

**USING FÖRSTER RESONANCE ENERGY TRANSFER (FRET)  
TO DEFINE THE CONFORMATIONAL CHANGES OF  
HUNTINGTIN AT THE CLINICAL THRESHOLD FOR  
HUNTINGTON'S DISEASE**

**USING FÖRSTER RESONANCE ENERGY TRANSFER (FRET)  
TO DEFINE THE CONFORMATIONAL CHANGES OF  
HUNTINGTIN AT THE CLINICAL THRESHOLD FOR  
HUNTINGTON'S DISEASE**

**By Nicholas Caron B.Sc.**

**A Thesis Submitted to the School of Graduate Studies in Partial Fulfilment of the  
Requirements for the Degree Doctor of Philosophy**

**McMaster University**

**© Copyright by Nicholas Caron, March 2014**

**Doctor of Philosophy – Biochemistry & Biomedical Sciences**

**McMaster University**

**Hamilton, Ontario**

**Title : Using Förster Resonance Energy Transfer (FRET) To Define the Conformational Changes of Huntingtin at the Clinical Threshold for Huntington’s Disease**

**Author : Nicholas S. Caron, Honours B.Sc.**

**Supervisor : Dr. Ray Truant**

**Number of Pages : xii, 181**

## Abstract

Huntington's disease (HD) is a progressive, neurodegenerative disorder that leads to the selective loss of neurons in the striatum and the cerebral cortex. HD is caused by a CAG trinucleotide repeat expansion beyond the normal length in the *IT15* (*Htt*) gene. The CAG stretch codes for an elongated polyglutamine tract within the amino-terminus of the huntingtin protein. Polyglutamine tracts with lengths exceeding 37 repeats cause HD whereas repeat lengths below do not. This phenomenon has plagued the HD community since the discovery of the gene in 1993. In this thesis, we sought to elucidate the molecular mechanism by which huntingtin becomes toxic at polyglutamine lengths above 37. Using Förster resonance energy transfer (FRET) techniques, we describe an intramolecular proximity between the first 17 residues (N17) and the proline-rich regions, which flank the polyglutamine tract of huntingtin. We report that we can precisely measure differences between the conformations adopted by the huntingtin protein with polyglutamine tracts below and above the pathogenic repeat threshold of 37 repeats. Our data supports the hypothesis that polyglutamine tracts below the pathogenic threshold can act as a flexible hinge allowing the N17 domain to freely fold back upon huntingtin and come into close 3D proximity with the polyproline region. This flexibility is lost in polyglutamine tracts with >37 repeats resulting in a diminished spatial proximity between N17 and the polyproline domain.

A hallmark of HD is the presence of nuclear and cytoplasmic inclusion bodies composed of mutant huntingtin within the brains of patients. The relevance of inclusions to HD pathology remains controversial. Some postulate that they are inherently neurotoxic, others that they are benign or protective. In this thesis, we sought to understand the mechanisms underlying the aggregation of mutant huntingtin into inclusion bodies. Using a combination of biophotonic methods, we describe two morphologically and structurally distinct inclusion types. Termed fibrillar and globular, these two inclusion types display different formation and maturation dynamics. Furthermore, by regulating post-translational modifications of N17, we show that we can push the cellular population of inclusions to one type or the other. Our results have led us to hypothesize that mutant huntingtin can form two unique inclusion types; one which is toxic while the other has a protective role in the cell.

## **Acknowledgements**

I would like to thank my supervisor, Dr. Ray Truant, for seeing my scientific potential and taking me on as a graduate student. You have provided me with invaluable support, insight and guidance throughout my PhD.

I would like to thank my committee members Dr. Jon Draper, Dr. David Andrews and Dr. Tony Collins for providing constructive feedback and helping me to achieve my research goals.

A sincere thank you to all the past members of the Truant lab: Dr. Randy Atwal, Dr. Carly Desmond, and Dr. Lise Munsie, for training me and helping me to adapt to the research environment. I would also like to thank the current members of the Truant lab: Jianrun Xia, Dr. Tam Maiuri, Dr. Leanne Stalker, Jenny Williamson, Tanya Woloshansky, Lisa Sequeira, Laura Bowie, Shreya Patel, Claudia Hung and Siddharth Nath, you have all contributed to making my PhD a productive and enjoyable experience.

Finally, I would like to acknowledge my family and friends for their unwavering motivation and support.

## List of Abbreviations

<b><sup>1</sup>H-NMR</b>	<sup>1</sup> H-nuclear magnetic resonance
<b>3-NP</b>	3-Nitropropionic acid
<b>A</b>	Adenine
<b>AAV</b>	Adeno-associated virus
<b>A<math>\beta</math></b>	Amyloid beta
<b>AD</b>	Alzheimer's disease
<b>ALS</b>	Amyotrophic lateral sclerosis
<b>AMPA</b>	$\alpha$ -amino-3-hydroxy-5-methyl-4-isoxazolepropionic acid
<b>APP</b>	Amyloid precursor protein
<b>ASO</b>	Antisense oligonucleotide
<b>ATP</b>	Adenosine triphosphate
<b>BAC</b>	Bacterial artificial chromosome
<b>BDNF</b>	Brain-derived neurotrophic factor
<b>C</b>	Cytosine
<b>C9orf72</b>	C9 open reading frame 72
<b>cAMP</b>	Cyclic adenosine monophosphate
<b>CBP</b>	CREB-binding protein
<b>CDK5</b>	Cyclin-dependent kinase 5
<b>CHIP</b>	Chromatin immunoprecipitation
<b>CJD</b>	Creutzfeldt–Jakob disease
<b>CK2</b>	Casein kinase 2
<b>CoQ10</b>	Coenzyme Q10
<b>CNS</b>	Central nervous system
<b>CREB</b>	cAMP response element-binding protein
<b>CRM1</b>	Chromosome region maintenance 1
<b>CSF</b>	Cerebrospinal fluid
<b>DM1/2</b>	Myotonic dystrophy 1 & 2
<b>DNA</b>	Deoxyribonucleic acid
<b>DRPLA</b>	Dentatorubial-pallidoluysian atrophy
<b>EMA</b>	European Medicines Agency
<b>ER</b>	Endoplasmic reticulum
<b>FBS</b>	Fetal bovine serum
<b>FDA</b>	United States Food and Drug Administration
<b>FLIM</b>	Fluorescence lifetime imaging microscopy
<b>FMR</b>	Fragile-X mental retardation
<b>FP</b>	Fluorescent protein
<b>FRAP</b>	Fluorescence recovery after photobleaching
<b>FRET</b>	Förster resonance energy transfer
<b>FTD</b>	Frontotemporal dementia
<b>G</b>	Guanine
<b>GFP</b>	Green fluorescent protein
<b>GTPase</b>	Guanosine triphosphate hydrolase
<b>H3K4</b>	Histone 3 lysine 4
<b>H3K27</b>	Histone 3 lysine 27

<b>HAT</b>	Histone acetyltransferase
<b>HAP</b>	Huntingtin-associated protein
<b>HD</b>	Huntington's disease
<b>HDAC</b>	Histone deacetylase
<b>HDF</b>	Hereditary disease foundation
<b>HEAT</b>	Huntingtin, elongation factor 3, the regulatory subunit of PP2A and TOR
<b>HIP</b>	Huntingtin-interacting protein
<b>HSP70</b>	Heat shock protein 70
<b>IHC</b>	Immunohistochemistry
<b>IKK</b>	I $\kappa$ B kinase
<b>MDPK</b>	Myotonic dystrophy protein kinase
<b>MSN</b>	Medium spiny neuron
<b>N17</b>	First 17 amino acids of huntingtin
<b>N-WASP</b>	Neural Wiskott–Aldrich syndrome protein
<b>NAD<sup>+</sup></b>	Nicotinamide adenine dinucleotide
<b>NES</b>	Nuclear export signal
<b>NFT</b>	Neurofibrillary tangle
<b>NLS</b>	Nuclear localization signal
<b>NMDA</b>	<i>N</i> -methyl-D-aspartate
<b>NR3A</b>	NMDA receptor subunit 3A
<b>PACSN1</b>	Protein kinase C and casein kinase substrate in neurons 1
<b>PD</b>	Parkinson's disease
<b>PET</b>	Positron emission tomography
<b>PGC-1<math>\alpha</math></b>	Peroxisome proliferator-activated receptor gamma coactivator 1-alpha
<b>PP2A</b>	Protein phosphatase 2A
<b>PRC2</b>	Polycomb repressive complex 2
<b>PrP</b>	Prion protein
<b>PSD-95</b>	Post synaptic density-95
<b>RFLP</b>	Restriction fragment-length polymorphism
<b>RNA</b>	Ribonucleic acid
<b>ROS</b>	Reactive oxygen species
<b>S13S16</b>	Serine 13 and 16
<b>S13AS16A</b>	Serine 13 to alanine and serine 16 to alanine
<b>S13DS16D</b>	Serine 13 to aspartic acid and serine 16 to aspartic acid
<b>S13ES16E</b>	Serine 13 to glutamic acid and serine 16 to glutamic acid
<b>SAHA</b>	Suberoylanilide hydroxamic acid
<b>SBMA</b>	Spinobulbal muscular atrophy
<b>SCA</b>	Spinocerebellar ataxia
<b>SH3</b>	SRC homology 3
<b>SIRT</b>	Sirtuin
<b>SOD1</b>	Superoxide dismutase 1
<b>SP1</b>	Specificity protein 1
<b>SUMO</b>	Small ubiquitin-like modifier
<b>T</b>	Thymidine
<b>TBP</b>	TATA-box binding protein
<b>TG2</b>	Transglutaminase type 2

<b>TOR</b>	Target of rapamycin
<b>UTR</b>	Untranslated region
<b>UHDRS</b>	Unified Huntington's disease rating scale
<b>UVCHD</b>	US-Venezuela Collaborative HD Project
<b>YAC</b>	Yeast artificial chromosome
<b>ZF9</b>	Zinc finger 9

## Table of Contents

<b>Chapter 1 - Introduction</b>	<b>1</b>
1.1 Overview of Huntington's Disease	1
1.2 History of HD	3
1.3 Genetics of HD	7
1.4 Neuropathology of HD	9
1.5 Symptoms of HD	11
1.6 CAG Trinucleotide Repeat Disorders	12
1.7 Non-Polyglutamine and Other Repeat Disorders	13
1.8 Huntingtin Cellular Localization and Evolution	14
1.9 Huntingtin Structure	15
1.9.1 Huntingtin Structural Domains	16
1.10 Huntingtin Function	19
1.10.1 The Role of Huntingtin in Development	19
1.10.2 The Role of Huntingtin in Vesicular Transport	20
1.10.3 The Role of Huntingtin in Axonal Transport	20
1.10.4 The Role of Huntingtin in Endocytosis	21
1.10.5 The Role of Huntingtin in Synaptic Transmission	22
1.10.6 The Role of Huntingtin in the Cell Stress Response	23
1.11 The Pathogenic Threshold for HD	25
1.12 Polyglutamine Flanking Sequences	26
1.12.1 The Rusty Hinge Hypothesis	29
1.13 Pathogenic Mechanisms in HD	31
1.13.1 Excitotoxicity in HD	31
1.13.2 Mitochondrial Dysfunction in HD	33
1.13.3 Altered Transcription in HD	34
1.13.4 Proteolytic Cleavage of Huntingtin in HD	36
1.13.5 Protein Aggregation in Neurodegenerative Diseases	37
1.13.6 Inclusion Bodies in HD	39
1.14 Therapeutic Efforts in HD	44
1.14.1 Pharmacologic Management of Symptoms in HD	44
1.14.2 A Need for Disease-Modifying Drugs for HD	46
1.14.3 Overview of Disease-Modifying Therapies in HD	46
1.14.4 Targeting Transglutaminase type 2 (TG2) as a Therapy for HD	52
1.14.5 Targeting Huntingtin as a Therapy for HD	54
1.14.6 Promoting Phosphorylation of Huntingtin N17 as a Prospective Therapy for HD	56
1.14.7 A Need for Better Animal Models	58

<b>1.15</b>	<b>Using FRET Techniques to Study HD and Other Neurodegenerative Diseases</b>	<b>58</b>
<b>1.16</b>	<b>Thesis Outline and Study Rationale</b>	<b>61</b>
<b>Chapter 2 - Measuring Conformational Changes of an Enzyme in Live Cells</b>		<b>63</b>
<b>2.1</b>	<b>Abstract</b>	<b>65</b>
<b>2.2</b>	<b>Introduction</b>	<b>66</b>
<b>2.3</b>	<b>Materials and Methods</b>	<b>69</b>
<b>2.4</b>	<b>Results</b>	<b>72</b>
<b>2.5</b>	<b>Discussion</b>	<b>76</b>
<b>2.6</b>	<b>Acknowledgements</b>	<b>82</b>
<b>Chapter 3 - Detecting the Conformational Change of Huntingtin at the Pathogenic Threshold for HD</b>		<b>83</b>
<b>3.1</b>	<b>Abstract</b>	<b>85</b>
<b>3.2</b>	<b>Introduction</b>	<b>86</b>
<b>3.3</b>	<b>Materials and Methods</b>	<b>89</b>
<b>3.4</b>	<b>Results</b>	<b>92</b>
<b>3.5</b>	<b>Discussion</b>	<b>99</b>
<b>3.6</b>	<b>Acknowledgements</b>	<b>113</b>
<b>Chapter 4 - Mutant Huntingtin Forms Toxic and Protective Inclusions</b>		<b>114</b>
<b>4.1</b>	<b>Abstract</b>	<b>116</b>
<b>4.2</b>	<b>Introduction</b>	<b>117</b>
<b>4.3</b>	<b>Materials and Methods</b>	<b>121</b>
<b>4.4</b>	<b>Results</b>	<b>125</b>
<b>4.5</b>	<b>Discussion</b>	<b>134</b>
<b>4.6</b>	<b>Acknowledgements</b>	<b>153</b>
<b>Chapter 5 - Discussion and Future Directions</b>		<b>154</b>
<b>5.1</b>	<b>TG2 Conformational Sensor</b>	<b>154</b>
	<b>5.1.1 Future Directions</b>	<b>155</b>
<b>5.2</b>	<b>Huntingtin Conformational Sensor</b>	<b>155</b>
	<b>5.2.1 Future Directions</b>	<b>159</b>
<b>5.3</b>	<b>Huntingtin Inclusions</b>	<b>159</b>
	<b>5.3.1 Future Directions</b>	<b>160</b>

## List of Figures

- Figure 1.1** CAG expansion within the *Htt* gene causes Huntington's disease (HD)
- Figure 1.2** The huntingtin protein
- Figure 1.3** The Rusty Hinge hypothesis
- Figure 1.4** Comparing symptomatic and disease-modifying treatments in HD
- Figure 2.1** The transglutaminase type 2 (TG2) conformational FRET sensor
- Figure 2.2** Point mutations and cell stresses affect TG2 conformation in live cells
- Figure 2.3** TG2 inhibitors differentially affect TG2 conformation
- Figure 3.1** Huntingtin exon1 FLIM-FRET sensor
- Figure 3.2** N17 phospho-mimicry mutants and kinase inhibitors can affect the conformation of huntingtin exon1
- Figure 3.3** PACSIN1 interacts with N17 and facilitates the proximity between N17 and the polyproline region of huntingtin
- Figure 3.4** An antibody-based FLIM-FRET assay to measure the conformations of the amino terminus of full-length huntingtin
- Figure 3.S1** Huntingtin FRET sensor in fibroblasts
- Figure 3.S2** Measuring the conformation of wild-type and mutant polyglutamine tracts in the context of longer huntingtin fragments
- Figure 3.S3** N17 phospho-mimicry mutants can affect the conformation of huntingtin exon1
- Figure 3.S4** Co-immunoprecipitation and siRNA of PACSIN1
- Figure 3.S5** FLIM-FRET of endogenous huntingtin using monoclonal antibodies
- Figure 4.1** Huntingtin fragments can form two morphologically unique inclusion types
- Figure 4.2** Fibrillar inclusions are detectable by thioflavin-T staining assay
- Figure 4.3** Comparing the fluorescence lifetime ( $\tau$ ) changes in globular versus fibrillar inclusion types

- Figure 4.4** Comparing the dynamics of globular versus fibrillar inclusions
- Figure 4.5** Active recruitment of mutant huntingtin into globular inclusions is microtubule-dependent
- Figure 4.6** Comparing the formation of fibrillar versus globular inclusions using temporal seFRET
- Figure 4.7** Full-length, endogenous huntingtin is actively recruited and sequestered within fibrillar inclusions
- Figure 4.8** Phosphorylation state of N17 S13 and S16 can influence the fate of the inclusion type
- Figure 4.9** Model of the dynamics of two distinct inclusion types formed from mutant huntingtin protein
- Figure 4.S1** HA-tagged mutant huntingtin exon1 forms two inclusion types
- Figure 4.S2** Fibrillar and globular inclusions are not differentially ubiquitinated
- Figure 4.S3** FLIM-FRET controls
- Figure 4.S4** Endogenous huntingtin is detectable within fibrillar inclusions with methanol fixation
- Figure 5.1** Comparing the effect of eight novel inhibitors on the conformation of TG2
- Figure 5.2** The polyglutamine tract of ataxin-7 behaves as a flexible hinge that is impaired at pathogenic lengths

# Chapter 1 – General Introduction

## 1.1 Huntington's Disease Overview

Huntington's disease (HD) is an autosomal dominant, neurodegenerative disorder for which there is no treatment. HD affects ~1:7000 people worldwide making it one of the most common inherited neurodegenerative diseases<sup>1</sup>. Neuropathological analysis of patients with HD shows selective and progressive degeneration of the medium spiny neurons (MSNs) of the striatum and pyramidal projection neurons of the cerebral cortex<sup>2</sup>. HD manifests as a spectrum of progressive motor, cognitive and psychiatric symptoms. Motor symptoms of HD include involuntary choreic movements, dystonia and a lack of motor coordination<sup>3</sup>. Cognitive symptoms range from dementia to impaired memory and executive functions<sup>4,5</sup> whereas psychiatric symptoms include depression, apathy, irritability and aggression<sup>6</sup>. Which symptoms appear first or have the greatest effect on functional ability varies greatly among the affected individuals. HD is a late-onset disease that typically affects individuals in the third to fourth decade of life. Symptoms manifest and progress over a 10-15 year period before leading to death.

At the molecular level, the cause of HD was found to be an expansion of a cytosine (C)-adenine (A)-guanine (G) trinucleotide repeat stretch beyond the normal repeat length within the coding region of the *IT15 (Htt)* gene<sup>7</sup>. This polymorphic CAG expansion encodes a polyglutamine tract within exon1 of the huntingtin protein (Figure 1.1). Individuals with CAG repeat lengths above the pathogenic threshold of 37 develop HD whereas those with lengths below 36 do not (Figure 1.1)<sup>8,9</sup>. An inverse correlation exists between the length of the CAG tract and age of symptom onset<sup>8,10</sup>, whereas there is a strong positive correlation between CAG length and symptom severity<sup>9</sup>. However, significant variability arises when making predictions of symptom-onset based on repeat length<sup>10</sup>, suggesting that additional genetic, environmental and disease-modifying factors are involved in HD pathology.

To date, therapeutic intervention in HD has been limited to drugs that have mild efficacy in managing symptoms and there are currently no disease-modifying treatments available to reverse or even slow the progression of the disease. The lack of

disease-modifying drugs may be a result of poor target selection or that the majority of clinical trials choose symptomatic patients that may be too far progressed in the course of the disease to show therapeutic benefits. However, the lack of effective drugs for treatment of HD likely stems from our poor understanding of the normal function of the huntingtin protein and the dysfunction that occurs as a result of the polyglutamine expansion.

Magnetic resonance imaging (MRI) of gene-positive, non-symptomatic patients reveals dramatic changes in brain physiology many years prior to the onset of symptoms and neurodegeneration in HD<sup>11,12</sup>. The availability of predictive genetic testing for HD provides the opportunity to begin treatment decades before the onset of the disease. Therefore, pre-symptomatic treatment likely represents the optimal therapeutic window for drugs that modify the course of HD. However, robust and reliable biomarkers are required to track the progression of the HD following drug treatments, in the absence of clinical symptomatic endpoints.

## 1.2 History of HD

The origins of HD can be traced back as far as the 16<sup>th</sup> century where Paracelsus, an alchemist and physician, first coined the term chorea (from the Greek khoreia = dance) to describe the uncoordinated, involuntary dance-like movements now known to be a characteristic motor symptom of HD. In the 17<sup>th</sup> century, individuals with HD were said to be afflicted with “that disorder” or “St. Vitus” dance, which was a term used to describe the choreic movements that manifest in the disease. Despite chorea being the most obvious symptom of HD, there is evidence as early as 1621 proposing that HD was not only a motor disorder but having cognitive and psychiatric components as well.

In the 1840's, HD was first described as being a ‘chronic hereditary chorea’ where physicians from Europe and North America independently wrote of individuals suffering from involuntary movements and cognitive disturbances that worsened with age and were inherited from similarly affected parents. A more comprehensive description of “that disorder” was done by a family medical practice located in East Hampton, New York during the 18<sup>th</sup> and 19<sup>th</sup> century. Abel Huntington was a physician that frequently encountered individuals with St. Vitus dance. Later the medical practice was taken over by his son, George Lee Huntington, who continued to observe, document and treat individuals from the East Hampton community afflicted with HD. These detailed longitudinal observations of patients over several generations laid the ground work for Dr. George Huntington, son of George Lee and grandson of Abel, to publish the seminal paper “On Choreia” in 1872 at the age of 22<sup>13</sup>. This paper detailed the classic symptoms and hereditary nature of this disease. As a result of George Huntington’s ground breaking work, St. Vitus dance was subsequently renamed Huntington’s chorea. It was not until the 20<sup>th</sup> century that Huntington’s chorea became known as HD to reflect the wide range of motor, cognitive and psychiatric symptoms associated with the disease. The neuropathology associated with HD was first described in the late 1800’s through the examination of *post mortem* brains of patients who died of Huntington’s chorea<sup>14,15</sup>. These doctors accurately described the loss of

neurons within the caudate nucleus, putamen and global pallidus that make up the corpus striatum<sup>14,15</sup>.

In the early 1900's, interest in the hereditary nature of Huntington's chorea was strengthened due to the rediscovery of Gregor Mendel's 1865 work on dominant inheritance. This led British geneticist William Bateson to definitively conclude in 1909 that Huntington's chorea was inherited as a Mendelian autosomal dominant disease. Around the same time, the emergence of eugenics, the concept of improving the genetic quality of the human race by promoting mating between individuals with desired traits and preventing mating between those with undesired traits, became popular in the scientific community. One of the early leaders of the eugenics movement was American biologist Charles B. Davenport, director of the Biological Laboratories at Cold Spring Harbour and founder of the Eugenics Records Office. In 1911, Davenport commissioned Elizabeth Muncey to conduct the first large-scale pedigree study of North American families with Huntington's chorea going back 12 generations. He concluded that the vast number of individuals affected with HD were the result of a small group of progenitors in the population. This led Davenport to lobby for eugenics policies around the world calling for surveillance, institutionalization, immigration restrictions and even sterilization of those affected.

Huntington's chorea garnered mainstream attention when prominent folk singer-songwriter Woody Guthrie was diagnosed in 1952, who had inherited the disease from his mother Nora. He wrote about his affliction:

*"Face seems to twist out of shape. Can't control it. Arms dangle all around. Can't control them. Wrists feel weak and my hands wave around in odd ways. I can't stop. All these docs keep asking me about how my mother died of Huntington's Chorea. They never tell me if its pass-onable or not. So I never know. I believe every doctor ought to speak plainer so us patients can begin to try to guess partly what's wrong with us. If it's not alcohol which has me, I wonder what it's going to be"*<sup>16</sup>

Woody Guthrie's passing from HD in 1967 led his wife Marjorie to found the Committee to Combat Huntington's Disease (now the Huntington's Disease Society of America), a non-profit organization that funds research and provides for support for families affected by the disease. Another prominent figure in HD research was Milton

Wexler, a Los Angeles psychoanalyst, who formed the Hereditary Disease Foundation (HDF) in 1968 after his wife was diagnosed with HD. The HDF was established with the aim of curing genetic diseases by organizing and funding research. In 1972, Milton Wexler learned of a fishing village near Lake Maracaibo in Venezuela with the largest kindred of HD in the world (14,000 individuals) from the work of a Venezuelan clinician named Dr. Amerigo Negrette. The staggering prevalence was attributed to a founder effect, where the arrival of a European sailor in ~1800 carrying the HD mutation left over 18,000 descendants with HD in the villages surrounding Lake Maracaibo. Dr. Nancy Wexler, daughter of Milton Wexler, realized the potential of studying a hereditary disease in a genetically related population and established the US-Venezuela Collaborative Huntington's Disease (UVCHD) project in 1979. This interdisciplinary consortium has travelled to Lake Maracaibo annually to identify families with HD, collect DNA samples and study the progression of the disease in these families. The genetic information collected by the UVCHD project was critical in enabling scientists to identify the gene responsible for HD.

In 1983, genetic linkage analysis was used to narrow down the HD locus to a region of human chromosome 4<sup>17</sup>. This was done by identifying a DNA probe with a specific restriction fragment length polymorphism (RFLP) pattern that was associated with HD families<sup>17</sup>. The location of the gene was subsequently refined using a location cloning approach and was mapped to the short arm of chromosome 4 at the 4p16.3 locus<sup>18</sup>. In an unprecedented global collaborative effort comprising the top researchers and medical doctors in the field, the Huntington's Disease Collaborative Research Group (HDCRG) spent the next 10 years trying to identify the HD gene and the mutation associated with HD. In 1993, the HDCRG identified the novel interesting transcript 15 (*IT15*, now on referred to as *Htt*) gene, which contained a polymorphic CAG trinucleotide repeat that was unstable and expanded in HD patient chromosomes<sup>7</sup>. They also discovered that the CAG expansion occurred within an open reading frame of the *Htt* gene predicted to code for a 348KDa protein. The seminal work done by the HDCRG along with the discovery of the gene responsible for spinal bulbar muscular atrophy (SBMA)<sup>19</sup> a few years prior led to the characterization of a new family of diseases, known collectively as CAG trinucleotide repeat disorders.

In 1996, the first mouse model of HD was generated expressing exon1 of huntingtin as a transgene<sup>20</sup>. The expression of this short fragment containing the polyglutamine tract was sufficient to elicit the progressive neurological symptoms seen in HD<sup>20</sup>. This was the first *in vivo* opportunity to study the molecular mechanisms underlying HD. Since then, many transgenic and knock-in, full-length huntingtin animal models have been generated in an effort to more closely recapitulate the disease process seen in humans. In 1997, mutant huntingtin-containing inclusion bodies were discovered within *post mortem* brains of patients with HD<sup>21</sup>. This discovery led researchers to hypothesize that the accumulation of misfolded, mutant huntingtin may be responsible for the neurodegeneration observed in HD.

### 1.3 Genetics of HD

HD is a devastating hereditary disorder that is inherited in an autosomal dominant manner. As such, only one copy of the mutated gene is required for disease and if one parent is affected (as a heterozygous carrier) then offspring have a 50% chance of developing HD. HD is a monogenetic disorder caused by a single mutation within the DNA sequence of the *Htt* gene located on the short arm of chromosome 4 at the locus 4p16.3<sup>7</sup>. The *Htt* gene codes for a protein named huntingtin, which is composed of 3144 amino acids, 67 exons and is 350KDa in size<sup>22</sup>. The single, causative mutation responsible for HD is a CAG trinucleotide repeat expansion within the open reading frame of the first exon1 of *Htt* (Figure 1.1). This CAG expansion results in an elongated glutamine tract near the amino-terminus of the huntingtin protein. Individuals with CAG repeat lengths of 36 or less within the *Htt* gene do not develop HD, whereas individuals having greater than 40 CAG repeats develop HD symptoms with full penetrance (Figure 1.1). CAG repeat lengths between 37-39 exhibit incomplete (reduced) penetrance and may or may not develop HD symptoms in their lifetime (Figure 1.1)<sup>23</sup>. Repeat lengths above 60 result in juvenile-onset HD (also known as the Westphal variant), where symptoms progress more severely than adult-onset HD and onset occurs before the age of 20 (Figure 1.1)<sup>24</sup>. Therefore, there is a strong inverse correlation between CAG repeat lengths and the age of symptom onset in HD<sup>25</sup>. However, despite CAG length being the dominant modifier of disease, additional environmental and genetic factors also contribute to the age of symptom onset.

Intermediate length alleles with CAG repeats between 29-36 are characterized as being unstable and can expand to pathogenic lengths in germ cells during meiosis<sup>26,27</sup>. This genetic anticipation is the cause of sporadic HD cases and can lead to progressively earlier onset of symptoms in subsequent generations. Although a rare occurrence, having two expanded copies of the *Htt* allele (homozygous HD) results in a HD pathology that is clinically indistinguishable from heterozygous HD and does not influence the severity or age of onset of HD symptoms<sup>28,29</sup>. Rather, the age of onset for homozygous individuals is strongly dependent on the length of the allele with the longest CAG expansion<sup>30</sup>.

A

<i>Htt</i> CAG Length	Clinical Phenotype	Resulting Polyglutamine (PolyQ) Expansion within Huntingtin Exon1
<36 CAG repeats	Normal	N17 PolyQ Proline-rich
37-39 CAG repeats	Adult-Onset HD Reduced Penetrance	N17 PolyQ Proline-rich
>40 CAG repeats	Adult-Onset HD Full Penetrance	N17 PolyQ Proline-rich
>60 CAG repeats	Juvenile HD	N17 PolyQ Proline-rich

**Figure 1.1. CAG expansion within the *Htt* gene causes Huntington's disease (HD).**

(A) Table representing different ranges of *Htt* CAG repeat lengths and the impact on penetrance, disease state and the expansion of the polyglutamine (polyQ) tract at the amino-terminus of the huntingtin protein. N17, the first 17 amino acids of huntingtin, the polyQ tract and the proline-rich domain represent the protein product of exon1 of *Htt*.

## 1.4 Neuropathology of HD

HD is characterized by the progressive and selective loss of neurons within the striatum and the cerebral cortex of the brain. The striatum is divided into two sections: the caudate nucleus and putamen, which together make-up the main input to the basal ganglia. The striatum undergoes diffuse atrophy during the progression of HD, where the caudate nucleus is more severely affected than the putamen<sup>2</sup>. Notably, there is a large variation in the degree of neuropathology of the striatum between individuals with HD<sup>2</sup>. The striatum is composed of two main sub-populations of neurons: the MSNs, which are projection neurons responsible for signalling to other regions of the brain, and interneurons, which are responsible for local signalling within the striatum. In HD, the medium spiny projection neurons are extremely vulnerable to neurodegeneration whereas the interneurons are largely spared<sup>31,32</sup>. The cerebral cortex, which sends efferent connections to the striatum, also undergoes some degree of atrophy during the progression of HD<sup>2</sup>. This atrophy is due to the loss of pyramidal projection neurons of the cerebral cortex.

The severity of neurodegeneration in HD is measured on a standardized 5 grade scale (0-4) based on the examination of striatal degeneration patterns in post mortem brains of patients<sup>2</sup>. Grade 0 refers to patients that were diagnosed with clinical HD but show no discernible neuropathological abnormalities relative to normal brains<sup>2</sup>. Grade 1 is characterized by striatal atrophy, neuronal loss up to 50% and astrocytosis<sup>2</sup>. Grades 2-3 show more severe striatal atrophy and neuronal loss than grade 1. Grade 4 is designated to the most severe cases of HD where there is gross atrophy of the striatum with up to 95% neuron loss<sup>2</sup>.

Despite the characteristic neuron loss seen in select brain regions of patients with late stage HD, it has been hypothesized that neuronal dysfunction occurs prior to the onset of neurodegeneration and is responsible for the early symptoms of HD. This phenomenon has been suggested in human HD<sup>2</sup> and has been fully documented in animal models that recapitulate the selective neurodegeneration associated with HD<sup>33,34</sup>. Advances in neuro-imaging techniques have provided a tool to correlate the morphological changes in the brain with the clinical symptoms experienced in HD. MRI-

based analysis of symptomatic HD patients has revealed global volume reductions in nearly all brain regions<sup>35</sup>. Furthermore, imaging of pre-symptomatic HD patients has revealed that drastic changes in the brain actually occur many years before the onset of symptoms or neurodegeneration<sup>11,36</sup>. These findings validate the need to utilize pre-symptomatic individuals in clinical trials for neuro-protective and disease-modifying drugs since dramatic neurophysiological abnormalities occur very early in the course of the disease.

## 1.5 Symptoms of HD

HD manifests as a spectrum of motor, cognitive and psychiatric disorders where there is significant variability in the severity of symptoms between affected individuals. The age of onset and severity of symptoms in HD is strongly dependent on the length of the CAG stretch<sup>25</sup>. On average, symptoms develop in the 4<sup>th</sup> decade of life and progress in severity for 10-15 years prior to death<sup>37</sup>. Clinical diagnosis of HD is based on the presence of choreic movements; however, due to the symptom variability between affected individuals, diagnosis can be delayed due to the absence of motor symptoms. The most common motor symptoms that develop during adult-onset HD include: chorea, dystonia (prolonged muscle contraction), bradykinesia (difficulty initiating movements), dysphagia (difficulty swallowing) and dysarthria (difficulty articulating)<sup>3</sup>. These include both voluntary and involuntary movement disorders. Chorea or choreatic movements refer to the involuntary, jerky, non-repetitive movement of hands and feet that resembles dancing. The most common cognitive symptoms associated with HD include: impaired communication, dementia, impaired memory, impaired organization, impaired regulation and overall loss of executive function<sup>4,5</sup>. Cognitive disorders of HD are typically the first symptoms to appear and often precede the onset of motor dysfunction. The most common psychiatric or behavioural disorders that occur in adult-onset HD include: aggression, apathy, anxiety, depression, sleep disturbances, hallucinations and sexual dysfunction<sup>6</sup>. Depression is the most common psychiatric symptom associated with HD, where major depression affects up to 40% of patients<sup>38</sup>. The debilitating cognitive and psychiatric symptoms of HD result in an incidence of suicide that is 5 times greater than the population average in unaffected individuals<sup>39</sup>. To date, therapeutics available for HD are limited to managing symptoms and are inadequate in their efficacy. Furthermore, no disease-modifying drugs exist to reverse or even slow the progression of the disease and its associated symptoms.

## 1.6 CAG Trinucleotide Repeat Disorders

CAG trinucleotide repeat disorders encompass a family of diseases caused by a CAG trinucleotide repeat expansion beyond the normal length in the open reading frame (ORF) of a coding gene. In these diseases, the CAG repeat expansion is translated into an elongated tract of glutamines within the disease protein which has led to the term, polyglutamine diseases. In 1991, it was first discovered that spinal bulbar muscular atrophy (SBMA) was caused by a CAG expansion within the androgen receptor (*AR*) gene located on the X-chromosome that coded for a polyglutamine tract within the protein<sup>19</sup>. Following this discovery, it was found that HD was caused by a CAG expansion within the *Htt* gene on chromosome 4<sup>7</sup>. In total, there are nine hereditary, neurodegenerative diseases caused by polyglutamine expansions in unrelated proteins. The polyglutamine diseases include: spinal and bulbar muscular atrophy (SBMA), spinocerebellar ataxia (SCA) types 1, 2, 3, 6, 7, 17, dentatorubral-pallidoluysian atrophy (DRPLA) and HD. All the polyglutamine diseases share a similar autosomal dominant inheritance, mid-age onset, genetic anticipation to future generations due to repeat instability and an inverse correlation between polyglutamine length and age of symptom onset<sup>40</sup>. Despite the common elements between these diseases, the CAG expansions occur within different genes and the resulting proteins do not share a common structure, function, or sequence identity aside from the polyglutamine tract. All of the polyglutamine diseases are caused by a repeat expansion beyond a specific pathogenic threshold. Some are similar to HD, requiring ~36-40 repeats, whereas SCA type 6 requires fewer (21) and DRPLA, SCA types 3 and 17 require many more to cause disease. Additionally, each polyglutamine disease causes neurodegeneration in a specific subset of neurons in the brain resulting in very different symptoms. Therefore, the context of the polyglutamine expansion within the specific disease protein could explain the differences in neurodegeneration and pathogenic thresholds seen in these diseases. Understanding the molecular dysfunction that occurs at the clinical threshold in one disorder may help to elucidate the pathogenic mechanisms in the other polyglutamine diseases.

## 1.7 Non-Polyglutamine and Other Repeat Disorders

To date, at least 22 inherited disorders involving the central nervous system (CNS) are known to be caused by repeat expansions<sup>41</sup>. Beyond the subcategory of polyglutamine diseases, where CAG expansions occur within the coding region of a gene, there is a larger family of repeat disorders caused by trinucleotide expansions (not CAG) that fall within non-coding or intronic regions and also those caused by non-trinucleotide repeat expansions. The class of diseases caused by non-CAG trinucleotide expansions within non-coding regions of DNA include diseases such as: fragile-X syndrome, where a CGG expansion occurs within the 5' untranslated region (UTR) of the fragile-X mental retardation 1 (*FMR1*) gene<sup>42</sup>; and myotonic dystrophy type 1 (DM1) which is caused by a CTG expansion within the 3' UTR of the myotonic dystrophy protein kinase (*MDPK*) gene. The CTG expansion in the *MDPK* gene results in a toxic RNA species with an expanded CUG repeat<sup>43</sup>. Non-trinucleotide repeat disorders can be caused by tetra-, penta- and even hexanucleotide microsatellite repeats. Myotonic dystrophy type 2 (DM2) is caused by a CCTG tetranucleotide expansion within intron 1 of the zinc finger 9 (*ZF9*) gene<sup>44</sup>. The tetranucleotide expansion in the *ZF9* gene results in a toxic RNA molecule with an expanded CCUG repeat<sup>44</sup>. Notably, the tetranucleotide repeat lengths on expanded alleles in DM2 can range from 75 to over 11,000, with a mean of ~5000<sup>44</sup>. A non-coding GGGGCC hexanucleotide repeat in the first intron of the C9 open reading frame 72 (*C9ORF72*) gene has been identified as the cause of a large percentage of familial amyotrophic lateral sclerosis (ALS) and frontal temporal dementia (FTD) cases<sup>45,46</sup>. Expanded hexanucleotide repeats within the *C9ORF72* gene have also been implicated in a variety of other neurodegenerative diseases including: HD-like syndrome, sporadic Creutzfeldt-Jakob disease and Alzheimer's disease (AD)<sup>47</sup>. The repeat expansion disorders encompass a broad spectrum of diseases where at least four mechanisms of disease have been proposed: a loss-of-function of the expansion-containing gene; a toxic gain-of-function of the expansion-containing gene; a gain-of-function as a result of an expansion within RNA; and the gain-of-function as a result of a polyalanine expansion<sup>41</sup>. Classification of the repeat disorders within these mechanistic categories provides insight into the sequence expansion and the location of the expansion within the gene<sup>41</sup>.

## 1.8 The Huntingtin Protein: Cellular Localization and Evolution

The huntingtin protein is composed of 3144 amino acids, 67 exons and has a molecular weight of 350KDa<sup>22</sup>. Huntingtin is ubiquitously expressed in all tissues with elevated levels in the brain and testis<sup>48,49</sup>. Despite the widespread expression of the protein, neurodegeneration in HD is limited mainly to the striatum and cerebral cortex regions of the brain<sup>2</sup>. At the cellular level, huntingtin is localized to the cytoplasm and the nucleus, and can associate with a number of organelles including: the endoplasmic reticulum, the Golgi apparatus, the mitochondria, endosomal compartments and the primary cilium (Figure 1.2C)<sup>50-55</sup>. Huntingtin has also been shown to interact directly with the actin and microtubule cytoskeleton where it can be detected at the mitotic spindle, the centrosome, the cleavage furrow and cofilin-actin stress rods (Figure 1.2C)<sup>56-60</sup>. In addition to associating with numerous proteins, huntingtin can also interact with deoxyribonucleic acid (DNA), messenger ribonucleic acid (mRNA) and lipids<sup>61-64</sup>. Therefore, huntingtin is a protein that interacts with a vast network of molecules and as a result has many functions within the cell.

Huntingtin is highly conserved among vertebrate species supporting an important evolutionary role for this protein in higher organisms. Aside from the polyglutamine tract, huntingtin does not share homology with any other cellular protein. A sequence comparison between different orthologs of the huntingtin protein revealed that the amino-terminus of huntingtin (amino acids 1-386) represents the most recently evolved section whereas the carboxyl-terminus (2437-3078) is the most conserved region of huntingtin<sup>65</sup>. That being said, the amino-terminal polyglutamine tract was an ancient evolutionary acquisition and is found in animals as far back as the deuterosome branch<sup>65</sup>. Notably, all vertebrates have evolved with at least four glutamines and this length is expanded in mammals with humans having the longest and most polymorphic polyglutamine tracts<sup>66</sup>. This suggests that the presence of the polyglutamine tract in huntingtin is an important evolutionary feature that may be critical for the normal function of huntingtin in vertebrates. The proline-rich region flanking the polyglutamine tract at the distal end seems to have been spontaneously acquired during the evolution of the protein<sup>65,66</sup>. Portions of the proline-rich tract are found in all mammals and its

length has increased with the expansion of the polyglutamine tract. Huntingtin, elongation factor 3 (EF3), the regulatory subunit A of protein phosphatase 2A (PP2A) and target of rapamycin (TOR) (HEAT) repeats<sup>67</sup>, which are dispersed along the length of huntingtin and make up a majority of the protein, are also highly conserved in vertebrates<sup>68</sup>.

## 1.9 Huntingtin Structure

For many years after the discovery of the *Htt* gene, the huntingtin protein was described as having an unknown function. This was due to the inherent challenges of performing experimental assays to test the functions of such a large protein. To gain insight into the normal functional roles of huntingtin in the cell, structural features of the protein must be analyzed. The huntingtin protein is believed to adopt an overall alpha ( $\alpha$ )-helical solenoid structure due to the numerous tandem HEAT repeat regions that make up the majority of the protein (Figure 1.2A)<sup>67,69,70</sup>. A single HEAT repeat unit is composed of two interacting  $\alpha$ -helices connected by a short 1-3 residue turn, thus forming an anti-parallel helical hairpin. These units can form linear arrays of 50 repeats or more. Parallel stacking of these repeats induces an overall  $\alpha$ -solenoid structure that instills conformational flexibility to the huntingtin protein. Based on bioinformatic analysis, huntingtin is believed to contain between 40-70 HEAT repeats clustered into 4 larger HEAT repeat domains dispersed throughout the protein<sup>71</sup>. The conformational flexibility of huntingtin allows it to sense and transduce cellular mechanical forces along the entire length of the protein that are believed to expose and/or conceal different molecular interaction domains<sup>72</sup>. Solenoid proteins, like huntingtin, are generally involved in protein-protein interactions suggesting that huntingtin behaves as a scaffold for its large network of interacting proteins<sup>70,72</sup>. This implicates huntingtin as a multifunctional protein that is involved in a number of cellular processes. The enormous size of huntingtin has made it impossible to perform mass spectroscopy or x-ray crystallography assays to determine the structure of the full length protein. It is therefore necessary to systematically analyze the structure of individual domains to further elucidate the normal function of huntingtin.

### 1.9.1 Huntingtin Structural Domains

Beyond the HEAT repeats, structural analysis of the huntingtin protein has revealed multiple structured domains along the length of the protein (Figure 1.2B). The characterization of these structured domains has elucidated many of the normal cellular functions of the huntingtin protein. The first 17 amino acids (a.a) of huntingtin (N17) adopt an amphipathic  $\alpha$ -helical structure. This domain is a stress-dependent, membrane targeting signal that modulates huntingtin localization<sup>50</sup>, and calcium homeostasis<sup>73</sup>. N17 has also been shown to have a vast network of molecular interactors that are required for the normal function of the protein<sup>74</sup>. N17 is subject to a number of post-translational modifications that affect the localization, inclusion formation properties and toxicity of polyglutamine expanded huntingtin. Additionally, N17 has been shown to behave as a chromosome region maintenance 1 (CRM1)/exportin-dependent nuclear export signal (NES)<sup>75</sup>. Immediately downstream of the N17 domain is the polyglutamine tract that is responsible for HD upon its expansion. X-ray crystal structures of the wild type polyglutamine tract (17 glutamines) in the context of huntingtin exon1 (a.a. 1-81) reveals that it adopts multiple structural conformations including an  $\alpha$ -helix, a random coil and an extended-loop<sup>76</sup>. We hypothesize that this flexibility is required to facilitate the interaction of N17 with critical molecular factors and downstream regions of huntingtin. The mutant polyglutamine-expanded tract of huntingtin has long been considered to adopt a beta ( $\beta$ )-sheet structure, and this was recently confirmed using x-ray crystallography<sup>77</sup>. This  $\beta$ -sheet structure of polyglutamine is postulated to result in the formation of 'polar zippers' via hydrogen bonds between the main chain glutamines and the side chain amides of huntingtin leading to aggregation of the protein. Distal to the polyglutamine tract is a polymorphic proline rich-region composed of two pure polyproline stretches separated by a short intervening region composed mostly of proline and glutamine residues. This region adopts a polyproline type II (PPII) helix that can influence the structure of the polyglutamine tract and the ability of mutant huntingtin to form inclusions<sup>76,78,79</sup>. The proline-rich region is also the site of a number of protein-protein interactions required for the normal function of huntingtin that are impaired in HD<sup>80,81</sup>. Downstream of the proline-rich region, between amino acids 174-207, is an active nuclear localization signal (NLS) that mediates transport of huntingtin through

both karyopherin  $\beta$ 1 and  $\beta$ 2 pathways<sup>82</sup>. This NLS domain adopts a  $\beta$ -sheet structure that is critical to its import function<sup>82</sup>. Downstream of the NLS are a cluster of calpain (a.a. 437-537) and caspase sites (a.a. 513-586). Cleavage of huntingtin at these sites increases the toxicity and aggregation of the mutant protein<sup>83-86</sup>. Residues 1184-1254 of huntingtin make up a highly conserved, unstructured hinge region<sup>71</sup>. This hinge separates two large, flexible,  $\alpha$ -helical domains composed of HEAT repeats that span nearly the entire length of the protein<sup>71</sup>. Near the carboxyl end of the protein is another highly conserved CRM1/exportin1 dependent NES<sup>87</sup>. The presence of an import and two export signals implicates huntingtin as a shuttling protein that has functional roles in both the nucleus and the cytoplasm.

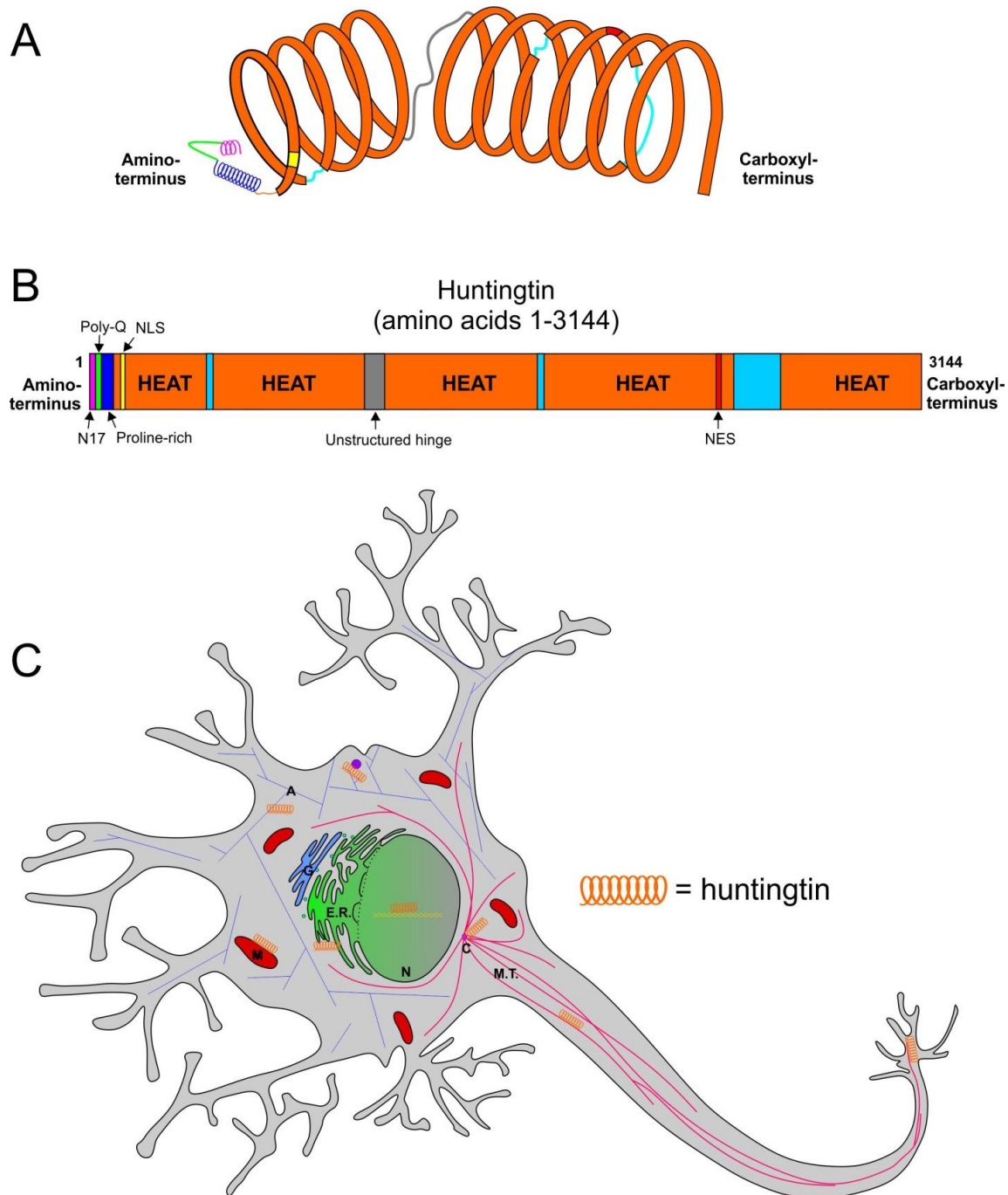


**Figure 1.2. The huntingtin protein.** (A) Speculative model showing overall  $\alpha$ -solenoid structure of the huntingtin protein. Different colours correspond to domains identified in (B). (B) Schematic representation of the huntingtin protein and its characterized domains (not to scale). (C) Subcellular localization of huntingtin within a neuron (not to scale). A=actin, M.T.=microtubules, N=nucleus, E.R.=endoplasmic reticulum, G=golgi, M=mitochondria, C=centrosome.

## 1.10 Huntingtin Function

Following the discovery of the *Htt* gene, huntingtin was long referred to as a protein of unknown function. The characterization of huntingtin as a flexible, HEAT repeat-rich structure and the identification of a large network of molecular interactors has implicated huntingtin as a scaffold protein with many critical cellular roles. The huntingtin protein has essential roles in embryonic development, axonal trafficking, endocytosis, synaptic regulation and the cell stress response. Many of these cellular roles are impaired in the presence of polyglutamine expanded huntingtin. This has led researchers to postulate that the mutation in HD results in the loss of function(s) of normal huntingtin.

### 1.10.1 The Role of Huntingtin in Development

Huntingtin is a critical cellular protein involved in a plethora of functions and has an essential role during development. Targeted inactivation of both copies of the *Hdh* gene (murine homolog of the *Htt* gene), generating a homozygous null mouse (-/-), impairs gastrulation and causes embryonic lethality at about day 7.5<sup>88-90</sup>. The timing of embryonic lethality in these nullizygous mice suggests that the huntingtin protein is a critical factor required for neurulation and the development of the anterior-posterior axis<sup>88,91</sup>. Therefore, huntingtin is expressed early in development, and that there are no functional redundancies to compensate for the complete loss of the *Hdh* gene. Inactivation of a single copy of the *Hdh* gene (+/-) is sufficient to rescue embryonic lethality and results in a normal phenotype in mice<sup>89,90</sup>. Notably, a single copy of either the wild type *Hdh* or CAG expanded *Hdh* results in normal development<sup>91</sup>. This was the first evidence that mutant huntingtin can perform all the required cellular functions during development but has a toxic gain or loss-of-function later in life. As a corollary, individuals with two copies of the CAG expanded *Htt* gene develop normally and are phenotypically identical to individuals that are heterozygous for the mutation<sup>29</sup>. Reducing huntingtin levels in mice below 50% causes defects in the development of the central nervous system (CNS) and structural anomalies in the brain. Unlike complete inactivation of *Hdh*, experimental reduction of huntingtin levels can overcome impaired gastrulation in mice but leads to developmental abnormalities later in gestation<sup>91</sup>. These

studies implicate huntingtin as an essential cellular protein where a certain dosage is required for normal embryonic development and for proper neurogenesis.

### **1.10.2 The Role of Huntingtin in Vesicular Transport**

Vesicular transport is a tightly regulated, active cellular process that involves the trafficking of molecules between specific membrane-enclosed organelles. In neurons, axonal transport is critical since essential factors produced in the soma must be transported along the cytoskeleton and delivered to the synapse. Thus, axonal trafficking in neurons requires the displacement of vesicles over extremely long distances. Huntingtin has an established role in axonal transport, endocytosis and synaptic recycling, suggesting that it plays a global cellular role as an essential integrator of vesicular trafficking<sup>92</sup>.

### **1.10.3 The Role of Huntingtin in Axonal Transport**

Consistent with a direct role in axonal transport, huntingtin has been shown to associate with actin, microtubules and vesicles<sup>51,56</sup>. Huntingtin-associated protein 1 (HAP1) has been proposed to facilitate interactions with microtubule-based motor proteins and interacts with the huntingtin protein in a polyglutamine-dependent manner<sup>93</sup>. HAP1 interacts with the p150<sup>glued</sup> subunit of dynactin, a co-activator of the motor protein dynein required for retrograde vesicular transport along microtubules<sup>94,95</sup>. Huntingtin can also interact directly with dynein in the absence HAP1<sup>96</sup>. Furthermore, huntingtin has been implicated in anterograde transport along microtubules through the interaction of HAP1 with the light chain of the kinesin motor protein. These interactions between huntingtin and motor protein complexes are critical for the transport of neurotrophic factors, such as brain-derived neurotrophic factor (BDNF), along axons<sup>97</sup>. The presence of mutant huntingtin or the experimental reduction of wild type huntingtin levels attenuates BDNF transport by impairing the association of motor proteins to microtubules<sup>97</sup>. Huntingtin is required for bi-directional vesicular transport along microtubules, and the aberrant interaction between mutant huntingtin and HAP1 impairs vesicular transport in neurons. Therefore, huntingtin acts as a scaffold between the cytoskeleton and motor proteins and is critical for the trafficking of cargo in the cell.

#### 1.10.4 The Role of Huntingtin in Endocytosis

Huntingtin has been found to localize to endosomal compartments and is a critical component of the endocytic pathway<sup>50,73,98,99</sup>. The function of huntingtin in endocytosis has been elucidated through the identification of several huntingtin interacting proteins. Huntingtin interacting protein 1 (HIP1) is a critical component of clathrin-mediated endocytosis and acts as an adaptor between clathrin and huntingtin<sup>100,101</sup>. HIP1 interacts with huntingtin in a polyglutamine-dependent manner, where mutant huntingtin has a reduced binding affinity for HIP1<sup>101</sup>. The huntingtin-associated protein 40 (HAP40) interacts with at the carboxyl-terminus of huntingtin<sup>102</sup>. HAP40 functions as an effector of the guanosine triphosphate hydrolase (GTPase) Rab5, an essential regulator of vesicular trafficking during early endocytosis<sup>103,104</sup>. HAP40 mediates the recruitment of huntingtin to early endosomes through its interaction with Rab5 and this complex is required for the regulation of endosome motility<sup>104</sup>. The interaction between Rab5 and huntingtin has also been shown to regulate the differential association of early endosomes to either the microtubule or actin cytoskeleton<sup>104</sup>. Protein kinase C and casein kinase 2 substrate in neurons type 1 (PACSIN1 or Syndapin I) is a neuron-specific protein that interacts with the proline-rich domain of huntingtin in a polyglutamine-length dependent manner via an SRC homology 3 (SH3) domain<sup>81</sup>. The SH3 domain of PACSIN1 can also interact with the endocytic proteins dynamin, synapsin and synaptojamin, as well as the neural Wiskott–Aldrich syndrome protein (N-WASP), an activator of actin-related protein 2/3 (Arp2/3) - mediated actin polymerization<sup>105</sup>. PACSIN1 forms tetramers through a FCH and Bin-Amphiphysin-Rvs (F-BAR) domain, which is critical for its interaction with numerous SH3 binding proteins simultaneously<sup>106</sup>. The F-BAR domain also mediates the interaction with lipid membranes where PACSIN1 is hypothesized to induce membrane curvature prior to vesicular fission by dynamin<sup>106</sup>. PACSIN1 also acts as an adaptor between N-WASP and dynamin, thus scaffolding vesicles to the actin cytoskeleton following endocytosis<sup>105,107</sup>. These results implicate PACSIN1 and huntingtin as critical components of the endocytic machinery. Huntingtin interacting protein 14 (HIP14) is a neuronal palmitoyl transferase (PAT) that catalyzes the addition of palmitate to a variety of protein substrates, including huntingtin<sup>108</sup>. Palmitoylation of huntingtin at cysteine 214

increases its hydrophobicity and promotes the association of huntingtin with membranes<sup>109,110</sup>. Furthermore, this modification is critical in modulating the sorting, targeting and trafficking of huntingtin between membrane compartments<sup>110</sup>.

Palmitoylation is critical to the trafficking of huntingtin to the Golgi apparatus. Expansion of the polyglutamine tract causes a decreased interaction between mutant huntingtin and HIP14, which in turn results in reduced palmitoylation of the mutant protein<sup>110</sup>. This decreased palmitoylation of mutant huntingtin promotes inclusion formation and increases neurotoxicity<sup>110</sup>. Therefore, huntingtin contributes to endocytosis through its interaction with proteins involved in vesicular transport, cytoskeletal reorganization and membrane dynamics. These interactions are critical to endocytic function since expression of mutant huntingtin leads to impaired endocytosis.

### **1.10.5 Role of Huntingtin in Synaptic Transmission**

Communication between neurons requires the regulation of proteins at the synapse. The huntingtin protein plays a critical role in synaptic activity by acting as a scaffold between components of the cytoskeleton and synaptic vesicle recycling. Post-synaptic density 95 (PSD-95) is a scaffolding protein that binds to *N*-methyl-D-aspartate (NMDA) and kainate receptors causing them to cluster at the post-synaptic membrane. This recruitment process governed by PSD-95 is critical in NMDA-mediated long term potentiation and depression<sup>111</sup>. The proline-rich region of huntingtin binds the SRC homology 3 (SH3) domain of PSD-95, leading to its sequestration and the resultant inhibition of NMDA activity<sup>112</sup>. The polyglutamine expansion impairs the interaction between huntingtin and PSD-95, leading to sensitization and increased activity of NMDA receptors<sup>112</sup>. Hyper-activation of NMDA receptors has been shown to induce excitotoxicity and contribute to neurodegeneration in HD. PACSIN1 can interact with NMDA receptor subunit 3A (NR3A, also known as GluN3A)-containing NMDA receptors via its SH3 domain and regulates the recycling of these receptors<sup>113</sup>. Mutant huntingtin can sequester PACSIN1, causing stores of immature NMDA receptors to be redirected to the synaptic membrane<sup>114</sup>. Elevating levels of the NR3A subunit at the synaptic membrane in the striatum of wild-type mice caused synaptic deficits comparable those observed in the full-length huntingtin, transgenic yeast artificial chromosome (YAC)128

mouse model, whereas deletion of NR3A reduced synapse loss, improved behavioural phenotypes and neurodegeneration in the YAC128 HD model<sup>114</sup>. Therefore, huntingtin influences synaptic activity through its interaction with PSD-95 and PACSIN1, where the polyglutamine expansion disrupts the proper localization, recycling and signalling of receptors at the synapse of neurons.

### **1.10.6 The Role of Huntingtin in the Cell Stress Response**

At the molecular level, the process of ageing causes cell stress and leads to the accumulation of damaged biomolecules over time. Many types of stress are utilized in cell biology to mimic the normal physiological stresses associated with ageing. Cells elicit a response to these chemical or physical stressors in order to re-establish cellular homeostasis. Heat shock for example, is a global cellular stress that causes the activation of chaperones, the induction of the unfolded protein response (UPR), a spike in calcium release from the ER and leads to a transient decrease in cellular ATP levels<sup>115</sup>.

Huntingtin has been shown in several studies to be a critical component of the cellular response to stress<sup>50</sup>. The N17 domain of huntingtin is a membrane association signal that targets the protein to the ER and other organelles<sup>50,73</sup>. In response to heat shock and other UPR-inducing cell stresses, N17 is phosphorylated at serine residues 13 and 16, causing huntingtin to dissociate from the ER and translocate to the nucleus<sup>57</sup>. Once in the nucleus, huntingtin localizes to stress-dependent, short rod-like structures known as cofilin-actin rods<sup>58</sup>. Cofilin is a small, actin-binding protein involved in the disassembly of actin filaments and is required for proper actin treadmilling<sup>116</sup>. Actin treadmilling is a constant dynamic process which is hypothesized to utilize up to 50% of the available cellular ATP under steady-state conditions<sup>117</sup>. Under cell stress conditions, treadmilling is halted and cofilin saturates actin filaments in an effort to free up ATP levels for more critical cellular processes<sup>117</sup>. The properties of cofilin-actin rod formation and clearance are strongly influenced by the polyglutamine expansion of huntingtin. Wild type huntingtin induces the formation of numerous, short rods in response to stress that are cleared rapidly once the insult is removed<sup>58</sup>. Conversely, mutant huntingtin induces the formation of only a few (1-3), longer rods that persist

following the removal of stress<sup>58</sup>. Notably, mutant cells that contain persistent rods have decreased survival relative to those where rods were cleared. Therefore, the persistence of mutant huntingtin rods and subsequent cell death suggests that these cells are unable to recover from stress. This likely stems from impaired energy metabolism observed in cell models of HD and HD patients.

Huntingtin has also been reported to translocate from the ER during stress and form huntingtin stress bodies (HSBs)<sup>118</sup>. These small, stress-dependent HSBs were shown to be unique from stress granules and processing bodies (P-bodies) that regulate mRNA translation and turnover, and were found to colocalize with early endosome markers<sup>118,119</sup>. The formation of HSBs is not affected by the polyglutamine length of huntingtin, however the clearance of the HSBs following the transient insult is significantly impaired by the mutant protein. Therefore, the formation of HSBs is hypothesized to be a cell stress response needed to conserve ATP levels that results in the transient arrest of early to late-endosome maturation<sup>118</sup>. The mechanism by which huntingtin HSBs arrest endosomal trafficking during cell stress events remains unknown. It is apparent, however, that huntingtin is integral to several cellular stress responses. Significantly, the recovery of cells to homeostatic conditions following insult is impaired upon expansion of the polyglutamine tract.

### 1.11 Pathogenic Threshold in HD

Since the discovery of the *Htt* gene in 1993, researchers have been trying to determine why CAG repeat lengths above 37 cause HD whereas repeat lengths below 36 do not. This has led researchers to query what is happening at the protein level at the disease-causing length of huntingtin. However, the large size of the huntingtin protein has made performing structural and functional assays a challenge. Therefore, most studies attempting to elucidate the pathogenic threshold of huntingtin have been conducted using amino-terminal fragments of the protein. Crystal structures of both wild type (Q17) and mutant (Q36) huntingtin exon1 fragments have been solved and have revealed a change in the structure of the polyglutamine tract just below the pathogenic threshold (36 repeats)<sup>76,77</sup>. However, the crystallization of mutant huntingtin was done on a small fragment of huntingtin and required the addition of 3 histidines in the polyglutamine tract to facilitate crystal formation. Furthermore, these assays were done *in vitro* with high concentrations of purified protein and in the absence of any interacting proteins. Due to the lack of reliable structural information available for the huntingtin protein, it remains unclear as to what is happening to the structure or conformation of the protein at the pathogenic threshold *in vivo*.

Huntingtin with polyglutamine lengths near the threshold are rarely used experimentally since they do not show robust phenotypes in cell culture or animal models of HD. Instead, researchers rely on extremely long polyglutamine lengths (>90) to study mutant huntingtin at the functional level. These extreme polyglutamine lengths are more in line with juvenile HD, which manifests as a clinically different disease process compared to adult-onset HD. Thus, *in vivo* research is moving away from elucidating the mechanism of huntingtin toxicity at the clinical pathogenic threshold in an effort to rapidly elicit phenotypes in animals to more closely recapitulate the symptoms and neurodegeneration seen late in HD.

A hallmark of HD is the presence of nuclear and cytoplasmic inclusions bodies within the brains of HD patients<sup>21</sup>. The formation of mutant huntingtin inclusions are strongly dependent on polyglutamine length, where huntingtin below the pathogenic threshold does not form inclusions. Therefore, it has been hypothesized that the

pathogenic length of polyglutamine exists to elicit the formation of toxic inclusion bodies responsible for HD pathology. However, inclusion formation may simply represent a functional consequence of polyglutamine expansion and not be the pathogenic cause of HD.

Examination of other CAG trinucleotide repeat disorders has revealed that the pathogenic threshold required for pathology in HD is not unique and is consistent with the threshold for SBMA, SCA-2 and SCA-7<sup>40</sup>. This has led researchers to postulate a common mechanism of pathology for these diseases. However, other CAG disorders require either more or fewer repeats to induce pathology, indicating that there is not a universal inherent toxicity associated with polyglutamine tracts at 37 repeats. The variance in the range of CAG repeats required for disease implicates the context of the polyglutamine tract within the specific disease protein.

### **1.12 Polyglutamine Flanking Sequences**

HD is one of 9 neurodegenerative diseases caused by the expansion of polyglutamine within a specific protein. Despite the common etiology, most of these diseases affect only a specific subset of neurons within the brain and they manifest as different spectra of symptoms<sup>40</sup>. Therefore, it has been hypothesized that the differential neurodegeneration patterns seen in the polyglutamine diseases can be attributed to the context of the polyglutamine tract within each respective disease protein<sup>120</sup>.

The polyglutamine tract of huntingtin is located at the amino-terminus of the protein where it is flanked at the proximal end (upstream) by the first 17 amino acids of huntingtin (N17) and at the distal end (downstream) by a proline-rich region. N17 is a highly conserved, amphipathic  $\alpha$ -helix that acts as a membrane association signal which reversibly targets huntingtin to the ER, late endosomes and autophagic vesicles<sup>50</sup>. The interaction of N17 with membranes does not require the aid of adaptor proteins, rather the N17  $\alpha$ -helix itself inserts into the membrane in a parallel orientation<sup>64</sup>. The association of N17 with the ER membrane is sensitive to stress, which causes the translocation of huntingtin into the nucleus<sup>50</sup>. The localization of mutant huntingtin to the

nucleus has been shown by many groups to increase the toxicity of the protein in cell culture models<sup>121-123</sup>.

N17 is subject to post-translational modifications by phosphorylation<sup>57,124</sup>, acetylation<sup>124</sup> and SUMOylation<sup>125</sup> that can affect the subcellular localization, protein-protein interactions, aggregation properties and toxicity of the mutant huntingtin protein. Mutant huntingtin has been shown to be hypo-phosphorylated at threonine 3 as well as serines 13 and 16 of N17<sup>57,124</sup>. The phospho-mimetic mutation of threonine 3 to an aspartic acid (T3D) was shown to reduce the neurodegeneration and promote aggregation of mutant huntingtin in a fly (*D. melanogaster*) model of HD. Introducing phospho-mimetic mutations to serines 13 and 16 (S13S16) by substitution with either glutamic (S13ES16E) or aspartic acids (S13DS16D) reduced the toxicity of mutant huntingtin fragments *in vitro* and *ex vivo*<sup>57,126</sup>. Furthermore, mice expressing full length, polyglutamine expanded huntingtin with phospho-mimetic mutations to S13 and 16 resulted in a normal phenotype with no detectable signs of HD pathology<sup>127</sup>. Promoting phosphorylation of S13S16 using ganglioside GM1 reduces mutant huntingtin toxicity and abrogates motor deficits in transgenic, full-length mutant huntingtin-expressing YAC128 HD mice<sup>128</sup>.

The N17 domain is also important in modulating the aggregation of mutant huntingtin into inclusion bodies. A single mutation of methionine 8 to a proline (M8P) abolishes the  $\alpha$ -helical structure of N17 by introducing a kink<sup>50</sup>. This mutant abrogates the formation of any huntingtin inclusions even with polyglutamine lengths exceeding 250 repeats<sup>50</sup>. Despite the M8P mutant preventing the formation of inclusions, this construct is more toxic than mutant huntingtin containing no N17 mutations and causes an increased localization of huntingtin to the nucleus<sup>50</sup>. Phospho-mimetic and alanine (S13AS16A) mutations of serines 13 and 16 on synthetic huntingtin fragments (amino acids 1-56 with 37 glutamines) have also been shown to modulate the aggregation of mutant huntingtin by affecting the rate of formation as well as the morphology of the inclusions *in vitro*<sup>127</sup>. Notably, the S13DS16D mutant slows the aggregation rate of mutant huntingtin, whereas the S13AS16A mutant accelerates the process relative to wild type N17 constructs<sup>127</sup>. Furthermore, electron microscopy (EM) of huntingtin

inclusions formed by S13DS16D and S13AS16A mutants reveals that they are morphologically different<sup>127</sup>. Therefore, these data strongly implicate the importance of the N17 domain on influencing the localization, toxicity and aggregation properties of the mutant huntingtin protein.

Directly flanking the polyglutamine tract on the distal end is a region known as the proline-rich region of huntingtin, composed of two pure poly-proline stretches (11 and 10 prolines, respectively) separated by a proline-glutamine rich intervening sequence. The proline-rich domain has been shown to mediate the aggregation and toxicity of mutant huntingtin through its protein-protein interactions. One such interactor is profilin, a small actin-binding protein that influences actin remodelling by sequestering G-actin monomers, acting as a nucleotide exchange factor and promoting the addition of monomeric actin subunits to a growing F-actin chain<sup>129</sup>. Profilin interacts directly with the poly-proline regions of the huntingtin proline-rich domain, and promoting this interaction reduces the aggregation and toxicity of mutant huntingtin<sup>130</sup> and plays a neuroprotective role in the cell<sup>80</sup>. Another interacting partner that is critical to mediating mutant huntingtin toxicity is the neuron-specific PACSIN1. PACSIN1 is required for synaptic vesicle recycling, endocytosis and cytoskeleton reorganization<sup>107,113,114,131</sup>. It interacts with a variety of poly-proline ligands, including huntingtin, by means of a carboxyl-terminus SH3 domain. As such, PACSIN1 binds the proline-glutamine rich intervening sequence within the proline-rich domain of huntingtin. PACSIN1 binds polyglutamine expanded huntingtin (Q44) with higher affinity than wild type huntingtin (Q18), leading to its sequestration and functional loss. Multiple PACSIN1 molecules can be bound to the intervening sequence at once, as it forms dimers and tetramers by means of a highly conserved F-BAR domain. Therefore, protein-protein interactions with the proline-rich region dramatically affect the aggregation and toxicity of the mutant huntingtin protein. As a proof-of-concept for the importance of proline-rich region, studies in *S. cerevisiae* have demonstrated that the removal of this domain from exon1 dramatically alters the number and morphology of huntingtin inclusions formed and increases the toxicity of mutant huntingtin<sup>120,132</sup>. The effect of the proline-rich region on the formation of mutant huntingtin inclusions has been attributed to the PPII structure of

this domain opposing the aggregation-prone  $\beta$ -sheet structure of the expanded polyglutamine tract<sup>78,79</sup>.

### 1.12.1 The Rusty Hinge Hypothesis

Many groups have hypothesized that the regions flanking the polyglutamine tract of huntingtin are critical in mediating the toxicity of the mutant protein<sup>78,79,120,132</sup>. Beyond N17 and the proline-rich region being able to independently mediate the toxicity of mutant huntingtin, it has been suggested that these two domains may be interacting together and working synergistically to affect toxicity. The Rusty Hinge hypothesis postulates that the normal polyglutamine tract of huntingtin is a flexible region that can act as a hinge that can facilitate the interaction of factors with N17 and downstream regions of the protein (Figure 1.3A)<sup>133</sup>. At the pathogenic threshold, the polyglutamine tract gains a rigid  $\beta$ -sheet structure that impairs flexibility of the hinge and thus the ability of N17 to interact with downstream regions of huntingtin (Figure 1.3B)<sup>133</sup>. As previously mentioned, huntingtin is a flexible, scaffolding protein that interacts with a large network of proteins and is involved in many cellular functions. Therefore, the flexibility of the polyglutamine tract may represent a necessary feature of huntingtin required for its molecular interactions and multiple cellular functions.

The concept that the polyglutamine tract of huntingtin behaves as a hinge between flanking sequences is supported by the crystal structure of huntingtin exon1 with 17 glutamines, which shows N17 in close spatial proximity with the proline-rich domain<sup>76</sup>. The crystal structures also demonstrate that the normal polyglutamine tract can switch between a number of conformations within the structure, including:  $\alpha$ -helix, extended loop and random coil - where this conformational flexibility is strongly influenced by the flanking sequences<sup>76</sup>. Replica-exchange molecular dynamic (REMD) simulations of huntingtin exon1 Q17 also show the polyglutamine tract behaving like a hinge allowing for the N17 domain to fold over and interact with the proline-rich region<sup>134</sup>. However, these structural studies of huntingtin exon1 were performed *in vitro*, in the absence of any other cellular factors. Therefore, it is not known whether the folding back of N17 onto the proline-rich domain and downstream regions of huntingtin requires other interactors in the cell.

PACSIN1, which has previously been shown to interact with the proline-rich region of huntingtin<sup>81</sup>, has also been found by our group to interact with the N17 domain using affinity chromatography and mass spectrometry (unpublished data). Therefore, PACSIN1 may represent a critical factor required for the interaction between N17 and the downstream proline-rich domain (Figure 1.3A). Another protein that may facilitate the interaction between flanking sequences to the polyglutamine tract of huntingtin is profilin, an actin-binding protein that interacts with the polyproline stretches of the proline-rich domain<sup>130</sup>. Filamentous actin, which has also been shown to interact with the first 14 residues of N17<sup>60</sup>, could interact with profilin bound to the proline-rich region and bring these domains together (Figure 1.3A). Notably, the interactions of PACSIN1 and profilin with huntingtin are dramatically altered when the polyglutamine tract is expanded. Therefore, the Rusty Hinge hypothesis supports the idea that protein context is important in mediating mutant huntingtin toxicity since the polyglutamine expansion-induced rigidity of the tract would alter protein-protein interaction dynamics of the flanking sequences. These altered interaction dynamics could translate to the differential vulnerability of specific neuronal subsets and different symptoms observed in other polyglutamine diseases.

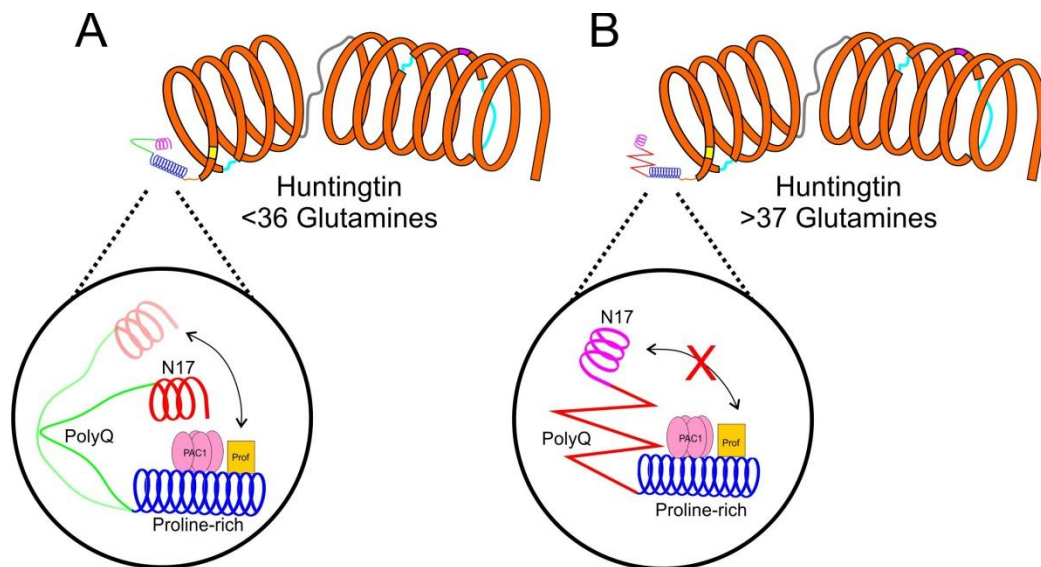


**Figure 1.3. The Rusty Hinge hypothesis.** (A) Wild type polyglutamine tract acts like a flexible region that allows N17 to freely fold back upon the proline-rich domain, and other downstream regions of huntingtin. (B) Flexibility of the polyglutamine tract is

impaired at lengths above the clinical pathogenic threshold for HD (>37 repeats).  
PAC1=PACSIN1, Prof=profilin.

### **1.13 Pathogenic Mechanisms in HD**

To date, research in the HD field has failed to identify the exact mechanism involved of mutant huntingtin-induced pathology. However, countless studies have provided evidence for the disruption of numerous cellular functions and pathways in the presence of polyglutamine-expanded huntingtin. Some of the mechanisms that have been proposed to contribute to HD pathology include excitotoxicity, mitochondrial dysfunction, transcriptional dysregulation, proteolytic cleavage of huntingtin and the formation of mutant huntingtin inclusion bodies. Many of these pathogenic mechanisms represent toxic gain-of-function(s) as a result of the polyglutamine expansion. It is postulated that the combination of these events accumulated over the life of an individual leads to the characteristic neuronal dysfunction and degeneration of HD.

#### **1.13.1 Excitotoxicity in HD**

HD results in the selective neurodegeneration of MSNs and cortical projection neurons of the brain. Excitotoxicity, a cytotoxic process that results from the excessive activation of receptors by excitatory neurotransmitters, has been proposed as a pathological mechanism to account for the selective neurodegeneration observed in HD. MSNs make up approximately 95% of the neuronal population within the striatum where they receive afferent inputs from glutamatergic projection neurons originating in the thalamus and cortex. Glutamate, the major excitatory neurotransmitter in the CNS, acts on NMDA,  $\alpha$ -amino-3-hydroxy-5-methyl-4-isoxazolepropionic acid (AMPA), kainate and several classes of metabotropic glutamate receptors. When NMDA receptors are activated by glutamate and the membrane potential has been sufficiently depolarized by the activation of surrounding AMPA receptors, NMDA receptors allow the influx of  $\text{Ca}^{2+}$  ions which activate downstream pathways required for gene transcription, neuronal survival and synaptic plasticity<sup>135</sup>. In the context of HD, it is hypothesized that aberrant over-activation of NMDA receptors on MSNs results from the increased release of glutamate from cortical afferents and the decreased uptake by surrounding glia.

Furthermore, it has also been postulated that hyper-sensitization of NMDA receptors to glutamate may also play a role in excitotoxicity and contribute to neurodegeneration. The resulting overload of calcium due to excessive activation of NMDA receptors can activate downstream pathways that lead to neuronal death<sup>136,137</sup>. These downstream pathways include the production of reactive oxygen species (ROS), the activation of caspases, mitochondrial dysfunction and impaired cellular calcium homeostasis<sup>138</sup>.

The first evidence supporting the role of excitotoxicity in HD pathogenesis stemmed from the observation that the intra-striatal injection of glutamate or NMDA receptor agonists quinolinic acid (QA) and kainic acid (KA) induced a striatal neurodegeneration phenotype in rodents similar to that seen in HD patient brains<sup>139,140</sup>. Furthermore, it was shown that glutamate receptors are lost and there is a decrease in the binding of glutamate to NMDA receptors in the striatum of *post mortem* pre- and early symptomatic HD patient brains<sup>141,142</sup>. This suggested that neurons containing NMDA receptors are lost early in the disease process.

The localization of NMDA receptors at the cortico-striatal synapse also plays a critical role in mediating NMDA receptor-mediated excitotoxicity. It has been shown that the activation of synaptic NMDA receptors promotes the transcription of neuro-protective genes whereas the activation of extra-synaptic NMDA receptors leads to the transcription of cell death genes<sup>143</sup>. Therefore, the balance between synaptic and extra-synaptic NMDA receptors is critical in determining the fate of a neuron. In the striatum of the YAC128 mouse model, expression and activity of extra-synaptic NMDA receptors are increased whereas levels of nuclear cyclic AMP receptor element-binding protein (CREB) are reduced relative to wild-type mice<sup>144</sup>. Treatment with memantine, a specific inhibitor of extra-synaptic NMDA receptors, was shown to reverse signalling deficits and improve the overall phenotype in the YAC128 HD mice.

NMDA-mediated excitotoxicity has also been linked to the energy deficiency observed in HD. Treatment of mice with 3-nitropropionic acid (3-NP), an irreversible inhibitor of mitochondrial complex II of the electron transport chain, results in the selective striatal degeneration and motor deficits similar to those seen in HD mice<sup>145</sup>. At the molecular level, 3-NP treatment results in the drop of cellular ATP levels and the

increase in ROS production<sup>146</sup>. Oxidative stress due to reactive oxygen species (ROS) causes damage to nucleic acids, proteins and lipids, activating downstream apoptotic pathways and leading to cell death. The study shows that 3-NP-induced ROS production occurs through secondary excitotoxicity via the activation of NMDA receptors, and that treatment of cultured neurons with glutamate receptor antagonist AP5 abolished the 3-NP-induced ROS increases and reduced mitochondrial fragmentation<sup>146</sup>. Therefore, inhibiting NMDA-mediated excitotoxicity represents a promising therapeutic target for the treatment HD, which may also have beneficial secondary effects on correcting mitochondrial dysfunction in the disease.

### 1.13.2 Mitochondrial Dysfunction in HD

Mitochondrial dysfunction, resulting in reduced energy production and impaired tolerance to calcium, has been implicated as a mechanism contributing to pathology in HD. Mutant huntingtin has been shown to interact directly with mitochondria, resulting in impaired motility along microtubules<sup>147,148</sup>. The proper distribution of mitochondria in neurons is highly regulated and required to maintain sufficient levels of ATP at specific sites of energy-dependent processes. Mutant huntingtin has also been shown to aberrantly interact with the mitochondrial fission GTPase dynamin-related protein-1 (DRP1), increasing its enzymatic activity and causing the fragmentation of mitochondria in HD patient fibroblasts and the YAC128 HD model<sup>52</sup>. The dynamic balance between mitochondrial fusion and fission is critical process required for their proper function and is impaired in many neurodegenerative diseases<sup>52</sup>. HD patient have an increased number of mitochondrial DNA mutations and deletions which affects mitochondrial respiration and overall energy metabolism<sup>149,150</sup>. Furthermore, cell extracts from HD knock-in mice show reduced levels of ATP and a decrease in the ratio of ATP:ADP in the early stages of disease<sup>147,151</sup>. Imaging studies of patient brains have further validated the energy metabolism defect in HD. The use of <sup>1</sup>H-nuclear magnetic resonance (<sup>1</sup>H-NMR) spectroscopy revealed decreased levels of N-acetylaspartate in the basal ganglia and thalamus of symptomatic HD patients<sup>152</sup>. N-acetylaspartate is synthesized from aspartic acid and acetyl-CoA in the mitochondria and is often used as a marker to reflect mitochondrial metabolic function. <sup>1</sup>H-NMR spectroscopy also

revealed increased levels of lactate in the basal ganglia and cortex of patient brains representing an increased glycolytic rate and the back-up of oxidative phosphorylation in HD<sup>152</sup>. As a corollary, positron emission tomography (PET) scans of HD patient brains show altered glucose metabolism early in the disease process<sup>153-155</sup>.

The uptake of calcium into mitochondria is a tightly regulated process that can influence energy production and can initiate cell death pathways. NMDA-mediated excitotoxicity in HD causes a drastic increase in intracellular calcium levels, which can in turn lead to an increase of calcium levels within the mitochondria and the ER<sup>156</sup>. The increase of mitochondrial calcium levels and presence of ROS can lead to secondary excitotoxicity and cause the mitochondrial transition permeability pore to open, releasing pro-apoptotic factors into the cell. Therefore, compounds that promote increased energy production and reduce oxidative stress represent promising therapeutic approaches to overcome the mitochondrial dysfunction that contributes to pathology in HD.

### 1.13.3 Altered Transcription in HD

Transcriptional dysregulation is an early feature of HD that precedes neurodegeneration and has been validated as a key mechanism in pathogenesis. Single gene and microarray studies have shown that the expression profiles of a large number of genes are dysregulated in HD patients<sup>157</sup>. Rather than being a consequence of the disease process, growing evidence suggests that huntingtin has a direct and essential role in regulation of gene expression. Brain-derived neurotrophic factor (BDNF) is a neuronal pro-survival factor that is produced in cortical neurons from which it is transported and secreted in the striatum. Levels of BDNF are decreased in the brains of HD patients<sup>158</sup>, which has been linked to a decrease of BDNF transcription in the cortex during disease progression<sup>159</sup>. Wild-type huntingtin has been shown to contribute to BDNF transcription in cultured cortical neurons and *in vivo* by inhibiting the repressor element 1 (RE1)/neuron restrictive silencer elements (NRSE) at the BDNF promoter<sup>159</sup>. More specifically, huntingtin promotes BDNF transcription by binding and sequestering RE1-silencing transcription factor (REST)/neuron restrictive silencing factor (NRSF) in the cytoplasm rendering it unable to translocate to the nucleus to form a repressor complex at the RE1/NRSE<sup>160</sup>. The mutant huntingtin protein, however,

cannot sequester REST/NRSF, allowing its aberrant entry into the nucleus and causing reduced transcription of the BDNF gene. This decreased neurotrophic support to striatal neurons can lead to death and has been proposed as a mechanism for the selective neurodegeneration in HD.

Huntingtin also interacts with specificity protein 1 (SP1), a transcription factor that binds G-C rich elements in specific promoters and activates transcription of SP1-regulated genes, including neurotransmitter receptors and growth factors<sup>161</sup>. The expansion of the huntingtin polyglutamine tract enhances its interaction with SP1, thus inhibiting the binding of nuclear SP1 to promoter sites to activate transcription<sup>161,162</sup>. Furthermore, mutant huntingtin can also alter transcription of specific genes through aberrant interactions CREB binding protein (CBP) and the TATA-box binding protein (TBP), both polyglutamine-containing proteins<sup>163,164</sup>. Mutant huntingtin has also been shown to repress transcription of the *PPARGC1A*, a gene that codes for the peroxisome proliferator-activated receptor-gamma coactivator 1 $\alpha$  (PGC-1 $\alpha$ ) transcription factor<sup>165</sup>. PGC-1 $\alpha$  is essential for the transcription of proteins required for proper mitochondrial function and energy metabolism.

Huntingtin can also modulate transcription of genes by interacting with different epigenetic modifiers. The polycomb repressive complex 2 (PRC2) has methyltransferase activity that primarily tri-methylates lysine 27 of histone 3 (H3K27), a marker of transcriptionally silent chromatin. Huntingtin has been shown to associate with PRC2 and facilitates methylation at the H3K27 mark *in vitro* and HD knock-in mice<sup>71</sup>. Full-length, polyglutamine expanded huntingtin protein increases the trimethylation at H3K27, leading to more transcriptional repression at specific promoters<sup>71</sup>. Huntingtin has also been shown to affect the trimethylation of lysine 4 of histone 3 (H3K4), a mark of transcriptionally active chromatin<sup>166</sup>. Mutant huntingtin causes a decrease in the trimethylation status of H3K4 at a number of promoters and results in diminished transcription of specific genes<sup>166</sup>. In general, histone acetylation causes a relaxation of the DNA and represents a more transcriptionally active form of chromatin. Mutant huntingtin is believed to alter the histone acetylation landscape by binding and sequestering histone acetyltransferase (HAT) enzymes leading to more

condensed chromatin and reduced transcription. Huntingtin can also bind directly to DNA *in vivo*, and chromatin immunoprecipitation (ChIP) studies have shown huntingtin binds to specific promoter regions in a polyglutamine-dependent manner<sup>61</sup>. Therefore, huntingtin can influence transcription indirectly, through interactions with transcription factors, regulators and epigenetic modifiers, or by directly interacting with DNA.

#### 1.13.4 Proteolytic Cleavage of Huntingtin in HD

The proteolytic cleavage of huntingtin has been shown by several groups to play a key role in the pathogenesis of HD. In 1996, the first transgenic mouse model of HD was generated expressing a small amino-terminal fragment (exon1) of human mutant huntingtin, known as the R6/2 mouse<sup>20</sup>. This mouse developed severe HD-like symptoms and demonstrated that a small piece of huntingtin, that included the mutant polyglutamine tract, was sufficient to recapitulate some of the clinical features of HD<sup>20</sup>. Subsequently, it was shown that full-length huntingtin is cleaved by the cysteine-aspartic acid protease 3 (caspase-3) to produce small amino-terminal fragments of huntingtin<sup>167</sup>. Mutant huntingtin was shown to be more susceptible than wild type to proteolytic cleavage by caspase-3<sup>167</sup>. These findings led to the formulation of the toxic fragment hypothesis which postulates that the proteolytic cleavage of mutant huntingtin generates toxic amino-terminal fragments that can accumulate and induce neurodegeneration. Notably, caspase-cleaved fragments of huntingtin have been detected in post mortem brains of HD and age-matched control patients<sup>168,169</sup>. To test the relationship between huntingtin cleavage and HD pathogenesis, YAC128 mice were generated expressing full-length, mutant huntingtin resistant to caspase-3 and caspase-6 cleavage<sup>170</sup>. The caspase-3 resistant mice developed pathology and behavioural deficits similar to the YAC128 mice, whereas the caspase-6 resistant mice maintained normal motor functions and showed no neurodegeneration<sup>170</sup>. This study demonstrated that cleavage of mutant huntingtin at residue 586 by caspase-6 is a key step required for neuronal dysfunction and neurodegeneration in HD. In addition to caspases, calpains<sup>85,168,171</sup> and aspartate proteases<sup>172</sup> have also been shown to cleave huntingtin at the amino-terminus of the protein. Furthermore, PTMs have been shown to be critical regulators of huntingtin cleavage. Phosphorylation of huntingtin at serine 421 by the

prosurvival kinase Akt (also known as protein kinase B)<sup>173</sup> reduces cleavage of mutant huntingtin by caspase-6<sup>174</sup>. Similarly, phosphorylation of huntingtin at serine 434 by cyclin-dependent kinase 5 (CDK5) has been shown to reduce cleavage by caspase-3 at residue 513<sup>175</sup>. Therefore, promoting phosphorylation at specific sites on huntingtin as a method of inhibiting proteolytic cleavage of mutant huntingtin may represent a promising therapeutic target for the treatment of HD.

### 1.13.5 Protein Aggregation in Neurodegenerative Diseases

Protein function and solubility often requires that proteins are folded into one or more specific conformations. The protein folding process is driven by the 'hydrophobic effect' whereby hydrophobic regions are buried into the interior of the protein and hydrophilic regions are exposed to the cellular environment on the exterior of the protein. Proteins that are not folded correctly by the cellular machinery or that spontaneously misfold can lead to the exposure of buried hydrophobic patches of the protein which can in turn associate with the hydrophobic regions of other misfolded proteins leading to aggregation and the formation of inclusion bodies. Therefore, protein aggregation refers to the self-association of partially folded or misfolded proteins into either intra- or extracellular inclusion structures.

The misfolding event that initiates protein aggregation can be caused by multiple molecular factors. Specific mutations can result in a protein that is more prone to misfolding, whereas other mutations can directly affect the overall structure of a protein which can promote the formation of inclusion bodies. This is clearly seen with polyglutamine proteins, where there is a strong correlation between the length of the CAG tract and the aggregation of the mutated protein<sup>176</sup>. Another factor that modulates the aggregation of a disease protein is post-translational modifications. Phosphorylation of polyglutamine expanded ataxin-1 (SCA1) at serine residue 776 has been shown to increase the aggregation of the mutant protein<sup>177</sup>. Similarly, hyper-phosphorylation of the microtubule-associated protein, tau, can promote self-assembly and lead to the formation of neurofibrillary tangles (NFTs) in AD<sup>178</sup> and other diseases collectively known as tauopathies. Proteolytic cleavage is also a factor that can affect the aggregation of disease proteins. In HD, the mutant huntingtin protein is proteolytically

cleaved, resulting in the formation of small-amino terminal fragments of huntingtin that aggregate more readily than the full-length protein<sup>83,167,169,170,179</sup>. The aberrant proteolytic cleavage of the amyloid precursor protein (APP) to amyloid- $\beta$  peptides leads to their aggregation and the formation of extracellular plaques in Alzheimer's disease (AD)<sup>180</sup>. Additional cellular mechanisms that cause protein misfolding and that can initiate the aggregation process include oxidation and nitration<sup>181</sup>.

Protein aggregates generally fall into two distinct categories termed either amyloid or amorphous. Amyloid inclusions are structured and are composed of misfolded protein oriented in a  $\beta$ -sheet conformation, whereas amorphous inclusions lack any defined structure or conformation. The process of protein aggregation follows complex pathways, likely with many intermediate species, and can thus form many types of amyloid or amorphous aggregates. The mechanism of protein aggregation for either type of inclusion, however, is initiated by protein misfolding resulting in an abnormal conformation of the monomeric protein. The misfolded protein can self-associate into several oligomeric intermediates prior to embarking on the divergent pathways that lead to the formation of either mature amyloid fibrils or amorphous aggregates.

Proteins aggregating into inclusion bodies is a characteristic feature of over half of the 25 defined neurodegenerative diseases, including Alzheimer's disease (AD), Parkinson's disease (PD), polyglutamine diseases, amyotrophic lateral sclerosis (ALS) and prion diseases, to name a few. Each of these diseases involves the aggregation of different disease-specific proteins, which share no functional relation. AD involves the characteristic formation of both extracellular plaques composed of predominantly amyloid- $\beta$  peptides<sup>182</sup> and intracellular neurofibrillary tangles (NFTs) made up of tau<sup>183</sup>. Misfolding of the  $\alpha$ -synuclein protein leads to the formation of insoluble amyloid fibrils, known as Lewy bodies, which are characteristic of PD, dementia with Lewy bodies and other synucleopathies<sup>184</sup>. Furthermore, in some forms of familial ALS, superoxide dismutase 1 (SOD1) is mutated causing it to misfold and aggregate<sup>185</sup>. The classic amyloid hypothesis describes the accumulation of misfolded amyloid- $\beta$  into plaques as being the primary pathogenic mechanism in AD<sup>186,187</sup>. This seminal hypothesis has

since been revised to explain a common pathogenic mechanism in all neurodegenerative diseases in which aggregates form<sup>188</sup>. Therefore, many of the pharmacologic treatment approaches being tested in these diseases are aimed at inhibiting the aggregation of the disease protein.

### 1.13.6 Inclusion Bodies in HD

The presence neuronal inclusions in HD were initially described in transgenic HD mice expressing exon1 of huntingtin<sup>189</sup> and subsequently in HD patients<sup>21</sup>. Examination of *post mortem* HD patient brain slices revealed numerous inclusion bodies within MSNs and cortical neurons that contained amino-terminal huntingtin fragments and stained positive for ubiquitin<sup>21,176</sup>. These seminal studies demonstrated a strong correlation between CAG repeat length and the prevalence of inclusion bodies, where brains of juvenile HD patients showed a more extreme aggregate phenotype than those of adult patients<sup>176</sup>.

Prior to being identified in HD-specific brain regions of mouse models and human patients, higher-order mutant huntingtin aggregate structures were predicted by Max Perutz<sup>190</sup>. He hypothesized that pure polyglutamine with 37 or more repeats could form an energetically stable  $\beta$ -sheet structure that acquires a toxic function<sup>191</sup>. Furthermore, he proposed that  $\beta$ -sheets of poly-L-glutamine may be linked together to form 'polar zippers' via hydrogen bonds between the main chain glutamine and the side chain amides of huntingtin<sup>192</sup>. The arrangement of anti-parallel  $\beta$ -sheets of polyglutamine would result in water molecule displacement, rendering the protein insoluble and leading to its aggregation. Perutz also predicted that the interaction between these polar zippers grows stronger with increasing glutamine tract lengths, making longer polyglutamine tracts more prone to aggregating into inclusion bodies. As a corollary, *in vitro* studies using small fragments of huntingtin have shown that there is a conformational transition to the  $\beta$ -sheet conformation of polyglutamine expanded monomers prior to self-associating into  $\beta$ -sheet containing amyloid inclusions<sup>193</sup>.

Despite being a hallmark feature of HD, the role of huntingtin inclusion bodies in HD pathology still remains a contentious issue in the field. Some researchers have

postulated that these inclusions are inherently toxic and are responsible for the selective neurodegeneration observed in HD<sup>21,189,194</sup>. Conversely, other groups have hypothesized that inclusions are neuro-protective, where the monomeric and oligomeric forms of mutant huntingtin act as the toxic species<sup>121,195</sup>.

Several mechanisms have been postulated to explain the toxicity of mutant huntingtin aggregates in HD. One such mechanism proposes that the formation of inclusion bodies in HD causes the recruitment and sequestration of other polyglutamine-containing and non-polyglutamine-containing cellular proteins<sup>196,197</sup>. Multiple studies have demonstrated that mutant huntingtin inclusions can contain transcription factors, components of the cytoskeleton, proteins involved in degradation as well as molecular chaperones<sup>197-199</sup>. Specifically, sequestration of proteins within mutant huntingtin inclusions has been shown to cause the functional depletion of transcription factors CBP, TATA-box binding protein (TBP), TBP-associated factor (TAFII130) and SP1<sup>162,163,200-202</sup>. The functional loss of these factors within huntingtin inclusions has been hypothesized to contribute to the transcriptional dysregulation observed in HD. Mutant huntingtin inclusions have also been shown to induce toxicity through the disruption of axonal transport in neurons by physically occluding the trafficking of essential factors<sup>148,203</sup>. Furthermore, mutant huntingtin inclusions have been shown to impair the ubiquitin-dependent proteolysis of misfolded proteins by the proteasome system<sup>194,204</sup>.

The toxic fragment hypothesis postulates that the toxic gain-of-function associated with the expansion of the polyglutamine tract involves the accumulation of amino-terminal fragments of huntingtin into inclusion bodies as the cause of neurodegeneration in HD. This hypothesis was formulated based on the observations that HD mice expressing exon1 of mutant huntingtin developed behavioural, neuropathological and inclusion phenotypes similar to that seen in human HD patients<sup>20,189</sup> and that full-length, mutant huntingtin could be cleaved to produce small, amino-terminal fragments<sup>167</sup>. The initial evidence supporting the toxicity of inclusions in HD was based on studies in cultured cells which showed that inclusion formation by truncated, amino-terminal fragments of mutant huntingtin increased the susceptibility of

cells to death<sup>122,123,205</sup>. Notably, there is a strong correlation between the threshold required for inclusion formation *in vitro* and the threshold for developing HD in humans<sup>200,205</sup>. These findings have led researchers to conclude that the formation of inclusion bodies must be integral to HD pathogenesis.

In a seminal study, immunohistochemistry (IHC) analysis of *post mortem* HD brains revealed positive labelling of neuronal inclusions using an antibody raised to an epitope at the extreme amino-terminus of huntingtin (a.a. 1-11) but not with an antibody against an internal site (a.a. 585-725)<sup>21</sup>. This suggested that the inclusions found in HD patient brains are composed of small, amino-terminal fragments of huntingtin or that internal epitopes of huntingtin are occluded during the aggregation process. The proteolytic cleavage of mutant huntingtin by a variety of caspases and calpains has been shown to generate small amino-terminal fragments both *in vitro* and *in vivo*<sup>83,85,167,168</sup>. Additionally, multiple *in vitro* studies have demonstrated that smaller, amino-terminal fragments are more prone to aggregate and the inclusions are more toxic than those formed by longer huntingtin fragments<sup>122</sup>. Therefore, the length of mutant huntingtin affects the properties of inclusion formation and the toxicity of the inclusions. In HD patient brains, inclusion bodies were identified in both the nucleus and the cytoplasm of select neurons<sup>21</sup>. However, *in vitro* evidence suggests that the sub-cellular localization of the inclusion is critical to inducing toxicity. In a proof-of-concept study, inclusions formed using polyglutamine peptides targeted to the cytoplasm of cells in culture had little effect on cellular viability. Conversely, targeting the inclusions to the nucleus using an exogenous nuclear localization signal (NLS) led to dramatic cell death<sup>206</sup>. Therefore, these findings implicate the length of mutant huntingtin and the subcellular localization of inclusions as key determinants of toxicity in HD.

The first study to suggest that the formation of inclusion bodies in HD may not be toxic was done in cultured primary neurons expressing fragments of mutant huntingtin<sup>121</sup>. They demonstrated that the formation of inclusions did not correlate with neurodegeneration and that neurons without inclusions showed a higher frequency of death relative to those with inclusions<sup>121</sup>. These seminal findings were validated by a subsequent study which utilized an automated microscope system to track individual

neurons temporally following the expression of mutant huntingtin fragments with various polyglutamine expansion lengths. They discovered that the formation of inclusion bodies by mutant huntingtin improved the survival of neurons, and that the diffuse, soluble species of mutant huntingtin caused neuron death. Moreover, inclusion formation reduced the level of diffuse mutant huntingtin over time via recruitment and sequestration. This led to the hypothesis that the formation of inclusion bodies may be a coping mechanism to accumulate and sequester the toxic species of mutant huntingtin. In another study, researchers serendipitously generated a 'short-stop' HD mouse expressing a truncated fragment (exons 1+2) of huntingtin with 128 glutamines<sup>207</sup>. Notably, the 'short-stop' mice showed no behavioural abnormalities or neurodegeneration despite the widespread presence of inclusions<sup>207</sup>. This study provided *in vivo* evidence that the presence of huntingtin inclusions in the brain do not necessarily correlate with the development of disease and neurodegeneration in HD models.

Perhaps the most convincing evidence against the toxic fragment hypothesis came from the structural analysis of the N17 domain of huntingtin<sup>50</sup>. Mutating methionine 8 to a proline (M8P) in the context of a 1-586 fragment of mutant huntingtin resulted in a construct that was unable to aggregate and form inclusion bodies, even with polyglutamine lengths exceeding 250<sup>50</sup>. Notably, this M8P mutation resulted in the most toxic construct of huntingtin tested despite its inability of this mutant huntingtin fragment to form inclusion bodies. This work has implicated the flanking sequences to the polyglutamine tract as being critical modulator of inclusion formation and toxicity of the mutant protein.

Taken together, these studies provide evidence that inclusions formed by mutant huntingtin can be toxic and protective to the cell. This discrepancy may be due to the different mutant huntingtin fragment lengths used to induce aggregation in these studies, or the models and assays used to measure toxicity. It is also possible that the conflicting observations regarding inclusion toxicity may be the result of mutant huntingtin having the capacity to form multiple inclusion species of varying toxicity. Depending on the size of the huntingtin fragment that forms the inclusion, the sub-

cellular localization of the inclusion, the cell type and factors sequestered within them, it is possible that mutant huntingtin can form both toxic and protective inclusion.

Therefore, further studies are required to elucidate the controversy surrounding the role of inclusions in HD and to investigate whether mutant huntingtin can form different inclusion types.

## 1.14 Therapeutic Efforts in HD

HD is a progressive neurodegenerative disease for which there are no disease-modifying therapeutics, instead, treatment efforts have been limited to managing the symptoms of HD. HD manifests as a triad of motor, psychiatric and cognitive disorders with a spectrum of signs and symptoms. The age-of-onset of symptoms in HD is strongly, but not entirely, influenced by the length of the CAG tract in the *Htt* gene. Furthermore, which symptoms appear first and have a more dominant effect on overall functional ability can differ greatly between affected individuals. Therefore, symptomatic treatment must be personalized to each individual patient. Currently, symptoms of HD are managed with modest efficacy through pharmacological intervention, rehabilitation and support.

Most clinical trials for HD rely on enrolling patients that are already symptomatic. This is due in large part to the lack of reliable biomarkers available to track early progression of the disease and the need to use symptom-based clinical endpoints to assess drug efficacy. Therefore, a standardized method was developed to measure the overall condition of a patient. The Unified Huntington's Disease Rating Scale (UHDRS) assesses clinical performance in four domains of HD: motor function, cognitive function, psychiatric abnormalities and overall functional ability<sup>208</sup>. The UHDRS provides a method of tracking clinical features of HD over time and is consistently used in clinical trials to measure drug efficacy.

### 1.14.1 Pharmacologic Management of Symptoms in HD

To date, drugs to manage the motor symptoms of HD have been limited to treating the chorea. Treatment is typically initiated when choreic movements become bothersome or begin to affect the overall functional ability of the individual. Tetrabenazine is the only United States Food and Drug Administration (FDA) approved drug shown to significantly reduce choreic movements associated with HD<sup>209</sup>. It functions by promoting the degradation of monoamine neurotransmitters, namely dopamine, in the brain. In a double-blind, placebo controlled, randomized trial, treatment of HD patients with tetrabenazine resulted in a significant reduction in chorea from

baseline values as measured by the UHDRS<sup>209</sup>. Treatment with tetrabenazine carries the risk of causing dyskinesia, parkinsonism and depression side effects in patients. Pridopidine (also known as ACR-16 or Huntexil) is a dopamine-stabilizing compound that helps counter the effects of excessive or reduced dopamine transmission in the brain and is intended for use in reducing the involuntary movements and chorea associated with HD. Two independent randomized, double-blind, placebo controlled clinical trials demonstrated that treatment with pridopidine improved UHDRS scores in HD patients, but failed to meet the established clinical endpoints in both studies<sup>210,211</sup>. An additional clinical trial showing efficacy of pridopidine on improving motor function in HD is required prior to FDA and European Medicines Agency (EMA) approval.

The psychiatric symptoms associated with HD are often the most distressing aspect of the disease to individuals and family members affected by the disease. Neuroleptics (or anti-psychotics) can be used in a multi-purpose capacity to reduce choreic movements and associated psychiatric disorders, and are often used in conjunction with antidepressants. Olanzapine is a neuroleptic drug that helps to manage the psychiatric symptoms of HD. In an open-label trial, individuals treated with olanzapine showed a significant improvement in the UHDRS score<sup>212</sup>. The drug was also shown to improve irritability, depression, anxiety and compulsive behaviour in an independent clinical trial<sup>213</sup>. Haloperidol, also a neuroleptic, has been shown to improve chorea over baseline values with efficacy comparable to tetrabenazine<sup>214</sup> but also helps to improve aggression, delusions and hallucinations associated with HD. Additional neuroleptics used to manage psychological symptoms of HD include valproic acid, risperidone, clonazepam and quetiapine. Neuroleptics are often used in concert with antidepressants to help treat the anxiety and depression associated with HD. Venlafaxine XR, a serotonin and noradrenaline reuptake inhibitor (SNRI) class of antidepressant, was shown to improve depression over baseline values in patients with HD experiencing depression<sup>215</sup>. Additionally, a wide range of selective serotonin-reuptake inhibitors (SSRIs), SNRIs, tricyclics and other classes of antidepressants have also been shown to be effective in managing the depression associated with HD. The choice of which neuroleptic or antidepressant is made based on the side-effects, the

patient response to the drug and the beneficial secondary effects of the drug on other symptoms<sup>216</sup>.

Treatment options for the cognitive symptoms of HD are aimed to improve daily functioning and quality of life. In a randomized, open-label clinical trial, rivastigmine, an acetylcholinesterase inhibitor, was shown to improve cognitive function and slow motor dysfunction in patients with HD relative to the untreated control group<sup>217,218</sup>. This compound has also been used to treat mild to moderate dementia in AD<sup>219</sup> and PD<sup>220</sup>. Other drugs such as methylphenidate have also been used to improve overall executive function in HD<sup>221</sup>.

#### **1.14.2 A Need for Disease-Modifying Drugs for HD**

Unlike other neurodegenerative diseases such as AD and PD which are predominantly idiopathic, all HD cases are caused by a CAG expansion within the *Htt* gene<sup>7</sup>. Therefore, predictive genetic testing for HD allows for a diagnosis to be made decades before the onset of symptoms and neurodegeneration, thus providing an opportunity to intervene early and modify the course of the disease. Therapeutic intervention prior to the onset of symptoms in HD likely represents the optimal window for disease modifying drugs. However, preventive clinical trials require reliable outcome measures to accurately track the progression of the disease in the absence of clinical symptoms. To date, there are no biomarkers that can reliably and accurately predict the course of HD. This has led to a number of multi-national, observational studies to examine clinical and biological markers of disease progression in gene-positive, pre-symptomatic and early stage-HD individuals<sup>222,223</sup>. Current studies being conducted in North America and Europe are collecting a variety of biological samples to identify biomarkers that will better reflect physiological changes that occur early in the disease.

#### **1.14.3 Overview of Disease-Modifying Therapies in HD**

Identifying compounds that can protect neurons from degeneration could have enormous benefits on slowing the progression of HD. Some of the approaches postulated to improve neuronal survival in HD patients have been to neutralize NMDA-induced excitotoxicity, decrease oxidative stress, increase the availability of cellular

ATP, enhance transcription of neuro-protective genes, inhibit mutant huntingtin cleavage, prevent inclusion formation of mutant huntingtin, inhibit transglutaminase type 2 (TG2) and target the huntingtin protein directly.

Excitotoxicity has been proposed by a number of groups to be a key pathogenic mechanism contributing to the degeneration of neurons in HD. Therefore, blocking activation of extra-synaptic NMDA receptors represents a potential therapeutic target to protect neurons against toxicity and death in HD. Memantine, an extrasynaptic NMDA receptor antagonist, has been shown by several groups to prevent neuronal excitotoxicity in cell culture and animal models of HD<sup>144,224,225</sup>. However, a pilot study to test the clinical efficacy of memantine in HD only showed modest efficacy on treating motor symptoms and had no effects on slowing the progression of the disease.

Mitochondrial dysfunction causes energy defects and oxidative stress that have been implicated as pathogenic mechanisms associated with neurodegeneration in HD. Therefore, compounds that increase the availability of intracellular ATP and act as antioxidants may play a neuroprotective role in HD. Creatine, a powerful mitochondrial antioxidant which is also involved in maintaining the availability of cellular ATP, has been shown to have beneficial effects in animal models of HD<sup>226</sup>. However, when tested in a 2-year pilot study, treatment of patients with high-doses of creatine was shown to be ineffective<sup>227</sup>. Despite this failure, a large phase III clinical trial to further test the efficacy of creatine is currently being conducted by the Huntington Study Group (HSG). Coenzyme Q10 (CoQ10), also an antioxidant that increases the availability of cellular ATP, has been shown to improve survival and motor function in the R6/2 transgenic model of HD<sup>228</sup>. However, a subsequent study in the same mouse model was unable to reproduce the beneficial effects of CoQ10<sup>229</sup>. A clinical trial testing the efficacy of CoQ10 as a neuroprotective agent in HD failed to show significant therapeutic effects above baseline values<sup>230</sup>. Despite the previous failures, high dose CoQ10 is currently being tested in a large, randomized, double-blind phase III clinical trial by the HSG aimed to determine if CoQ10 has any therapeutic value in the treatment of HD (2Care trial, results unpublished). Notably, in 2009, the HSG received funding to assay the

safety and tolerability of CoQ10 in the first clinical trial using gene-positive, presymptomatic HD patients (PREQUEL trial, results unpublished).

Transcriptional dysfunction is another mechanism proposed to contribute to pathogenesis in HD. Inhibiting histone deacetylases (HDACs) renders chromatin more relaxed which is associated with increased levels of transcription. Therefore, HDAC inhibitors could represent a class of drugs that could promote the transcription of pro-survival genes and protect neurons from death in HD. In a seminal study, suberoylanilide hydroxamic acid (SAHA), an HDAC inhibitor, was found to improve the motor phenotype and increase histone acetylation in the brains of R6/2 transgenic mice<sup>231</sup>. Sirtuins (SIRT), a family of proteins that belong to class III HDACs, are critical in influencing transcription, inflammation and apoptosis. Class I SIRT (SIRT1-3) act as nicotinamide adenine dinucleotide (NAD<sup>+</sup>) -dependent deacetylases on a number of histone and non-histone substrates. EX-527 (also known as SEN0014196) was discovered in a high-throughput screen to be a potent and selective inhibitor of SIRT1<sup>232</sup>. EX-527/SEN0014196, which received orphan drug status in 2009, is currently being tested in a phase I clinical trial for the treatment of HD. Conversely, promoting the activation of SIRT1 using resveratrol (SRT501-M) was shown to improve longevity and survival of transgenic HD mice<sup>233</sup>. The beneficial effects of SIRT1 activation in this study were hypothesized to be due to the deacetylation of PGC-1 $\alpha$ <sup>233</sup>, which can activate the PGC-1 $\alpha$  signalling pathway and increase mitochondrial biogenesis<sup>234</sup>. Inhibition of SIRT2 by the compound AK-7 *in vivo* improved motor functions, extended survival, reduced neurodegeneration and lowered levels of mutant huntingtin inclusions in two mouse models of HD<sup>235</sup>.

Cleavage of mutant huntingtin by a variety of cellular proteases (caspases, calpains and aspartic proteases) leading to the production of toxic, amino-terminal fragments has been proposed as a key initiating pathogenic mechanism in HD. Therefore, targeting these proteases pharmacologically has been proposed to prevent neuronal dysfunction and subsequent neurodegeneration in HD. This approach is based on the finding that HD mice resistant to cleavage at residue 586 by caspase-6 do not develop HD-like symptoms and are protected against stress-induced neurotoxicity<sup>170</sup>.

Minocycline, a broad-spectrum tetracycline derivative, has been shown to improve the disease phenotype in R6/2 HD mice by inhibiting caspase-1 and 3<sup>236</sup>. However, in a double-blind, placebo-controlled phase II clinical trial conducted by the HSG, minocycline had no significant effect on delaying the onset of symptoms<sup>237</sup>. Subsequent studies have used high-throughput screening in HD cell models to identify neuroprotective compounds (R1-R4) that act by inhibiting specific caspases<sup>238</sup>. Furthermore, a group of sulfonamide isatin acceptors have been developed that show specificity for inhibiting caspase-6 compared to caspase-3<sup>239</sup>. These compounds need to be tested in preclinical models of HD to assess their efficacy *in vivo* prior to being tested in humans. However, since caspases are critical for many cellular functions, inhibition of specific caspases may not represent a feasible therapeutic target and could lead to significant adverse effects. Therefore, recent efforts have focused on identifying synthetic molecules that bind to mutant huntingtin at specific residues to prevent the cleavage by caspases.

The formation of mutant huntingtin inclusion bodies has also been proposed as a pathogenic mechanism contributing to HD. Since the discovery of nuclear and cytoplasmic inclusion bodies within patient brains, significant efforts have been invested into identifying compounds that reduce or inhibit the aggregation of mutant huntingtin. Riluzole is one of several benzothiazole derivatives that were identified in an *in vitro* screen to inhibit the aggregation of mutant huntingtin<sup>240</sup>. In addition to preventing aggregation, riluzole also protects neurons against excitotoxicity by indirectly reducing activation of glutamate receptors in the CNS<sup>241</sup>. In a preclinical trial for HD, riluzole was shown to alter nuclear inclusion properties, reduce neuronal loss and improve survival in R6/2 HD mice<sup>242</sup>. However, in a randomized, double-blind clinical trial, riluzole was not found to have any neuroprotective or beneficial symptomatic effects in the treatment of HD<sup>243</sup>. C2-8 is a compound that was identified in a high-throughput screen to reduce the aggregation of mutant huntingtin in mammalian cell models of HD and in brain slices of HD mice<sup>244</sup>. In a subsequent study, R6/2 HD mice treated with the C2-8 compound displayed an improved motor phenotype, reduced neurodegeneration and decreased size of huntingtin inclusions relative to untreated R6/2 mice<sup>245</sup>. The benefits of C2-8 observed in a preclinical model of HD have made this compound (and other derivatives)

a promising therapeutic lead to enter clinical trials for HD. Other compounds such as Congo red and trehalose have also been found to reduce the aggregation of mutant huntingtin into inclusion bodies<sup>246,247</sup>. The caveat of huntingtin aggregation inhibitors is that they do not prevent the initial misfolding of mutant huntingtin. Furthermore, many lines of evidence implicate huntingtin inclusions as being benign or even neuroprotective, where inhibiting their formation could cause toxicity and the neuronal death observed in HD. This has led to studies attempting to identify compounds that promote the aggregation of mutant huntingtin into inclusion bodies. B2 is a compound that was identified in a high-throughput screen to promote the aggregation of small amino-terminal fragments of mutant huntingtin in cell culture models of HD<sup>248,249</sup>. This compound was found to reduce cellular toxicity by preventing mutant huntingtin-associated proteasome dysfunction<sup>249</sup>. These results are in direct conflict with the toxic fragment hypothesis and may suggest that some inclusions may be toxic whereas others may have a protective role. Thus, assays that can identify different species of inclusions based structural or biophysical properties could represent a useful tool in efforts to identify compounds that inhibit/promote specific inclusion types.

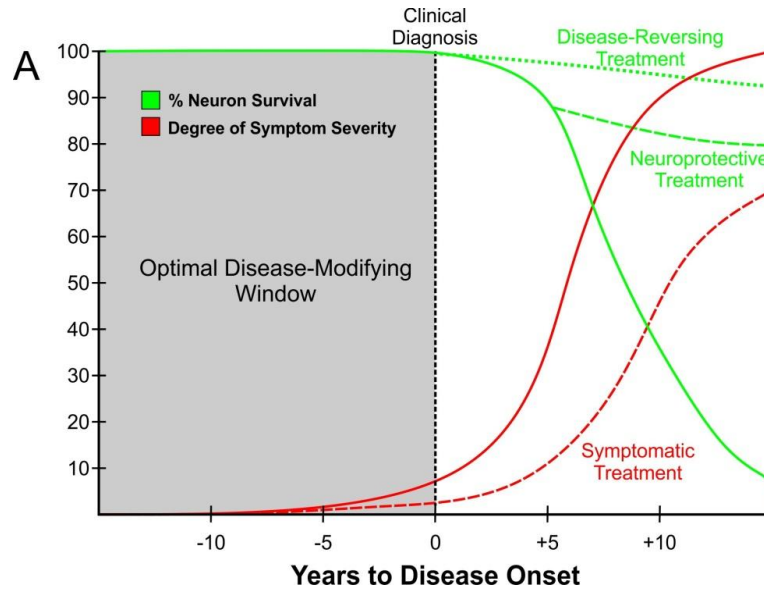


**Figure 1.4. Comparing symptomatic and disease-modifying treatments in HD. (A)** Representation of the neurodegeneration (solid green line) and severity of symptoms (solid red line) during the progression of typical adult-onset HD. Dashed red line represents the effect of available symptomatic treatment options on the severity of symptoms in HD. Grey box identifies the decades prior to clinical diagnosis as being the optimal window for treatments options that will modify the course of the disease. Dashed green line represents the prospective effect of neuroprotective treatments on neurodegeneration in HD. Dotted green line represents the prospective effect of disease-reversing treatments on neurodegeneration in HD.

#### 1.14.4 Targeting Transglutaminase type 2 (TG2) as a Therapy for HD

TG2 is a multi-functional enzyme that can catalyze the calcium-dependent transamidation (covalent cross-linking) between the  $\gamma$ -carboxamide group of a peptide bound glutamine and the primary  $\epsilon$ -amine group of a peptide bound lysine residue<sup>250</sup>. In addition to cross-linking, TG2 can catalyze other calcium-dependent protein modifications including deamidation and the incorporation of free amines<sup>251</sup>. Furthermore, TG2 can also bind and hydrolyze GTP, behaving as a G-protein that couples adrenergic, thromboxane and oxytocin receptors to the phospholipase C signalling (PLC) pathway<sup>252,253</sup>. These cellular roles of TG2 are mutually exclusive: GDP/GTP bound TG2 cannot catalyze calcium-dependent reactions and vice versa. This reciprocal activation of TG2 by calcium and guanosine nucleotides is mediated by a large conformational change between its enzymatically active states<sup>254</sup>. TG2 is ubiquitously expressed in body and is the predominant TG found in the brain. It has been proposed to have a role in cell death since its expression is upregulated in cells undergoing apoptosis<sup>255</sup>. However, it has been hypothesized that TG2 can play both a pro- and anti-apoptotic role depending on the cell type, the type of cell stress, as well as the subcellular localization and conformation of the protein<sup>256-258</sup>.

Notably, up-regulation of TG2 cross-linking activity has been implicated in many neurodegenerative diseases<sup>259,260</sup>, cancer<sup>261</sup>, atherosclerosis<sup>262</sup>, cataract formation<sup>263</sup> and celiac disease<sup>264,265</sup>. In neurodegenerative diseases, the pathological role of TG2 was initially hypothesized to be through the aberrant covalent cross-linking of specific disease proteins leading to the formation of toxic inclusions. This has been reported for amyloid- $\beta$  plaques and neurofibrillary tangles in AD<sup>104,105</sup>, Lewy bodies in PD<sup>266,267</sup> as well as huntingtin inclusions in HD<sup>268-271</sup>. Further investigation into the role of TG2 in HD has revealed that aberrant cross-linking of huntingtin into aggregates may not contribute to cell death<sup>272</sup>. The cross between a TG2 knockout mouse (-/-) and a HD transgenic mouse model (R6/2) improved survival, reduced neuronal death yet resulted in the significant increase of mutant huntingtin inclusions<sup>273</sup>. Increased levels and activity of TG2 have been reported in the brains and cerebrospinal fluid (CSF) of HD patients<sup>274,275</sup>, where dysregulated cross-linking activity has been proposed to

contribute to striatal neuron loss. This dysregulation of TG2 cross-linking activity likely stems from the altered calcium signalling observed in HD models<sup>276</sup> and patients. Therefore, inhibitors of TG2 cross-linking activity have been tested for their efficacy in treating HD.

Cystamine, and its reduced form cysteamine, are potent, competitive amine inhibitors of transglutaminase activity. Treatment with cystamine has been shown to improve survival and behaviour, as well as prevent neuronal loss in the small-fragment R6/2<sup>277,278</sup> and the full length YAC128 mouse models of HD<sup>279</sup>. However, treatment with cystamine was subsequently shown to have similar beneficial effects on survival and motor behaviour in R6/2 mouse with the normal TG2 complement compared to the R6/2 without TG2<sup>280</sup>. This suggests that the therapeutic effects of cystamine in HD mouse models are not primarily due to its ability to inhibit transglutaminase activity. Instead, evidence suggests that cystamine may have other beneficial effects *in vivo* by inhibiting caspase-3 activation<sup>281</sup>, increasing levels of antioxidants<sup>282</sup>, promoting the expression of heat shock proteins<sup>278</sup> and by increasing BDNF levels in the brain<sup>283</sup>. The reduced form of cystamine, cysteamine, is an FDA approved drug for the treatment of cystinosis in children and adults. Cysteamine is currently being tested in a randomized, controlled, double-blind phase 2/3 clinical trial for the treatment of HD. A caveat of cystamine/cysteamine is that they are not specific to inhibiting TG2 and inhibit other members of the TG family, which could cause adverse effects. This has led to the discovery of several selective, covalent inhibitors of TG2 for the treatment of HD<sup>284</sup>. There is also a need to synthesize competitive, reversible inhibitors of TG2 that block access of substrates to the active site without covalently modifying the enzyme. These compounds can reversibly inhibit TG2 cross-linking activity without affecting the other cellular roles of the enzyme<sup>285</sup>. Therefore, with the right properties, inhibitors of TG2 may represent a promising therapy for the treatment of HD and many other diseases. However, since the activity, conformation and subcellular localization of TG2 are critical to influencing cell fate, assays need to be developed to gain insight into how inhibitors are affecting these factors in biological systems.

### 1.14.5 Targeting Huntingtin as a Therapy for HD

The huntingtin protein is widely regarded as the best therapeutic target for the treatment of HD. Significant efforts have been invested into testing the safety, tolerability and efficacy of decreasing huntingtin levels *in vivo* as a treatment for HD. Reducing huntingtin levels can be achieved through specifically silencing the disease-causing mutant allele or by non-allele specific silencing of total huntingtin expression. HD is caused by a CAG expansion within the *Htt* gene that results in a toxic gain-of-function in the huntingtin protein. Therefore, silencing only mutant huntingtin expression could be a direct and effective therapy for the treatment of HD. Previous studies have shown that post-natal inactivation of the mutant *Htt* transgene in conditional HD mice can reverse neuropathology and motor dysfunctions<sup>286</sup>. However, targeting the expanded CAG tract of *Htt* presents dramatic challenges since repeat elements are common throughout the genome. Instead, genomic sequencing of HD patients has identified numerous single nucleotide polymorphisms (SNPs) that are strongly associated with the CAG expanded allele and can therefore be used to selectively target the mutant allele for knockdown<sup>287</sup>. Reports suggest that targeting as little as three SNPs associated with the mutant allele would be sufficient to cover up to 85% of the population with HD<sup>288</sup>.

Other approaches have tested silencing total huntingtin expression as a therapy for HD. The wild type huntingtin protein is essential for development and is required for many critical cellular functions including vesicular transport, transcriptional regulation and promoting neuronal health. Therefore, silencing of the wild type allele may have some detrimental effects when combined with the silencing of the mutant allele. Studies have shown that post-natal inactivation of the *Hdh* gene (murine *Htt* homolog) causes progressive neurodegeneration in mice suggesting a loss-of-function mechanism in HD pathogenesis<sup>289</sup>. Despite this finding, many studies have demonstrated that partial reduction of *Htt* expression has been well tolerated in both mice and non-human primates<sup>290-293</sup>. Furthermore, non-allele specific silencing of *Htt* has been shown to improve clinical features of HD in animal models<sup>290,293,294</sup>. However, the threshold for

how much and how long wild-type huntingtin reduction can be tolerated without eliciting negative effects has not been extensively tested.

Therefore, both the allele specific and non-specific approaches to silencing *Htt* expression may be viable therapeutic strategies for HD. The two methods currently being tested to lower huntingtin levels are RNA interference (RNAi) and anti-sense oligonucleotide (ASO) technologies. RNAi is a cellular process that inhibits gene expression post-transcriptionally by targeting specific mRNAs for destruction through the endogenous silencing machinery<sup>295</sup>. The initial studies tested RNAi using short hairpin RNA (shRNA) to evaluate the benefits of lowering mutant huntingtin levels *in vivo*<sup>296</sup>. These studies used adeno-associated virus (AAV) to deliver the shRNA targeted to human huntingtin directly into the striatum of transgenic mice expressing a small, mutant fragment of human huntingtin (a.a. 1-171, Q82)<sup>296</sup>. Lowering mutant huntingtin levels improved motor and neuropathological abnormalities in these HD mice<sup>296</sup>. However, the shRNA used in this study was designed to a sequence that is unique to the human mutant huntingtin transgene. Therefore, the selective silencing of only the mutant allele was achieved by targeting sequence differences between species. Notably, shRNAs have been shown to have off-target effects and to cause *in vivo* toxicity by saturating the endogenous RNAi machinery<sup>297</sup>. Thus, the use of shRNA for therapeutic silencing of *Htt* has been replaced by safer approaches such as artificial microRNAs<sup>297,298</sup>.

Short synthetic ASOs have also been tested for their efficacy in silencing *Htt* gene expression in both an allele specific and non-specific manner. ASOs silence gene expression post-transcriptionally by a variety of mechanisms<sup>299</sup> and can be modified to specifically target any SNPs. A benefit of ASOs is that they can target SNPs in the pre-mRNA, including SNPs that fall within intronic regions, thus increasing the number of SNP's that can be targeted. Another benefit of ASOs is that efficient delivery throughout the brain is accomplished via simple infusion without the need for a viral delivery system. This allows dosing of ASO levels in the brain to be stringently controlled. Furthermore, rather than requiring continuous treatment, transient infusions of ASOs are sufficient to sustain *Htt* silencing for several months after the initial knock-down<sup>290</sup>.

Studies with ASOs have targeted the expanded CAG tract and SNPs of human *Htt* with a high degree of specificity for the mutant relative to the wild type allele<sup>287,300</sup>. However, further studies are required to test the efficacy of allele specific silencing of mutant huntingtin on the progression of HD.

Isis pharmaceuticals, in collaboration with Roche, are currently working to push ASO technology into clinical trials for the treatment of HD. Isis has successfully completed a pilot safety study of a huntingtin-silencing ASO in non-human primates<sup>290</sup>, which is a major step towards moving into human clinical trials. Since most efficacy studies of ASOs in animal models have only tested benefits of silencing total *Htt* levels, the first clinical trial for ASOs in HD will test the non-allele specific approach to reducing *Htt*. A pilot study testing the safety of ASOs in the treatment of familial ALS showed that ASOs delivered directly into the CNS of humans are well tolerated<sup>301</sup>.

Another approach to reducing huntingtin-induced toxicity has focused on targeting the mutant protein at the post-translational level using intracellular antibodies (intrabodies)<sup>302-305</sup>. Intrabodies bind to huntingtin with high specificity and have been shown to improve behavioural phenotypes in multiple mouse models of HD<sup>303,305</sup>. Therefore, strategies that decrease levels of huntingtin or reduce mutant huntingtin-induced toxicity represent promising therapeutic options for the treatment of HD.

#### **1.14.6 Promoting Phosphorylation of Huntingtin N17 as a Prospective Therapy for HD**

The N17 domain of huntingtin is subject to a number of PTMs that can alter the localization, inclusion formation properties and toxicity of the mutant protein<sup>50,57,73,124,125</sup>. Previously, our group has demonstrated that N17 is a membrane association signal that targets huntingtin to the E.R. and that cell stress conditions can cause huntingtin to translocate into the nucleus<sup>50</sup>. The shuttling of huntingtin between cellular compartments during stress is initiated by the reversible phosphorylation of N17 at S13S16<sup>57</sup>. Mutant huntingtin is hypo-phosphorylated at S13S16 which results in an impaired response to stress in HD<sup>57</sup>.

Notably, bacterial artificial chromosome (BAC) HD transgenic mice expressing full-length mutant huntingtin with S13DS16D mutations showed a normal phenotype with no HD-like symptoms or neurodegeneration. This study identified S13S16 phosphorylation as a therapeutic target for HD. Subsequently, a high-content screen of kinase inhibitors in live cells identified a number of compounds that could modulate the phosphorylation of S13S16. Notably, compounds that increased phosphorylation at these residues decreased the toxicity of mutant huntingtin in a cell model of HD<sup>57</sup>. Furthermore, we discovered that inhibitors of casein kinase 2 (CK2) reduced phosphorylation at S13S16, whereas inhibitors of I $\kappa$ B kinase (IKK) paradoxically increased phosphorylation at these sites. We hypothesized that this is due to IKK and CK2 having similar substrates, where inhibiting IKK can be compensated by an increase in CK2 activity.

GM1 ganglioside is a glycosphingolipid that is enriched in the brain and is critical in neuronal plasticity and cell signalling<sup>306</sup>. Synthesis of GM1 ganglioside has been found to be impaired in HD patients and has been postulated to contribute to the increased susceptibility of HD cells to apoptosis<sup>307</sup>. The direct administration of GM1 into the brains of YAC128 transgenic mice expressing full-length mutant huntingtin was sufficient to reduce neuropathology and restore motor, cognitive and psychiatric behavior to normal in these mice<sup>128</sup>. Notably, GM1 ganglioside was found to increase the phosphorylation at S13S16 of mutant huntingtin in cell culture, suggesting that the beneficial role of restoring GM1 levels in HD mouse models may be due to the modulation of phosphorylation<sup>128</sup>. The use of GM1 ganglioside as a therapy for HD is currently being validated in other HD animal models (non-human primates) and is an attractive candidate to move into human clinical trials. A clinical trial was recently conducted to test the efficacy of GM1 ganglioside in the treatment of PD. GM1 was shown to significantly improve motor function and slow symptom progression in patients with PD<sup>308</sup>. Therefore, identifying compounds that can modify the post-translational status of the huntingtin protein provides a promising therapeutic avenue for the treatment of HD.

### 1.14.7 A Need for Better Animal Models

Although many drugs have shown beneficial effects in mouse models of HD, most have failed when tested in human clinical trials. These failures highlight the difficulty of predicting the efficacy of drugs in humans based on beneficial effects seen in mice. This suggests that potential therapeutic candidates should be tested in multiple mouse models, both fragment and full-length models, prior to advancing into humans. This also implies the need for better models to study HD and test drug candidates. In the past decade, transgenic sheep<sup>309</sup> and non-human primate<sup>310,311</sup> models of HD have been developed in order to more closely mimic the brain size and physiology seen in humans. Furthermore, a knock-in non-human primate HD model is currently being developed that will represent the most accurate animal model of HD to date. Testing compounds in these emerging models may help to reduce the failures of potential drug candidates that make it to human clinical trials.

### 1.15 Using FRET Techniques to Study HD and Other Neurodegenerative Diseases

The discovery and development of fluorescent proteins (FPs) for use in molecular and cell biology has revolutionized our ability to visualize the complex environment of the cell<sup>312</sup>. The constant development of new FPs and novel applications for their use has led to the parallel evolution of improved microscopes and imaging technologies. Conventional widefield and confocal imaging modalities are restricted by the overall limit of optical resolution imposed by the diffraction of light through the objective lens. This limitation, known as the diffraction barrier, restricts the ability of the optical instrument to laterally resolve two objects separated by approximately half of the excitation wavelength used (based on the formula :  $\text{Abbe Resolution}_{x,y} = \lambda/2(\text{Numerical Aperture})$ ). Depending on the objective lens, standard widefield and confocal modalities can optimally resolve objects approximately >200nm apart. The need to improve resolution beyond the diffraction-limit in biological samples has led to the development of super-resolution imaging modalities and the emergence of Förster resonance energy transfer (FRET) techniques.

FRET refers to the non-radiative transfer of an electronic excitation from a donor molecule to an acceptor molecule through a dipole-dipole interaction<sup>313</sup>. The rate constant of energy transfer is proportional to the inverse sixth power of distance between the donor and acceptor FRET pair<sup>313</sup>. Thus, FRET efficiency is extremely sensitive to small changes in distances probes. FRET requires that the distance between the donor and acceptor molecules to be small, typically on the order of 1-10 nanometres (nm), depending on the FRET pair<sup>314</sup>. For practical applications, FRET pairs are characterized by the Förster radius ( $R_0$ ), the distance between fluorophores at which FRET efficiency is 50%<sup>313</sup>. FRET also requires a sufficient overlap between the emission spectrum of the donor and the excitation spectrum of the acceptor. The theoretical maximum of FRET efficiency is strongly dependent on the degree of overlap between the FRET pair spectra<sup>313</sup>. Additionally, FRET requires the proper orientation of dipoles between the donor and acceptor probes. Therefore, FRET represents a powerful tool to assay direct molecular interactions and subtle conformational changes at nm resolution in live cells<sup>314-317</sup>.

Using FRET techniques to gain insight into the molecular mechanisms underlying neurodegenerative diseases have gained increased interest over the past decade and have been used in variety of applications. In HD, the first uses of FRET were to measure the aggregation of mutant huntingtin fragments into inclusion bodies<sup>201,318</sup>. In these studies, intermolecular FRET between individual huntingtin fragment fusions (with either donor or acceptor probes) is detected as they are recruited and sequestered at nanometer proximity into inclusion bodies. FRET has also been used to measure sequestration of CBP, TBP, heat shock protein 70 (Hsp70) and other critical cellular proteins into huntingtin inclusions<sup>199</sup>. Furthermore, FRET has been used as part of a high throughput screen to selectively identify compounds that reduce or inhibit aggregation of the mutant huntingtin protein into inclusion bodies<sup>318</sup>. However, the use of FRET techniques in HD has not been limited to looking at aggregation of huntingtin but has recently been implemented to quantify levels of mutant huntingtin relative to total huntingtin in patient brain, plasma and cerebral spinal fluid samples<sup>319</sup>. This novel assay utilizes lanthanide conjugated-antibodies raised to specific epitopes on mutant huntingtin (expanded polyglutamine tract) and to total huntingtin in conjunction with

time-resolved detection of FRET (TR-FRET) to quantify levels of soluble mutant huntingtin *in vivo*. Biological samples contain many naturally fluorescent compounds, thus, TR-FRET exploits the long fluorescent emission times and large Stokes shift of rare earth elements, such as lanthanides, to minimize signal interference due to background auto-fluorescence. This TR-FRET assay was developed at Novartis and has since been adapted to quantify FMR1 protein levels in Fragile-X syndrome<sup>320</sup> and  $\alpha$ -synuclein levels in PD<sup>321</sup>.

FRET has also been used for a variety of applications in other neurodegenerative diseases. In AD, FRET has been used to study defective calcium homeostasis, a mechanism hypothesized to contribute to AD pathology. In this study, a FRET-based high-throughput phenotypic screen was used to identify lead compounds that could reverse agonist-evoked release of intracellular calcium in cells stably co-expressing a familial AD-linked presenilin-1 M146L mutant and a calcium FRET sensor<sup>322</sup>. In prion diseases like Creutzfeldt-Jakob disease (CJD), it is hypothesized that the prion protein (PrP) becomes misfolded and can propagate this misfolded state to other PrP, thus leading to pathology. In CJD, an antibody-based FRET assay has been developed to quantify levels of PrP in live cells<sup>323</sup>. This assay has been used as part of a high-throughput screen to identify compounds that could decrease expression of the PrP in live cells<sup>323</sup>. These compounds were found to reduce levels of PrP at the cell surface and to inhibit PrP replication. Therefore, FRET represents a powerful tool used in many neurodegenerative diseases to elucidate molecular mechanisms of pathology, quantify levels of mutant proteins and to identify therapeutic compounds.

## 1.16 Thesis Outline and Study Rationale

Dynamic conformational changes are required for the proper function of many proteins. Previously, crystal structures of TG2 have revealed that the enzyme undergoes a large conformational change between its enzymatic roles<sup>254</sup>. However, all of this work was done *in vitro* with purified TG2, providing no insight into the conformational dynamics of the enzyme inside native environments. In chapter 2 of this thesis, we describe the use of a TG2 FRET sensor to measure the conformation of TG2 in live cells. Based upon structural studies of TG2<sup>254</sup>, we hypothesize that FRET can be used to measure the effect of cell stresses, functional point mutations and small-molecule inhibitors on the conformation of TG2 in live cells. To test this hypothesis, we generated a FRET sensor with TG2 fused between a donor and an acceptor fluorophore. In an effort to optimize the sensor for FRET detection, several iterations of this sensor were generated with different linker regions between TG2 and the fluorophores.

Huntingtin is a scaffolding protein that interacts with a large network of factors and has many cellular roles. The expansion of polyglutamine beyond a specific threshold in huntingtin results in both the loss of normal huntingtin function(s) and the gain of toxic function(s) that ultimately lead to HD. The question of why CAG lengths at or greater than 37 repeats cause HD and fewer repeats do not has plagued the HD field since the discovery of the *Htt* gene in 1993. At the level of huntingtin, many *in vitro* studies have implicated a transition of the protein to a mutant, toxic conformer above the pathogenic threshold for HD<sup>77,193</sup>. Based on these findings, we hypothesize that mutant huntingtin undergoes a conformational change at the pathogenic threshold for HD in live cells. To test this hypothesis, we developed a FRET sensor similar to that used to measure the conformational change of TG2 (chapter 2). Chapter 3 of this thesis describes a conformational change of huntingtin at the pathogenic threshold due to the loss of flexibility of mutant polyglutamine tracts.

The implication of mutant huntingtin inclusions in HD pathology remains a controversial issue in the field, with evidence supporting both a toxic and protective role in the cell<sup>121,195</sup>. Based on these conflicting lines of evidence, we hypothesize that

mutant huntingtin can form multiple inclusion types with different structural and functional properties in live cells. To test this hypothesis, we used the mutant huntingtin exon1 FRET sensor developed in chapter two and implemented a combination of super-resolution imaging, FRET and FRAP techniques. In chapter 4 of this thesis, we describe the characterization of two different mutant huntingtin inclusion types based on morphology, structure and, formation and maturation dynamics.

## **Chapter 2 - Measuring Conformational Changes of an Enzyme in Live Cells**

### Preface

The material presented in this chapter is a representation of the following publication.

**Caron, N.S., Munsie, L.N., Keillor, J.W. & Truant, R.** Using FLIM-FRET to measure conformational changes of transglutaminase type 2 in live cells. *PLoS One* **7**, e44159 (2012)

The only changes made to this publication were for thesis continuity and formatting.

This work with the transglutaminase type 2 (TG2) enzyme has helped to develop and optimize the methodology of studying protein conformations in live cells. This study of TG2 conformation has laid the groundwork for studying the conformation of the huntingtin protein and other polyglutamine-containing proteins.

## **Using FLIM-FRET to Measure Conformational Changes of Transglutaminase Type 2 in Live Cells**

Caron, N.S.<sup>1</sup>, Munsie, L.N.<sup>1</sup>, Keillor, J.W.<sup>2</sup>, Truant, R.<sup>1\*</sup>

<sup>1</sup>Department of Biochemistry and Biomedical Sciences, McMaster University, Hamilton, Ontario, Canada, L8N3Z5.

<sup>2</sup>Department of Chemistry, University of Ottawa, 30 Marie-Curie, Ottawa, Ontario, Canada. K1N 6H5,

\*Address correspondence to: Ray Truant, HSC 4N54, 1200 Main Street West, Hamilton, Ontario, Canada L8N3Z5; Fax: 905-522-9033; email: [truantr@mcmaster.ca](mailto:truantr@mcmaster.ca)

## 2.1 Abstract

Transglutaminase type 2 (TG2) is a ubiquitously expressed member of the transglutaminase family, capable of mediating a transamidation reaction between a variety of protein substrates. TG2 also has a unique role as a G-protein with GTPase activity. In response to GDP/GTP binding and increases in intracellular calcium levels, TG2 can undergo a large conformational change that reciprocally modulates the enzymatic activities of TG2. We have generated a TG2 biosensor that allows for quantitative assessment of TG2 conformational changes in live cells using Förster resonance energy transfer (FRET), as measured by fluorescence lifetime imaging microscopy (FLIM). Quantifying FRET efficiency with this biosensor provides a robust assay to quickly measure the effects of cell stress, changes in calcium levels, point mutations and chemical inhibitors on the conformation and localization of TG2 in living cells. The TG2 FRET biosensor was validated using established TG2 conformational point mutants, as well as cell stress events known to elevate intracellular calcium levels. We demonstrate in live cells that inhibitors of TG2 transamidation activity can differentially influence the conformation of the enzyme. The irreversible inhibitor of TG2, NC9, forces the enzyme into an open conformation, whereas the reversible inhibitor CP4d traps TG2 in the closed conformation. Thus, this biosensor provides new mechanistic insights into the action of two TG2 inhibitors and defines two new classes based on ability to alter TG2 conformation in addition to inhibiting transamidation activity. Future applications of this biosensor could be to discover small molecules that specifically alter TG2 conformation to affect GDP/GTP or calcium binding.

## 2.2 Introduction

Transglutaminase type 2 (TG2; EC 2.3.2.13) is a multi-functional enzyme capable of catalyzing several calcium-dependent reactions, including a transamidation reaction (covalent cross-link) between the  $\gamma$ -carboxamide group of a peptide bound glutamine and a variety of amine substrates<sup>250</sup>, in both an intra- and extracellular context<sup>324</sup>. Alternatively, TG2 can also hydrolyze GTP, where it acts as a G-protein mediating the phospholipase C signalling cascade<sup>253,325</sup>. These cellular roles of TG2 are reciprocally regulated by a large conformational change<sup>254,326</sup>. Crystal structures of TG2 have been solved indicating that GDP/GTP bound TG2 adopts a 'closed' conformation that is catalytically inactive as a cross-linking enzyme<sup>254</sup>. Conversely, an additional crystal structure shows that a substrate-mimicking peptide inhibitor bound to TG2 extends the enzyme to an 'open' conformation<sup>254</sup>. This suggests that the open conformation represents the enzymatically active version of the enzyme, yet to date no crystal has been solved with both calcium ions and a substrate bound to TG2. Under normal physiological conditions, intracellular calcium levels are low and the majority of the TG2 population is bound with guanosine nucleotides in a closed conformation<sup>257</sup>. However, under specific cell stress conditions, calcium levels rise dramatically causing a shift in the TG2 population towards its open and enzymatically active cross-linking conformation.

Despite the breadth of information that can be extracted from generating crystal structures, this work is time-consuming and assumes that the purified protein that packs into crystal arrays *in vitro* is representative of the protein conformation *in vivo*. As an alternative method, we generated a triple fusion of human TG2 between two fluorescent probes in order to measure conformational differences between the enzymatic roles of TG2 in live cells using Förster resonance energy transfer (FRET). FRET is a well-established method of measuring molecular interactions as well as conformational changes in live cells. FRET involves the non-radiative transfer of energy between a donor and an acceptor molecule<sup>327</sup>. FRET requires that the donor and the acceptor molecule be within a close spatial proximity of each other, where the Förster radius of a FRET pair refers to the distance at which the efficiency of energy transfer is 50% (~8

nanometres for mCer and eYFP)<sup>327-329</sup>. This 8 nm spacing represents the distance between the fluorophore cores, yet when the outer valence shell diameters of the fluorescent proteins are considered, this proximity essentially represents a direct protein-protein interaction. Another requirement of FRET is a high degree of overlap between the emission spectrum of the donor molecule and the excitation spectrum of the acceptor molecule. The most quantitative method of measuring FRET in live cells is by using fluorescent lifetime imaging microscopy (FLIM)<sup>330</sup>. Fluorescence lifetime refers to the period of time a fluorescent molecule stays in an excited state prior to returning to ground state and emitting a photon<sup>330</sup>. The lifetime of a fluorophore can be affected by the biochemical and biophysical properties of its microenvironment, where FRET leads to a decrease in the fluorescence lifetime of the donor molecule that can accurately be measured<sup>316</sup>. Contrary to other spectral methods of measuring FRET, such as sensitized emission FRET (SE-FRET)<sup>331</sup>, the ability to measure fluorescence lifetime of fluorescent proteins expressed in live cells is less dependent of relative probe concentrations and intensities, photo-bleaching as well as spectral bleed through<sup>316,332</sup>. The accuracy of FRET measurement is further enhanced by this genetically-encoded triple fusion that insures a relative donor-acceptor fluorophore concentration of 1:1. To measure lifetimes in the time-domain (TD-FLIM), the fluorescent samples are excited with a femtosecond pulsing laser coupled to a time-correlated single photon counting (TCSPC) system<sup>333</sup>. Using FLIM to measure FRET, we have generated a biosensor that provides a novel tool to quantitatively measure TG2 conformations in a live cell context. This sensor provides an assay to quickly measure the effects of cell stresses, point mutations and chemical inhibitors on the conformation of TG2. Using this assay, we have uncovered new mechanistic insights into the activity of TG2 inhibitors NC9 and Cp4d and have established a new way to classify TG2 inhibitors based on their ability to affect the conformation of the protein.

TG2 has been linked to a myriad of human disorders including: inflammatory, autoimmune and neurodegenerative diseases, yet the pathological role of TG2 in these conditions remains elusive. Much of the early work done on TG2 has focused on its aberrant cross-linking of substrates as being the cause of pathology; however growing evidence suggests that the subcellular localization and the conformation of TG2 are

also critical in the regulation of cell death processes<sup>257</sup>. Therefore, we believe that examining TG2 *in vivo* is critical to improving our understanding of TG2 and its role in multiple disease pathologies. This biosensor provides a universal tool capable of rapidly assessing the conformations of TG2 while providing additional information about the subcellular localization of TG2 in live cells.

## 2.3 Materials and Methods

**Ethics Statement** : Full details of the study approval by the McMaster University Biosafety Committee.

**Tissue Culture** : Immortalized mouse striatal *STHdh*<sup>Q7/Q7</sup> cells were derived from normal WT mice and were grown as previously described<sup>50</sup>. Cells were a kind gift from Dr. Marcy Macdonald (MGH/Harvard) and were previously characterized<sup>334</sup>.

**Cell Transfection** : *STHdh*<sup>Q7/Q7</sup> cells were transfected using TurboFect *in vitro* transfection reagent (Fermentas) for 24-36 hours prior to imaging as previously described<sup>58</sup>.

**Plasmid Constructs** : TG2 constructs were generated using PCR on human TG2 cDNA (generous gift from G.V.W. Johnson) with forward primer GATCAGATCTGGTGGCGGAGGGATGGCCGAGGAGCTGGTCTTAG with a BglII restriction site and reverse primer CTATGGTACCCCCTCCGCCACCGGCGGGGCCAATGATGACATTC with an Acc65I restriction site. TG2 R580A point mutation was introduced using inverse PCR on wild type TG2 with forward primer GCGGACCTCTACCTGGAGAATC and reverse primer CTCAGCCAGCAGGTAGCTGTTG. TG2 W241A mutation was introduced using inverse PCR on wild type TG2 with forward primer GCGGACAACAACACTACGGG and reverse primer GCGTCCCAGCAGCACACC. All insert PCR products were cloned into a modified mCerulean-C1 plasmid with an eYFP insert cloned into BamHI and XbaI sites at the opposing end of the multiple cloning site (MCS).

**TG2 Inhibitor Treatments** : CP4d and NC9 inhibitor treatments were left on transfected *STHdh*<sup>Q7/Q7</sup> cells for ~14-16 hours prior to use in FLIM-FRET experiments. TG2 inhibitors (NC9, CP4d) were confirmed to be active using an *in vitro* colorimetric transglutaminase assay (Sigma Cat # CS1070-1KT) at concentrations ranging from 500nM to 15µM. This assay was also used to confirm transglutaminase activity of the mCer-TG2-eYFP protein expressed in *STHdh* cells, which have little/no measureable endogenous TG2 activity.

**Fluorescence Lifetime Imaging Microscopy (FLIM)** : FLIM was performed as previously described<sup>58</sup>.

**FLIM - ImageJ Analysis** : Using a Becker and Hickl FLIM plug-in for ImageJ (from [www.macbiophotonics.ca](http://www.macbiophotonics.ca)), we imported both the tau and photon images for each cell to be quantified. The values on the tau ( $\tau$ ) images represent the fluorescent lifetimes of the donor fluorophore (mCerulean) at each pixel within the image, whereas the photon image represents the number of photons collected at each pixel. The values on the  $\tau$  image were then set to only display a range from 1750 – 3250 picoseconds in order to minimize the contribution of background signal and auto-fluorescence in each image to the final quantifications. Using the freehand selection tool, each cell was then fully outlined on the photon image to reduce experimental bias, where this region of interest (ROI) was then applied to the  $\tau$  image for measurement. Mean intensity measurements on the  $\tau$  image represent the mean fluorescence lifetime at each R.O.I. FRET efficiency for each image was determined using the equation % FRET  $E = 1 - (\text{average lifetime D.A} / \text{average lifetime D})$ , where average lifetime D.A indicates the average lifetime of mCerulean-exon1 fusions in the presence of the indicated acceptor and average lifetime D indicates the overall average lifetime of mCerulean-exon1 fusions alone (no acceptor present). A minimum of 10 cells were quantified on each condition for every trial and subsequently graphed on a box-whisker plot. The box represents the 25% to 75% confidence intervals and the line within in represents the data median. The whiskers represent the 5% to 95% confidence intervals whereby outliers were removed if they fell outside 2 standard deviations from the mean.

**Statistical Analysis** : All statistical analysis was done using the SigmaPlot software 11.0 (Systat Software Inc.). For comparisons between two groups, Student's T-tests were performed if data passed the normality assumptions. If data did not pass the normality test, it was analyzed by the Mann–Whitney method. For multiple pairwise comparisons, one-way analysis of variance (ANOVA) using the Student-Newman-Keuls method was performed if the data passed the normality test of distribution. If the data did not pass the normality assumptions, then we performed a one-way ANOVA on ranks using the Tukey test. For all FLIM quantifications, every cell was represented as its own

N for that construct/treatment. Therefore, every box-whisker blot graph was generated using data from a single representative trial. Every construct/treatment trial was repeated a minimum of 3 times to ensure that trends were consistent between trials.

## 2.4 Results

Using the molecular modelling software, PyMol<sup>335</sup>, and previously published crystal structures of TG2 (PDB ID: 2Q3Z)<sup>254</sup>, we measured the distances between the amino and carboxyl termini residues of TG2 in 3D space for both of its known conformations. The transition of TG2 from a closed to an open conformation shifts the distance between its termini from less than 10 nm to approximately 150 nm apart. We hypothesized that these distances would be amenable to detecting FRET and could be used to generate a conformational biosensor to analyze both the conformation and cellular localization of TG2 in live cells. We fused a donor mCerulean fluorescent protein and an acceptor yellow fluorescent protein (eYFP) fluorophore to the amino and carboxyl termini of TG2, respectively, and tested this construct under various conditions in live cells using TD-FLIM. Monomeric cerulean was chosen as a donor for FRET as this CFP variant has a mono-exponential lifetime decay and has significant spectral overlap with eYFP, making this pair optimal for FLIM-FRET<sup>328</sup>. As demonstrated by our model, when TG2 is bound to guanosine nucleotides in its closed conformation we would predict a robust increase in FRET efficiency, correlating with a decrease in the donor lifetime (Figure 2.1A). Alternatively, when a substrate molecule and/or calcium are bound to TG2 in the open conformation, the fluorophores are no longer in close spatial proximity and thus we would predict a reduction in FRET efficiency (Figure 2.1B).

Prior to testing our conformational sensor in live *STHdh* cells we determined that the mCerulean-TG2 fusion in the absence or presence of an acceptor (using eYFP alone, Figure 2.1C) had a lifetime of approximately 2.8 ns, consistent with the natural lifetime of mCerulean measured by others<sup>328</sup>. As predicted, we noted a significant decrease in donor lifetime (represented by the orange to red pseudo-colours in the photon-weighted lifetime image and a left shift in the lifetime histogram peak) with our mCerulean-TG2-eYFP sensor (Figure 2.1E and 2.1F). This can be interpreted as the TG2 population in the cell adopting a closed conformation. These results are consistent with the biochemical data which suggests that the majority of TG2 in cells under steady state conditions behaves as a GTPase/G-protein<sup>257</sup>. To establish that the observed

decrease in lifetime was due to intramolecular FRET between individual TG2 molecules and not due to intermolecular FRET as an artefact of over-expression or protein aggregation, we co-expressed mCerulean-TG2 and TG2-eYFP constructs together on separate expression plasmids and saw no change in lifetime relative to the mCerulean-TG2 + eYFP alone control (Figure 2.1D and 2.1F). Despite the simplicity of this sensor, glycine linkers between the fluorophores and TG2 were tested in order to optimize the efficiency of energy transfer between the probes as well as increase the dynamic range for quantification (Figure 2.1G). We found that adding 4 glycines as linkers to both the amino and carboxyl termini provided the optimal FRET efficiency values. This was likely accomplished by less steric hindrance of TG2 protein dynamics by the fluorophores, as well as a better potential to align the fluorophore dipole moments in 3D space.

Next, we wanted to assay the effects of substitution mutations at critical residues on the conformation of TG2. Mutating arginine 580 of human TG2 to an alanine (R580A) abolishes all guanosine nucleotide binding<sup>336</sup>, however, little is known regarding the effects of this mutation on the conformation of TG2. This R580A mutation causes a significant decrease in percent FRET efficiency ( $p < 0.001$ ) relative to the wild type (WT) TG2 biosensor (Figure 2.2A). This suggests that when TG2 cannot bind GDP/GTP, an increased amount of TG2 in the cell can be found in an open conformation. Tryptophan 241 is a conserved residue within human TG2 that is critical for its transamidating activity<sup>337</sup>. Mutating this residue to an alanine (W241A) abolishes its transamidating activity, while maintaining the ability of the enzyme to bind GDP/GTP<sup>337</sup>. As expected, this mutation had little effect on the conformation of the TG2 population relative to WT (Figure 2.2A). This is likely due to the ability of this TG2 mutant to still bind guanosine nucleotides.

To further validate this TG2 sensor, we tested the effect of various stresses on the conformation of TG2. Heat shock is a global cellular stress that activates many chaperones and signalling cascades involved in the heat shock response<sup>338</sup>. Heat shock causes a decrease in cellular ATP levels<sup>339</sup> and an increase in intracellular calcium levels<sup>115</sup>, which we hypothesized would shift the intracellular population of TG2 towards an open conformation. Our data showed that a 30 minute heat shock treatment (at

42.5°C) causes a significant ( $p < 0.001$ ) decrease in the overall percent FRET efficiency within cells expressing the TG2 sensor (Figure 2.2B). All controls were also performed under the same conditions to ensure that this decrease in FRET efficiency was not due to an artefact of heat-denaturing the sensor fluorescent proteins. We also tested A23187 (calcimycin), an ionophore that makes the plasma membrane of cells permeable to divalent ions, rapidly increasing intracellular levels of calcium<sup>340</sup>. Treatment with the A23187 compound for 10 minutes had a similar effect on the conformation of TG2 as the heat shock treatment (Figure 2.2B), demonstrating that TG2 adopts an open conformation in live cells when exposed to high concentrations of calcium.

Lastly, we wanted to test the effects of various transamidation inhibitors on the conformation of TG2 to get more mechanistic insight into their mode of action in vivo. NC9 ( $\alpha$ -N-carbobenzyloxy- $\gamma$ -N-acryloyl-L-lysine(2-(2-dansylaminoethoxy)ethoxy)ethanamide) is an irreversible inhibitor of the transglutaminase family that reacts with the active site of the enzyme and has a similar mode of action as the synthetic pentapeptide inhibitor used to generate the open conformation crystal structure of TG2<sup>254</sup>. Therefore, NC9 has been hypothesized to stabilize the protein in an open conformation<sup>341,342</sup>. To test this hypothesis, cells expressing the TG2 FRET sensor were treated with the NC9 compound for 16 hours. We measured a significant decrease in the percent FRET efficiency (Figure 2.3A and 2.3C;  $p < 0.001$ ) over non-treated cells. To test the conformational kinetics of this inhibition, we treated *STHdh* cells expressing the TG2 sensor with 10  $\mu$ M NC9 and measured percent FRET efficiency temporally over a 24 hour time course (Figure 2.3C). We noted that NC9 elicited its most significant effects after 1 hour of treatment.

CP4d ((E)-1-(1-(4-nitrobenzyl)-1H-1,2,3-triazol-4-yl)-3-(4-nitrophenyl)prop-2-en-1-one) is a competitive, reversible and selective TG2 inhibitor with no known effect on the conformation of TG2 in cells<sup>285</sup>. In cells expressing the TG2 sensor, we noted that treatment with CP4d caused an increase in the percent FRET efficiency compared to no treatment, suggesting that this inhibitor maintains TG2 in the closed conformation to prevent transamidating activity. Treating cells with a range of CP4d concentrations

ranging from 500nM to 10 $\mu$ M (Figure 2.3B) caused a progressive dose-response effect of this inhibitor on the conformation of TG2 with increasing concentrations of CP4d.

## 2.5 Discussion

The various activities of TG2 have been directly implicated in the progression of celiac disease, atherosclerosis, diabetes, cancer, glaucoma and the formation of cataracts<sup>343</sup>. Additionally, TG2 has a role in multiple neurodegenerative diseases including Huntington's (HD)<sup>58</sup>, Parkinson's (PD) as well as Alzheimer's disease (AD)<sup>344,345</sup>. Studies of patient brains have shown that expression levels and transamidating activity of TG2 are highly elevated in these diseases, where it has been proposed that cell death may be caused by the aberrant cross-linking of substrates<sup>345</sup>. The role of TG2 in the cell death process is dependent on cell type, the stressor, its subcellular localization, its enzymatic role, and its conformation<sup>257,341</sup>. Using FLIM-FRET, the TG2 FRET biosensor not only provides a measure of the conformation and enzymatic role of TG2 but also provides resolution of the subcellular localization of TG2 in live cells. Therefore, this assay quickly provides several levels of information regarding TG2 and can be done under physiological conditions in living cells. Additionally, this TG2 sensor is a tool to determine if specific inhibitors are affecting both the conformation and/or localization of the enzyme under steady-state and cell stress conditions, and may be amenable to transgene expression in a mouse model.

While here we used FLIM to detect FRET changes, since both the donor and acceptor are on one molecule in a ratio of 1:1, detection and quantification of FRET by the less costly methods amenable to high content or high throughput screening, i.e. sensitized emission<sup>331</sup> or acceptor photo-bleaching FRET<sup>314</sup>. It is also possible to image the temporal changes of FRET in live cells by the use of ratiometric imaging with SE-FRET.

Using this assay we were able to compare the effects of NC9 and Cp4d inhibitors both by dose-response and time-response in live cells expressing the TG2 FRET biosensor. As predicted by the original authors of the work describing NC9<sup>336,342</sup>, this inhibitor was shown to force TG2 open and to stabilize it in this conformation<sup>336</sup>. Conversely, the Cp4d reversible TG2 inhibitor, was shown to promote the closed conformation of the TG2 biosensor<sup>285</sup>. This suggests that this inhibitor may still maintain

GTP binding within the closed conformation, while completely inhibiting transamidation activity of TG2.

The differing activities of these TG2 inhibitors suggests that they may fall into three potential classes: Class I, which can promote a closed conformation of the enzyme while bound; class II, which can lock the enzyme in an open conformation; and a third class, class III, which does not have any conformational effects at all, yet can still inhibit the transamidation activity of TG2. Therefore, depending on the disease context, therapeutics targeted towards inhibiting the cross-linking activity of TG2 could be designed with the conformation of the enzyme in mind as to not affect the other potentially beneficial biological functions of TG2, such as calcium and/or GTP binding. Conversely, this biosensor could be used to screen new molecule inhibitors that specifically target the conformation of TG2, hence the calcium or GTP binding activities, if these are relevant to the disease pathology being studied.

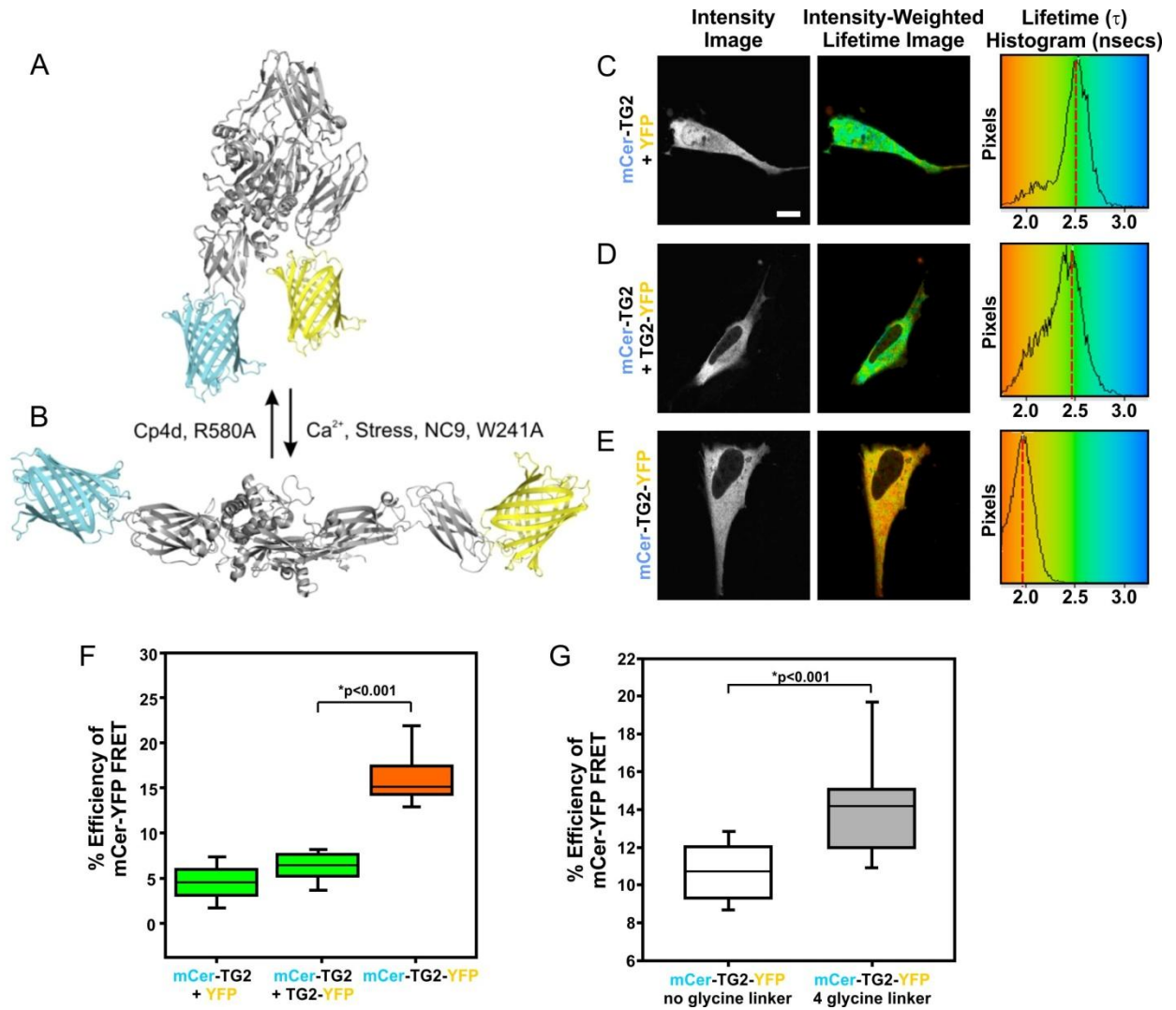


**Figure 2.1. The transglutaminase type 2 (TG2) conformational FRET sensor. (A and B)** Speculative models of mCerulean-TG2-eYFP FRET sensor in a GDP/GTP bound closed conformation and of mCerulean-TG2-eYFP sensor in a  $\text{Ca}^{2+}$  and substrate bound open conformation. **(C)** Sample FLIM image of mCerulean-TG2 with eYFP alone negative control. Intensity, intensity-weighted lifetime images and lifetime histograms are shown for every construct. Lifetimes shown in the intensity-weighted lifetime images are pseudo-colored using a rainbow LUT that corresponds to the lifetime scale represented in the histogram. Dashed red lines within the histograms represents the approximate lifetime with the highest number of pixels. **(D)** Sample FLIM image of mCerulean-TG2 with TG2-eYFP, a negative control for intermolecular FRET. **(E)** Sample FLIM image of mCerulean-TG2-eYFP conformational FRET sensor. **(F)** Quantitative FLIM-FRET data shown as percent FRET efficiency for TG2 negative controls, as well as the mCerulean-TG2-eYFP FRET sensor. **(G)** Quantification of effect of adding 4X glycine linkers between the fluorophores and TG2 on FRET efficiency of TG2 in the closed or resting state. Black line represents median values, boxes encompass 25% and 75% confidence intervals and whiskers indicate the 5% to 95% confidence intervals. \* $p < 0.001$ . N=15 for 5 replicates. Scale bar represents 10 $\mu\text{m}$ .

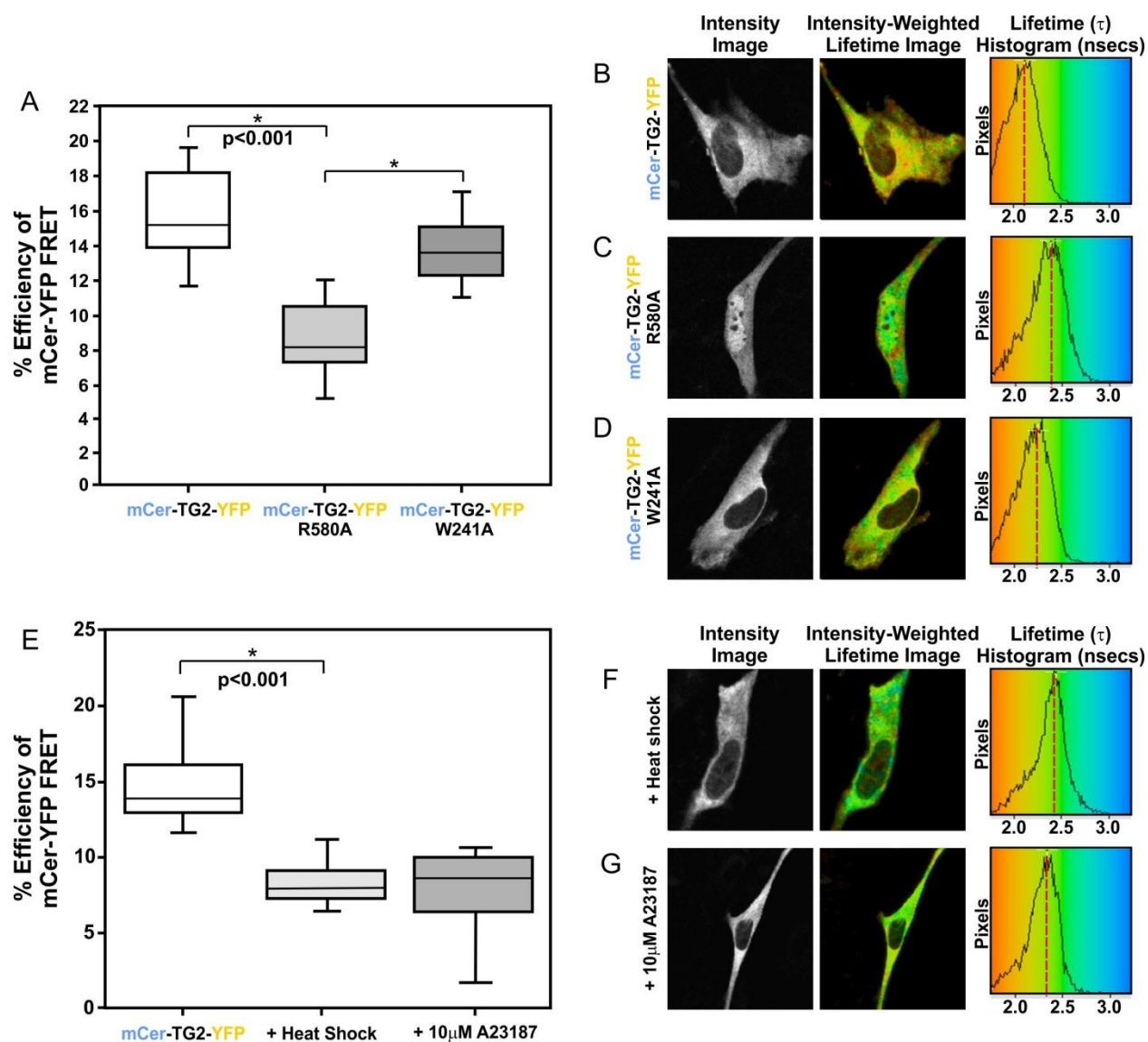


**Figure 2.2. Point mutations and cell Stresses affect TG2 conformation in live cells. (A)**

Quantitative FLIM-FRET data shown as percent FRET efficiency for the mCerulean-TG2-eYFP FRET sensor, GDP/GTP insensitive R580A mutant and catalytically inactive W241A mutant. Black line represents median values, boxes encompass 25% and 75% confidence intervals and whiskers indicate the 5% to 95% confidence intervals. \* $p < 0.001$ .  $N = 15$  for 3 replicates. **(B-D)** Representative FLIM images of data in **(A)**. **(E)** Quantitative FLIM-FRET data shown as percent FRET efficiency for the mCerulean-TG2-eYFP FRET sensor, or the sensor following either a 30 minute heat shock (42.5°C) treatment or a treatment with  $\text{Ca}^{2+}$  ionophore A23187 for 10 minutes. **(F,G)** Representative FLIM images of data in **(E)**.

\* $p < 0.001$ .  $N > 10$  for 4 replicates. Scale bar represents 10 $\mu\text{m}$ .

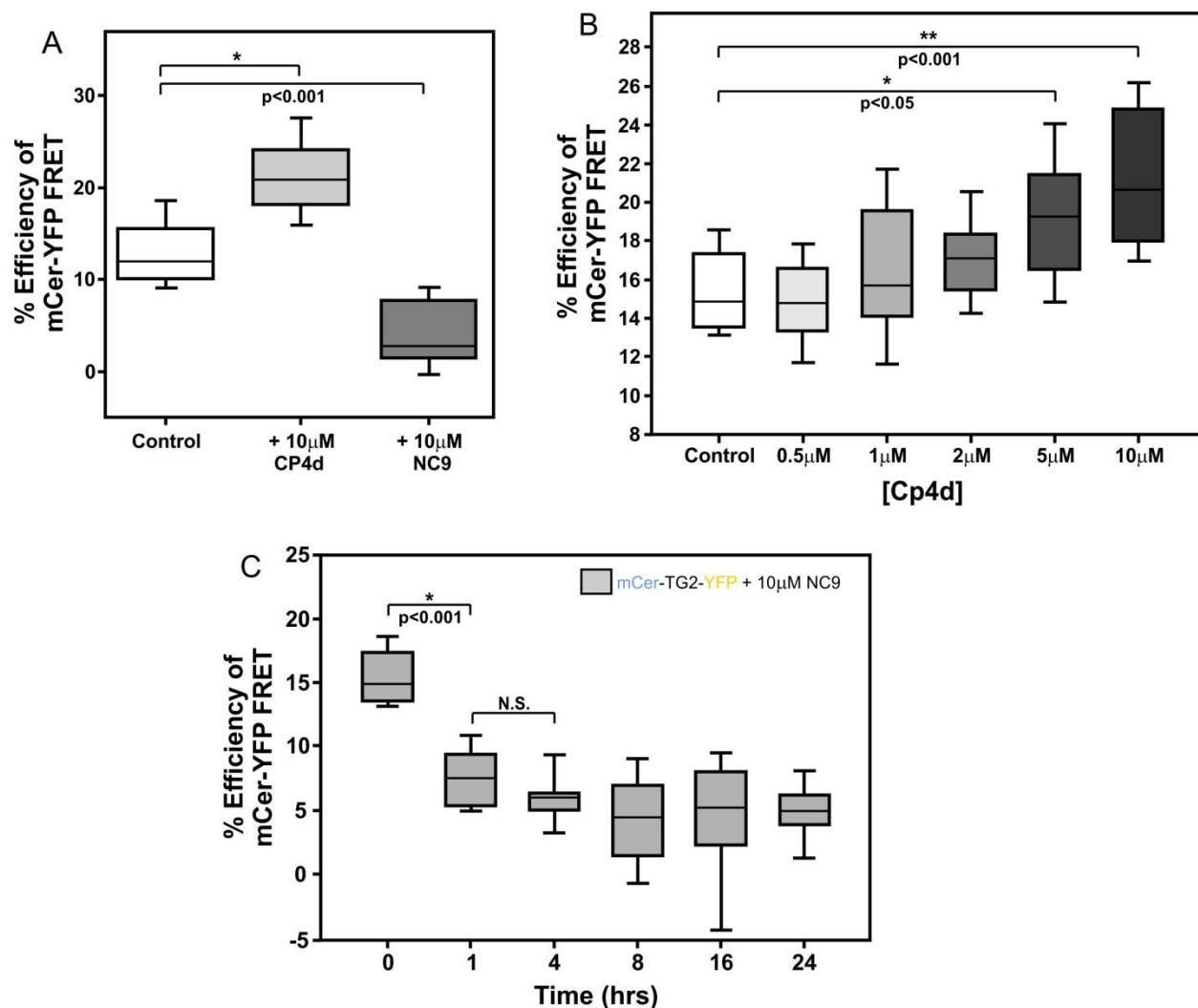


**Figure 2.3. TG2 inhibitors differentially affect TG2 conformation.** (A) Quantitative FLIM-FRET data shown as percent FRET efficiency for the mCerulean-TG2-eYFP FRET sensor after a 16 hour treatment with either the irreversible TG2 inhibitor, NC9, or the reversible TG2 inhibitor, CP4d. (B) Percent FRET efficiency graph generated following treatment of TG2 sensor with 5 increasing concentrations of CP4d. (C) Percent FRET efficiency graph of TG2 sensor following treatment with 10µM NC9 for 5 different time points from 0 to 24 hours. Black line represents median values, boxes encompass 25% and 75% confidence intervals and whiskers indicate the 5% to 95% confidence intervals. \* $p < 0.001$ . \*\* $p < 0.05$ .  $N > 10$  for 4 replicates. Scale bar represents 10µm.

## **2.6 Acknowledgements**

This work was funded by the Canadian Institutes of Health Research, grant MOP-119391, support from CHDI Inc. (Los Angeles) and the Krembil Foundation to RT. The authors would like to thank the invaluable advice and gifts of reagents by Prof. G.V. Johnson at the University of Rochester, NY, and Dr. Douglas Macdonald at CHDI Inc.

## **Chapter 3 – Detecting the Conformational Change of Huntingtin at the Pathogenic Threshold for HD**

### **Preamble**

The material presented in this chapter is a representation of the following publication.

**Caron, N.S., Desmond, C.R., Xia, J. & Truant, R.** Polyglutamine domain flexibility mediates the proximity between flanking sequences in huntingtin. *Proc Natl Acad Sci U S A* **110**, 14610-5 (2013).

The only changes made to this publication were for thesis continuity and formatting.

NC performed all the experiments and data analysis

CD and JX generated the original construct used as a FRET sensor in this publication

NC and RT wrote the manuscript

## **Polyglutamine Domain Flexibility Mediates the Proximity Between Flanking Sequences in Huntingtin**

Caron, N.S.<sup>1</sup>, Desmond, C.R.<sup>1</sup>, Xia, J.<sup>1</sup>, Truant, R<sup>1\*</sup>.

<sup>1</sup>Department of Biochemistry and Biomedical Sciences. McMaster University, Hamilton, Ontario, Canada. L8N 3Z5.

\*To whom Correspondence should be addressed. HSC 4N54, 1200 Main Street West, Hamilton, ON, Canada L8N3Z5. [Truantr@mcmaster.ca](mailto:Truantr@mcmaster.ca)

### 3.1 Abstract

Huntington's disease (HD) is a neurodegenerative disorder caused by a CAG expansion within the *Htt* gene that encodes a polymorphic glutamine tract at the amino terminus of the huntingtin protein. HD is one of nine polyglutamine expansion diseases. The clinical threshold of polyglutamine expansion for HD is near 37 repeats, but the mechanism of this pathogenic length is poorly understood. Using Förster resonance energy transfer (FRET), we describe an intramolecular proximity between the N17 domain and the downstream polyproline region that flank the polyglutamine tract of huntingtin. Our data supports the hypothesis that the polyglutamine tract can act as a flexible domain allowing the flanking domains to come into close spatial proximity. This flexibility is impaired with expanded polyglutamine tracts, and we can detect changes in huntingtin conformation at the pathogenic threshold for HD. Altering the structure of N17, either via phospho-mimicry or with small molecules, also affects the proximity between the flanking domains. The structural capacity of N17 to fold back towards distal regions within huntingtin requires an interacting protein, PACSIN1. This protein has the ability to bind both N17 and the polyproline region, stabilizing the interaction between these two domains. We also developed an antibody-based FRET assay that can detect conformational changes within endogenous huntingtin in wild-type versus HD fibroblasts. Therefore, we hypothesize that wild-type length polyglutamine tracts within huntingtin can form a flexible domain that is essential for proper functional intramolecular proximity, conformations, and dynamics.

### 3.2 Introduction

Huntington's disease (HD) is an autosomal dominant, progressive neurodegenerative disorder caused by the expansion of a CAG trinucleotide repeat within the *Htt* gene<sup>7</sup>. The pathogenic threshold of CAG expansion is approximately 37 repeats, with increased repeats leading to an earlier age-onset of HD<sup>8-10</sup>. This CAG mutation results in an expanded polyglutamine tract in the amino-terminus of the gene's protein product, huntingtin<sup>7</sup>. To date, no phenotypes at the level of huntingtin molecular biology or animal models can be attributed to polyglutamine lengths near the human pathogenic disease threshold<sup>346</sup>.

Polyglutamine or glutamine-rich domains are also found in transcription factors such as the Sp-family and cAMP response element-binding protein (CREB), and are defined as protein-protein interaction motifs used to scaffold, and regulate transcription by RNA polymerase II<sup>347,348</sup>. In the transducin-like enhancer of split (TLE) co-repressor proteins, the glutamine-rich domains are thought to allow dimerization<sup>349</sup>. However, the role of polyglutamine in proteins like huntingtin may be distinct from that of a protein-protein interaction or dimerization domain.

The polyglutamine tract of huntingtin is flanked on the amino-terminal side by the first 17 amino acids, termed N17, an amphipathic  $\alpha$ -helical targeting domain that can mediate huntingtin localization to membranes<sup>50,73</sup>. The N17 domain can be modified post-translationally at multiple residues<sup>57,124,126,128</sup>. Within N17, phosphorylation of two serines at positions 13 and 16 are critical for modulating huntingtin localization during stress<sup>50,57</sup>, N17 structure<sup>57</sup>, and the toxicity of mutant huntingtin in cell biological and mouse models of HD<sup>57,126-128</sup>. We have previously demonstrated that mutant huntingtin is hypo-phosphorylated at serines 13 and 16; this results in an inability to respond to cell stress<sup>57</sup>.

On the carboxyl-terminal side of the polyglutamine tract is a region containing two pure proline tracts separated by a leucine-proline rich intervening region within the human huntingtin protein<sup>132</sup>. Similar to the N17 domain, interacting proteins within this polyproline region have been found to affect mutant huntingtin toxicity<sup>132</sup>. PACSIN1

(Protein kinase C and casein kinase 2 substrate in neurons) or syndapin1, binds directly to the polyproline domain<sup>350</sup>. This interaction is enhanced in the presence of expanded polyglutamine<sup>81</sup>. PACSIN1 is a predominantly cytoplasmic neuronal protein that has functions in NMDA receptor recycling<sup>81,113</sup>, actin/microtubule reorganization<sup>131</sup> and neuronal spine formation<sup>351</sup>. Both N17 and PACSIN1 are substrates of casein kinase 2 (CK2)<sup>57,350</sup>.

Since both of the flanking regions to the polyglutamine tract are critical in mediating the toxicity of the mutant huntingtin protein in mammalian and yeast models<sup>120</sup>, we wanted to determine whether the two domains could be interacting with each other in 3D space using the polyglutamine tract as a flexible region. To test this hypothesis, we developed a Förster resonance energy transfer (FRET) sensor with donor and acceptor fluorophores at the amino and carboxyl-termini of huntingtin fragments, respectively. Using fluorescence lifetime imaging microscopy (FLIM), we quantified the FRET efficiency of live cells expressing huntingtin fragments with multiple polyglutamine lengths. We discovered that the N17 domain folds back to the polyproline region of huntingtin and that this conformation is altered by expanded polyglutamine at the clinical pathogenic threshold for HD of 37 repeats.

We have previously used a chemical biology approach to determine that CK2 can phosphorylate huntingtin within N17. This could be prevented by treatment of cells with CK2 inhibitors<sup>57</sup>. Conversely, I $\kappa$ B kinase (IKK) inhibitors paradoxically increased phosphorylation of N17<sup>57</sup>. This suggested that the protective effect of serine 13 and 16 phospho-mimicry in the BACHD mouse model<sup>127</sup> may be attainable using small molecule treatments. The lipid ganglioside GM1 treatment of the YAC128 mouse model resulted in reversion of the HD motor phenotype to normal, and was found to restore the hypo-phosphorylation of mutant huntingtin at N17 to normal levels<sup>128</sup>. Therefore, we wanted to test if there was a direct effect of serines 13 and 16 on the conformation of the amino-terminus of huntingtin, and whether the conformations of huntingtin could be affected by phospho-mutants or true phospho-modulation of N17.

In order to translate this conformational sensor to look at endogenous huntingtin, we developed an antibody-based FLIM-FRET assay to measure the conformation of the

amino-terminus of huntingtin in the context of the full length protein. This assay confirmed the finding in human patient HD cells that N17 folds back to the vicinity of the polyproline region in endogenous huntingtin.

### 3.3 Materials & Methods

**Tissue Culture** : Immortalized mouse striatal *STHdh*<sup>Q7/Q7</sup> and *STHdh*<sup>Q111/Q111</sup> cell lines were cultured as previously described (10). Primary human fibroblasts from either a 54 year old unaffected female (Coriell catalogue #GM02149) or a 51 year old male with HD (Coriell catalogue # GM01061) were cultured as per Coriell Guidelines.

**Plasmid Constructs** : The huntingtin exon1 fragments with various glutamine lengths were generated from cDNA using forward primer GATCTCCGGAATGGCGACCCTG with a BSPEI restriction site and reverse primer GATCGGTACCGGGTCGGTGCAGCGGCTC with an ACC65I site. Huntingtin exon1 M8P, S13 and S16 mutants were generated from larger huntingtin 1-586 fragments described previously<sup>57</sup>, using forward and reverse primers described above. 1-117 fragments were generated using the same forward primer as for the exon1 constructs and the reverse primer GATCGGTACCGACAGACTGTGCCAC with an ACC65I restriction site. 1-171 fragments were also generated using the same forward primer as for the exon1 constructs and the reverse primer GATCGGTACCCTCGAGCTGTAACCTTGG with an ACC65I restriction site. 1-220 fragments were also generated using the same forward primer as for the exon1 constructs and the reverse primer GATCGGTACCCTTGCTTGTTCGAGTCAG with an ACC65I restriction site. 1-465 fragments were also generated using the same forward primer as for the exon1 constructs and the reverse primer GATCGGTACCGCTGCTGACATCCGATCT with an ACC65I restriction site. All insert PCR products were cloned into a modified mCer-C1 plasmid with an eYFP insert cloned into BamHI and XbaI sites at the opposing end of the multiple cloning site.

**Transfection** : Transfection of *STHdh* cells was done using TurboFect *in vitro* reagent (Fermentas, cat. # R0531) as previously described<sup>352</sup>. Transfection of human fibroblasts was done using the Lonza Amaxa 4D-Nucleofector X Kit L (Lonza, cat. # V4XC-3024) according to the instructions provided.

**Antibody Conjugation** : 2B7 (Novartis), 4C9 (Novartis) and C20 (Santa Cruz) antibodies were all conjugated using Alexa Fluor 488 (Invitrogen, cat.# A20181) or 546 (Invitrogen, cat. # A20183) monoclonal antibody labelling kit.

**Immunofluorescence** : *STHdh*<sup>Q7/Q7</sup> cells were seeded to ~80% confluency prior to fixation and permeabilization with ice cold methanol at -20°C for 12 minutes. Cells were then washed two times with PBS and blocked two times with 2% FBS in PBS. Primary antibodies for PACSIN1 (A-3, cat. # sc-166756, 1:50-100), N17 (generated to epitope MKAFESLKSFC, 1:250) and phospho-N17 S13 and S16 (generated to epitope MKAFESpLKSFC, 1:250) were then added to cells in a solution with 0.0005% Tween 20 (Sigma cat.# P9416), 2% FBS in PBS overnight and subsequently washed two times with blocker solution. Secondary antibodies raised against rabbit (Alexa Fluor 488 donkey anti-rabbit, cat. #A21206, 1:500) or mouse (Alexa Fluor 594 goat anti-mouse, cat. #A11032, 1:500) were then added to cells in antibody solution for 45 minutes and subsequently washed two times with PBS prior to imaging.

**Immunofluorescence for Antibody-Based FLIM** : Cells were seeded to 80% confluency prior to fixation for 30 minutes using 4% paraformaldehyde. Cells were washed three times with phosphate buffered saline (PBS) prior to being permeabilized with 0.5% Triton X-100, 2% FBS in PBS for 15 minutes. Cells were then washed two times with PBS and blocked two times with 2% FBS in PBS. Primary conjugated antibodies were then added to cells at optimized concentrations in a solution with 0.0005% Tween 20 (Sigma cat.# P9416), 2% FBS in PBS for ~16 hours each and subsequently washed two times with PBS.

**SiRNA Treatment** : *STHdh*<sup>Q7/Q7</sup> cells were treated with three PACSIN1 siRNAs (Santa Cruz cat. # SC-36172) as previously described<sup>58</sup>.

**Microscopy** : Widefield fluorescence images were captured on a Nikon TE200 epifluorescence inverted microscope equipped with a 63x oil immersion NA1.4 plan apochromat objective using a Hamamatsu Orca ER camera (Hamamatsu Photonics, Japan).

**Small Molecule and Kinase Inhibitor Treatments** : All compounds were used from sources and at concentrations optimized previously<sup>57,128</sup>. Ganglioside GM1 from bovine brain was sourced from Merck Millipore (cat. #345724).

**FLIM Image Analysis and subsequent statistical analysis** : Analysis of FLIM images was completed as previously described<sup>58,352</sup>.

### 3.4 Results

#### Huntingtin N17 Folds Back to the Polyproline Region

To test for an intramolecular interaction between the regions flanking the polyglutamine tract of huntingtin, we developed a conformational sensor using FRET efficiency as readout. We chose a fluorophore pair for FRET that consisted of a mCerulean donor and an enhanced yellow fluorescent protein (eYFP) acceptor<sup>329</sup>. FRET was calculated using fluorescence lifetime imaging microscopy (FLIM) by time-correlated single photon counting (TCSPC)<sup>333</sup>. Fluorescence lifetime refers to the amount of time a valence electron from a fluorophore remains in the excited state prior to returning to ground state and emitting a photon. The lifetime of a fluorophore can be directly affected by FRET, which results in a decrease in the donor fluorophore lifetime. All the necessary controls were performed to validate the fluorophore lifetime values in our live cell system (Figure 3.1A-C).

We constructed a FRET sensor using exon1 fragments of varying polyglutamine lengths with a donor and an acceptor fluorophore at the amino and carboxyl termini of exon1, with a 1:1 ratio of donor:acceptor. At a wild-type length of 17 polyglutamine repeats, we noted a robust lifetime decrease, thus a relative increase in percent FRET efficiency, indicating a close proximity of the donor and acceptor fluorophores (Figure 3.1D, H). This FRET was intramolecular, since co-expression of mCerulean-huntingtin exon1 and huntingtin exon1-eYFP together, on separate plasmids, did not result in a donor lifetime change at these expression levels (Figure 3.1E, G). When a similar sensor with a polyglutamine expansion of 138 repeats was tested, the fluorescence lifetime values were increased relative to the wild-type polyglutamine length, resulting in a reduced FRET efficiency (Figure 3.1F, H). We controlled for expression of huntingtin fragments levels in the assays to avoid the effects of protein aggregation on lifetime values.

Typical pathogenic polyglutamine lengths for mid-life onset of HD are between 45-50 repeats<sup>7</sup>, however HD is fully penetrant at any length over 40 repeats. Most HD models use huntingtin genes with very long CAG repeats (>100), in order to induce a

robust phenotype<sup>346</sup>. To date, no assay in live cells has noted a phenotype at polyglutamine lengths close to 37 repeats, or even typical HD repeat lengths. Using the huntingtin exon1 FRET sensor, we tested the effect of varying glutamine repeat lengths to determine if we could detect a conformational change at the pathogenic threshold for HD. We detected a significant decrease in FRET efficiency between 32 and 37 repeats, however minimal changes were measured between 37, 46 and 138 repeats (Figure 3.1H). To prove that the FRET efficiency changes we detected were not due to simply moving the acceptor probe farther away from the donor, we synthesized and tested an exon1 FRET sensor with only two glutamines. This construct resulted in a lower FRET efficiency relative to all other polyglutamine lengths tested, despite the shorter  $\alpha$ -carbon backbone (Figure 3.1H). To demonstrate that the intramolecular FRET between N17 and the polyproline region was not an artifact of the *STHdh*<sup>Q7/Q7</sup> cell type used, we repeated experiments using the exon1 FRET sensor with wild-type (Q17) and mutant (Q138) polyglutamine tracts in both NIH3T3 fibroblasts and primary human fibroblasts (Figure 3.S1A and B). Consistent with the data generated in the *STHdh*<sup>Q7/Q7</sup> cells, we measured higher percent FRET efficiencies with the wild-type versus the mutant sensor in both fibroblast cell lines.

Since we consistently measured the highest FRET efficiencies for huntingtin fragments with wild-type polyglutamine lengths, this suggested that the polyglutamine tract may exist as a flexible 'hinge' to allow the N17 domain to loop back and come into close spatial proximity with the polyproline region (Fig.1H, K and L). To test this hypothesis, we designed a synthetic exon1 fragment where we substituted the polyglutamine tract with a four glycine linker<sup>353</sup>. We detected a similar change in FRET efficiency with the exon1  $\Delta$ Q + 4 glycine construct relative to the exon1 Q17 FRET sensor, suggesting that wild-type polyglutamine tracts can behave similar to a flexible glycine linker (Figure 3.1I). Conversely, we hypothesized that the mutant polyglutamine expansion results in a diminished flexibility, which induces a conformational change in the amino terminus of huntingtin. To test the importance of the flanking sequences on the flexibility of the polyglutamine tract, we inserted pure polyglutamine tracts with either 17 or 46 repeats into the FRET sensor. For both constructs, we measured lower FRET efficiencies relative to the exon1 constructs. There was only a modest difference

between the wild-type and mutant pure polyglutamine constructs, indicating that just polyglutamine was not sufficient to properly place the amino and carboxyl termini in close proximity in the absence of flanking sequences of huntingtin (Figure 3.1J). Our next step was to analyze if we could detect polyglutamine dependent conformational changes in larger huntingtin fragments.

We then constructed FRET sensors with increasing fragment lengths of huntingtin in both the wild-type and mutant context (Figure 3.S2). FRET efficiency of the huntingtin 1-117 (exon1+2) sensor was higher than that of the exon1 sensor. This indicated that N17 was likely in closer proximity to a distal region of huntingtin beyond the polyproline region, or that additional amino acids beyond this domain were important to stabilize this conformation. As with the huntingtin exon1 sensor, polyglutamine expansion of huntingtin 1-117 resulted in a similar drop of FRET efficiency. Placement of the FRET acceptor at amino acids 171, 220 or 465 in huntingtin resulted in a drop in FRET efficiency, with no significant difference between polyglutamine lengths.

### **N17 Serine Phospho-Mimetics Affect Huntingtin Conformation**

To test the importance of serines 13 and 16 on the conformation of huntingtin exon1 in live cells, we generated constructs with N17 phospho-mimetic mutants in the context of the FRET sensor (Figure 3.S3). S13A/S16A mutations in either the Q17 (Figure 3.S3A) or Q142 (Figure 3.S3C) context of exon1 had little effect on the FRET efficiency of the sensor relative to wild-type N17 constructs (Figure 3.2A). However, S13E/S16E substitutions in both the wild-type (Figure 3.S3B) and mutant (Figure 3.S3D) context significantly reduced FRET efficiency (Figure 3.2A). Previously, we demonstrated that phosphorylation and phospho-mimicry at serine residues 13 and 16 disrupted the structure of N17<sup>57</sup>, whereas a proline substitution at methionine 8 (M8P) completely abolished N17 structure<sup>50</sup>. In the context of the FRET sensor, the M8P mutation with either Q17 (Figure 3.S3E) or Q150 (Figure 3.S3F), both resulted in a significant decrease in FRET efficiency (Figure 3.2A). The result with the M8P mutant was consistent with the control experiment of just 17 or 46 glutamines in the FRET sensor (Figure 3.1J). Thus, we conclude that the structure of N17 contributes to the overall conformation of the amino terminus of huntingtin as well as the proximity of N17

to the polyproline region. The caveat of this data is that phospho-mimicry is not true phosphorylation. To address this, we used a chemical biology approach with kinase inhibitors that we previously described as modulating the phosphorylation of huntingtin in N17<sup>57</sup>.

### **Kinase Inhibitors Directly Affect the Conformation of Amino-Terminus of Huntingtin**

In order to study the effects of phospho-modulation on the conformation of the amino-terminus of huntingtin, we used kinase inhibitors known to either inhibit or promote phosphorylation at serine residues 13 and 16 of N17<sup>57</sup>. N17 phosphorylation can be inhibited by CK2 inhibitors DMAT (2-Dimethylamino-4,5,6,7-tetrabromo-1H-benzimidazole) and quinalizarin (1,2,5,8-tetrahydroxyanthraquinone). Alternatively, N17 phosphorylation can be promoted by treatments with IKK inhibitors, the ATP analog Bay 11-7082 ((E)-3-(4-methylphenylsulfonyl)-2-propenenitrile) and the allosteric inhibitor BMS-345541 (N-(1,8-Dimethylimidazo[1,2-a]quinoxalin-4-yl)-1,2-ethanediamine hydrochloride). These compounds were tested on *STHdh*<sup>Q7/Q7</sup> cells expressing the polyglutamine expanded (Q138) huntingtin FRET sensor (Figure 3.2B). Unlike alanine substitutions, CK2 inhibition by DMAT and quinalizarin caused an increase in FRET efficiency by affecting the conformation of mutant huntingtin exon1. This indicates that the hydroxyl side group of the serine is important for the contribution of N17 to huntingtin conformation. IKK inhibition by Bay-11-7082 and BMS-345541, leading to hyper-phosphorylation of N17<sup>57</sup>, resulted in reduced FRET efficiency to a greater extent than phospho-mimicry (Figure 3.2B versus Figure 3.2A). From these data, we concluded that the promotion of huntingtin N17 phosphorylation by IKK inhibitors showed similar effects to phospho-mimicry on the conformation of soluble mutant huntingtin.

### **PACSIN1 Interacts with Both the N17 and Polyproline Domains of Huntingtin**

PACSIN1 has previously been reported to interact with the proline-rich intervening region of the polyproline domain of huntingtin, in a polyglutamine length-dependent manner<sup>81</sup>. Using co-immunoprecipitation, we were able to purify PACSIN1

using the N17 domain alone (Figure 3.S4A). Importantly, although both N17 and PACSIN1 are substrates of CK2, treatment of cells with the DMAT prior to co-immunoprecipitation had little effect on the amount of PACSIN1 recovered using N17. This indicated that the phosphorylation state of N17 or PACSIN1 does not affect the interaction between the two proteins.

Co-immunofluorescence with antibodies recognizing PACSIN1 and N17 demonstrated that these two proteins show a high degree of signal overlap in the cytoplasm (Figure 3.3A). When co-immunofluorescence was done using antibodies raised towards PACSIN1 and N17 S13pS16p, we observed no signal overlap in the cytoplasm, instead both proteins were strongly co-localized to nuclear puncta (Figure 3.3B). When we treated cells with compounds that are known to decrease (DMAT; Figure 3.3C) or increase (BMS-345541; Figure 3.3D) the phosphorylation of huntingtin at residues S13 and S16<sup>57</sup>, we noted a profound effect on the larger morphology and reduced number of the puncta present in the nucleus.

PACSIN1 interacts with both the N17 and polyproline domains that flank the polyglutamine tract of huntingtin, which we hypothesized may stabilize the positioning of these two domains in close 3D proximity. To determine the involvement of PACSIN1 between these domains, we tested our huntingtin exon1 FRET sensor following treatment of the cells with a cocktail of three small interfering RNAs (siRNA) directed to mouse PACSIN1. Both a western blot and immunofluorescence were performed to confirm the efficacy of the knock-down (Figure 3.S4B-D). In cells expressing the wild-type huntingtin FRET sensor (Q17), treatment with PACSIN1 siRNAs significantly reduced FRET efficiency, whereas this was not seen with the mutant polyglutamine expanded FRET sensor (Q138) (Figure 3.S4E). Our data indicates that PACSIN1 may facilitate the proximity of N17 and polyproline by acting as a scaffold to bridge these two domains.

## Measuring the Conformation of the Amino-Terminus within the Context of Full Length, Endogenous Huntingtin

Making protein fusions with fluorophores at both termini can alter the folding dynamics and conformations of huntingtin fragments. We were also limited by the need to overexpress the FRET sensor to super-physiological concentrations in order to collect enough photons to generate accurate fluorophore lifetime decay curves. Thus, we wanted to determine if we could measure the conformation of the amino-terminus of huntingtin within the context of the full length protein at endogenous expression levels, based on evidence of a N17-polyproline proximity learned from the exon1 FRET sensor. We conjugated several primary antibodies raised to epitopes known to fall between residues 1 and 117 of huntingtin. We chose to use both the 2B7 and the 4C9 monoclonal antibodies that target residues 8-13 of the N17 domain and residues 61-71 of the polyproline region of huntingtin, respectively<sup>319</sup>. As an optimal pair for FLIM-FRET, we chose to conjugate the antibodies with either alexa488 or alexa546 dyes.

We tested the lifetime of both alexa488 alone and the alexa488-2B7 conjugate *in vitro* and measured a lifetime of ~4.0 nsecs, consistent with others<sup>354</sup>. Despite these values, the lifetimes of the 2B7-alexa488 conjugate alone in the *STHdh*<sup>Q7/Q7</sup> and *STHdh*<sup>Q111/Q111</sup> cell lines was consistently reduced to ~2.6 nsecs (Figure 3.S5A). The fluorescent lifetime of a molecule is dependent on many factors, which may be affected by the fixative and/or permeabilization agent used to perform immunofluorescence. However, since the calculation of FRET efficiency in the cell is dependent on the relative lifetimes of donor with and without acceptor present, we felt confident that using alexa488 as a donor in fixed cells remained valid. When we compared FRET efficiency values between *STHdh*<sup>Q7/Q7</sup> and *STHdh*<sup>Q111/Q111</sup> lines both stained with 2B7-alexa488 and 4C9-alexa546 conjugates, we measured a significantly lower percent FRET efficiency in the mutant compared to the wild-type cells (Figure 3.4A). As a negative control, we used an acceptor conjugated to an antibody that recognized an epitope at the carboxyl terminus of huntingtin (C-20) and saw no significant change in the donor lifetime. This was due to the acceptor conjugate now being too far away from the donor

for FRET. Thus, using this antibody-based assay on full length, endogenous huntingtin, we were able to recapitulate our earlier findings with the huntingtin exon1 FRET sensor.

In order to assess the effects of phosphorylation on the conformation of the amino-terminus within the context of the full length huntingtin protein, we used two compounds known to promote phosphorylation at serine residues 13 and 16 of N17: BMS-345541 and ganglioside GM1<sup>57,128</sup>. Treatment of *STHdh*<sup>Q7/Q7</sup> cells with either BMS-345541 or GM1 for 16 hours caused a significant reduction of the percent FRET efficiency relative to the non-treated control (Figure 3.4B). These data were consistent with our earlier findings using the exon1 FRET sensor, that phosphorylation of N17 affects the conformation of the amino-terminus of huntingtin.

Next, we wanted to test our antibody-based FLIM-FRET assay on human HD patient cells, rather than models of HD. We chose to use untransformed human fibroblasts from a 54 year old unaffected female and a 51 year old male with HD. Using 2B7 and 4C9 conjugates in these cells, we were able to detect a robust conformational difference of huntingtin in these HD patient fibroblast samples relative to those from the unaffected individual (Figure 3.4C,D). This conformational difference was measured as a significant decrease in the overall FRET efficiency in the HD versus the wild-type fibroblasts (Figure 3.4E). Thus, using this assay, we measured a difference in huntingtin conformation in fibroblasts between normal and HD individuals.

### 3.5 Discussion

A long-standing question in HD research has been why clinical CAG repeat lengths beyond 37 repeats result in pathogenesis, while even a few repeats below this number do not<sup>355</sup>. Animal models of HD require very long polyglutamine tracts to elicit any obvious phenotypic changes; however, using our huntingtin exon1 FRET sensor, we have been able to detect a conformational switch between 32 and 37 glutamine repeats in live cells.

Huntingtin is one of nine polyglutamine expansion disease proteins, where the biological role of normal polyglutamine tracts in these proteins is not understood<sup>40</sup>. In transcription factors such as the Sp-family, CREB and TLE, glutamine-rich domains are thought to mediate protein-protein interactions and/or dimerization<sup>347-349</sup>. Our data demonstrates that polyglutamine or glutamine-rich regions may also represent a domain of required flexibility to mediate interactions between flanking protein-protein interaction domains.

All mammalian species have a huntingtin protein that contains at least four glutamines in their polyglutamine tract. In vertebrate species that contain only two glutamines, the proline-rich region is absent<sup>68</sup>. The reduced FRET efficiency observed with the synthetic huntingtin exon1 Q2 FRET construct suggests that the polyglutamine tract may be a critical conformational hinge in the amino-terminus, allowing N17 to interact with regions downstream. This hinge hypothesis is consistent with the X-ray crystal structures that have been solved with wild-type exon 1<sup>76</sup>, and molecular dynamics simulations<sup>134</sup>.

We hypothesize that the decrease of FRET efficiency with mutant fragments is due to a gain of structure in the polyglutamine tract, leading to a reduced flexibility of the hinge region. *In vitro*, expanded polyglutamine tracts can adopt a rigid  $\beta$ -sheet structure<sup>193</sup>. Therefore, our FLIM-FRET data are consistent with the “rusty hinge” hypothesis<sup>133</sup>, where the expansion of polyglutamine leads to reduced flexibility of the tract, resulting in multiple inflexible conformations of the amino-terminus. We hypothesize, as have others, that the normal polyglutamine tract in huntingtin is

disordered<sup>356</sup>. We suggest that polyglutamine tract in proteins may contribute to a phenomenon of stochastic protein conformations and interactions termed “fuzzy complexes”<sup>357</sup>. A caveat of using FLIM-FRET to measure conformations of huntingtin is that the data do not tell us exactly what the conformations of the tested proteins are, only the differences between the tested constructs.

The effects of CK2 and IKK inhibitors on skewing the conformation of soluble huntingtin indicate that a protective conformation of mutant huntingtin may be pharmacologically induced by correcting the hypo-phosphorylation seen in mutant huntingtin<sup>57</sup>. Treatment of cells with IKK inhibitors caused an increase in phosphorylation at serines 13 and 16 of N17, which we measured as a decrease in the percent FRET efficiency and interpreted as a change in conformation of the huntingtin. We hypothesized that this decrease in FRET efficiency was either due to a loss of the  $\alpha$ -helical structure of N17 or due to a change in the interaction network with N17 as a result of phosphorylation. However, since the readout for FLIM is either an increase or a decrease in FRET efficiency values relative to a control, the decrease in FRET efficiency seen following promoting phosphorylation of N17 cannot be compared to the decrease measured when the sensor has an expanded polyglutamine tract.

IKK is a critical regulator of neuroinflammation which has been implicated in the pathogenesis of HD<sup>358</sup>. IKK inhibitors form a class of compounds in development for disease therapy<sup>359</sup>. In terms of potential therapy for HD, the inhibition of IKK may have two complementary effects, on promoting the phosphorylation of N17 and reducing mutant huntingtin induced neuroinflammation. The challenges for the future will be to develop compounds that increase or stabilize the phosphorylation of N17 and can effectively cross the blood-brain barrier.

The antibody-based FRET assay on endogenous huntingtin could be useful to track huntingtin conformational changes with respect to disease progression, as well as act as a biomarker for compounds that may affect huntingtin conformation by altering huntingtin post-translational modifications.

The biology of PACSIN1 overlaps heavily with known pathways affected in Huntington's disease, namely the recycling of NMDA receptors<sup>113</sup> and the formation of neuronal spines<sup>351</sup>. PACSIN1 is known to directly interact with human huntingtin within the polyproline region<sup>81</sup>, and we have additionally shown that PACSIN1 interacts with the N17 domain. This suggests that PACSIN1 may stabilize or modulate the conformation of the amino-terminus of huntingtin. Both N17 and PACSIN1 are substrates for CK2<sup>57,350</sup>. Therefore, the effect of the CK2 inhibitors on the conformation of the exon1 sensor may not only be due to post-translational modification of N17 but also that of PACSIN1. As a corollary, both the N17 and polyproline regions of huntingtin exon1 are also known to interact with actin, either directly with N17<sup>60</sup>, or indirectly through the actin-binding protein, profilin, with the polyproline domain<sup>80</sup>. This may indicate the consequence of proper huntingtin conformation and conformational switching on the regulation of actin dynamics during stress<sup>58</sup>. The role of PACSIN1 in the nucleus is not known, but the properties of F-BAR domains<sup>106</sup> suggest that its role at nuclear puncta may be to either induce or recognize structure of chromatin.

In another polyglutamine expansion disease, spinocerebellar ataxia type 1 (SCA1), individuals have been described with a CAG expansion in the ATXN1 gene, yet with no disease pathology. This is due to the presence of interrupting CAT codons that result in histidine amino acids within the polyglutamine tracts<sup>360</sup>, that reduce aggregation and enhance solubility<sup>361</sup>. This suggests that interrupting codons within the polyglutamine tract in these proteins may have a phenotypic effect on disease by affecting the flexibility of the polyglutamine tract and/or the ability of expanded polyglutamine to form structure.

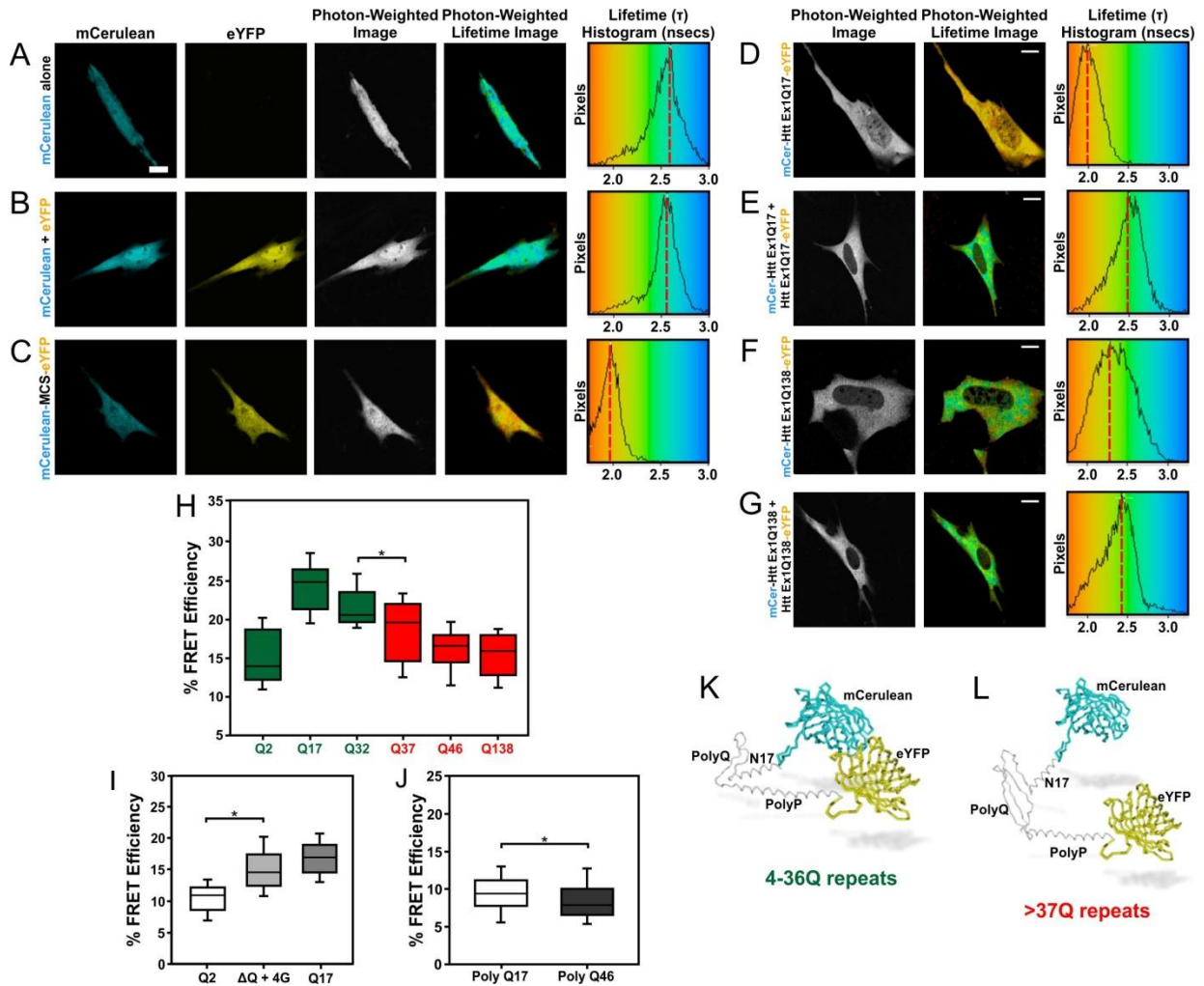


**Figure 3.1. Huntingtin exon1 FLIM-FRET sensor.** Sample live cell fluorescence and FLIM images for the (A) mCerulean (mCer) donor alone control, (B) mCer co-expressed with the YFP acceptor control and for (C) mCer-MCS-YFP positive control. Sample FLIM images of (D) mCer-huntingtin exon1 Q17-eYFP (mCer-HttEx1 Q17-eYFP) fusion, (E) mCer-HttEx1 Q17 + HttEx1 Q17-eYFP control for inter-molecular FRET, (F) mCer-HttEx1 Q138-eYFP fusion, and (G) mCer-HttEx1 Q138 + HttEx1 Q138-eYFP control for inter-molecular FRET expressed in *STHdh<sup>Q7/Q7</sup>* cells. (H) FLIM-FRET data using the mCer-HttEx1-eYFP FRET sensor with varying lengths of polyglutamine. Black lines represent the median value, boxes encompass 25% and 75% confidence intervals, and whiskers indicate the 5% and 95% confidence intervals. \*  $P < 0.001$ .  $N = 50$ , 4 replicates. Box-whisker plot shows data for all trials. (I) FRET efficiency comparing mCer-HttEx1 Q2-YFP and the mCer-HttEx1 Q17-YFP FRET sensor to the mCer-HttEx1  $\Delta Q + 4$  glycines-YFP positive control. \* $P < 0.001$ .  $N = 90$ , 3 replicates. (J) FRET efficiency of 17 and 46 glutamines. \* $P < 0.001$ .  $N = 100$ , 3 replicates. Models of huntingtin FRET sensor with (K) wild-type and (L) mutant polyglutamine lengths. Scale bars are 10  $\mu\text{m}$ .

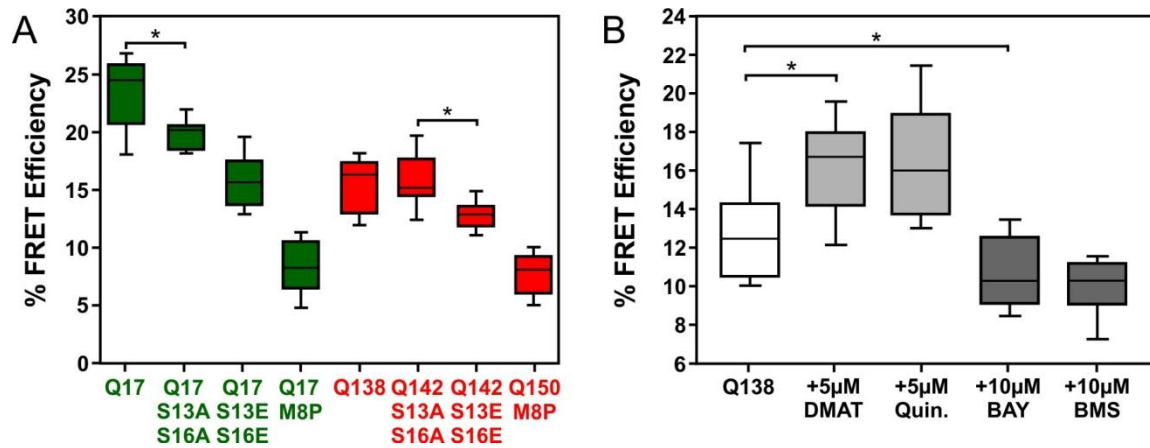


**Figure 3.2. N17 phospho-mimicry mutants and kinase inhibitors can affect the conformation of huntingtin exon1.** (A) Percent FRET efficiency for mCer-HttEx1 Q17 or Q142-eYFP with serines 13 and 16 mutated to alanines or glutamic acids, mCer-HttEx1 Q17 or Q150-eYFP with the M8P mutation. \* $P < 0.001$ .  $N = 40$ , 4 replicates. (B) Percent FRET efficiency for the mCer-HttEx1 Q138-eYFP sensor following no treatment, treatment with CK2 inhibitors (DMAT, Quinalizarin), or treatment with IKK inhibitors (Bay 11-7082, BMS-345541). \* $P < 0.001$ .  $N = 30$ , 3 replicates.

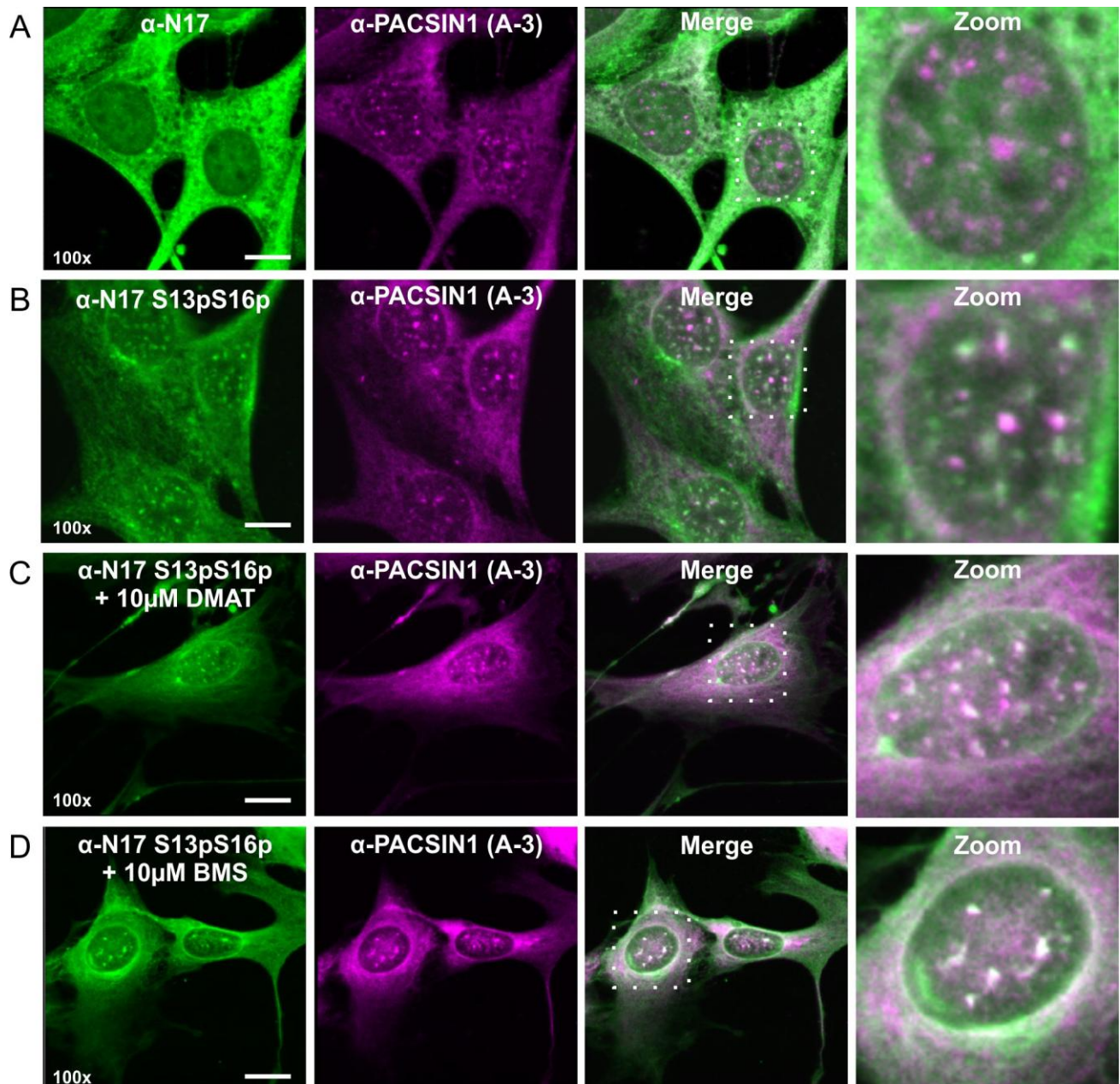


**Figure 3.3. PACSIN1 interacts with N17 and facilitates the proximity between N17 and the polyproline region of huntingtin.** Co-immunofluorescence images of *STHdh*<sup>Q7/Q7</sup> cells taken at 100x magnification using an anti-PACSIN1 antibody (A-3) and (A) N17 or (B) N17 S13pS16p, respectively. Immunofluorescence against PACSIN1 and N17 S13pS16p was also done on *STHdh*<sup>Q7/Q7</sup> cells following 16hr treatments with either (C) 10μM DMAT or (D) 10μM BMS-345541. Scale bars are 10μm.

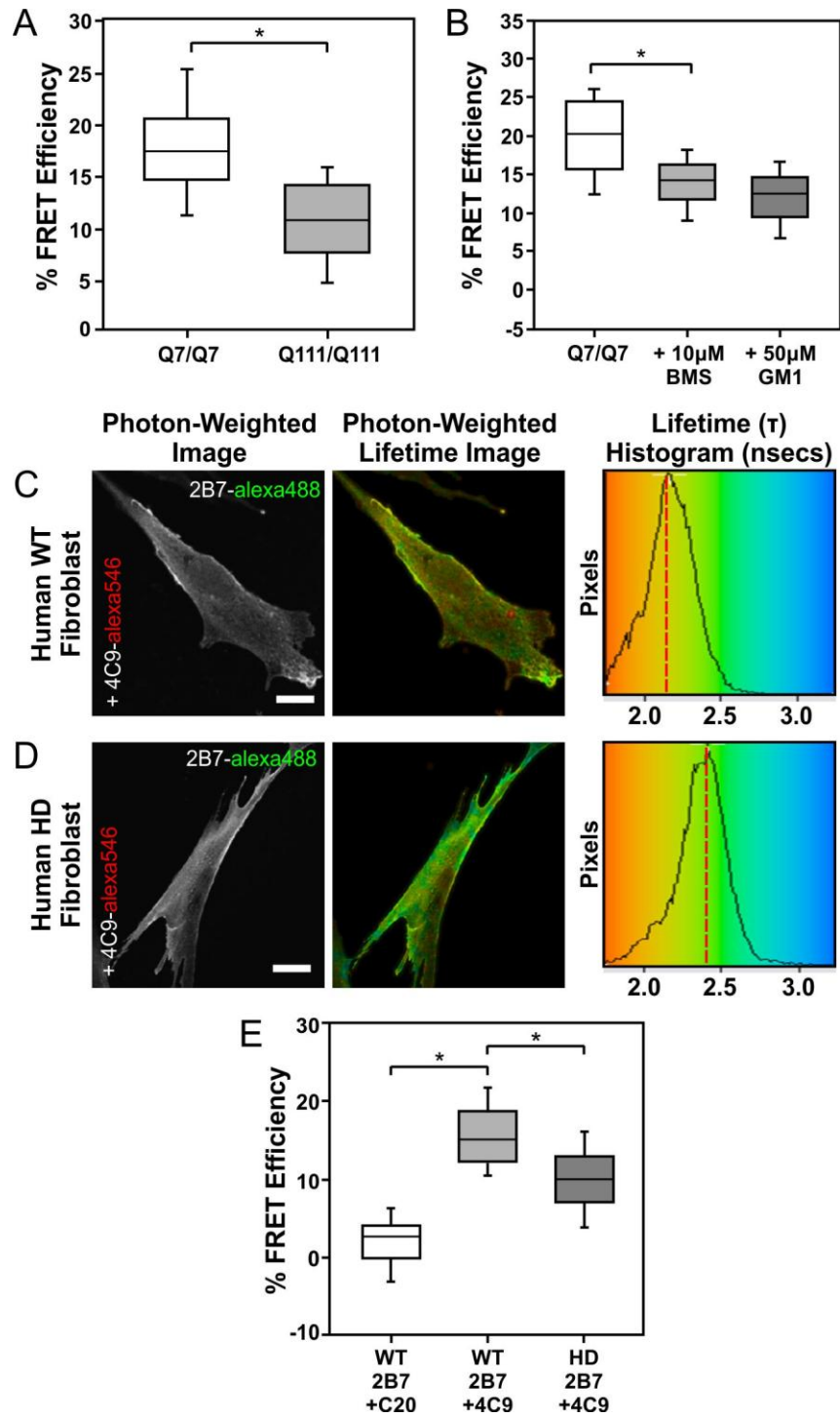


**Figure 3.4. An antibody-based FLIM-FRET assay to measure the conformations of the amino-terminus of full-length huntingtin.** (A) Percent FRET efficiency for the amino-terminus of huntingtin in *STHdh*<sup>Q7/Q7</sup> versus *STHdh*<sup>Q111/Q111</sup> cells following immunofluorescence with conjugated primary antibodies 2B7 and 4C9. \*P <0.001. N=150, 5 replicates. (B) Percent FRET efficiency for the amino-terminus of huntingtin in *STHdh*<sup>Q7/Q7</sup> following treatment with 10µM BMS-345541 or 50µM ganglioside GM1. \*P <0.001. N=100, 3 replicate trials. FLIM images of 2B7-alexa488 and 4C9-alexa546 conjugates in fixed (C) wild-type or (D) HD patient fibroblasts. (E) FRET efficiency for the amino-terminus of huntingtin in wild-type vs HD fibroblasts with conjugated primary antibodies 2B7/C20 or 2B7/4C9. \*P <0.001. N=100, 3 replicates. Scale bars are 10µm.

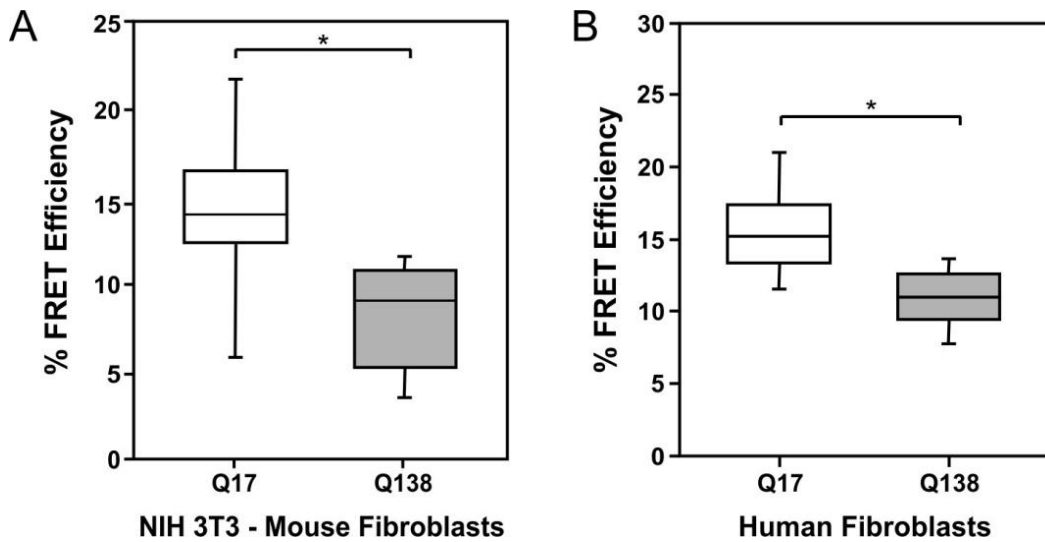


**Figure 3.S1. Huntingtin FRET sensor in fibroblasts.** Quantification of huntingtin exon1 FRET sensor with either wild-type (Q17) or mutant (Q138) polyglutamine lengths in (A) NIH3T3 mouse fibroblasts or (B) human fibroblasts. \*P < 0.001. N=30, 3 replicate trials and N=70, 3 replicate trials, respectively. Scale bars are 10 $\mu$ m.

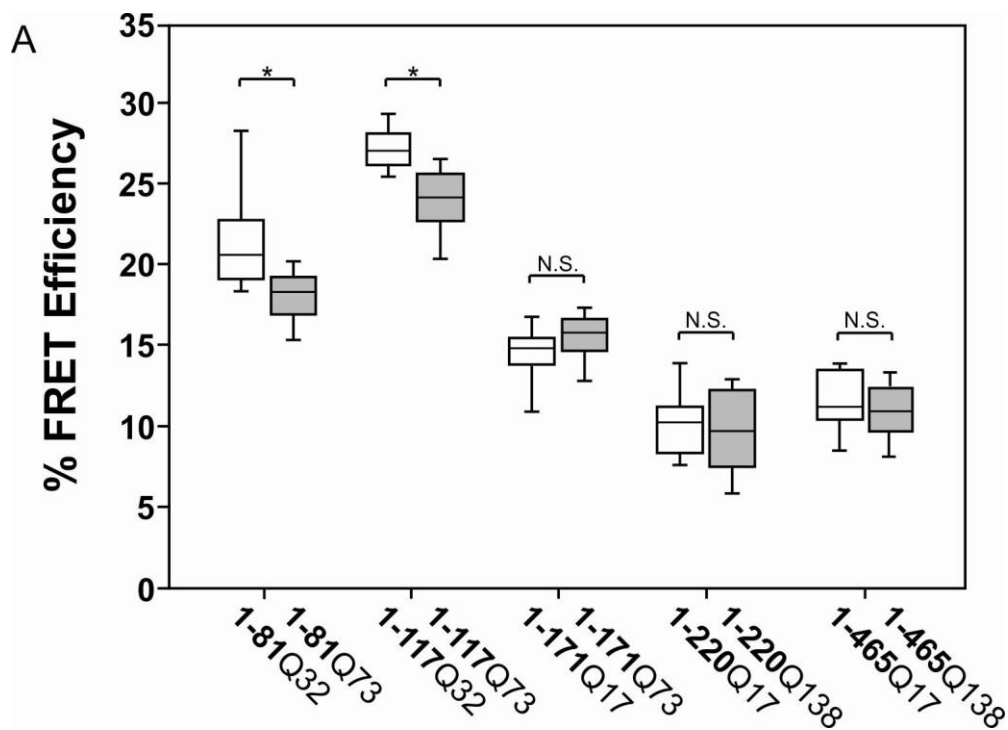


**Figure 3.S2. Measuring the conformation of wild-type and mutant polyglutamine tracts in the context of longer huntingtin fragments. (A)** Quantification of various huntingtin FRET sensors in different fragment length contexts with either wild-type or mutant polyglutamine lengths. FRET efficiency drops when the acceptor is placed at 171 or further downstream, with no notable differences between wild-type and expanded polyglutamine lengths. \* $P < 0.001$ , NS= not statistically significant.  $N=15$ , 3 replicate trials. Scale bars are  $10\mu\text{m}$ .

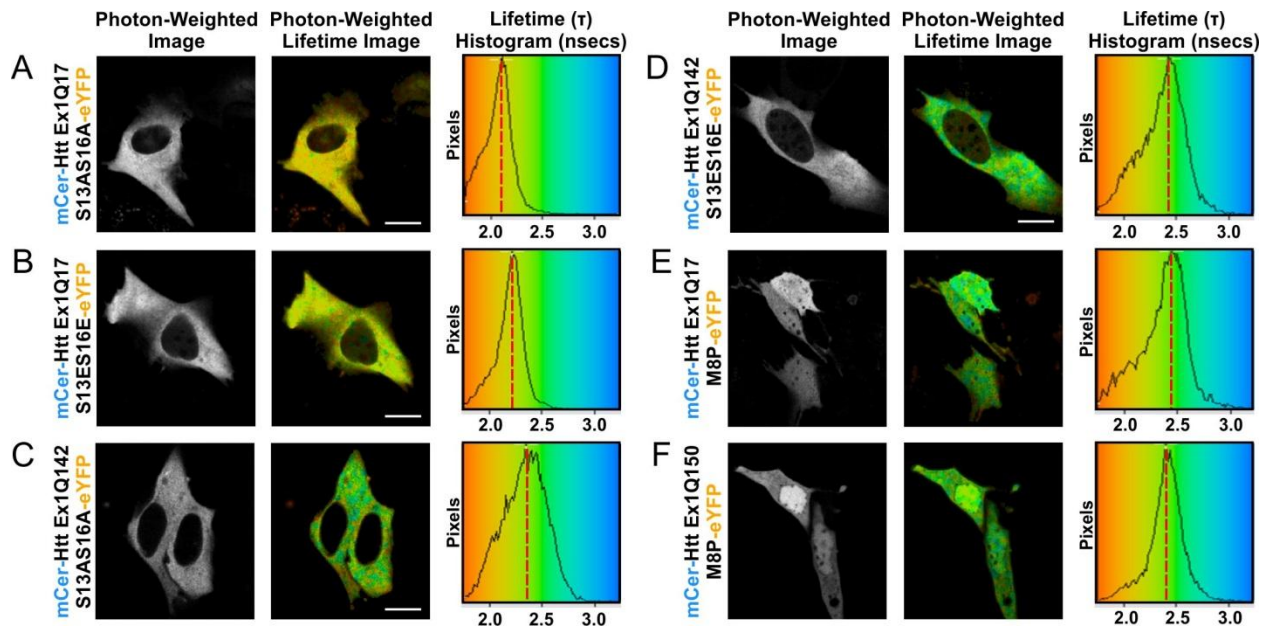


**Figure 3.S3. N17 phospho-mimicry mutants can affect the conformation of huntingtin exon1.** (A-D) Sample live cell FLIM images of mCerulean-HttEx1 Q17 or Q142-eYFP constructs with serine 13 & 16 point mutations expressed in *STHdh*<sup>Q7/Q7</sup> cells. Sample FLIM images of (E) mCerulean-HttEx1 Q17-YFP or (F) mCerulean-HttEx1 Q150-eYFP with the M8P loss-of-structure mutation in N17 (note nuclear localization).

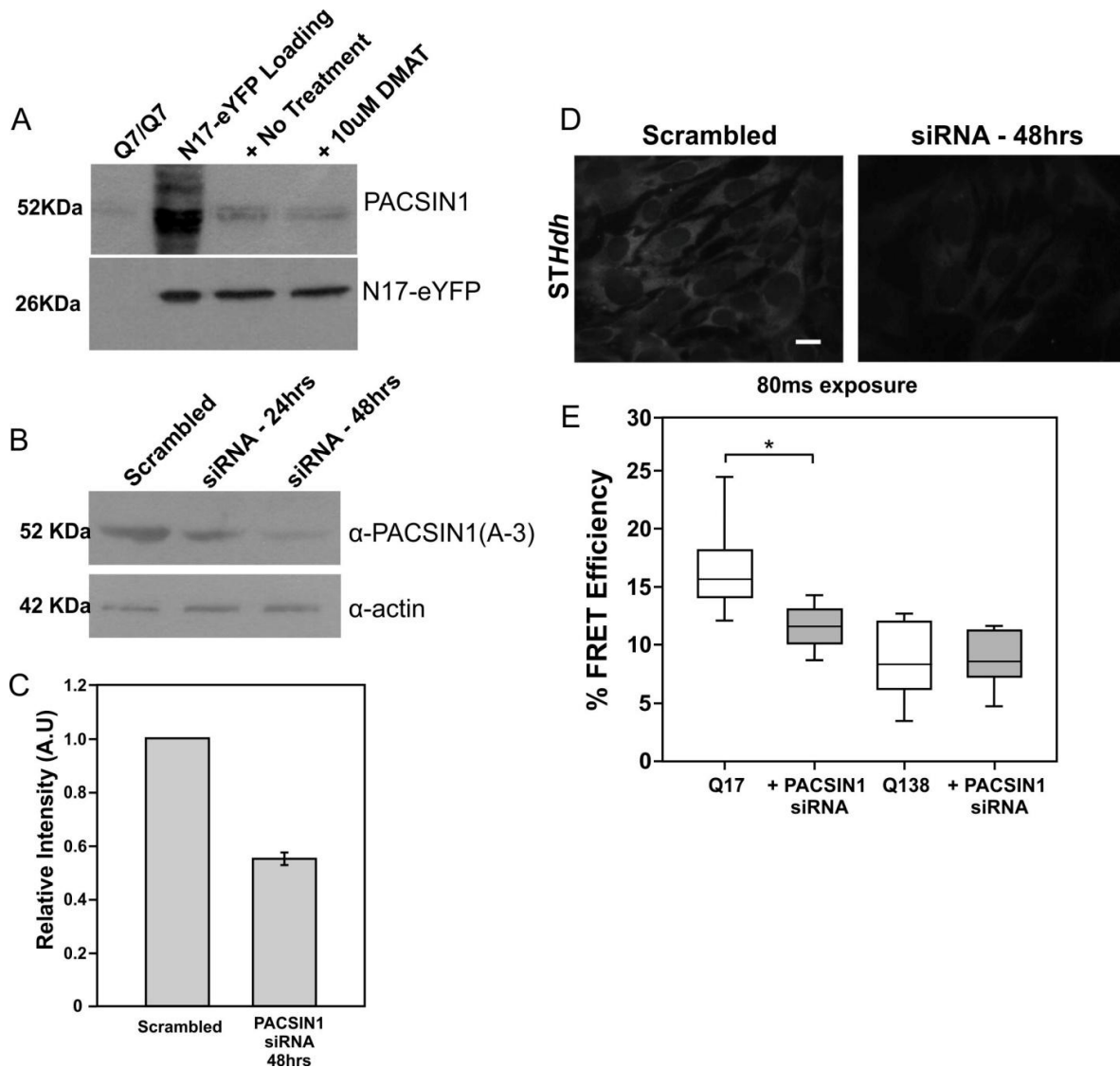


**Figure 3.S4. Co-immunoprecipitation and siRNA of PACSIN1.** (A) Representative co-immunoprecipitation of endogenous PACSIN1 using a N17-eYFP fusion in *STHdh*<sup>Q7/Q7</sup>. Scale bars are 10 $\mu$ m. (B) Western blot showing levels of PACSIN1 knock-down following treatment of *STHdh*<sup>Q7/Q7</sup> cells with 3 siRNA's targeted towards mouse PACSIN1. Actin was used to control for equal loading. (C) Quantification on Western blots of PACSIN1 knockdown following 48 hour treatments with PACSIN1 siRNA. (D) Immunofluorescence for PACSIN1 following treatment of cells with siRNA to PACSIN1. Images were taken at 80 msec exposure. Scale bars are 10 $\mu$ m. (E) FRET efficiency for either venus-HttEx1 Q17-mCherry or venus-HttEx1 Q138-mCherry following treatment with a control siRNA or against endogenous PACSIN1. \*P <0.001. N=15, 3 replicate trials.

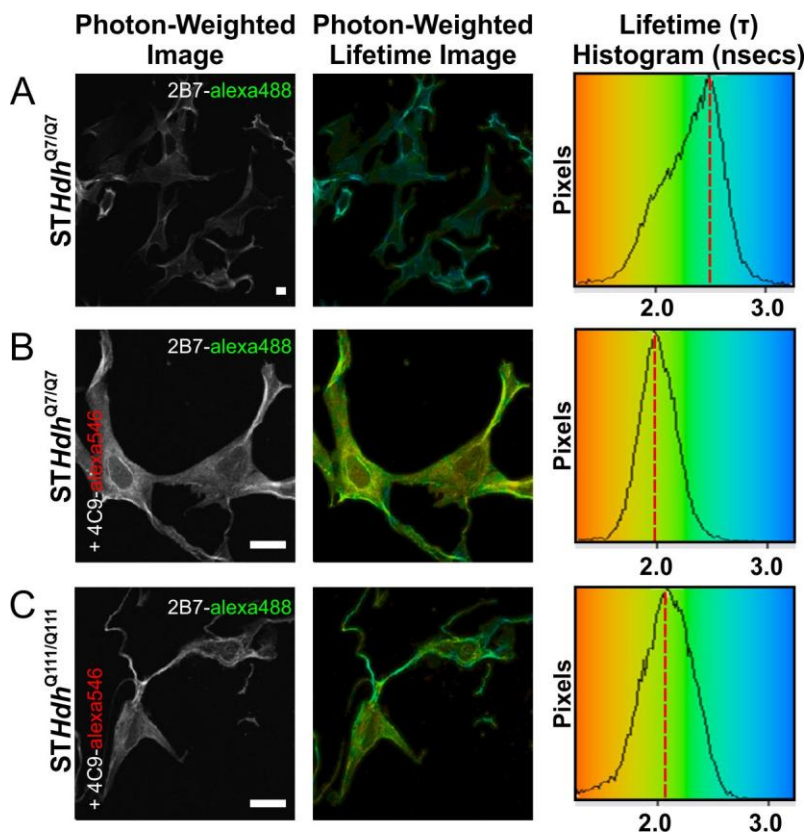


**Figure 3.S5. FLIM-FRET of endogenous huntingtin using monoclonal antibodies.**

(A) FLIM image of 2B7-alexa488 conjugate in fixed *STHdh*Q7/Q7 cells. FLIM image of 2B7-alexa488 and 4C9-alexa555 conjugates in fixed (B) *STHdh*Q7/Q7 cells or (C) *STHdh*Q111/Q111 cells.

### **3.6 Acknowledgements**

This work is supported by a Canadian Institutes of Health Research grant, MOP-119391, and a grant from the Krembil Family Foundation of Toronto with the Huntington Society of Canada. We would like to thank Dr. Andreas Weiss (IRBM Promidis Srl) for providing us with monoclonal antibodies for use with the full-length huntingtin FLIM-FRET assay.

## Chapter 4 - Mutant Huntingtin Forms Toxic and Protective Inclusions

### Preamble

This is a pre-copy-editing, author-produced PDF of an article accepted for publication in *Human Molecular Genetics* following peer review. The definitive publisher-authenticated version of:

**Caron, N.S., Hung, C.L., Atwal, R.S. & Truant, R.** Live cell imaging and biophotonic methods reveal two types of mutant huntingtin inclusions. *Hum Mol Genet* (2014)

is available online at:

<http://hmg.oxfordjournals.org/content/early/2014/01/09/hmg.ddt625.long>

The only changes made to this publication were for thesis continuity and formatting.

NC & CH performed all the experiments

NC performed data analysis

NC, RSA & RT designed the experiments

NC wrote the manuscript and CH helped with editing and revisions

## **Live Cell Imaging and Biophotonic Methods Reveal Two Types of Mutant Huntingtin Inclusions**

Nicholas S. Caron<sup>1§</sup>, Claudia L. Hung<sup>1§</sup>, Randy S. Atwal<sup>2</sup>, Ray Truant<sup>1\*</sup>.

<sup>1</sup>Department of Biochemistry and Biomedical Sciences. McMaster University, Hamilton, Ontario, Canada. L8N 3Z5.

<sup>2</sup> Department of Neurology, Harvard Medical School, Massachusetts General Hospital, Boston, Massachusetts, USA. 02114.

§ Equal contribution on experiments for manuscript.

\*To whom correspondence should be addressed. HSC 4N54, 1200 Main Street West, Hamilton, ON, Canada L8N3Z5. [truantr@mcmaster.ca](mailto:truantr@mcmaster.ca)

## 4.1 Abstract

Huntington's disease (HD) is an autosomal dominant, neurodegenerative disorder that can be characterized by the presence of protein inclusions containing mutant huntingtin within a subset of neurons in the brain. Since their discovery, the relevance of inclusions to disease pathology has been controversial. We show using super-resolution fluorescence imaging and Förster resonance energy transfer (FRET) in live cells, that mutant huntingtin fragments can form two morphologically and conformationally distinct inclusion types. Using fluorescence recovery after photobleaching (FRAP), we demonstrate that the two huntingtin inclusion types have unique dynamic properties. The ability to form one or the other type of inclusion can be influenced by the phosphorylation state of serine residues at amino acid positions 13 and 16 within the huntingtin protein. We can define two types of inclusions: fibrillar, which are tightly packed, do not exchange protein with the soluble phase, and result from phospho-modification at serines 13 and 16 of the N17 domain, and globular, which are loosely packed, can readily exchange with the soluble phase, and are not phosphorylated in N17. We hypothesize that the protective effect of N17 phosphorylation or phospho-mimicry seen in animal models, at the level of protein inclusions with elevated huntingtin levels, is to induce a conformation of the huntingtin amino-terminus that causes fragments to form tightly packed inclusions that do not exit the insoluble phase, and hence exert less toxicity. The identification of these sub-types of huntingtin inclusions could allow for drug discovery to promote protective inclusions of mutant huntingtin protein in HD.

## 4.2 Introduction

Huntington's disease (HD) is a progressive, neurodegenerative disease caused by a CAG trinucleotide expansion within the *Htt* gene that codes for a polymorphic polyglutamine tract near the amino-terminus of the 350kDa huntingtin protein<sup>7</sup>. Individuals having polyglutamine tracts with 4 to 36 repeats do not develop disease, whereas those with tracts exceeding the critical threshold of 37 glutamines develop HD pathology with an inverse correlation between age-onset and CAG expansion length<sup>8,10</sup>. The huntingtin protein is ubiquitously expressed in every human cell, yet neurodegeneration in early HD is selectively restricted to the basal ganglia and cerebral cortex of the brain. Huntingtin is a highly conserved protein across vertebrates and is involved in a variety of cellular functions including roles in vesicular transport<sup>96,97,362</sup>, transcriptional regulation<sup>159-161,363</sup> and cytoskeletal dynamics<sup>58,364</sup>. The diverse functions of huntingtin likely stem from its ability to promote molecular interactions by behaving as a scaffold protein<sup>74</sup>. The polyglutamine expanded mutant huntingtin protein disrupts many of these critical cellular functions. Notably, polyglutamine expanded huntingtin can aggregate to form inclusion bodies, where a cellular hallmark of HD is the presence of mutant huntingtin containing inclusions within neurons and glia of human patient brains<sup>21</sup>.

The ability of mutant huntingtin fragments to form cytoplasmic and nuclear inclusions was initially described in the R6/2 transgenic HD mouse model, which expresses human huntingtin exon1 with a CAG expansion<sup>20,189</sup>. Brain slices from the R6/2 mice revealed the presence of numerous inclusion bodies composed of mutant huntingtin fragments that stained positive for ubiquitin<sup>189</sup>. Similar inclusions reported in human HD patient brains also contained amino-terminal fragments of huntingtin and stained positive for ubiquitin<sup>21</sup>.

Many studies have demonstrated that full-length huntingtin can be proteolytically cleaved to produce several prominent amino-terminal fragments, the smallest being exon1 (huntingtin 1-81)<sup>83,167-169,179,365</sup>. Furthermore, aberrant splicing of the huntingtin mRNA transcript can lead to the translation of the pathogenic exon1 huntingtin protein in HD mouse models and HD human fibroblasts<sup>366</sup>. Therefore, it is hypothesized that

small fragments of mutant huntingtin occur naturally in HD brains where they self-associate to form inclusions.

Protein aggregation occurs in most neurodegenerative disorders including Alzheimer's disease (AD), Parkinson's disease (PD), amyotrophic lateral sclerosis (ALS) and the polyglutamine disorders. In these diseases, aggregated protein commonly forms either amyloid or amorphous aggregates. Amyloid aggregates are highly insoluble and have a rigid  $\beta$ -sheet structure, whereas amorphous aggregates are unstructured<sup>367</sup>. The classic amyloid hypothesis defines the deposition of misfolded amyloid- $\beta$  protein into insoluble plaques within the brain as one of the primary pathogenic causes of neurodegeneration in AD<sup>186,187</sup>. The amyloid hypothesis has since been revised and adapted to describe a common pathogenic mechanism for most neurodegenerative diseases<sup>188</sup>. In HD, this hypothesis is often referred to as the toxic fragment hypothesis<sup>122,123,167</sup>. It postulates that the proteolytic cleavage of mutant huntingtin generates toxic amino-terminal fragments that can misfold and accumulate in neuronal inclusions, leading to the neurodegeneration associated with HD. For the sake of nomenclature consistency, this manuscript will refer to aggregated mutant huntingtin in concentrated puncta as inclusion bodies.

Several pathogenic mechanisms have been proposed to describe the toxicity of mutant huntingtin inclusions in HD. Inclusions have been implicated in neuronal death by sequestering critical cellular proteins leading to their functional loss<sup>196</sup>, physically occluding active vesicle trafficking between the nucleus and neuronal extremities<sup>203</sup>, and by impairing ubiquitin-dependent proteolysis of misfolded proteins by the proteasome<sup>194</sup>. Alternative hypotheses view inclusion formation as being either benign or even neuroprotective<sup>121</sup>. Live cell imaging in neurons reveals that the presence of huntingtin exon1 fragment inclusions correlates with enhanced survival, relative to neurons expressing exon1 without inclusions<sup>121,195</sup>. It has been proposed that the response to mutant huntingtin-induced cell stress is the formation of these inclusions, which accumulate and sequester mutant protein. These studies identify the soluble monomeric or oligomeric forms of mutant huntingtin as being the cytotoxic species. This is observed by the protective effect of the polyglutamine-binding peptide (QBP1) in

cultured cells, which preferentially binds soluble mutant huntingtin<sup>193</sup>. Using high-throughput screens, compounds have been identified that can paradoxically reduce cellular toxicity by either inhibiting<sup>245</sup> or promoting<sup>248</sup> the formation of mutant huntingtin inclusions. Studies like these have necessitated the need to revisit the toxic fragment hypothesis for HD<sup>133</sup>.

HD is one of nine CAG trinucleotide repeat disorders that are all caused by expanded polyglutamine tract lengths within different cellular proteins<sup>40</sup>. Despite the commonality between the polyglutamine disorders, each of these diseases typically affect only a specific subset of neurons within the brain<sup>40</sup>. Furthermore, the polyglutamine thresholds for disease pathology in most of the CAG trinucleotide diseases differ from the 37 repeats required for HD, which suggests that the context of polyglutamine within the pathogenic protein is important. Thus, some studies have focused on the importance of the sequences flanking the polyglutamine tract in mediating the toxicity of mutant huntingtin as well as its ability to form inclusions<sup>120,368</sup>. The N17 domain of huntingtin comprises the first 17 residues of the protein prior to the polyglutamine tract. N17 adopts an amphipathic alpha-helical structure that allows it to interact with various proteins in the cytoskeleton and to associate with membranes<sup>50,73</sup>. Recent studies performed by our group and others have shown that introducing serine 13 and 16 mutations within N17 can influence the ability of mutant huntingtin to form inclusions, the rate of inclusion formation, and also the morphology of the huntingtin inclusions<sup>57,127</sup>. Additionally, promoting phosphorylation at residues 13 and 16 of the N17 domain has been shown to alleviate mutant huntingtin toxicity in an animal model of HD<sup>128</sup>. Flanking the polyglutamine tract on the carboxyl-terminus is a region with two pure proline tracts separated by a proline-rich region. This domain has also been shown to interact with a variety of proteins that directly impact the toxicity of mutant huntingtin and its ability to form inclusions<sup>80,81</sup>. Therefore, these studies strongly implicate the importance of flanking sequences to the polyglutamine tract in modulating toxicity and inclusion formation.

Previously, our group developed a Förster resonance energy transfer (FRET) sensor to demonstrate that the polyglutamine tract of huntingtin can behave as a hinge,

allowing the N17 domain to fold back onto the distal polyproline region of huntingtin<sup>368</sup>. FRET involves the non-radiative transfer of energy between a donor and an acceptor molecule, which allows for the high spatial resolution of dynamic molecular interactions and conformational changes in live cells<sup>58,327,352</sup>. The exon1 FRET sensor was used to measure the intramolecular interactions between N17 and the polyproline domain as an indication of the conformation of soluble huntingtin in live cells. Here, we have applied the mutant huntingtin exon 1 fragment FRET sensor to observe the organization of polyglutamine expanded huntingtin within protein inclusions, measuring the intermolecular interaction between individual huntingtin fragments. We demonstrate using FRET, fluorescence recovery after photobleaching (FRAP) and super-resolution fluorescence imaging that mutant huntingtin fragments can form two morphologically and dynamically distinct inclusion types. We also show that the morphology of inclusions can be influenced by altering the phosphorylation state of serines 13 and 16 of N17. The definition of two distinct inclusion types, and the ability to identify them could lead to new insights into the controversy of the role of protein inclusions in HD and other polyglutamine diseases.

### 4.3 Materials and Methods

**Tissue Culture** : Immortalized mouse striatal *STHdh*<sup>Q7/Q7</sup> cells were grown as previously described<sup>50</sup>.

**Plasmid Construct** : The huntingtin exon1 Q138 sensor was generated from cDNA using forward primer GATCTCCGGAATGGCGACCCTG with a *BspEI* restriction site and reverse primer GATCGGTACCGGGTTCGGTGCAGCGGCTC with an *Acc65I* site. The PCR insert was then cloned into either a YFP-N1 plasmid (Clontech) or a modified mCerulean-C1 plasmid (Clontech) with an eYFP insert cloned into *BamHI* and *XbaI* sites at the opposing end of the multiple cloning site. The HA-tagged constructs were generated using synthetic oligos (MOBIX) GATCCTACCCATACGATGTTCCAGATTACGCTT with a *BamHI* restriction site overhang and CTAGAAGCGTAATCTGGAACATCGTATGGGTAG with an *XbaI* restriction site overhang. The insert was then cloned into a huntingtin exon 1 Q138 or huntingtin 1-171 Q138 vector.

**Transfection** : Transfection of *STHdh*<sup>Q7/Q7</sup> cells was done using TurboFect *in vitro* reagent (Fermentas, R0531) as previously described<sup>368</sup>.

**Primary Antibodies** : The huntingtin specific mouse monoclonal 1HU-4C8 (Millipore International, MAB2166) and HDC8A4 (Pierce Antibodies, MA1-82100) antibodies were used to perform immunofluorescence (IF) of endogenous huntingtin in *STHdh*<sup>Q7/Q7</sup> cells.

**Immunofluorescence** : IF on *STHdh*<sup>Q7/Q7</sup> cells to visualize endogenous huntingtin was done either using the antigen retrieval or the methanol method. For the antigen retrieval method, cells were fixed with 4% paraformaldehyde for 20 min at 4°C. Cells were then washed 2X with PBS and treated with 10% formic acid for 20 min at room temperature. Cells were then washed again 2X with PBS and subsequently permeabilized with Triton X-100 detergent (BioShop, TRX777.100) for 10 min at room temperature. Using the methanol method, cells were fixed and permeabilized using ice-cold methanol for 12 min at -20°C. Consistent between both methods, cells were then blocked 3X with 2% FBS in PBS blocking solution. Primary antibodies were added to cells at a concentration of 1:100 in a solution of 2% FBS in PBS with 0.02% TWEEN 20 (Sigma, P9416).

Antibodies were then labelled with the far-red Cy5 (Molecular Probes, A10524) (ex 650 nm/em 670 nm) dye at a concentration of 1:500.

To visualize overexpressed huntingtin HA-tagged constructs, IF was done using the antigen retrieval method described above. Primary antibody to the HA tag (Abcam, AB16918) was added to the cells at a concentration of 1:250 in a solution of 2% FBS in PBS with 0.02% TWEEN20. Antibodies were then labeled with the AlexaFluor 488 (Molecular Probes, A21206) (ex 499 nm/em 519 nm) dye at a concentration of 1:500.

For visualization of ubiquitin, immunofluorescence was done using antigen retrieval method with an anti-ubiquitin antibody (Sigma, SAB4503053) added to the cells at a concentration of 1:100 in a solution of 2% FBS in PBS with 0.02% TWEEN20. For visualization of  $\beta$ -tubulin, IF was done with 4% PFA fixation without antigen retrieval with an anti  $\beta$ -tubulin antibody (University of Iowa Hybridoma Bank, E7-S) at a concentration of 1:250 in 2% FBS in PBS with 0.02% TWEEN20. Both anti-ubiquitin and anti  $\beta$ -tubulin primary antibodies were labelled with Cy5 dye at a concentration of 1:500.

**Imaging** : Live cell temporal videos of inclusion formation were acquired with a 40x air objective using a Lumascope 500 inverted widefield epifluorescent microscope (Etaluma Inc., Carlsbad, CA, USA) housed in an incubator regulated at 33°C with 5% CO<sub>2</sub>.

Inclusion imaging was done with a 60x oil immersion objective (PlanApo N.A.= 1.4) on a Nikon Eclipse Ti2000 inverted widefield epifluorescent microscope using the Orca-Flash4.0 CMOS camera (Hamamatsu, Japan). Image acquisition was done using the NIS-Elements Advanced Research version 4.10.01 64-bit acquisition software from Nikon (Nikon, USA). Z-stacks of inclusions were acquired using a motorized stage (Prior Scientific, USA) with step sizes of 0.3 – 0.5 $\mu$ m. Deconvolution was done on z-stacks using the AutoQuant blind deconvolution module as part of the NIS-Elements version 4.10.01 software package (Nikon, USA). Iso-surface rendering on inclusions was applied using the Imaris software from Bitplane (AG).

**Thioflavin-T Amyloid Fibril Staining** : After 24 h of expression of Ex1 Q138-mRFP, transfected *STHdh*<sup>Q7/Q7</sup> cells were fixed with 4% PFA for 30 min and stained with 0.05%

thioflavin-T for 8 min (Sigma, T3516). Cells were washed 3x with PBS and imaged. Positive control for the assay was *STHdh*<sup>Q7/Q7</sup> cells transfected with A $\beta$  1-42-mRFP with 24 h of expression. Cells were fixed and stained as described above.

**Native Polyacrylamide Gel Electrophoresis** : Cell samples were lysed using an NP-40 lysis buffer on ice for 15 min. Supernatants were collected and the remaining pellet was resuspended in NP-40 lysis buffer and sonicated. Protein concentrations for soluble and insoluble fractions were calculated using a Bradford assay. Samples were prepared with a non-reducing loading buffer without boiling. The 7% acrylamide gels and running buffers were prepared without SDS or any other reducing agents.

**Small Molecule Treatments** : Transfected *STHdh*<sup>Q7/Q7</sup> cells were treated with compounds at concentrations optimized previously<sup>57</sup>. Cells were treated with compounds for ~16 h prior to experiments.

**Time-Domain Fluorescence Lifetime Imaging Microscopy (FLIM) and Analysis** : Time-domain FLIM and analysis of FLIM data was performed as previously described<sup>352</sup>.

**Sensitized Emission FRET (seFRET)** : seFRET was performed using the FRET module as part of NIS-Elements version 4.10.01. All controls were performed as required by the FRET module. Percent FRET efficiency values were calculated by the module using equations derived from the Gordon method. A rainbow look-up table was applied to the ratiometric FRET image to show the range of FRET efficiency values.

**Statistical Analysis** : All statistical analyses were done using the SigmaPlot software 11.0 (Systat Software Inc.). For comparisons between two groups, Student's *t*-tests were performed if data passed the normality assumptions. If data did not pass the normality test, it was analyzed by the Mann-Whitney method. For multiple pairwise comparisons, one-way analysis of variance (ANOVA) using the Student-Newman-Keuls method was performed if the data passed the normality test of distribution. If the data did not pass the normality assumptions, then we performed a one-way ANOVA on ranks using the Tukey test. For FLIM quantifications, every cell was represented as its own N

and the box-whisker plot graph was generated using cumulative data from 3 independent trials.

## 4.4 Results

### Huntingtin Fragments Can Form Morphologically Unique Inclusion Types

Using fluorescence microscopy imaging, deconvolution and iso-surface rendering, we were able to identify two morphologically distinct types of inclusions formed by the overexpression of mutant huntingtin fragments in striatal neuron derived *STHdh<sup>Q7/Q7</sup>* cells (Figure 4.1). Image deconvolution involves capturing multiple images in the z plane and using algorithms to restore the out-of focus light to one focal point in a quantitative manner, increasing the signal-to-noise ratio and resolution. Two different mutant huntingtin (Q138) fragments were generated by fusing a fluorophore at the carboxyl-terminus to generate huntingtin exon1 Q138-YFP (Ex1 Q138-YFP) and huntingtin amino acids 1-171 Q138-YFP (1-171 Q138-YFP). The first type of inclusion, which we termed fibrillar, appears to lack a defined shape and is composed of mutant huntingtin fibres organized in an astral morphology (Figure 4.1A). The second type, which we termed globular, tends to be spherically shaped with discrete and well-defined edges (Figure 4.1B). To further distinguish the morphologies of these inclusions, super-resolution structured illumination microscopy (SR-SIM) was used, a method that improves lateral resolution to ~100nm by illuminating the sample with a series of excitation light patterns<sup>369</sup>. Imaging revealed very distinct morphologies between the globular inclusions (Figure 4.1C) and fibrillar inclusions (Figure 4.1D), highlighting a cytoskeletal element in the globular inclusion.

To confirm that these different inclusion types were not just an artifact of the fluorescent protein fusion, we also generated huntingtin constructs with a small hemagglutinin (HA) tag and expressed them in *STHdh<sup>Q7/Q7</sup>* cells. Immunofluorescence with additional antigen retrieval revealed that both huntingtin exon1 Q138-HA (Ex1 Q138-HA) and 1-171 Q138-HA fragments can form both fibrillar and globular inclusion types (Figure 4.S1). Thus, these morphologies were validated as fluorescent protein fusions, allowing further observations in live cells.

In addition to characterizing the inclusions by their morphology, the fibrillar type of inclusion can be distinguished from the globular type using a thioflavin-T staining

assay. Thioflavin-T is commonly used to stain amyloid fibrils with a detectable  $\beta$ -sheet structure<sup>370</sup>. Fibrillar inclusions were thioflavin-T positive (Figure 4.2A), while globular inclusions did not show thioflavin-T specific staining (Figure 4.2B). As a positive control, *STHdh*<sup>Q7/Q7</sup> cells were transfected with amyloid-beta 1-42-mRFP ( $A\beta$  1-42-mRFP), the amyloid fibril-forming cleavage product of the amyloid precursor protein in AD. Inclusions formed from the overexpression of the amyloid- $\beta$  construct stained positive for thioflavin-T ((Figure 4.2C).

IF against ubiquitin was performed to test whether one or both types of inclusions consisted of misfolded protein. Both types of inclusions formed in *STHdh*<sup>Q7/Q7</sup> cells transfected with Ex1 Q138-HA revealed ubiquitinated protein, however, no difference in ubiquitination between types was detected (Figure 4.S2).

### **FLIM-FRET Reveals Two Conformationally Distinct Inclusion Types Formed by Mutant Huntingtin Fragments**

Despite their unique phenotypes, visually distinguishing between the two types of inclusions was challenging due to the high intensity and diffraction-limited spatial resolution of these inclusions using standard microscopy. To overcome these limitations, we implemented FRET-based techniques to study these two types of inclusions at nanometer (nm) resolution in live cells. FRET is a well-established technique used to measure molecular interactions and conformational changes in live cells<sup>327</sup>. As donor and acceptor probes for FRET, we chose a well-established FRET pair consisting of a cyan fluorescent protein variant, mCerulean (mCer), and an enhanced yellow fluorescent protein (eYFP)<sup>328,329</sup>. The most accurate method of measuring FRET is using FLIM, where fluorescence lifetime refers to the amount of time a valence electron remains in the excited state prior to returning to ground state and emitting a photon<sup>316,330</sup>. The lifetime of a fluorophore can be directly affected by the biochemical and biophysical properties of the surrounding microenvironment; notably, FRET between two molecules causes a decrease<sup>316</sup> in the donor fluorophore lifetime<sup>316</sup>. All controls for FLIM were performed to validate the use of mCer and eYFP as a FRET pair in our live cell system (Figure 4.S3).

To determine if we could detect FRET changes when huntingtin fragments were organized into higher-order inclusion structures within live *STHdh<sup>Q7/Q7</sup>* cells, we tested the huntingtin exon1 Q138 sensor tagged at the amino-terminus with mCer and at the carboxyl-terminus with eYFP (mCer-Ex1 Q138-eYFP). Using FLIM to measure FRET, we were able to accurately measure intra- and intermolecular interactions between individual huntingtin molecules during the nucleation and maturation of inclusions, allowing us to differentiate between the two inclusion types based on overall structure. The fibrillar type of inclusion consistently had significantly higher percent FRET efficiency values relative to the globular type of inclusion (Figure 4.3A, B, D). This suggested a higher degree of interaction within or between huntingtin molecules in the fibrillar inclusions compared to the globular type. To determine whether the FRET we measured was a result of intra- or intermolecular FRET, we co-expressed mCer-Ex1 Q138 and Ex1 Q138-eYFP constructs on separate plasmids and measured fluorescence lifetime at both fibrillar (Figure 4.3C) and globular (data not shown) inclusions. Since the lifetimes at fibrillar and globular inclusions were similar to those found using the FRET sensor, we concluded that the majority of the FRET measured at each type of inclusion was a result of intermolecular FRET between huntingtin fragments.

In order to acquire higher spatial resolution of FRET values within each inclusion type, we collected z-stacks and performed deconvolution on both fibrillar and globular inclusions formed by the huntingtin exon1 FRET sensor. FRET efficiency was calculated using seFRET as an alternative to FLIM-FRET. seFRET is a technique in which the excitation of the donor leads to the non-radiative transfer of energy between the probes, causing an increase in fluorescence intensity of the acceptor (sensitized emission) that can be quantified to generate ratiometric FRET images<sup>315</sup>. Consistent with the data collected using FLIM, we observed that the FRET within fibrillar inclusions was dramatically higher than that in the globular type of inclusions (Figure 4.3E, F). Additionally, we noted a heterogeneous distribution of FRET efficiency values within the fibrillar inclusions; ranging from high FRET in the centre to progressively lower FRET towards the edges of the inclusion (Figure 4.3F). This suggested tighter, more densely packed huntingtin molecules at the core of fibrillar inclusions relative to the edges, and

overall more loosely packed protein in globular inclusions (Figure 4.3E), throughout the entire volume of the inclusion.

### **FRAP Demonstrates that the Fibrillar and Globular Inclusion Types have Distinct Exchange Dynamics**

Next, we used FRAP to gain insight into the recruitment dynamics of the mutant huntingtin protein entering both fibrillar and globular inclusions within live *STHdh*<sup>Q7/Q7</sup> cells. FRAP uses photolysis to permanently destroy the fluorophore of a fluorescent protein with high-intensity light. Any signal seen in a region of interest (ROI) over time is the result of unbleached molecules entering this space, thus giving a read-out of protein dynamics<sup>371,372</sup>. We precisely photobleached both types of inclusions and measured the recovery of fluorescence to these ROI over time. The fluorescence recovery to the ROI in this assay represented the recruitment of soluble polyglutamine expanded huntingtin into inclusions. We observed that the fluorescence recovery within the globular type of inclusion occurred rapidly relative to the fibrillar inclusion type (Figure 4.4A, B). The recovery of fluorescence to each inclusion type was temporally quantified for both Ex1 Q138-YFP and 1-171 Q138-YFP. The globular inclusions recovered significantly faster than the fibrillar types for both constructs (Figure 4.4C, D).

To test whether inclusion formation could recruit and sequester the soluble huntingtin protein, we monitored inclusion formation temporally within *STHdh*<sup>Q7/Q7</sup> cells over 24 h periods using an environmentally controlled microscope system (33°C, 5% CO<sub>2</sub>). We observed that the formation of the globular inclusions did not affect the fluorescence of the soluble mutant huntingtin within the cells (Figure 4.4E). Conversely, the formation of fibrillar inclusions progressively caused all the soluble mutant huntingtin in the cell to be absorbed and sequestered to the inclusion (Figure 4.4F). We quantified the recruitment of soluble huntingtin into inclusions by temporally measuring the loss of fluorescence from a specific ROI in the cytoplasm of cells forming inclusions following expression of either Ex1 Q138-YFP (Figure 4.4G) or 1-171 Q138-YFP (Figure 4.4H). We measured significantly more fluorescence loss in cells forming fibrillar compared to globular inclusions at multiple time points (Figure 4.4G, H).

## **Mutant Huntingtin is Actively Recruited to Globular Inclusions by Microtubules**

In order to investigate whether mutant huntingtin inclusions localized to components of the cytoskeleton, IF was performed against  $\beta$ -tubulin, actin and vimentin. Globular inclusions were found to localize along microtubule filaments (Figure 4.5A) whereas fibrillar inclusions did not (Figure 4.5B). To test if mutant huntingtin was being actively recruited to either inclusion type along cytoskeletal structures, we treated cells expressing the mutant exon1 fragment with compounds that would inhibit microtubule or actin polymerization. We noted that live cells expressing mutant exon1 for ~10 hours treated with low concentrations of nocodazole, a potent inhibitor of microtubule polymerization, greatly reduced the formation of large globular inclusions and caused many smaller inclusions to be dispersed throughout the cytoplasm after ~3 hours of treatment (Figure 4.5C). These results complement our FRAP data which demonstrated that fluorescence within the globular inclusions recovered rapidly as if recruitment of mutant huntingtin was driven via an active process. This was further demonstrated by temporal observation of the effect of nocodazole on fully formed globular inclusions (Figure 4.5E). Cells expressing mutant exon1 for 24 hours revealed that large globular inclusions could break up into smaller inclusions due to the disruption of the active recruitment of mutant huntingtin. Notably, treatment with the highest concentrations of nocodazole had no effect on the formation of fibrillar inclusions within the cell (Figure 4.5D). Treatment of live cells with phalloidin, a potent inhibitor of actin polymerization, had no effect on the formation or size of either fibrillar or globular inclusion types (data not shown). Therefore, these data support the hypothesis that mutant huntingtin is being shuttled into globular inclusions via molecular motors on microtubules, whereas mutant huntingtin is being recruited to fibrillar inclusions by passive diffusion.

## **Temporal FRET Reveals Distinct Formation and Maturation Dynamics of Fibrillar and Globular Inclusions**

To gain further insight into the structure of both inclusion types during their formation and maturation in live cells, we used the huntingtin exon1 sensor to generate temporal FRET videos using the seFRET technique. For these temporal experiments we substituted mCerulean for mTurquoise2 (mTq2) due to its increased brightness and

photostability over other cyan fluorescent protein variants<sup>373</sup>. seFRET is an appropriate method in this context because the donor and acceptor fluorophores have approximately the same quantum yield, and expression levels are identical due to the fixed 1:1 ratio of the sensor. This method allows rapid and continuous temporal measurements of FRET. The FRET images were pseudocoloured with a lookup table (LUT) where FRET efficiency values correspond to the color ramp presented in the bottom left corner of each image. Following expression of mTq2-Ex1 Q138-eYFP in *STHdh*<sup>Q7/Q7</sup> cells for ~24 h, we measured the changes in FRET efficiency at 2 min intervals for 60 min. The formation of fibrillar inclusions caused a dramatic increase in relative FRET efficiency over the period of observation (Figure 4.6A, B). These high FRET values measured in fibrillar inclusions using seFRET were consistent with the relative values measured using FLIM, and thus validated the use of seFRET in our system with the huntingtin sensor. Conversely, the formation and maturation of globular inclusions did not cause any significant increase in FRET efficiency over time, despite having comparable fluorescence intensities to the fibrillar inclusions (Figure 4.6C, D). As a control to normalize FRET values between inclusion types, we captured a cell that formed both a fibrillar and globular inclusions (Figure 4.6E, F, white arrows F, G). As seen in cells forming only one type inclusion, fibrillar formation caused a drastic increase in FRET efficiency whereas globular formation caused little to no FRET changes above background values (Figure 4.6E, F).

### **Full-Length, Endogenous Huntingtin Is Actively Recruited to Globular Inclusions and Sequestered Within Fibrillar Inclusions**

In order to validate the physiological relevance of studying huntingtin exon1 inclusions, we wanted to test whether endogenous huntingtin could be recruited and sequestered to sites of mutant huntingtin aggregation. Most standard methods of cell fixation for IF fall within two categories: the crosslinking (aldehydes) and the denaturing (alcohol) fixatives. Therefore, we tried both fixation methods with a variety of permeabilization techniques to determine which would be optimal to assay the presence of endogenous huntingtin within exon1 inclusions. To label endogenous huntingtin we chose validated huntingtin monoclonal antibodies 1HU-4C8 (MAB2166) which

recognizes an epitope between amino acids 181-810 of huntingtin and HDC8A4 which recognizes amino acids 2703-2911. These antibodies were generated to huntingtin epitopes downstream of exon1 (amino acids 1-81) and therefore do not recognize the overexpressed Ex1 Q138-YFP. To control for spectral bleed through between channels due to the high fluorescence intensity of the inclusions, all primary antibodies were indirectly labelled with a Cy5 conjugated secondary antibody that is spectrally distinct from YFP. Fixation with PFA followed by antigen retrieval using formic acid and permeabilization with a detergent allowed us to detect full length, endogenous huntingtin at fibrillar (Figure 4.7A, C) but not globular (Figure 4.7B, D) inclusions using both 1HU-4C8 (Figure 4.7A, B) and HDC8A4 (Figure 4.7C, D) antibodies. Alternatively, fixation and permeabilization with methanol, which denatures cellular proteins by disrupting hydrophobic interactions, caused loss of the fluorescence at the globular but not the fibrillar type of inclusion (Figure 4.S4A). Notably, 1HU-4C8 (Figure 4.S4B), MAB2168 (Figure 4.S4C) and HDC8A4 (Figure 4.S4D) antibodies detected full-length huntingtin within the fibrillar inclusions under these conditions. Despite attempting every permutation of fixative and permeabilization agents to perform IF, we were never able to identify increased endogenous huntingtin at globular inclusions. This result was consistent with the fragment FRET and FRAP data, where soluble huntingtin had a low residence time in globular inclusions.

### **N17 Phospho-Mutants Influence Huntingtin Inclusion Morphology**

Phospho-modifications of serine residues 13 and 16 within N17 have been shown to affect the localization and toxicity of huntingtin within the cell<sup>50,57,127</sup>. Previous work by others with synthetic huntingtin 1-50 peptides have shown that phospho-mimicry at serines 13 and 16 alters inclusion morphology *in vitro*<sup>127</sup>. In order to assay the effects of phospho-mutations on the type of inclusions formed in live cells, we generated mutant huntingtin Ex1 Q142-YFP constructs with serines 13 and 16 mutated to glutamic acids (S13E/S16E) to mimic phosphorylation or to alanines (S13A/S16A) to render N17 resistant to phosphorylation. A polyglutamine repeat length of 142 was considered to be similar to the 138 polyglutamine length, so Ex1 Q138-YFP without serine mutations was used as a control. When overexpressed in *STHdh*<sup>Q7/Q7</sup> cells, the

huntingtin phospho-mimetic (S13E/S16E) mutant predominantly formed the fibrillar type of inclusion (Figure 4.8A). Conversely, the alanine mutation skewed the inclusion population towards the globular type of inclusion (Figure 4.8A). As expected, the polyglutamine expanded N17 wild type constructs produced a mixed phenotype of both fibrillar and globular types of inclusions, as residues S13 and S16 can exist in both phospho-states (Figure 4.8A). We also observed the effect on inclusion morphology of fusing YFP to the amino-terminus of the exon 1 mutants (Figure 4.8B). Consistent with the carboxyl-terminus tagged constructs, phospho-mimetic mutants formed more fibrillar and phospho-resistant mutants formed more globular inclusions (Figure 4.8B). This suggested that the location of the fluorescent tag on huntingtin fragments can alter inclusion formation properties, but does not affect the type of inclusion formed by altering the phosphorylation status.

### **Kinase Inhibitors Influence Huntingtin Inclusion Morphology**

In order to study the effects of true phospho-modulation on the type of inclusion formed by amino-terminal huntingtin fragments, we used kinase inhibitors known to either inhibit or promote phosphorylation of huntingtin at serine residues 13 and 16 of N17. Phosphorylation at N17 can be inhibited by casein kinase 2 (CK2) inhibitors DMAT and quinalizarin<sup>57</sup>. Conversely, N17 phosphorylation can be promoted by treatments with IKK inhibitors, the ATP analog Bay 11-7082, and the allosteric inhibitors BMS-345541 and IMD-0354<sup>57</sup>. *STHdh*<sup>Q7/Q7</sup> cells overexpressing Ex1 Q138-YFP treated with CK2 inhibitors had little effect on the type of inclusion formed in the cell, whereas the IKK inhibitors skewed the cellular inclusion population towards the fibrillar type (Figure 4.8C). These results suggest that the fate of inclusions that form in the cell can be influenced by kinase inhibitors or other small molecules that alter the phosphorylation state of serines 13 and 16 of N17.

To further validate the effect of small molecules on inclusion type, we treated *STHdh*<sup>Q7/Q7</sup> cells expressing Ex1 Q138-YFP with either CK2 or IKK inhibitors and looked at inclusion migration under non-denaturing conditions using polyacrylamide gel electrophoresis (PAGE). Native PAGE maintains the folded structure/conformation and the hydrodynamic size of proteins, thus mobility varies with changes in the biophysical

properties of the huntingtin inclusions. Consistent with data that IKK inhibitors skew the cellular inclusion population towards the fibrillar type of inclusions, we noted that these inclusions migrated further since they are more tightly packed (Figure 4.8D). Conversely, CK2 inhibitor treatment of cells had little effect on inclusion type (Figure 4.8C) and also did not alter the migration of inclusions relative to untreated lysates using native PAGE (Figure 4.8D).

## 4.5 Discussion

The concept that mutant huntingtin can form multiple types of inclusions has previously been proposed by others, based on observations with small mutant huntingtin fragments in cell culture and with synthetic protein *in vitro* at super-physiological concentrations<sup>120,127,205</sup>. Fibrillar and heterogeneous morphology inclusions have also been noted in HD brains<sup>21</sup>. The formation of amorphous or amyloid aggregates is initiated by the presence of abnormally folded protein. Past studies have described a pathway for the formation of amyloid aggregates where the abnormally folded monomers initiate the formation of oligomeric intermediates<sup>246</sup>. These intermediates have been described to be globular in shape and lead to the formation of fibrillar aggregates<sup>246</sup>. The globular inclusions described in this study were not the same as the intermediates since we never observed the direct conversion of globular to fibrillar inclusions. These two types of inclusions were therefore identified as two distinct terminal forms of aggregated mutant huntingtin. We also concluded that these inclusions were not aggresomes, a type of cytoplasmic aggregate that forms at the centrosome, since neither inclusion type were found to localize to the centrosome or to cause the characteristic redistribution of vimentin to the periphery of the inclusions<sup>374</sup>.

This manuscript characterizes different inclusion types based on a number of biophysical properties in live cells. A thioflavin-T fluorescent staining assay shows that the fibrillar type of inclusion has a detectable amyloid fibril structure and that the globular type does not. Notably, both types of inclusions were positive for ubiquitin, a characteristic of misfolded protein. Using biophotonic techniques including FLIM-FRET, seFRET, FRAP, deconvolution and temporal imaging, we observed that the fibrillar and globular inclusion types formed by polyglutamine expanded huntingtin have distinct morphological, structural and dynamic properties in live cells. We consistently measured increased FRET efficiency of the huntingtin sensor in fibrillar inclusions relative to the globular type, regardless of the intensity and size of the inclusion formed. Notably, intermolecular FRET between multiple huntingtin molecules represented the majority of the FRET measured at both inclusion types, with a small contribution of intramolecular FRET between the N17 and polyproline domains. Therefore, the higher FRET values

we observed within fibrillar inclusions represented a tighter, more compact and structured organization of huntingtin fragments, as compared with the globular inclusions.

Using FRAP, we demonstrated that globular and fibrillar inclusions formed by mutant huntingtin fragments have very distinct recruitment dynamics. FRAP studies have been performed on multiple polyglutamine disease inclusions to show heterogeneity in the dynamics of inclusions from different diseases. This implies that the context of polyglutamine is important and regions flanking the polyglutamine tracts may contribute to different dynamic properties in different polyglutamine disease proteins<sup>375</sup>. Here, we describe that inclusion heterogeneity can exist within one polyglutamine disease protein, mediated by post-translational modification of a flanking region. We noted that following photobleaching of inclusions, the soluble huntingtin in the cell was recruited back into globular inclusions significantly more rapidly relative to the fibrillar type of inclusions. We demonstrated that soluble huntingtin was actively being shuttled into globular inclusions along microtubules. Treatment of cells expressing mutant exon1 fragments with low concentrations of nocodazole prevented the formation of large globular inclusions and caused a redistribution of smaller inclusions throughout the cell. These results are consistent with previous research that has shown that huntingtin plays a critical role in cytoskeletal dynamics and interacts directly with microtubules<sup>56</sup>.

Temporal experiments done with an incubated microscope showed that the fibrillar inclusion formation caused all the soluble mutant huntingtin in the cell to be progressively recruited and sequestered within the inclusion. These data suggested that the huntingtin within fibrillar inclusions remained relatively static and was not being dynamically exchanged between the soluble and insoluble phases. Conversely, when the globular type formed, these inclusions quickly grew and maintained their size without affecting the fluorescence of the soluble huntingtin within the cells. This suggested that there was a constant dynamic exchange between the soluble and insoluble phases in these inclusions, data that was consistent with the FRAP studies.

Using site directed mutagenesis, we demonstrated that S13ES16E or S13AS16A in the context of polyglutamine-expanded exon1 were enough to push the cellular

population of inclusions towards the fibrillar or globular type, respectively. This observation is consistent with work done by others using purified synthetic huntingtin 1-56 Q37 constructs with either phospho-mimetic or alanine mutations at serine residues 13 and 16 expressed *in vitro*<sup>127</sup>. Using electron microscopy they discovered that huntingtin peptides with S13 and S16 mutations can associate to form morphologically different inclusion types<sup>127</sup>. Despite this, our data showed that constitutive phospho-mimicry or alanine mutations at these sites did not skew the population of inclusions entirely to one form or the other, suggesting that other factors can influence inclusion fate within the cell. We hypothesize that these auxiliary factors could be other post-translational modifications or molecular interactions with either N17 or the polyproline domain. A recent study by our group has shown that N17 phosphorylation can affect soluble huntingtin conformation<sup>368</sup>, and we hypothesize that these conformational differences can influence the nucleation and properties of an inclusion when high levels of protein are present.

Previous work has shown that mutant huntingtin is hypo-phosphorylated at serines 13 and 16 of N17 and that increasing phosphorylation at these sites can reduce the toxicity of the mutant protein<sup>57</sup>. Others have demonstrated that promoting phosphorylation at these residues can dramatically improve motor function in an HD mouse model<sup>128</sup>. In this study, we show that the type of inclusion formed by mutant huntingtin can be affected by small molecule kinase inhibitors that modulate the phospho-state of serine residues 13 and 16 of N17, described by us previously<sup>57</sup>.

The distinct properties of these huntingtin inclusions suggest that one type may represent a toxic form whereas the other may be benign or even protective to the cell. The globular inclusions were shown to have a looser packing of mutant huntingtin, which allowed for the rapid recruitment and continuous exchange of mutant protein with the soluble phase. Additionally, S13AS16A mutations skewed the population of inclusions towards the globular type. Conversely, fibrillar inclusions were shown to be densely packed and soluble mutant huntingtin was slowly recruited and sequestered within these inclusions (see model, Figure 4.9). This sequestration of the mutant protein

within the fibrillar inclusions could represent a cellular stress response to cope with mutant huntingtin load.

Many groups have shown that transgenic mice expressing exon1 of huntingtin rapidly develop motor and cognitive symptoms comparable to HD<sup>20</sup>. Despite the striking phenotypes in these transgenic animals, the question of whether this small fragment occurs naturally in the brains of HD patients has been controversial. However, recent work has elegantly shown that aberrant splicing of the huntingtin pre-mRNA leads to the translation of an exon1 fragment in a variety of HD models and human HD fibroblasts<sup>366</sup>. This work supports the hypothesis that exon1 fragments can occur naturally in abundance within neurons and other cells. However, a caveat of our studies, and those of others using small fragment over-expression, is that the protein concentrations are either super-physiological, or only relevant to neurons in late-stage HD with a massive accumulation of mutant protein. Regardless, the characterization of inclusions in late or severe HD could provide insight into huntingtin properties in early HD or even premanifest HD, which is likely the therapeutic window in this disease.

Using FRET techniques in live cells to visualize inclusions provides a valuable tool to accurately measure the unique conformational/structural differences for each type of inclusion within a cell. Additionally, FRET offers an added level of information by providing high spatial-resolution, beyond even that of super-resolution microscopy. This assay is amenable to high-content screening since it provides a reliable and robust phenotypic read-out of inclusion type. This would allow for the screening of compounds that could skew the cellular population of inclusions towards one type or the other. Furthermore, since inclusion formation is a characteristic of most neurodegenerative disorders, a FRET sensor to quantify different inclusion types could be adapted to other neurodegenerative disease proteins.

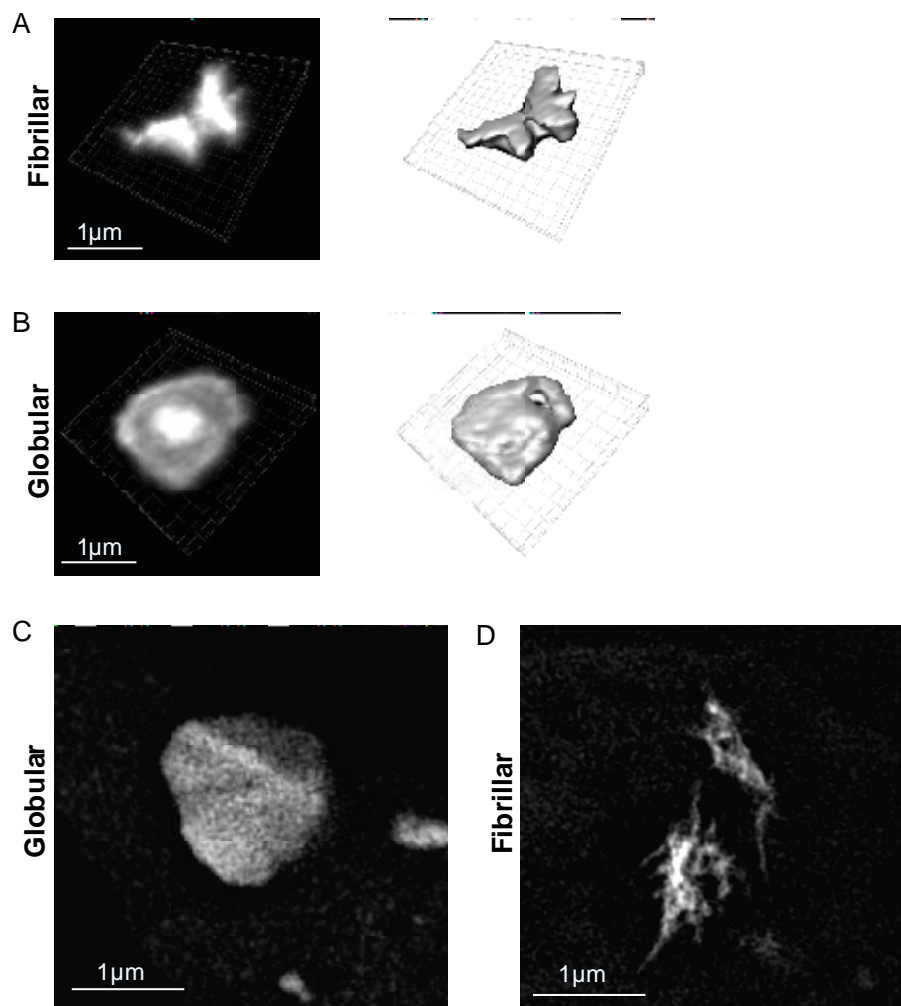


**Figure 4.1. Huntingtin fragments can form two morphologically unique inclusion types.** Maximum intensity projections of deconvolved z-stacks followed by iso-surface rendering of (A) fibrillar and (B) globular inclusion types formed in *STHdh<sup>Q7/Q7</sup>* cells using Ex1 Q138-YFP. (C) SR-SIM images of a globular inclusion with a cytoskeletal structure present in the inclusion. (D) SR-SIM image of a fibrillar inclusion. Scale bar = 1 μm.

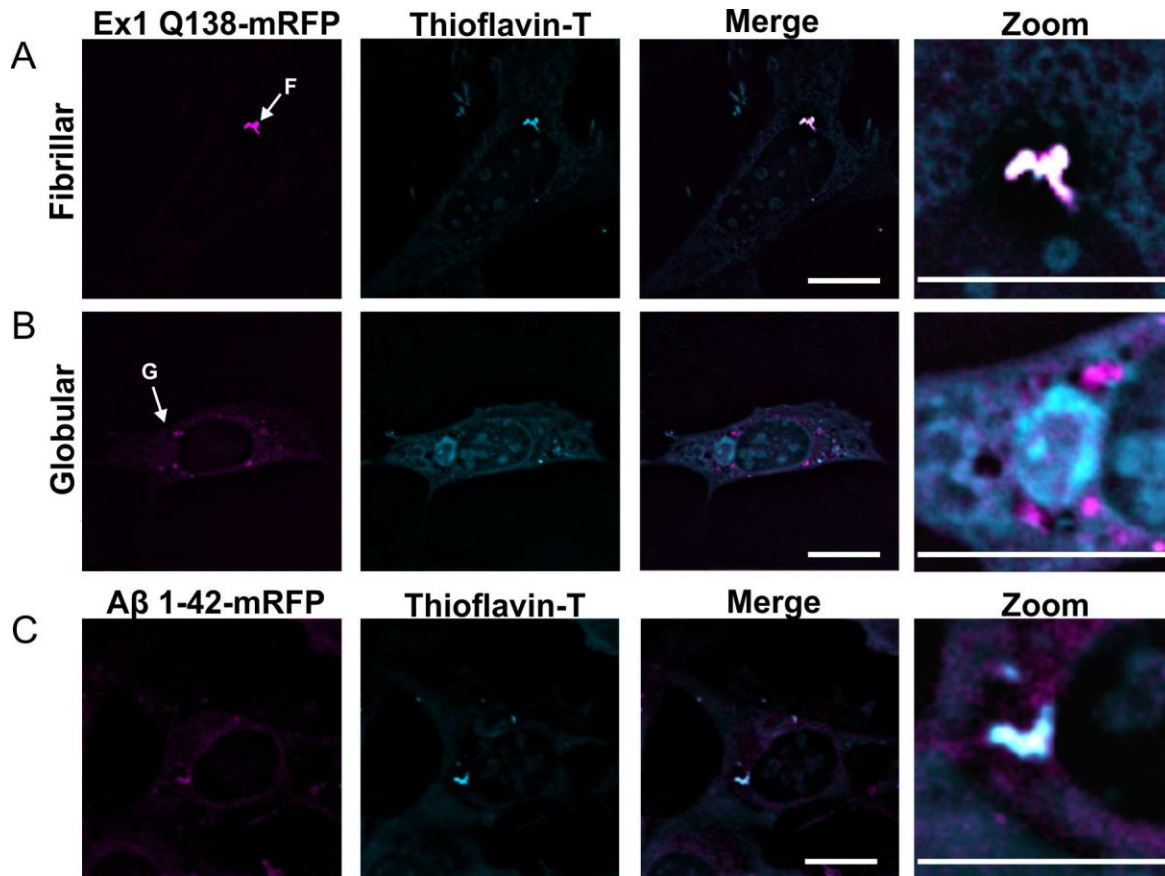


**Figure 4.2. Fibrillar inclusions are detectable by thioflavin-T staining assay.**

Thioflavin-T staining of *STHdh*<sup>Q7/Q7</sup> cells that formed either (A) fibrillar or (B) globular inclusions following 24 h expression of Ex1 Q138-mRFP. (C) Positive control for thioflavin-T assay showing staining of *STHdh*<sup>Q7/Q7</sup> cells expressing Aβ 1-42-mRFP for 24 hours that have formed amyloid fibril aggregates. Inclusions of interest are denoted with an arrow, where G refers to a globular inclusion, and F refers to a fibrillar inclusion. Scale bar = 10µm.

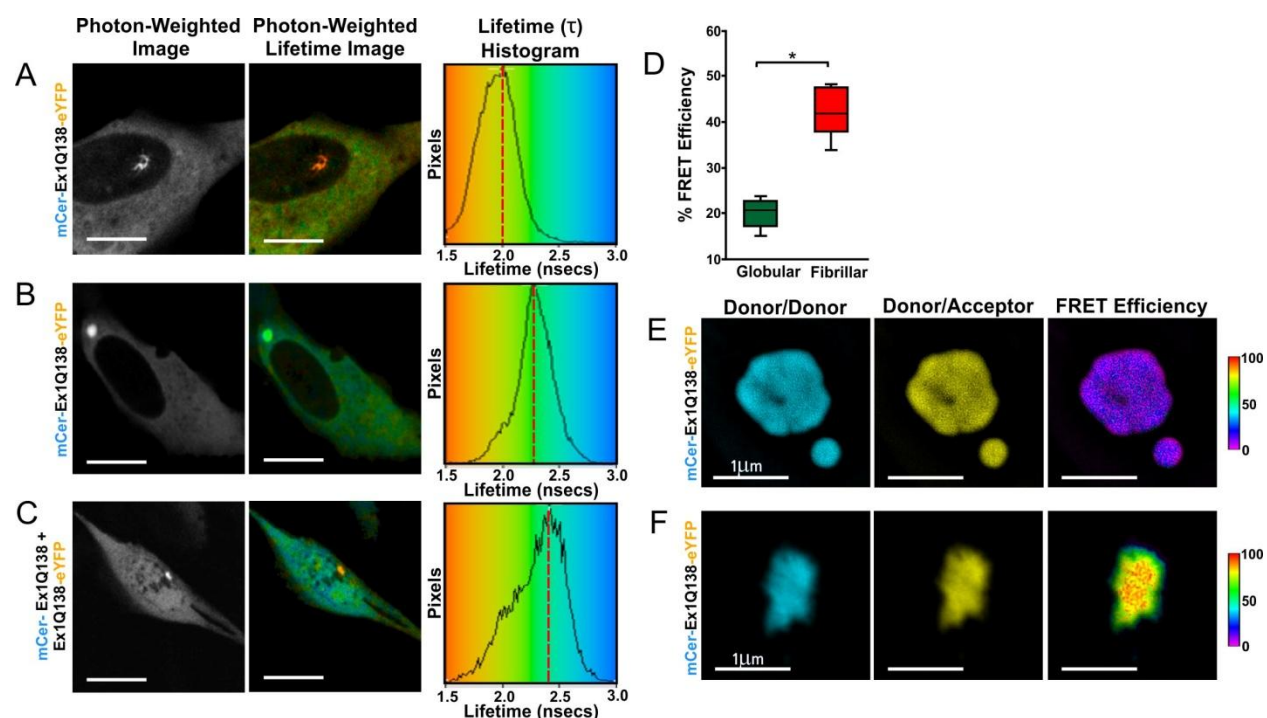


**Figure 4.3. Comparing the fluorescence lifetime ( $\tau$ ) changes in globular versus fibrillar inclusion types.** Sample FLIM images of (A) fibrillar and (B) globular inclusions formed using the mCer-Ex1 Q138-eYFP FRET sensor. (C) Co-expression of mCer-Ex1 Q138 and Ex1 Q138-eYFP as a control to show contribution of intermolecular versus intramolecular FRET. Photon-weighted images, photon-weighted lifetime images and lifetime histograms of each image are presented. Lifetimes shown in the photon-weighted lifetime images are pseudo-coloured using the rainbow scale lookup table (LUT) and correspond to lifetime values represented in the histogram. The dashed red lines within each histogram represents the approximate lifetime with the most representative pixels (mode). Scale bar = 10 $\mu$ m. (D) Quantification of FRET efficiency using the huntingtin FRET sensor comparing globular versus fibrillar inclusion types under steady state conditions in live cells (n=30, N=3, \*p<0.001). All imaging was done in Hank's balanced salt solution (HBSS) pH 7.3. Sample deconvolved z-stacks of (E) globular and (F) fibrillar inclusions generated using seFRET. The donor/donor image represents excitation and emission of mCerulean. Donor/acceptor image represents excitation of mCerulean and emission of eYFP. FRET efficiency images have been pseudocoloured using a rainbow LUT that corresponds to the corrected FRET efficiency values represented on the scale at the bottom left of the panel. Scale bar = 1 $\mu$ m

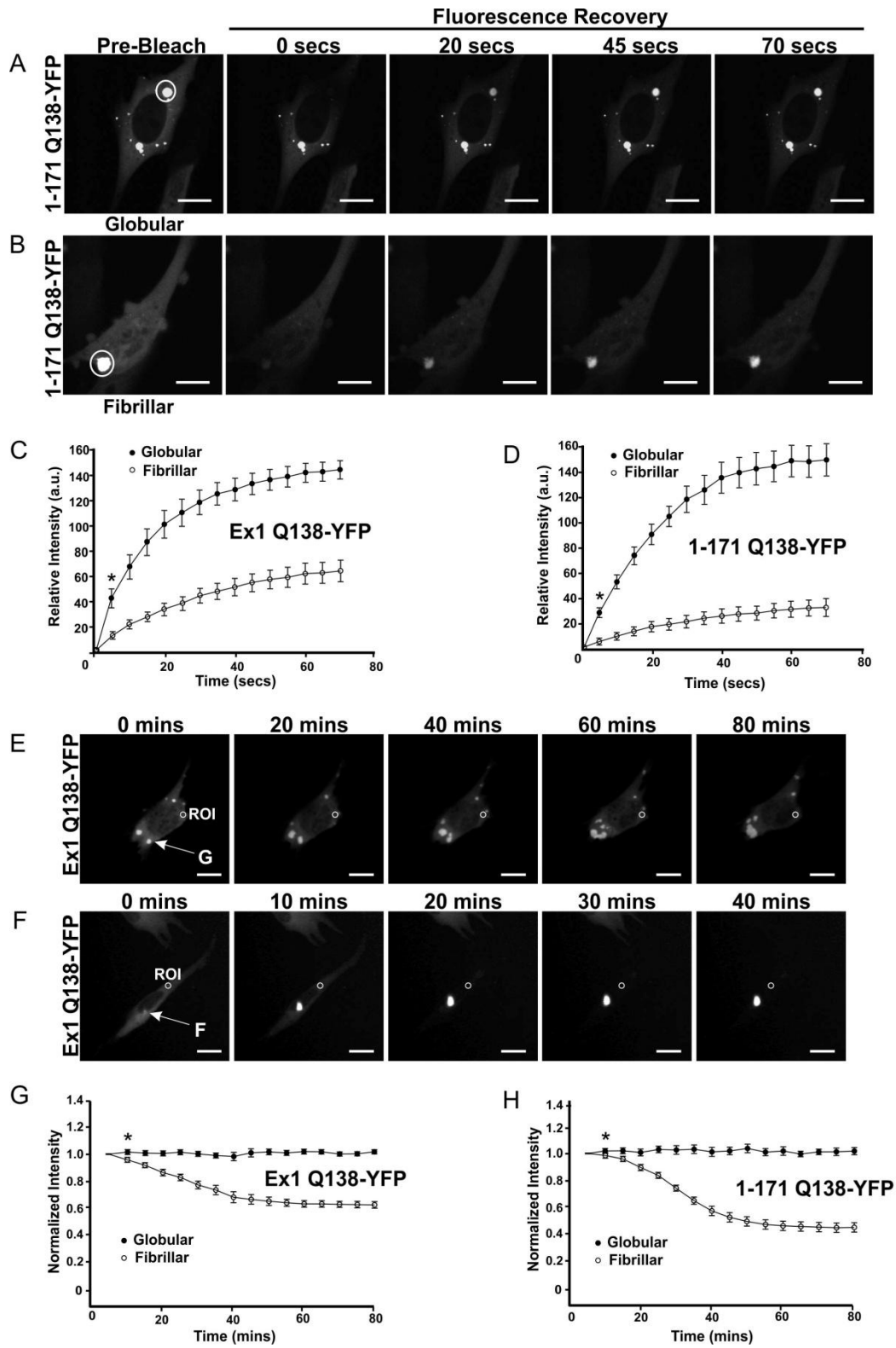


**Figure 4.4. Comparing the dynamics of globular versus fibrillar inclusions.** Live cell assay showing the recovery of fluorescence following bleaching of either (A) globular or (B) fibrillar inclusion using a high-intensity 488nm laser in *STHdh<sup>Q7/Q7</sup>* cells overexpressing 1-171 Q138-YFP. Pre-bleach acquisition shows the cell prior to ROI (circle) photobleaching. Quantifications of relative fluorescence recovery to either fibrillar or globular inclusions (over a 75 s time period) following expression of either (C) Ex1 Q138-YFP or (D) 1-171 Q138-YFP huntingtin fragments in *STHdh<sup>Q7/Q7</sup>* cells for 24 h. Plotted values represent arbitrary units (A.U.) of fluorescence intensity and error bars represent standard error. The \* represents time point where  $p < 0.001$  (N=3, n=10). Temporal movies of live cells expressing Ex1 Q138-YFP constructs forming either (E) globular or (F) fibrillar inclusions. Movies were made with an environmentally controlled microscope at 33°C, 5% CO<sub>2</sub> using a 40x objective where images were taken every 5 m for 24 h. Quantification of temporal fluorescence loss at a specific ROI for both fibrillar and globular inclusions following expression of either (G) Ex1 Q138-YFP or (H) 1-171 Q138-YFP in *STHdh<sup>Q7/Q7</sup>* cells for 24 h. Plotted values represent normalized intensity and error bars represent standard error (n=5, N=10 for Ex1 and n=9, N=8 for 1-171, \* $p < 0.001$ ).

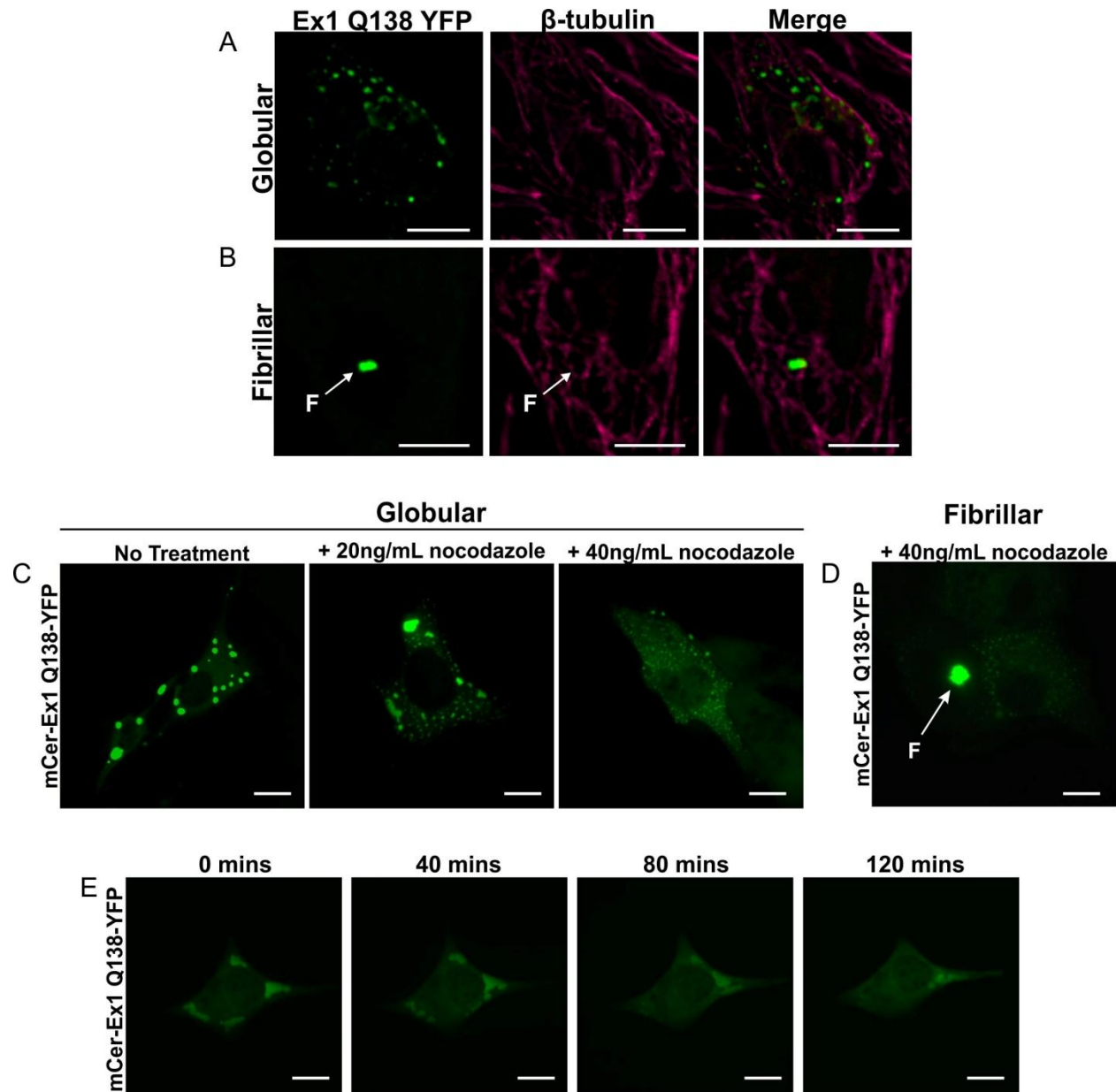


**Figure 4.5. Active recruitment of mutant huntingtin into globular inclusions is microtubule dependent.** IF for  $\beta$ -tubulin performed on  $STHdh^{Q7/Q7}$  cells that formed either (A) globular or (B) fibrillar inclusions following 24 h expression of Ex1 Q138-YFP. Effect of  $\sim 3$  h nocodazole treatment on  $STHdh^{Q7/Q7}$  cells expressing mCer-Ex1 Q138-YFP for  $\sim 10$  h forming either (C) globular or (D) fibrillar inclusions. (E) Temporal movie of a live cell with fully formed globular inclusions after expression of mCer-Ex1 Q138-YFP for 24 h treated with 40ng/mL nocodazole over 2 h. Inclusions of interest are denoted with an arrow, where F refers to a fibrillar inclusion. Scale bar = 10 $\mu$ m.

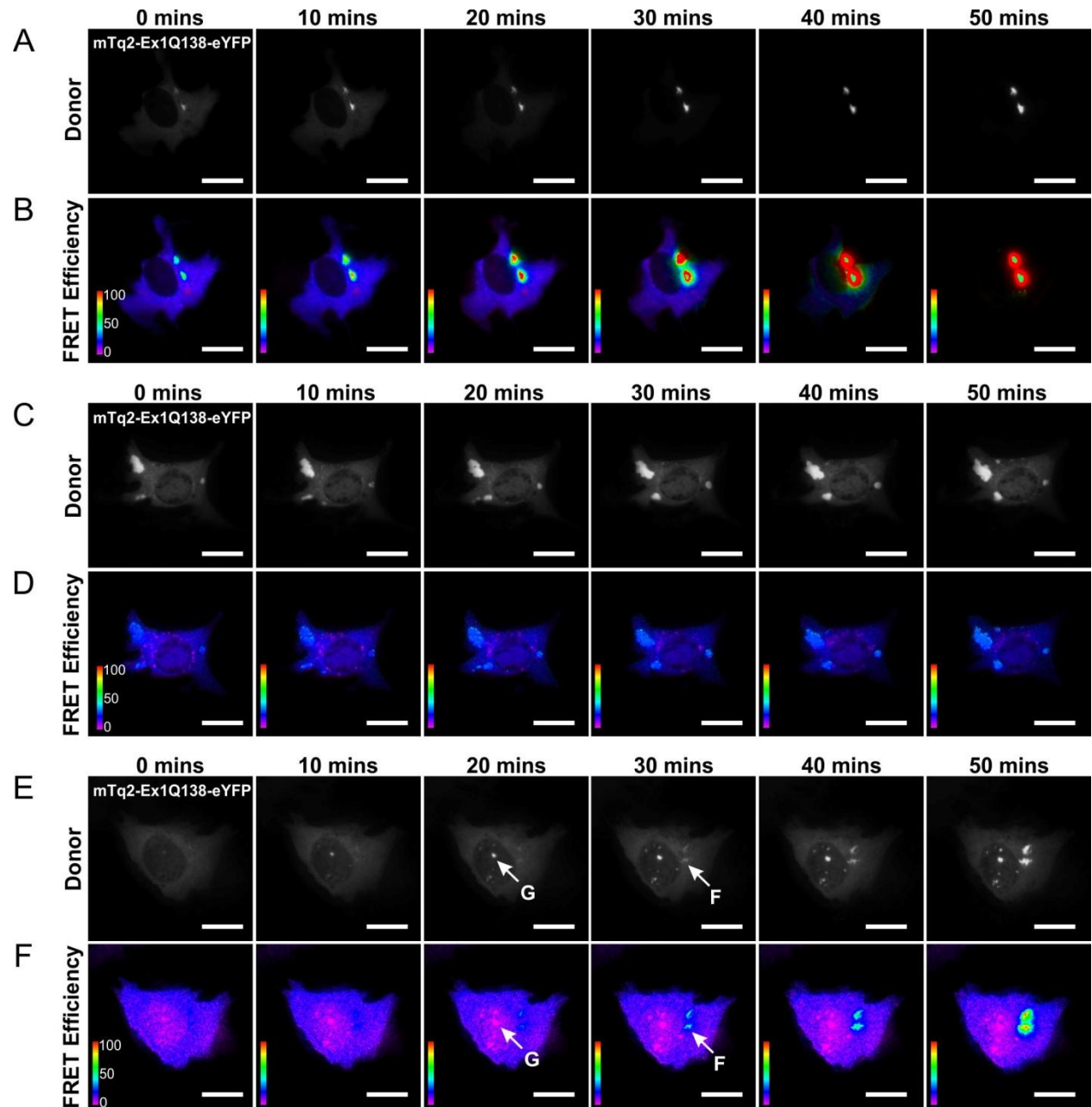


**Figure 4.6. Comparing the formation of fibrillar versus globular inclusions using temporal seFRET.** (A, C, E) Temporal fluorescence intensity images of *STHdh*<sup>Q71/Q7</sup> cells expressing mTq2-Ex1 Q138-eYFP FRET sensor during the formation of (A, E) fibrillar and (C, E) globular inclusions. (B, D, F) Corresponding temporal corrected FRET efficiency images generated using seFRET module showing the formation of (B, F) fibrillar and (D, F) globular inclusions. FRET images have been pseudocoloured using a rainbow LUT that corresponds to corrected FRET efficiency values represented on the scale at the bottom left of each panel. Inclusions of interest are denoted with an arrow, where G refers to a globular inclusion, and F refers to a fibrillar inclusion. Scale bar = 10µm.

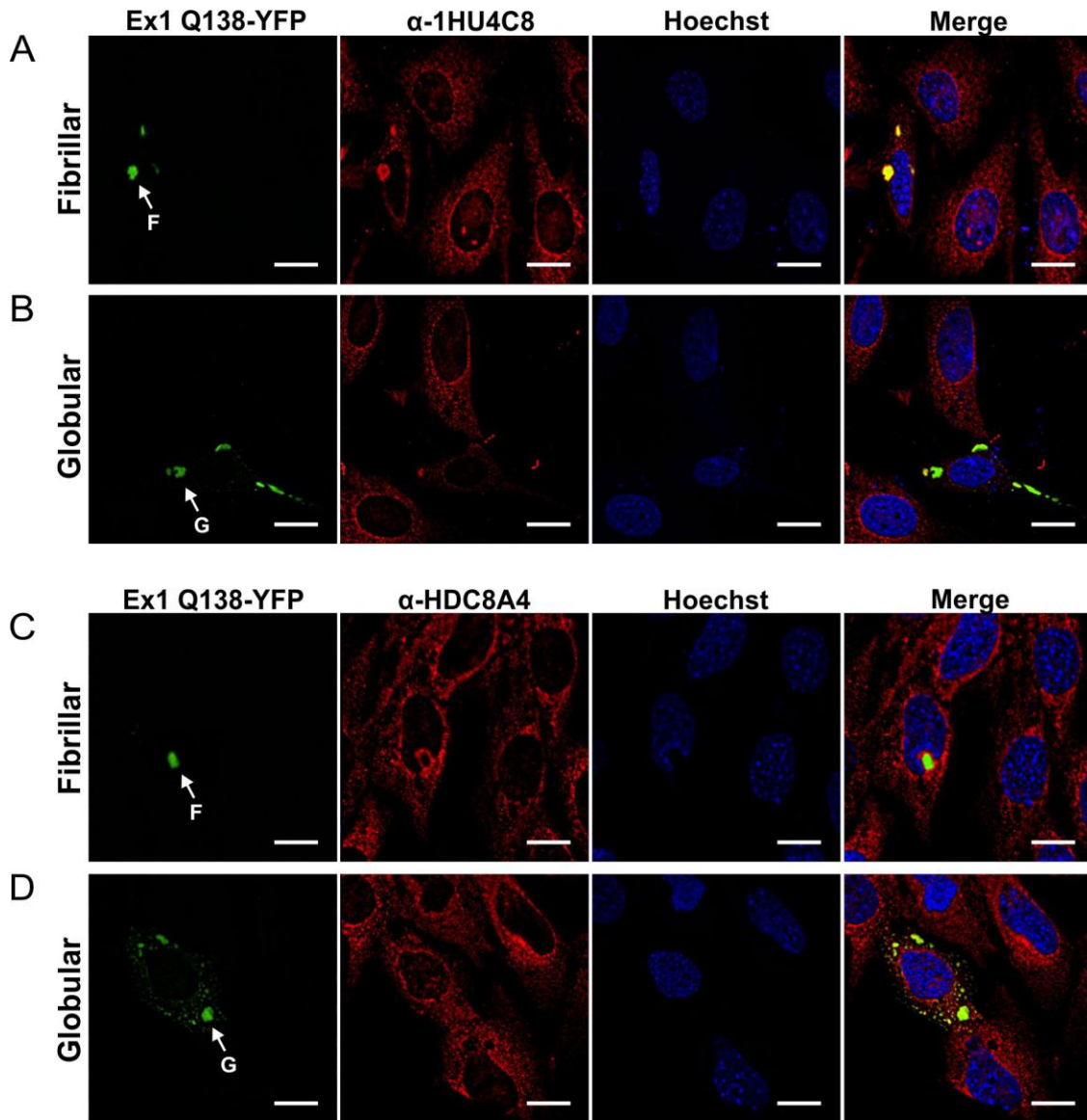


**Figure 4.7. Full-length, endogenous huntingtin is actively recruited and sequestered within fibrillar inclusions.** Representative IF images of *STHdh*<sup>Q7/Q7</sup> cells expressing Ex1 Q138-YFP followed by fixation with 4% paraformaldehyde, antigen retrieval using 10% formic acid and permeabilization using Triton X-100 detergent. IF was performed using both (A, B) 1HU4C8 and (C, D) HDC8A4 monoclonal antibodies on either (A, C) fibrillar or (B, D) globular huntingtin inclusions. Primary antibodies were indirectly labelled with secondary antibodies conjugated with Cy5 to prevent spectral bleedthrough due to the high fluorescence intensity of the inclusions. Inclusions of interest are denoted with an arrow, where G refers to a globular inclusion, and F refers to a fibrillar inclusion. Scale bar = 10 $\mu$ m.

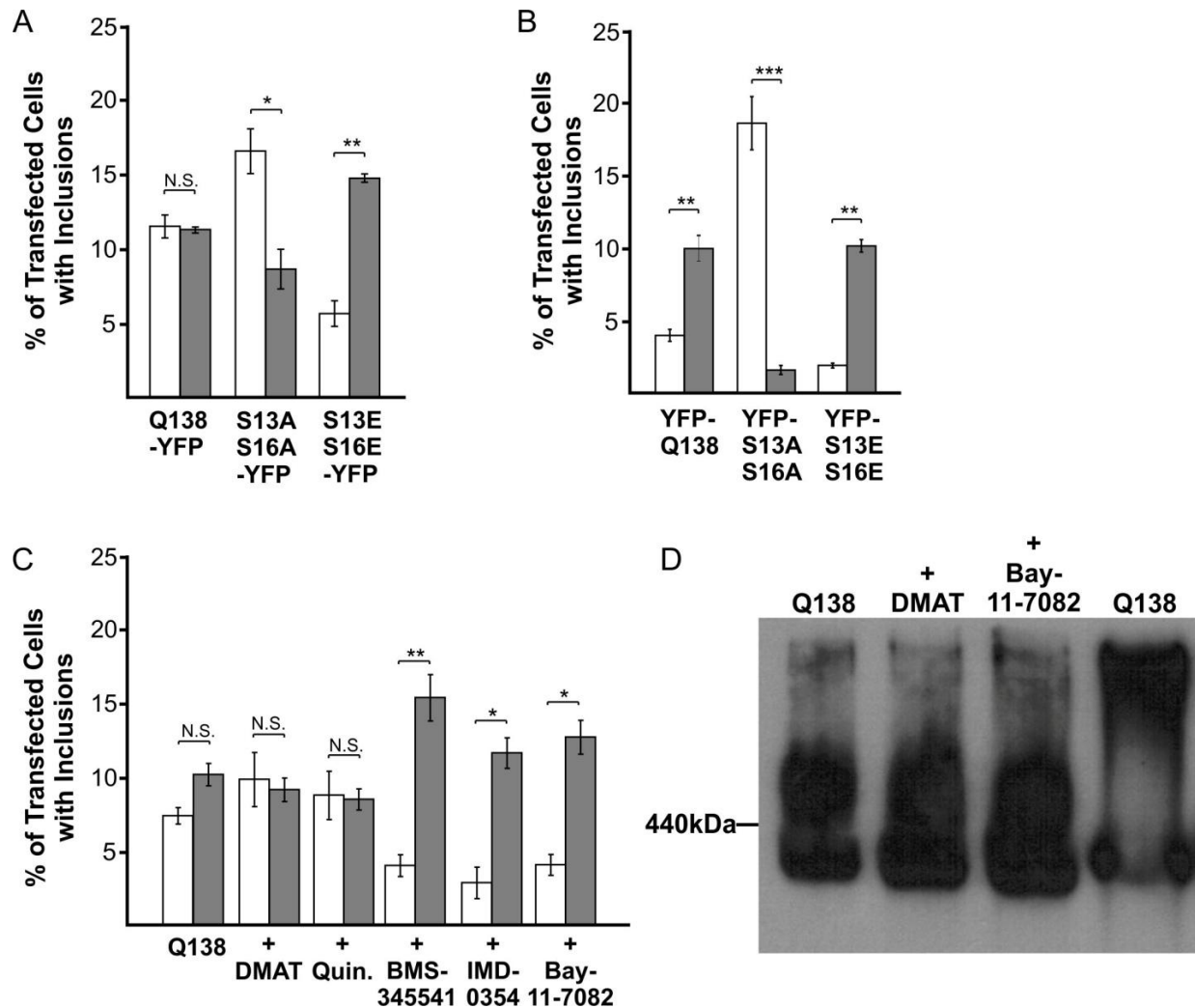


**Figure 4.8. Phosphorylation state of N17 S13 and S16 can influence the fate of the inclusion type.** Quantification of percent transfected cells with globular (white bars) or fibrillar (grey bars) inclusions following expression in *STHdh*<sup>Q7/Q7</sup> of (A) Ex1 Q138-YFP or (B) YFP-Ex1 Q138 constructs with serines 13 and 16 mutated to either alanines (S13AS16A) or glutamic acids (S13ES16E). N.S.= not significant, \*p=0.029, \*\*p=0.009, \*\*\*p<0.001. N=4, n=150. (C) Quantification of percent transfected cells with either fibrillar or globular inclusions for Ex1 Q138-YFP following either no treatment or treatment with CK2 and IKK inhibitors (2μM DMAT, 1μM quinalizarin, 4μM BMS-345541, 2μM IMD-0354 and 5μM Bay 11-7082). N.S. = not significant, \*p=0.029, \*\*p=0.009. n=150, N=3. (D) Differential migration of mCer-Ex1 Q138-YFP inclusions following treatment with CK2 or IKK inhibitors (1μM DMAT and 5μM Bay 11-7082) under native non-denaturing conditions. 440kDa protein marker position indicated.

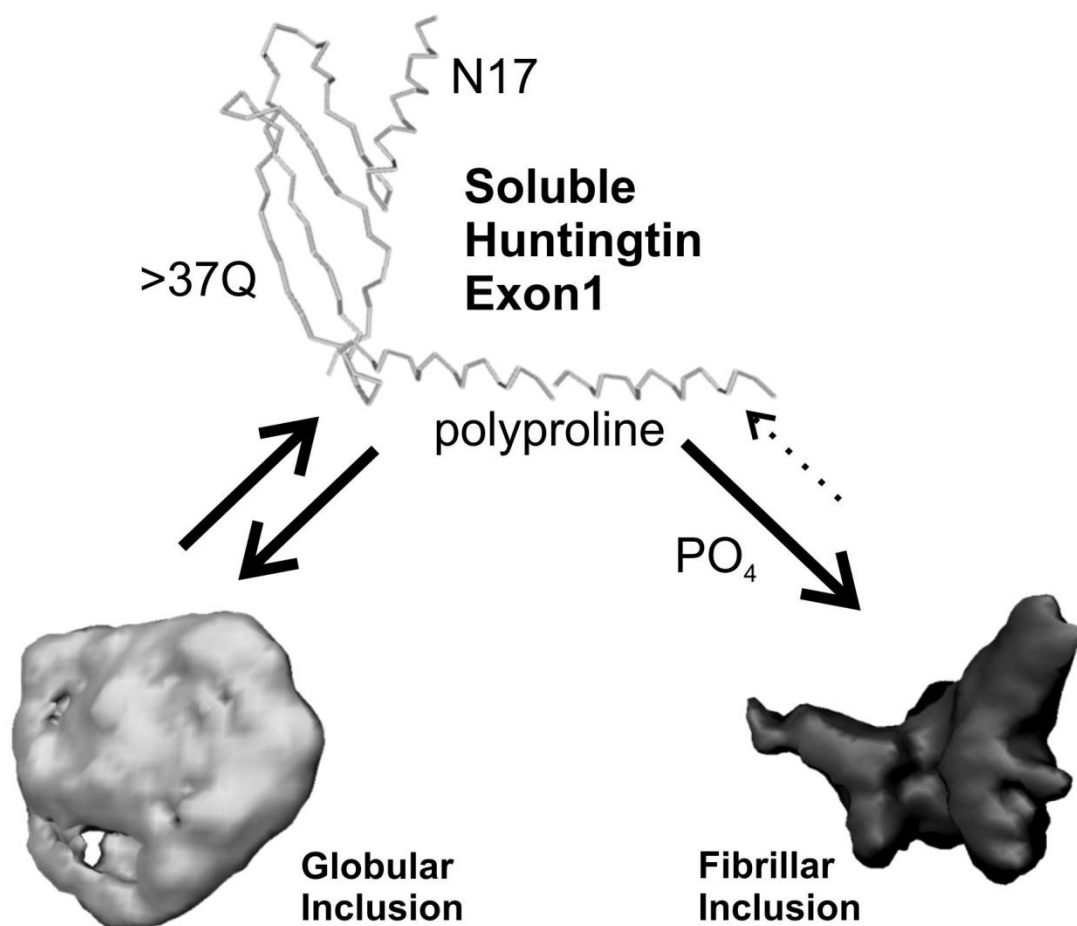


**Figure 4.9. Model of the dynamics of two distinct inclusion types formed from mutant huntingtin protein.** Soluble huntingtin exon1 with a CAG expansion beyond 37 repeats adopts an open conformation, pushing N17 and polyproline out of alignment. Globular inclusions can form, and readily exchange protein with the soluble phase, likely allowing mutant huntingtin to interact functionally in pathways required by normal huntingtin. Fibrillar inclusions can also form, especially if N17 is phosphorylated, causing tight-packed protein deposits that rapidly form and do not exchange with the soluble phase, thus are protective in HD. We did not observe one inclusion type directly converting to another.

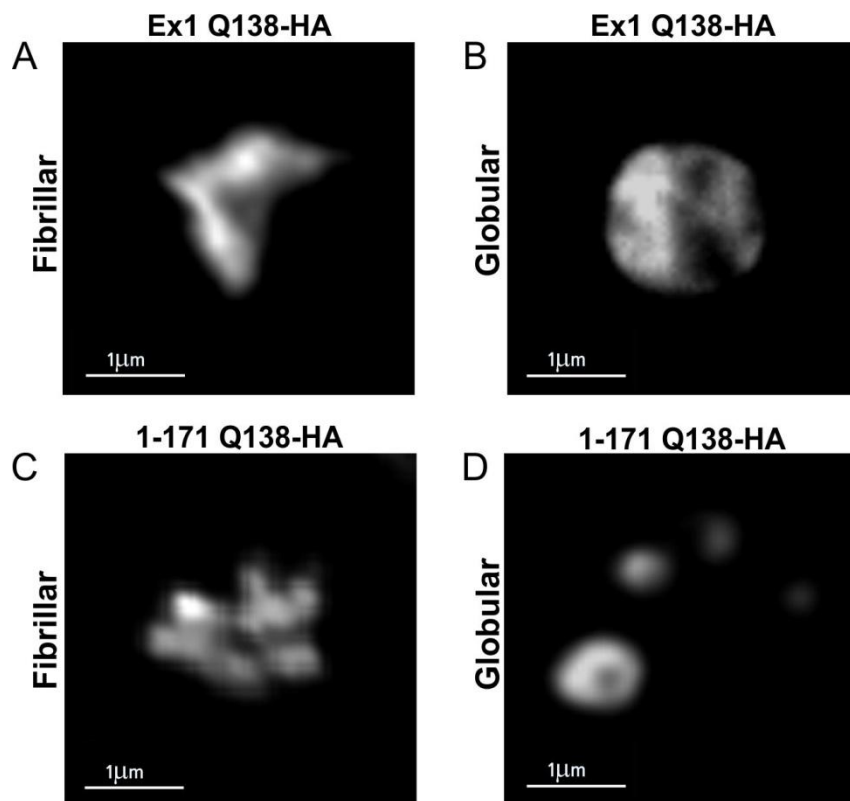


**Figure 4.S1. HA-Tagged Mutant Huntingtin exon1 forms two inclusion types.**

Representative images of the two inclusion types as HA-tagged constructs in fixed cells. Both (A, C) fibrillar and (B, D) globular inclusions were observed with both Ex1 Q138-HA and 1-171 Q138-HA contexts. Scale bar = 1 μm.

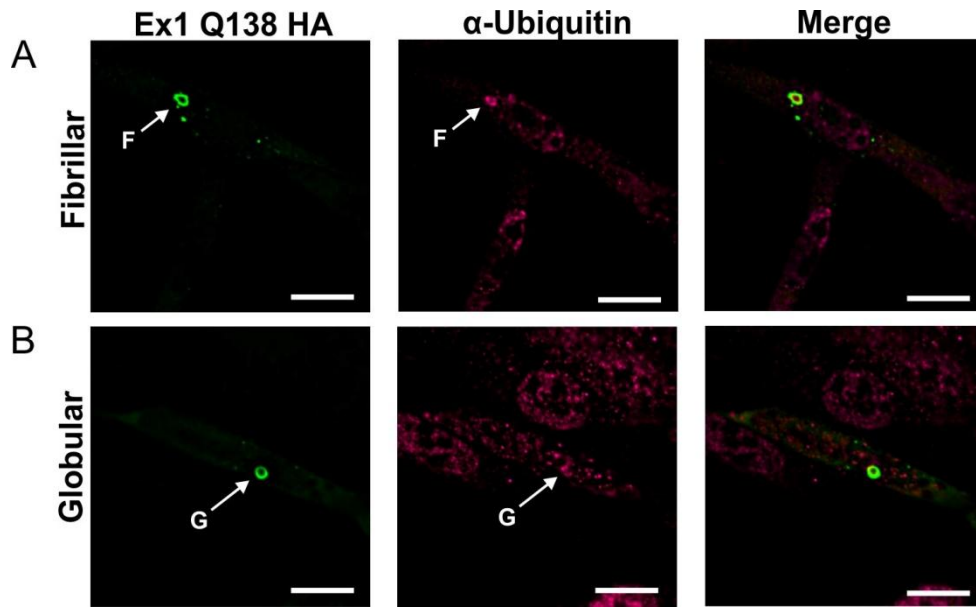


**Figure 4.S2. Fibrillar and globular inclusions are not differentially ubiquitinated.** Immunofluorescence for ubiquitin performed on ST*Hdh*<sup>Q7/Q7</sup> cells that formed either (A) fibrillar or (B) globular inclusions following 24 hours expression of Ex1 Q138-HA. Primary antibodies for HA-tag and ubiquitin were indirectly labelled with secondary antibodies conjugated with AlexaFluor488 and Cy5 respectively. Scale bar = 10µm.

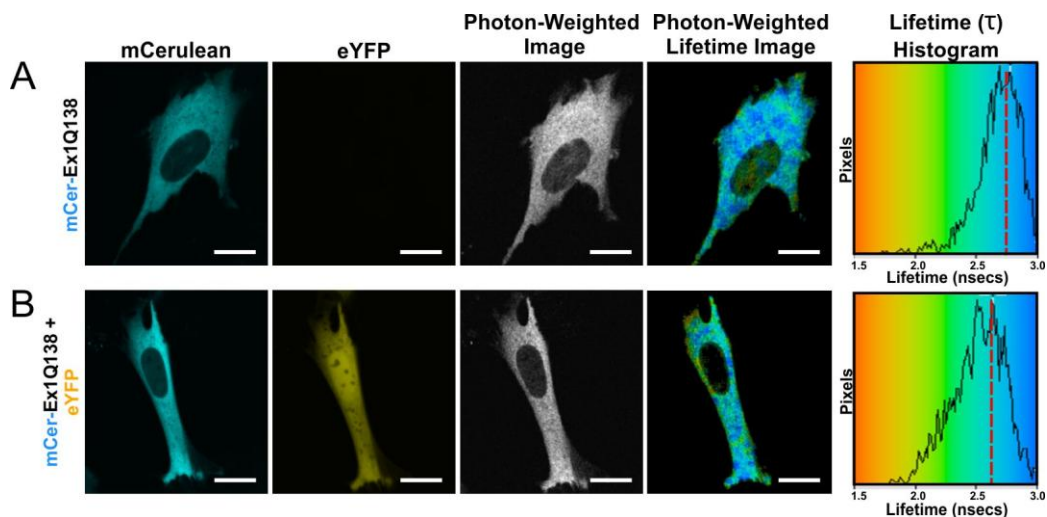


**Figure 4.S3. FLIM-FRET controls.** Sample negative control FLIM images for mCer-Ex1 Q138 in the (A) absence and in the (B) presence of an eYFP acceptor co-expressed in *STHdh*<sup>Q7/Q7</sup> cells for ~36 hours. Photon-weighted images, photon-weighted lifetime images and lifetime histograms of each image are presented. Lifetimes shown in the photon-weighted lifetime images are pseudo-coloured using the rainbow scale lookup table (LUT) and correspond to lifetime values represented in the histogram. The dashed red lines within each histogram represent the approximate lifetime with the most representative pixels (mode). Scale bar = 10 μm.

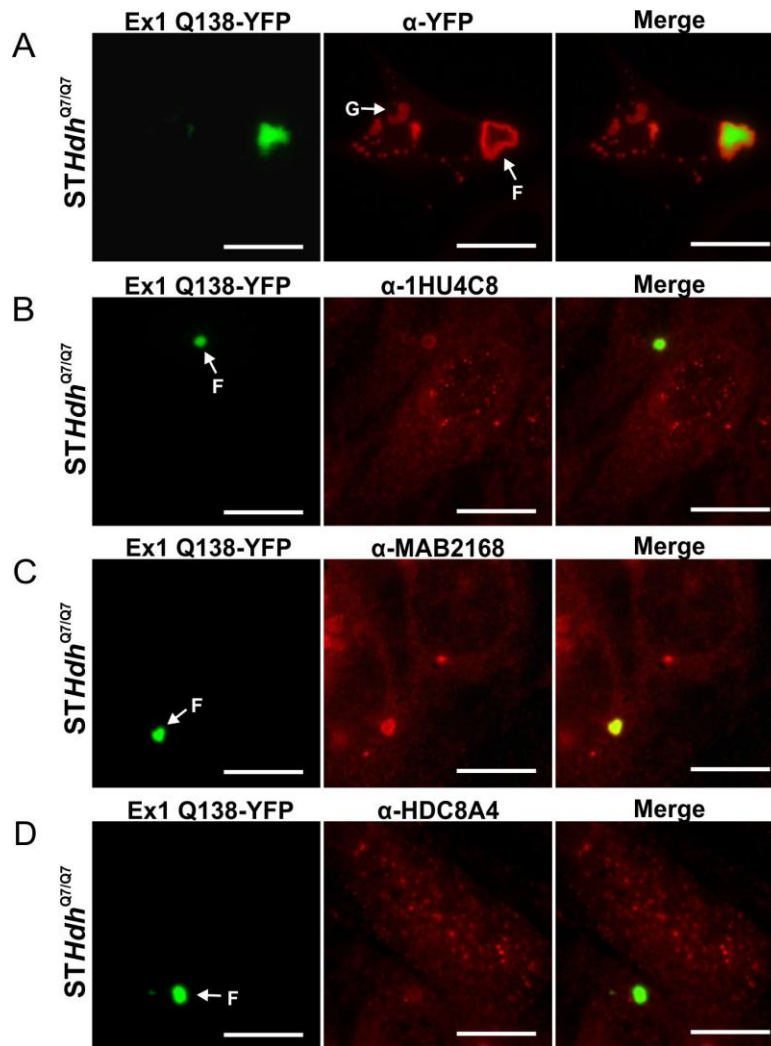


**Figure 4.S4. Endogenous huntingtin is detectable within fibrillar inclusions with**

**methanol fixation.** (A) Representative images showing that methanol fixation/permeabilization causes a loss of fluorescence at globular but not fibrillar inclusions following expression of Ex1 Q138-YFP and immunofluorescence with an anti-YFP antibody and an AlexaFluor488 secondary. Representative images of *STHdh*<sup>Q7/Q7</sup> cells fixed and permeabilized using methanol followed by immunofluorescence using (B) 1HU4C8, (C) MAB2168 and (D) HDC8A4 monoclonal antibodies showing that fibrillar inclusions formed by huntingtin exon1 Q138 constructs can recruit endogenous full-length huntingtin.

Antibodies were labelled with secondary antibodies conjugated with Cy5 to prevent spectral bleed through due to the high fluorescence intensity of the inclusions. Inclusions of interest are denoted with an arrow, where G refers to a globular inclusion, and F refers to a fibrillar inclusion. Scale bar = 10 $\mu$ m.

## **Acknowledgements**

This work was supported with operating grants to RT from the Huntington Society of Canada, the Canadian Institutes of Health Research (CIHR MOP-119391) and the Krembil Family foundation.

## Chapter 5 - Discussion and Future Directions

### 5.1 TG2 Conformational Sensor

In chapter two of this thesis we described a conformational FRET sensor for TG2 in live cells. This sensor was developed and optimized to test the conformation of TG2 in response to cell stress, structural mutations and TG2 inhibitors. In addition to a read-out of conformation, the sensor also provides additional information about the subcellular localization and activity of TG2 in the cell; factors known to mediate the role of TG2 in cell death processes. Therefore, this FRET sensor provides a novel tool to rapidly assay many properties of TG2 simultaneously in the context of live cells.

Additionally, this sensor provides a tool for screening TG2 inhibitors based on their effect on conformation. In chapter two, we described three classes of TG2 inhibitors: class I, which can promote a closed conformation of the enzyme while bound; class II, which can lock the enzyme in an open conformation; and class III, which does not have any conformational effects at all, yet can still inhibit the transamidation activity of TG2. We further validated the classification of TG2 inhibitors based on the conformational effect by testing eight previously described inhibitors<sup>284</sup> using the TG2 FRET sensor in a blinded manner (compounds were labelled 1-8). Of the eight TG2 inhibitors, compounds #1 and 3 locked the enzyme in the open conformation; compounds #4, 6 and 8 had no effect on conformation; whereas compounds #2, 5 and 7 promoted the closed conformation of TG2 (Figure 5.1A). Therefore, classifying compounds based on their effect on the conformation of a protein represents a novel method to identify inhibitors and could be adapted to a number of disease proteins where pathology is not due to aberrant enzymatic activity but rather a mutant conformation. For example, in prion diseases, where pathology is due to a mutated conformation of the PrP, developing a conformational sensor to identify the misfolded protein could be utilized to screen for compounds that restore the wild-type conformation in a live cell system that models the disease state. In chapter three of this thesis, we adapted and modified the TG2 sensor to look at the conformation of mutant huntingtin in live cells. By generating the huntingtin FRET sensor with a range of wild-type and mutant polyglutamine lengths, we detected a robust conformational change of

polyglutamine-expanded huntingtin at the clinical pathogenic threshold for HD. In addition to detecting a change in soluble mutant huntingtin conformation relative to wild-type (chapter 3), we were also able to detect differences in the conformation and organization of sub-populations of mutant huntingtin within fibrillar and globular inclusions using FRET techniques (chapter 4). Therefore, the TG2 sensor has laid the groundwork for the optimization of the huntingtin sensor for use in two critical applications.

### **5.1.1 Future Directions**

Increased TG2 activity has been implicated in a number of neurodegenerative disorders, cancer, atherosclerosis and celiac disease<sup>58,260,261,263,265,266,270</sup>. Therefore, the TG2 conformational sensor is amenable for use in many other applications. Future work could entail generating stable cell lines (cell type depends on application and disease being studied) expressing the TG2 sensor to conduct a FRET-based high-content screen of TG2 inhibitors using the conformation and subcellular localization of the enzyme as the read-out. Furthermore, this assay could be adapted to look at endogenous TG2 in HD patient samples. Using conjugated primary antibodies against epitopes at the extreme amino and carboxyl-termini, respectively, FRET could be used to measure the conformation, activity and subcellular localization of the enzyme throughout the progression of the disease.

## **5.2 Huntingtin Conformational Sensor**

In chapter three of this thesis we described a FRET-based assay to measure the conformation of amino-terminal huntingtin fragments in live cells. We demonstrated that the polyglutamine tract of huntingtin can behave like a flexible hinge allowing an intramolecular proximity between N17 and the proline-rich region of huntingtin. We showed that this flexibility of the polyglutamine tract is impaired at lengths beyond the clinical pathogenic threshold for HD and results in a diminished proximity between the flanking regions. Notably, this assay provides the first evidence of a robust conformational change of the mutant huntingtin protein at 37 repeats in live cells. Furthermore, we developed an antibody-based FRET assay to compare the

conformation of huntingtin between HD patient and age-matched control fibroblasts. Consistent with the huntingtin fragment FRET sensor, we detected a decreased proximity between flanking regions in the HD fibroblasts relative to wild type fibroblasts. Therefore, we were able to translate the observation of a conformational change with the huntingtin fragment FRET sensor at pathogenic lengths, into detecting a robust conformational change in the amino-terminus of full-length, endogenous huntingtin in HD patient fibroblast samples.

Polyglutamine or polyglutamine-rich domains are found in a number of cellular proteins where they act as scaffolding domains to promote dimerization and other protein-protein interactions<sup>347-349</sup>. In chapter three of this thesis we demonstrated that the polyglutamine tract of huntingtin behaves like a flexible hinge region to facilitate intramolecular proximities between flanking regions. Since HD is one of nine other diseases caused by an expansion of a polyglutamine tract beyond a normal length, we hypothesize that the polyglutamine tract in these disease proteins may also represent flexible regions required to promote intramolecular interactions. Sequence analysis of the polyglutamine disease proteins reveals that ataxin-1 (mutated in SCA1), 2 (SCA2), 7 (SCA7), TBP (SCA17), atrophin-1 (DRPLA) and the androgen receptor (SBMA) have polyglutamine tracts near the amino-terminus of the protein, similar to huntingtin. Furthermore, ataxin-2, 7 and atrophin also have polyglutamine tracts that are flanked at the carboxyl-terminus by a poly-proline stretch (minimum 3). The ataxin-7 protein, the most similar to huntingtin, has a polyglutamine tract directly at the amino terminus of the protein where it is flanked by a highly conserved domain (a.a. 1-15 or N15) at the extreme proximal end and a proline-rich region at the distal end of the tract (Figure 5.2A). Therefore, we postulated that the wild-type polyglutamine tract within ataxin-7 also behaves as a flexible domain allowing the N15 region to fold back onto the proline-rich region of the protein. To test this, we generated an ataxin-7 FRET sensor using the first 81 amino acids of ataxin-7 in the context of 10 or 64 glutamines, where we fused a mCerulean donor to the amino-terminus and an eYFP acceptor at the carboxyl-terminus, respectively (Figure 5.2B,C). Consistent with the results from the exon1 huntingtin sensor, we detected a significantly lower FRET efficiency with mutant ataxin-7 relative to the wild-type (Figure 5.2D). We interpreted this result as a decrease in

intramolecular proximity between flanking regions of ataxin-7 in the context of the mutant polyglutamine tract. In an effort to further investigate polyglutamine flexibility within ataxin-7, we introduced a single nucleotide substitution within the middle of the wild-type CAG tract of ataxin-7 to mutate a glutamine to a proline residue (CAG to CCG; resulting in a Q<sub>4</sub>-P<sub>1</sub>-Q<sub>5</sub> tract). We postulated that adding a proline residue within a polyglutamine stretch would induce a structural kink that would limit the flexibility of the tract in a manner analogous to an expansion. Notably, we detected as a significant increase in FRET efficiency in the ataxin-7 proline FRET sensor relative to wild-type (Figure 5.2D). We interpreted this result as an increase in the intramolecular proximity of ataxin-7 flanking sequences as a result of the proline mutation inducing structure and locking the donor/acceptor probes in close spatial proximity. Taken together, these results with huntingtin and ataxin-7 suggest that the unique pathogenic thresholds in each CAG trinucleotide disorder may result from reduced flexibility of the polyglutamine tracts at a specific length that is strongly influenced by the flanking sequences. However, further investigation is required with other polyglutamine-containing disease proteins to validate this hypothesis.

CAG trinucleotide stretches have been shown to be unstable in all polyglutamine diseases<sup>8,26,376</sup>. However, the current genetic test for polyglutamine diseases relies on PCR assays reporting the number of CAG repeats based on size. Therefore, limited sequence information is available to determine if mutations occur within the polyglutamine tract in these diseases. In normal individuals, the *ATXN1* gene contains a stretch of 6-39 CAG repeats that are interrupted by 1-2 CAT repeats<sup>376</sup>. These interrupting CAT codons result in histidine residues ((Q)<sub>n</sub>-H-Q-H-(Q)<sub>n</sub>) that are believed to stabilize the CAG tract during DNA replication and prevent expansion<sup>377</sup>. In SCA1, the CAG tract is expanded beyond the normal length and the CAT interruptions are lost<sup>376</sup>. This suggests that repeat instability in SCA1 extends beyond a variation in the CAG length, where the loss of interrupting codons predisposes the CAG tract in *ATXN1* to expansion<sup>376</sup>. However, individuals have been described with a CAG expansion in the *ATXN1* gene, yet with no disease pathology<sup>360,378</sup>. Upon sequencing, it was discovered that these individuals have histidine interruptions in the pure expanded polyglutamine tract of ataxin-1 (45 repeats) in the configuration (Q)<sub>12</sub>-H-Q-H-(Q)<sub>12</sub>-H-Q-H-(Q)<sub>14</sub><sup>360</sup>. In an

effort to elucidate the role of histidines in mitigating the toxicity of expanded polyglutamine in SCA1, a comparative study using synthetic polyglutamine peptides with ((Q)<sub>12</sub>-H-Q-H-(Q)<sub>12</sub>-H-Q-H-(Q)<sub>12</sub>) and without ((Q)<sub>42</sub>) histidine interruptions demonstrated that histidine mutations increase the solubility and decrease the propensity of aggregation of long polyglutamine stretches<sup>361</sup>. Furthermore, this study also showed that the incorporation of proline residues within pure, expanded polyglutamine altered the aggregation properties of the peptide to a greater extent than with histidines<sup>361</sup>. The effects of histidine and proline mutations on aggregation propensity were shown to be due to the induction of conformational change within the polyglutamine stretch. We hypothesize that the beneficial effect of histidine interruptions in the expanded polyglutamine tract of ataxin-1 is due to the restored flexibility of the mutant tract in these individuals. Expansion of pure, uninterrupted CTG beyond a 110 repeats in the *ATXN8OS* gene causes SCA8. Notably, sequencing of a number of SCA8 patients has revealed that expanded alleles can also contain one or more CCG, CTA, CTC, CTT or CCA interruptions<sup>379</sup>. These mutations have been postulated to affect penetrance of SCA8.

Therefore, these findings provide evidence that mutations do occur in triplet repeat sequences, and that current methods of genetic testing would overlook mutations in the expanded repeat regions of disease genes. In the past, accurately sequencing repeat stretches was a costly and challenging process, and likely represents the reason why testing based on repeat size was adopted as the preferred method of genetic diagnosis for triplet repeat diseases. However, advances in sequencing technology have made it a relatively rapid and inexpensive method for genetic testing. In the context of HD, we hypothesize that structural-mutations within the expanded polyglutamine tract of huntingtin occur and may contribute to the variability of disease-onset between patients with the same repeat lengths. Furthermore, we hypothesize that the sequencing of patients that present to the clinic with HD-like symptoms, but do not have a CAG expansion in *Htt*, may reveal mutations that affect the conformational flexibility of the polyglutamine tract.

### 5.2.1 Future Directions

Due to the accuracy and reliability of the huntingtin exon1 conformational sensor and the antibody-based FRET assay on endogenous, full-length huntingtin in a variety of cell systems, we hypothesize that they may be amenable for use as part of a high-content screen. Currently, our group is conducting an antibody-based, phenotypic screen using a natural compound library to identify small molecules that increase phosphorylation at serines 13 and 16 of huntingtin. Phosphorylation at these sites was shown to have a robust effect on the conformation of huntingtin in the context of exon1 as well as the full-length protein (chapter 3). Therefore, hits from the primary screen will be tested on previously generated *STHdh*<sup>Q7/Q7</sup> cells stably-expressing the mutant huntingtin exon1 sensor (~138 glutamines) and on HD fibroblasts using the antibody-based FLIM-FRET (chapter 3) assay to determine if novel compounds that promote phosphorylation at serines 13 and 16 can restore the conformation of mutant huntingtin to normal.

Furthermore, there are many disease proteins that undergo a change in conformation as part of the pathogenic process. We hypothesize, that a sensor like the one developed in chapter three of this thesis could be used to detect conformational changes of a wide variety of protein. Perhaps the most promising candidate to test is PrP, which becomes misfolded and propagates its toxic conformer to other PrP proteins in CJD. A conformational sensor that can detect the mutant PrP conformer in live cells or in patient samples could be used for a number of applications.

### 5.3 Huntingtin Inclusions

In chapter four of this thesis, we characterized two unique mutant huntingtin inclusion types, which we termed globular and fibrillar, based on morphology, structure and exchange dynamics in live cells. This was accomplished using a combination of super-resolution imaging, FRET, FRAP and IF techniques. Globular inclusions are loosely packed and readily exchange mutant huntingtin in and out of these inclusions on the microtubule cytoskeleton. Conversely, fibrillar inclusions are densely packed, sequester mutant huntingtin within the inclusion and their formation is independent of

the cytoskeleton. Thioflavin-T staining of the inclusions revealed that the fibrillar type contains a  $\beta$ -sheet-rich structure and are genuine amyloid fibrils. Additionally, both types of inclusions stained positive for ubiquitin, a marker used to identify misfolded protein. Notably, we demonstrated that we could skew the cellular population of inclusions towards the fibrillar type using phospho-mimetic mutations at serines 13 and 16 of N17 and by promoting the phosphorylation at these residues using small molecules. Previous studies have shown that mutant huntingtin is hypo-phosphorylated at serines 13 and 16 and that promoting phosphorylation at these residues abrogates the toxicity of mutant huntingtin<sup>57,128</sup>.

Therefore, this combination of assays provides the first evidence that mutant huntingtin can form two different inclusion types with unique properties in live cells. Based on these findings, we hypothesized that the globular type may represent a toxic inclusion species and that the fibrillar type may be protective. The definition of two distinct inclusion types, and the ability to reliably identify them, could lead to new insights into the controversy of the role of protein inclusions in HD and other polyglutamine diseases. Furthermore, the ability of small molecules to promote the formation of fibrillar inclusions may represent a novel therapeutic target for the treatment of HD.

### 5.3.1 Future directions

Protein aggregation is a common characteristic of many neurodegenerative diseases. Consistent with HD, it remains controversial whether inclusions in these diseases play a toxic or a protective role in the cell. Since mutant huntingtin can form at least two different inclusion types, we hypothesize that inclusion heterogeneity exists with other disease proteins. Therefore, by adapting the mutant huntingtin FRET sensor and the assays optimized in chapter four of this thesis, we postulate that we can detect if other disease proteins form different inclusion types. This hypothesis will first be tested on other polyglutamine disease proteins which can readily form inclusions.

Furthermore, due to the robust FRET differences measured between inclusions using the mutant huntingtin sensor, we hypothesize that it may be amenable for use in a

FRET-based high-content screen to identify compounds that can promote the formation of fibrillar inclusion formation or decrease globular inclusion formation. *STHdh*<sup>Q7/Q7</sup> and *STHdh*<sup>Q111/Q111</sup> HD knock-in cells stably-expressing the mutant huntingtin FRET sensor with 138 glutamines have already been generated for use in this screen.

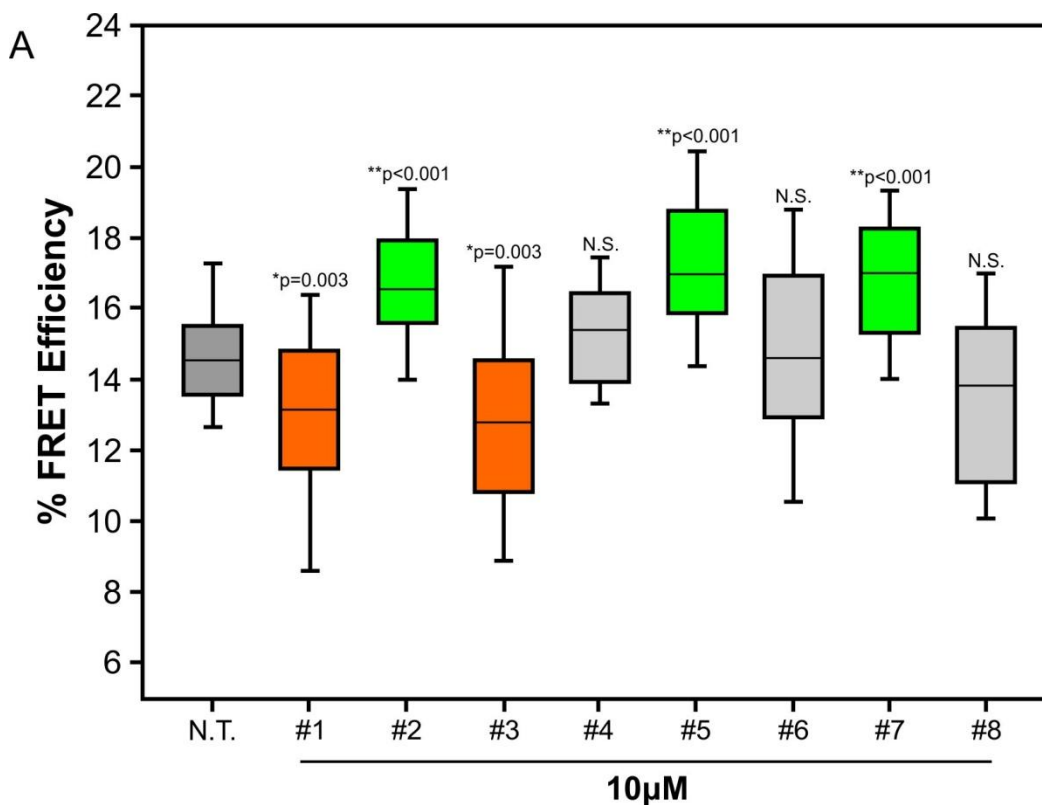


**Figure 5.1. Comparing the effect of eight novel inhibitors on the conformation of TG2. (A)** Quantitative FLIM-FRET data shown as percent FRET efficiency for the mCerulean-TG2-eYFP FRET sensor after a 16 hour treatment with eight TG2 inhibitors (labelled 1-8) at 10 $\mu$ M. Compound #1: CHDI-00340192-0000-002, #2: CHDI-00316470-0000-002, #3: CHDI-00339899-0000-002, #4: CHDI-00316226-0000-003, #5: CHDI-00329618-0000-002, #6: CHDI-00339972-0000-002, #7: CHDI-00339824-0000-002, #8: CHDI-00315225-0000-002.

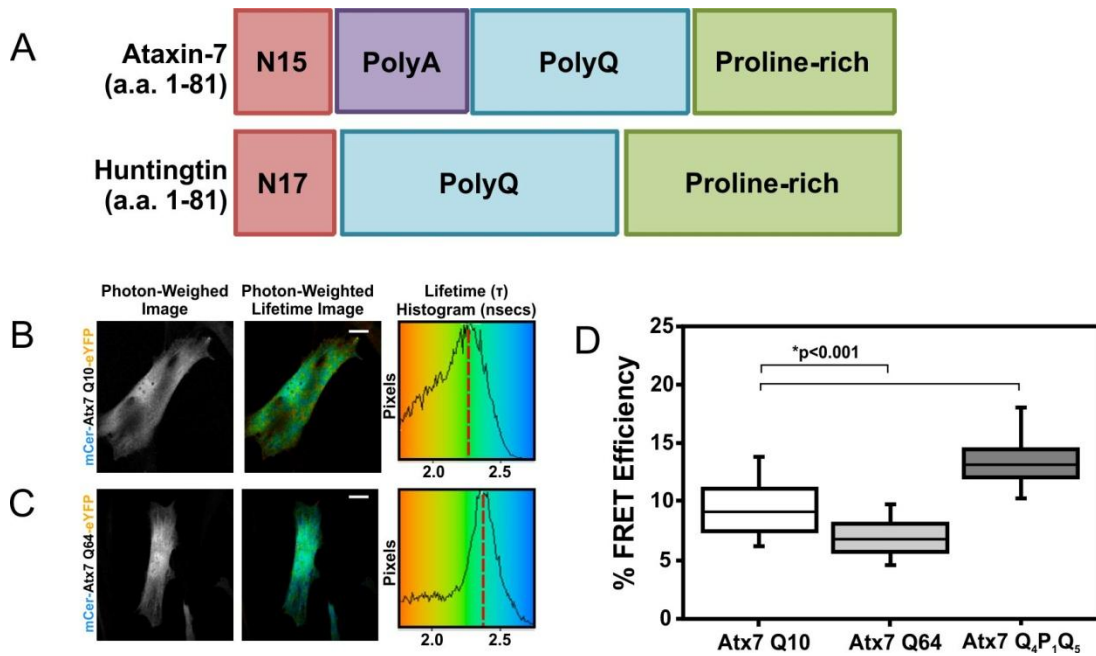


**Figure 5.2. The polyglutamine tract of ataxin-7 behaves as a flexible hinge that is impaired at pathogenic lengths.** (A) Schematic representation comparing the similarity of domains between the first 81 a.a. of huntingtin and ataxin-7 (Atx7). Sample FLIM images of (B) mCer-Atx7 Q10-eYFP and (C) mCer-Atx7 Q64-eYFP constructs expressed in wild-type human fibroblasts. (D) Quantitative FLIM-FRET data shown as percent FRET efficiency for the mCer-Atx7 Q10-eYFP, mCer-Atx7 Q64-eYFP and mCer-Atx7 Q<sub>4</sub>P<sub>1</sub>Q<sub>5</sub>-eYFP constructs.

## Reference List

1. Evans, S.J. et al. Prevalence of adult Huntington's disease in the UK based on diagnoses recorded in general practice records. *J Neurol Neurosurg Psychiatry* **84**, 1156-60 (2013).
2. Vonsattel, J.P. et al. Neuropathological classification of Huntington's disease. *J Neuropathol Exp Neurol* **44**, 559-77 (1985).
3. Yanagisawa, N. The spectrum of motor disorders in Huntington's disease. *Clin Neurol Neurosurg* **94 Suppl**, S182-4 (1992).
4. Norton, J.C. Patterns of neuropsychological test performance in Huntington's disease. *J Nerv Ment Dis* **161**, 276-9 (1975).
5. Josiassen, R.C., Curry, L.M. & Mancall, E.L. Development of neuropsychological deficits in Huntington's disease. *Arch Neurol* **40**, 791-6 (1983).
6. Caine, E.D. & Shoulson, I. Psychiatric syndromes in Huntington's disease. *Am J Psychiatry* **140**, 728-33 (1983).
7. A novel gene containing a trinucleotide repeat that is expanded and unstable on Huntington's disease chromosomes. The Huntington's Disease Collaborative Research Group. *Cell* **72**, 971-983 (1993).
8. Duyao, M. et al. Trinucleotide repeat length instability and age of onset in Huntington's disease. *Nat Genet* **4**, 387-92 (1993).
9. Snell, R.G. et al. Relationship between trinucleotide repeat expansion and phenotypic variation in Huntington's disease. *Nat Genet* **4**, 393-7 (1993).
10. Stine, O.C. et al. Correlation between the onset age of Huntington's disease and length of the trinucleotide repeat in IT-15. *Hum Mol Genet* **2**, 1547-9 (1993).
11. Kloppel, S. et al. Automatic detection of preclinical neurodegeneration: presymptomatic Huntington disease. *Neurology* **72**, 426-31 (2009).
12. Rizk-Jackson, A. et al. Evaluating imaging biomarkers for neurodegeneration in pre-symptomatic Huntington's disease using machine learning techniques. *Neuroimage* **56**, 788-96 (2011).
13. Huntington, G. On chorea. George Huntington, M.D. *J Neuropsychiatry Clin Neurosci* **15**, 109-12 (2003).
14. Lannois, M., Paviot, J. Deux cas de chorée héréditaire avec autopsies. *Arch Neurol (Paris)* **4**, 333-334 (1897).
15. Macleod, M.D. Cases of choreic convulsions in persons of advanced age. *British Journal of Psychiatry* **27**, 194-200 (1881).
16. Klein, J. *Woody Guthrie: a life*, (Dell Publishing/Random House, Inc., New York, NY, 1980).
17. Gusella, J.F. et al. A polymorphic DNA marker genetically linked to Huntington's disease. *Nature* **306**, 234-8 (1983).
18. Robbins, C. et al. Evidence from family studies that the gene causing Huntington disease is telomeric to D4S95 and D4S90. *Am J Hum Genet* **44**, 422-5 (1989).
19. La Spada, A.R., Wilson, E.M., Lubahn, D.B., Harding, A.E. & Fischbeck, K.H. Androgen receptor gene mutations in X-linked spinal and bulbar muscular atrophy. *Nature* **352**, 77-9 (1991).
20. Mangiarini, L. et al. Exon 1 of the HD gene with an expanded CAG repeat is sufficient to cause a progressive neurological phenotype in transgenic mice. *Cell* **87**, 493-506 (1996).
21. DiFiglia, M. et al. Aggregation of huntingtin in neuronal intranuclear inclusions and dystrophic neurites in brain. *Science* **277**, 1990-3 (1997).
22. Ambrose, C.M. et al. Structure and expression of the Huntington's disease gene: evidence against simple inactivation due to an expanded CAG repeat. *Somat Cell Mol Genet* **20**, 27-38 (1994).

23. McNeil, S.M. et al. Reduced penetrance of the Huntington's disease mutation. *Hum Mol Genet* **6**, 775-9 (1997).
24. Topper, R., Schwarz, M., Lange, H.W., Hefter, H. & Noth, J. Neurophysiological abnormalities in the Westphal variant of Huntington's disease. *Mov Disord* **13**, 920-8 (1998).
25. Kiebertz, K. et al. Trinucleotide repeat length and progression of illness in Huntington's disease. *J Med Genet* **31**, 872-4 (1994).
26. Trottier, Y., Biancalana, V. & Mandel, J.L. Instability of CAG repeats in Huntington's disease: relation to parental transmission and age of onset. *J Med Genet* **31**, 377-82 (1994).
27. Kremer, B. et al. Sex-dependent mechanisms for expansions and contractions of the CAG repeat on affected Huntington disease chromosomes. *Am J Hum Genet* **57**, 343-50 (1995).
28. Durr, A. et al. Homozygosity in Huntington's disease. *J Med Genet* **36**, 172-3 (1999).
29. Wexler, N.S. et al. Homozygotes for Huntington's disease. *Nature* **326**, 194-7 (1987).
30. Lee, J.M. et al. CAG repeat expansion in Huntington disease determines age at onset in a fully dominant fashion. *Neurology* **78**, 690-5 (2012).
31. Reiner, A. et al. Differential loss of striatal projection neurons in Huntington disease. *Proc Natl Acad Sci U S A* **85**, 5733-7 (1988).
32. Cicchetti, F. & Parent, A. Striatal interneurons in Huntington's disease: selective increase in the density of calretinin-immunoreactive medium-sized neurons. *Mov Disord* **11**, 619-26 (1996).
33. Slow, E.J. et al. Selective striatal neuronal loss in a YAC128 mouse model of Huntington disease. *Hum Mol Genet* **12**, 1555-67 (2003).
34. Gray, M. et al. Full-length human mutant huntingtin with a stable polyglutamine repeat can elicit progressive and selective neuropathogenesis in BACHD mice. *J Neurosci* **28**, 6182-95 (2008).
35. Rosas, H.D. et al. Evidence for more widespread cerebral pathology in early HD: an MRI-based morphometric analysis. *Neurology* **60**, 1615-20 (2003).
36. Rosas, H.D. et al. Diffusion tensor imaging in presymptomatic and early Huntington's disease: Selective white matter pathology and its relationship to clinical measures. *Mov Disord* **21**, 1317-25 (2006).
37. Sturrock, A. & Leavitt, B.R. The clinical and genetic features of Huntington disease. *J Geriatr Psychiatry Neurol* **23**, 243-59 (2010).
38. Shiwach, R. Psychopathology in Huntington's disease patients. *Acta Psychiatr Scand* **90**, 241-6 (1994).
39. Schoenfeld, M. et al. Increased rate of suicide among patients with Huntington's disease. *J Neurol Neurosurg Psychiatry* **47**, 1283-7 (1984).
40. Truant, R. et al. Canadian Association of Neurosciences Review: polyglutamine expansion neurodegenerative diseases. *Can J Neurol Sci* **33**, 278-91 (2006).
41. La Spada, A.R. & Taylor, J.P. Repeat expansion disease: progress and puzzles in disease pathogenesis. *Nat Rev Genet* **11**, 247-58 (2010).
42. Verkerk, A.J. et al. Identification of a gene (FMR-1) containing a CGG repeat coincident with a breakpoint cluster region exhibiting length variation in fragile X syndrome. *Cell* **65**, 905-14 (1991).
43. Brook, J.D. et al. Molecular basis of myotonic dystrophy: expansion of a trinucleotide (CTG) repeat at the 3' end of a transcript encoding a protein kinase family member. *Cell* **69**, 385 (1992).
44. Liquori, C.L. et al. Myotonic dystrophy type 2 caused by a CCTG expansion in intron 1 of ZNF9. *Science* **293**, 864-7 (2001).
45. DeJesus-Hernandez, M. et al. Expanded GGGGCC hexanucleotide repeat in noncoding region of C9ORF72 causes chromosome 9p-linked FTD and ALS. *Neuron* **72**, 245-56 (2011).

46. Renton, A.E. et al. A hexanucleotide repeat expansion in C9ORF72 is the cause of chromosome 9p21-linked ALS-FTD. *Neuron* **72**, 257-68 (2011).
47. Beck, J. et al. Large C9orf72 hexanucleotide repeat expansions are seen in multiple neurodegenerative syndromes and are more frequent than expected in the UK population. *Am J Hum Genet* **92**, 345-53 (2013).
48. Strong, T.V. et al. Widespread expression of the human and rat Huntington's disease gene in brain and nonneural tissues. *Nat Genet* **5**, 259-65 (1993).
49. Li, S.H. et al. Huntington's disease gene (IT15) is widely expressed in human and rat tissues. *Neuron* **11**, 985-93 (1993).
50. Atwal, R.S. et al. Huntingtin has a membrane association signal that can modulate huntingtin aggregation, nuclear entry and toxicity. *Hum Mol Genet* **16**, 2600-15 (2007).
51. DiFiglia, M. et al. Huntingtin is a cytoplasmic protein associated with vesicles in human and rat brain neurons. *Neuron* **14**, 1075-81 (1995).
52. Song, W. et al. Mutant huntingtin binds the mitochondrial fission GTPase dynamin-related protein-1 and increases its enzymatic activity. *Nat Med* **17**, 377-82 (2011).
53. Choo, Y.S., Johnson, G.V., MacDonald, M., Detloff, P.J. & Lesort, M. Mutant huntingtin directly increases susceptibility of mitochondria to the calcium-induced permeability transition and cytochrome c release. *Hum Mol Genet* **13**, 1407-20 (2004).
54. Strehlow, A.N., Li, J.Z. & Myers, R.M. Wild-type huntingtin participates in protein trafficking between the Golgi and the extracellular space. *Hum Mol Genet* **16**, 391-409 (2007).
55. Keryer, G. et al. Ciliogenesis is regulated by a huntingtin-HAP1-PCM1 pathway and is altered in Huntington disease. *J Clin Invest* **121**, 4372-82 (2011).
56. Hoffner, G., Kahlem, P. & Djian, P. Perinuclear localization of huntingtin as a consequence of its binding to microtubules through an interaction with beta-tubulin: relevance to Huntington's disease. *J Cell Sci* **115**, 941-8 (2002).
57. Atwal, R.S. et al. Kinase inhibitors modulate huntingtin cell localization and toxicity. *Nat Chem Biol* **7**, 453-60 (2011).
58. Munsie, L. et al. Mutant huntingtin causes defective actin remodeling during stress: defining a new role for transglutaminase 2 in neurodegenerative disease. *Hum Mol Genet* **20**, 1937-51 (2011).
59. Godin, J.D. et al. Huntingtin is required for mitotic spindle orientation and mammalian neurogenesis. *Neuron* **67**, 392-406 (2010).
60. Angeli, S., Shao, J. & Diamond, M.I. F-actin binding regions on the androgen receptor and huntingtin increase aggregation and alter aggregate characteristics. *PLoS One* **5**, e9053 (2010).
61. Benn, C.L. et al. Huntingtin modulates transcription, occupies gene promoters in vivo, and binds directly to DNA in a polyglutamine-dependent manner. *J Neurosci* **28**, 10720-33 (2008).
62. Savas, J.N. et al. A role for huntington disease protein in dendritic RNA granules. *J Biol Chem* **285**, 13142-53 (2010).
63. Burke, K.A., Hensal, K.M., Umbaugh, C.S., Chaibva, M. & Legleiter, J. Huntingtin disrupts lipid bilayers in a polyQ-length dependent manner. *Biochim Biophys Acta* **1828**, 1953-61 (2013).
64. Michalek, M., Salnikov, E.S., Werten, S. & Bechinger, B. Membrane interactions of the amphipathic amino terminus of huntingtin. *Biochemistry* **52**, 847-58 (2013).
65. Tartari, M. et al. Phylogenetic comparison of huntingtin homologues reveals the appearance of a primitive polyQ in sea urchin. *Mol Biol Evol* **25**, 330-8 (2008).
66. Cattaneo, E., Zuccato, C. & Tartari, M. Normal huntingtin function: an alternative approach to Huntington's disease. *Nat Rev Neurosci* **6**, 919-30 (2005).
67. Andrade, M.A. & Bork, P. HEAT repeats in the Huntington's disease protein. *Nat Genet* **11**, 115-6 (1995).

68. Candiani, S., Pestarino, M., Cattaneo, E. & Tartari, M. Characterization, developmental expression and evolutionary features of the huntingtin gene in the amphioxus *Branchiostoma floridae*. *BMC Dev Biol* **7**, 127 (2007).
69. Takano, H. & Gusella, J.F. The predominantly HEAT-like motif structure of huntingtin and its association and coincident nuclear entry with dorsal, an NF- $\kappa$ B/Rel/dorsal family transcription factor. *BMC Neurosci* **3**, 15 (2002).
70. Kobe, B. & Kajava, A.V. When protein folding is simplified to protein coiling: the continuum of solenoid protein structures. *Trends Biochem Sci* **25**, 509-15 (2000).
71. Seong, I.S. et al. Huntingtin facilitates polycomb repressive complex 2. *Hum Mol Genet* **19**, 573-83 (2010).
72. Grinthal, A., Adamovic, I., Weiner, B., Karplus, M. & Kleckner, N. PR65, the HEAT-repeat scaffold of phosphatase PP2A, is an elastic connector that links force and catalysis. *Proc Natl Acad Sci U S A* **107**, 2467-72 (2010).
73. Rockabrand, E. et al. The first 17 amino acids of Huntingtin modulate its sub-cellular localization, aggregation and effects on calcium homeostasis. *Hum Mol Genet* **16**, 61-77 (2007).
74. Shirasaki, D.I. et al. Network organization of the huntingtin proteomic interactome in mammalian brain. *Neuron* **75**, 41-57 (2012).
75. Maiuri, T., Woloshansky, T., Xia, J. & Truant, R. The huntingtin N17 domain is a multifunctional CRM1 and Ran-dependent nuclear and cilial export signal. *Hum Mol Genet* **22**, 1383-94 (2013).
76. Kim, M.W., Chelliah, Y., Kim, S.W., Otwinowski, Z. & Bezprozvanny, I. Secondary structure of Huntingtin amino-terminal region. *Structure* **17**, 1205-12 (2009).
77. Kim, M. Beta conformation of polyglutamine track revealed by a crystal structure of Huntingtin N-terminal region with insertion of three histidine residues. *Prion* **7**, 221-8 (2013).
78. Lakhani, V.V., Ding, F. & Dokholyan, N.V. Polyglutamine induced misfolding of huntingtin exon1 is modulated by the flanking sequences. *PLoS Comput Biol* **6**, e1000772 (2010).
79. Darnell, G., Orgel, J.P., Pahl, R. & Meredith, S.C. Flanking polyproline sequences inhibit beta-sheet structure in polyglutamine segments by inducing PPII-like helix structure. *J Mol Biol* **374**, 688-704 (2007).
80. Burnett, B.G., Andrews, J., Ranganathan, S., Fischbeck, K.H. & Di Prospero, N.A. Expression of expanded polyglutamine targets profilin for degradation and alters actin dynamics. *Neurobiol Dis* **30**, 365-74 (2008).
81. Modregger, J., DiProspero, N.A., Charles, V., Tagle, D.A. & Plomann, M. PACSIN 1 interacts with huntingtin and is absent from synaptic varicosities in presymptomatic Huntington's disease brains. *Hum Mol Genet* **11**, 2547-58 (2002).
82. Desmond, C.R., Atwal, R.S., Xia, J. & Truant, R. Identification of a karyopherin beta1/beta2 proline-tyrosine nuclear localization signal in huntingtin protein. *J Biol Chem* **287**, 39626-33 (2012).
83. Wellington, C.L. et al. Caspase cleavage of gene products associated with triplet expansion disorders generates truncated fragments containing the polyglutamine tract. *J Biol Chem* **273**, 9158-67 (1998).
84. Wellington, C.L. et al. Inhibiting caspase cleavage of huntingtin reduces toxicity and aggregate formation in neuronal and nonneuronal cells. *J Biol Chem* **275**, 19831-8 (2000).
85. Gafni, J. & Ellerby, L.M. Calpain activation in Huntington's disease. *J Neurosci* **22**, 4842-9 (2002).
86. Gafni, J. et al. Inhibition of calpain cleavage of huntingtin reduces toxicity: accumulation of calpain/caspase fragments in the nucleus. *J Biol Chem* **279**, 20211-20 (2004).
87. Xia, J., Lee, D.H., Taylor, J., Vandelft, M. & Truant, R. Huntingtin contains a highly conserved nuclear export signal. *Hum Mol Genet* **12**, 1393-403 (2003).

88. Nasir, J. et al. Targeted disruption of the Huntington's disease gene results in embryonic lethality and behavioral and morphological changes in heterozygotes. *Cell* **81**, 811-23 (1995).
89. Duyao, M.P. et al. Inactivation of the mouse Huntington's disease gene homolog Hdh. *Science* **269**, 407-10 (1995).
90. Zeitlin, S., Liu, J.P., Chapman, D.L., Papaioannou, V.E. & Efstratiadis, A. Increased apoptosis and early embryonic lethality in mice nullizygous for the Huntington's disease gene homologue. *Nat Genet* **11**, 155-63 (1995).
91. White, J.K. et al. Huntingtin is required for neurogenesis and is not impaired by the Huntington's disease CAG expansion. *Nat Genet* **17**, 404-10 (1997).
92. Caviston, J.P. & Holzbaur, E.L. Huntingtin as an essential integrator of intracellular vesicular trafficking. *Trends Cell Biol* **19**, 147-55 (2009).
93. Li, X.J. et al. A huntingtin-associated protein enriched in brain with implications for pathology. *Nature* **378**, 398-402 (1995).
94. Engelen, S. et al. Huntingtin-associated protein 1 (HAP1) interacts with the p150Glued subunit of dynactin. *Hum Mol Genet* **6**, 2205-12 (1997).
95. Li, S.H., Gutekunst, C.A., Hersch, S.M. & Li, X.J. Interaction of huntingtin-associated protein with dynactin P150Glued. *J Neurosci* **18**, 1261-9 (1998).
96. Caviston, J.P., Ross, J.L., Antony, S.M., Tokito, M. & Holzbaur, E.L. Huntingtin facilitates dynein/dynactin-mediated vesicle transport. *Proc Natl Acad Sci U S A* **104**, 10045-50 (2007).
97. Gauthier, L.R. et al. Huntingtin controls neurotrophic support and survival of neurons by enhancing BDNF vesicular transport along microtubules. *Cell* **118**, 127-38 (2004).
98. Trushina, E. et al. Mutant huntingtin inhibits clathrin-independent endocytosis and causes accumulation of cholesterol in vitro and in vivo. *Hum Mol Genet* **15**, 3578-91 (2006).
99. Li, X. et al. Mutant huntingtin impairs vesicle formation from recycling endosomes by interfering with Rab11 activity. *Mol Cell Biol* **29**, 6106-16 (2009).
100. Waelter, S. et al. The huntingtin interacting protein HIP1 is a clathrin and alpha-adaptin-binding protein involved in receptor-mediated endocytosis. *Hum Mol Genet* **10**, 1807-17 (2001).
101. Metzler, M. et al. HIP1 functions in clathrin-mediated endocytosis through binding to clathrin and adaptor protein 2. *J Biol Chem* **276**, 39271-6 (2001).
102. Peters, M.F. & Ross, C.A. Isolation of a 40-kDa Huntingtin-associated protein. *J Biol Chem* **276**, 3188-94 (2001).
103. Zerial, M. & McBride, H. Rab proteins as membrane organizers. *Nat Rev Mol Cell Biol* **2**, 107-17 (2001).
104. Pal, A., Severin, F., Lommer, B., Shevchenko, A. & Zerial, M. Huntingtin-HAP40 complex is a novel Rab5 effector that regulates early endosome motility and is up-regulated in Huntington's disease. *J Cell Biol* **172**, 605-18 (2006).
105. Qualmann, B., Roos, J., DiGregorio, P.J. & Kelly, R.B. Syndapin I, a synaptic dynamin-binding protein that associates with the neural Wiskott-Aldrich syndrome protein. *Mol Biol Cell* **10**, 501-13 (1999).
106. Halbach, A. et al. PACSIN 1 forms tetramers via its N-terminal F-BAR domain. *FEBS J* **274**, 773-82 (2007).
107. Qualmann, B. & Kelly, R.B. Syndapin isoforms participate in receptor-mediated endocytosis and actin organization. *J Cell Biol* **148**, 1047-62 (2000).
108. Singaraja, R.R. et al. HIP14, a novel ankyrin domain-containing protein, links huntingtin to intracellular trafficking and endocytosis. *Hum Mol Genet* **11**, 2815-28 (2002).
109. Huang, K. et al. Huntingtin-interacting protein HIP14 is a palmitoyl transferase involved in palmitoylation and trafficking of multiple neuronal proteins. *Neuron* **44**, 977-86 (2004).

110. Yanai, A. et al. Palmitoylation of huntingtin by HIP14 is essential for its trafficking and function. *Nat Neurosci* **9**, 824-31 (2006).
111. Garcia, E.P. et al. SAP90 binds and clusters kainate receptors causing incomplete desensitization. *Neuron* **21**, 727-39 (1998).
112. Sun, Y., Savanenin, A., Reddy, P.H. & Liu, Y.F. Polyglutamine-expanded huntingtin promotes sensitization of N-methyl-D-aspartate receptors via post-synaptic density 95. *J Biol Chem* **276**, 24713-8 (2001).
113. Perez-Otano, I. et al. Endocytosis and synaptic removal of NR3A-containing NMDA receptors by PACSIN1/syndapin1. *Nat Neurosci* **9**, 611-21 (2006).
114. Marco, S. et al. Suppressing aberrant GluN3A expression rescues synaptic and behavioral impairments in Huntington's disease models. *Nat Med* **19**, 1030-8 (2013).
115. Drummond, I.A., McClure, S.A., Poenie, M., Tsien, R.Y. & Steinhardt, R.A. Large changes in intracellular pH and calcium observed during heat shock are not responsible for the induction of heat shock proteins in *Drosophila melanogaster*. *Mol Cell Biol* **6**, 1767-75 (1986).
116. Nishida, E., Maekawa, S. & Sakai, H. Cofilin, a protein in porcine brain that binds to actin filaments and inhibits their interactions with myosin and tropomyosin. *Biochemistry* **23**, 5307-13 (1984).
117. Bernstein, B.W. & Bamberg, J.R. Actin-ATP hydrolysis is a major energy drain for neurons. *J Neurosci* **23**, 1-6 (2003).
118. Nath, S., Munsie, L.N., Truant, R. A novel cell stress response involving the huntingtin protein results in the arrest of energy-dependent endosomal trafficking. (2013).
119. Kedersha, N. & Anderson, P. Mammalian stress granules and processing bodies. *Methods Enzymol* **431**, 61-81 (2007).
120. Duennwald, M.L., Jagadish, S., Muchowski, P.J. & Lindquist, S. Flanking sequences profoundly alter polyglutamine toxicity in yeast. *Proc Natl Acad Sci U S A* **103**, 11045-50 (2006).
121. Saudou, F., Finkbeiner, S., Devys, D. & Greenberg, M.E. Huntingtin acts in the nucleus to induce apoptosis but death does not correlate with the formation of intranuclear inclusions. *Cell* **95**, 55-66 (1998).
122. Hackam, A.S. et al. The influence of huntingtin protein size on nuclear localization and cellular toxicity. *J Cell Biol* **141**, 1097-105 (1998).
123. Cooper, J.K. et al. Truncated N-terminal fragments of huntingtin with expanded glutamine repeats form nuclear and cytoplasmic aggregates in cell culture. *Hum Mol Genet* **7**, 783-90 (1998).
124. Aiken, C.T. et al. Phosphorylation of threonine 3: implications for Huntingtin aggregation and neurotoxicity. *J Biol Chem* **284**, 29427-36 (2009).
125. Steffan, J.S. et al. SUMO modification of Huntingtin and Huntington's disease pathology. *Science* **304**, 100-4 (2004).
126. Thompson, L.M. et al. IKK phosphorylates Huntingtin and targets it for degradation by the proteasome and lysosome. *J Cell Biol* **187**, 1083-99 (2009).
127. Gu, X. et al. Serines 13 and 16 are critical determinants of full-length human mutant huntingtin induced disease pathogenesis in HD mice. *Neuron* **64**, 828-40 (2009).
128. Di Pardo, A. et al. Ganglioside GM1 induces phosphorylation of mutant huntingtin and restores normal motor behavior in Huntington disease mice. *Proc Natl Acad Sci U S A* **109**, 3528-33 (2012).
129. Witke, W. The role of profilin complexes in cell motility and other cellular processes. *Trends Cell Biol* **14**, 461-9 (2004).
130. Shao, J., Welch, W.J., Diprospero, N.A. & Diamond, M.I. Phosphorylation of profilin by ROCK1 regulates polyglutamine aggregation. *Mol Cell Biol* **28**, 5196-208 (2008).

131. Grimm-Gunter, E.M., Milbrandt, M., Merkl, B., Paulsson, M. & Plomann, M. PACSIN proteins bind tubulin and promote microtubule assembly. *Exp Cell Res* **314**, 1991-2003 (2008).
132. Dehay, B. & Bertolotti, A. Critical role of the proline-rich region in Huntingtin for aggregation and cytotoxicity in yeast. *J Biol Chem* **281**, 35608-15 (2006).
133. Truant, R., Atwal, R.S., Desmond, C., Munsie, L. & Tran, T. Huntington's disease: revisiting the aggregation hypothesis in polyglutamine neurodegenerative diseases. *FEBS J* **275**, 4252-62 (2008).
134. Dlugosz, M. & Trylska, J. Secondary structures of native and pathogenic huntingtin N-terminal fragments. *J Phys Chem B* **115**, 11597-608 (2011).
135. Bliss, T.V. & Collingridge, G.L. A synaptic model of memory: long-term potentiation in the hippocampus. *Nature* **361**, 31-9 (1993).
136. Arundine, M. & Tymianski, M. Molecular mechanisms of calcium-dependent neurodegeneration in excitotoxicity. *Cell Calcium* **34**, 325-37 (2003).
137. Dong, X.X., Wang, Y. & Qin, Z.H. Molecular mechanisms of excitotoxicity and their relevance to pathogenesis of neurodegenerative diseases. *Acta Pharmacol Sin* **30**, 379-87 (2009).
138. Fan, M.M. & Raymond, L.A. N-methyl-D-aspartate (NMDA) receptor function and excitotoxicity in Huntington's disease. *Prog Neurobiol* **81**, 272-93 (2007).
139. McGeer, E.G. & McGeer, P.L. Duplication of biochemical changes of Huntington's chorea by intrastriatal injections of glutamic and kainic acids. *Nature* **263**, 517-9 (1976).
140. Schwarcz, R., Foster, A.C., French, E.D., Whetsell, W.O., Jr. & Kohler, C. Excitotoxic models for neurodegenerative disorders. *Life Sci* **35**, 19-32 (1984).
141. Young, A.B. et al. NMDA receptor losses in putamen from patients with Huntington's disease. *Science* **241**, 981-3 (1988).
142. London, E.D., Yamamura, H.I., Bird, E.D. & Coyle, J.T. Decreased receptor-binding sites for kainic acid in brains of patients with Huntington's disease. *Biol Psychiatry* **16**, 155-62 (1981).
143. Hardingham, G.E., Fukunaga, Y. & Bading, H. Extrasynaptic NMDARs oppose synaptic NMDARs by triggering CREB shut-off and cell death pathways. *Nat Neurosci* **5**, 405-14 (2002).
144. Milnerwood, A.J. et al. Early increase in extrasynaptic NMDA receptor signaling and expression contributes to phenotype onset in Huntington's disease mice. *Neuron* **65**, 178-90 (2010).
145. Borlongan, C.V., Koutouzis, T.K. & Sanberg, P.R. 3-Nitropropionic acid animal model and Huntington's disease. *Neurosci Biobehav Rev* **21**, 289-93 (1997).
146. Liot, G. et al. Complex II inhibition by 3-NP causes mitochondrial fragmentation and neuronal cell death via an NMDA- and ROS-dependent pathway. *Cell Death Differ* **16**, 899-909 (2009).
147. Orr, A.L. et al. N-terminal mutant huntingtin associates with mitochondria and impairs mitochondrial trafficking. *J Neurosci* **28**, 2783-92 (2008).
148. Trushina, E. et al. Mutant huntingtin impairs axonal trafficking in mammalian neurons in vivo and in vitro. *Mol Cell Biol* **24**, 8195-209 (2004).
149. Horton, T.M. et al. Marked increase in mitochondrial DNA deletion levels in the cerebral cortex of Huntington's disease patients. *Neurology* **45**, 1879-83 (1995).
150. Cantuti-Castelvetri, I. et al. Somatic mitochondrial DNA mutations in single neurons and glia. *Neurobiol Aging* **26**, 1343-55 (2005).
151. Gines, S. et al. Specific progressive cAMP reduction implicates energy deficit in presymptomatic Huntington's disease knock-in mice. *Hum Mol Genet* **12**, 497-508 (2003).
152. Jenkins, B.G., Koroshetz, W.J., Beal, M.F. & Rosen, B.R. Evidence for impairment of energy metabolism in vivo in Huntington's disease using localized <sup>1</sup>H NMR spectroscopy. *Neurology* **43**, 2689-95 (1993).
153. Kuhl, D.E. et al. Cerebral metabolism and atrophy in Huntington's disease determined by <sup>18</sup>F-DG and computed tomographic scan. *Ann Neurol* **12**, 425-34 (1982).

154. Kuhl, D.E. et al. Local cerebral glucose utilization in symptomatic and presymptomatic Huntington's disease. *Res Publ Assoc Res Nerv Ment Dis* **63**, 199-209 (1985).
155. Feigin, A. et al. Metabolic network abnormalities in early Huntington's disease: an [(18)F]FDG PET study. *J Nucl Med* **42**, 1591-5 (2001).
156. Friedman, L.K. Calcium: a role for neuroprotection and sustained adaptation. *Mol Interv* **6**, 315-29 (2006).
157. Cha, J.H. Transcriptional signatures in Huntington's disease. *Prog Neurobiol* **83**, 228-48 (2007).
158. Ferrer, I., Goutan, E., Marin, C., Rey, M.J. & Ribalta, T. Brain-derived neurotrophic factor in Huntington disease. *Brain Res* **866**, 257-61 (2000).
159. Zuccato, C. et al. Loss of huntingtin-mediated BDNF gene transcription in Huntington's disease. *Science* **293**, 493-8 (2001).
160. Zuccato, C. et al. Huntingtin interacts with REST/NRSF to modulate the transcription of NRSE-controlled neuronal genes. *Nat Genet* **35**, 76-83 (2003).
161. Li, S.H. et al. Interaction of Huntington disease protein with transcriptional activator Sp1. *Mol Cell Biol* **22**, 1277-87 (2002).
162. Dunah, A.W. et al. Sp1 and TAFII130 transcriptional activity disrupted in early Huntington's disease. *Science* **296**, 2238-43 (2002).
163. Steffan, J.S. et al. The Huntington's disease protein interacts with p53 and CREB-binding protein and represses transcription. *Proc Natl Acad Sci U S A* **97**, 6763-8 (2000).
164. Cong, S.Y. et al. Mutant huntingtin represses CBP, but not p300, by binding and protein degradation. *Mol Cell Neurosci* **30**, 560-71 (2005).
165. Cui, L. et al. Transcriptional repression of PGC-1alpha by mutant huntingtin leads to mitochondrial dysfunction and neurodegeneration. *Cell* **127**, 59-69 (2006).
166. Vashishtha, M. et al. Targeting H3K4 trimethylation in Huntington disease. *Proc Natl Acad Sci U S A* **110**, E3027-36 (2013).
167. Goldberg, Y.P. et al. Cleavage of huntingtin by apopain, a proapoptotic cysteine protease, is modulated by the polyglutamine tract. *Nat Genet* **13**, 442-9 (1996).
168. Kim, Y.J. et al. Caspase 3-cleaved N-terminal fragments of wild-type and mutant huntingtin are present in normal and Huntington's disease brains, associate with membranes, and undergo calpain-dependent proteolysis. *Proc Natl Acad Sci U S A* **98**, 12784-9 (2001).
169. Wellington, C.L. et al. Caspase cleavage of mutant huntingtin precedes neurodegeneration in Huntington's disease. *J Neurosci* **22**, 7862-72 (2002).
170. Graham, R.K. et al. Cleavage at the caspase-6 site is required for neuronal dysfunction and degeneration due to mutant huntingtin. *Cell* **125**, 1179-91 (2006).
171. Bizat, N. et al. Calpain is a major cell death effector in selective striatal degeneration induced in vivo by 3-nitropropionate: implications for Huntington's disease. *J Neurosci* **23**, 5020-30 (2003).
172. Lunke, A. et al. Proteases acting on mutant huntingtin generate cleaved products that differentially build up cytoplasmic and nuclear inclusions. *Mol Cell* **10**, 259-69 (2002).
173. Humbert, S. et al. The IGF-1/Akt pathway is neuroprotective in Huntington's disease and involves Huntingtin phosphorylation by Akt. *Dev Cell* **2**, 831-7 (2002).
174. Warby, S.C. et al. Phosphorylation of huntingtin reduces the accumulation of its nuclear fragments. *Mol Cell Neurosci* **40**, 121-7 (2009).
175. Luo, S., Vacher, C., Davies, J.E. & Rubinsztein, D.C. Cdk5 phosphorylation of huntingtin reduces its cleavage by caspases: implications for mutant huntingtin toxicity. *J Cell Biol* **169**, 647-56 (2005).
176. Becher, M.W. et al. Intranuclear neuronal inclusions in Huntington's disease and dentatorubral and pallidolulsian atrophy: correlation between the density of inclusions and IT15 CAG triplet repeat length. *Neurobiol Dis* **4**, 387-97 (1998).

177. Emamian, E.S. et al. Serine 776 of ataxin-1 is critical for polyglutamine-induced disease in SCA1 transgenic mice. *Neuron* **38**, 375-87 (2003).
178. Grundke-Iqbal, I. et al. Abnormal phosphorylation of the microtubule-associated protein tau (tau) in Alzheimer cytoskeletal pathology. *Proc Natl Acad Sci U S A* **83**, 4913-7 (1986).
179. Landles, C. et al. Proteolysis of mutant huntingtin produces an exon 1 fragment that accumulates as an aggregated protein in neuronal nuclei in Huntington disease. *J Biol Chem* **285**, 8808-23 (2010).
180. Dewji, N.N. et al. Processing of Alzheimer's disease-associated beta-amyloid precursor protein. *J Mol Neurosci* **2**, 19-27 (1990).
181. Giasson, B.I. et al. Oxidative damage linked to neurodegeneration by selective alpha-synuclein nitration in synucleinopathy lesions. *Science* **290**, 985-9 (2000).
182. Masters, C.L. et al. Amyloid plaque core protein in Alzheimer disease and Down syndrome. *Proc Natl Acad Sci U S A* **82**, 4245-9 (1985).
183. Kosik, K.S., Joachim, C.L. & Selkoe, D.J. Microtubule-associated protein tau (tau) is a major antigenic component of paired helical filaments in Alzheimer disease. *Proc Natl Acad Sci U S A* **83**, 4044-8 (1986).
184. Spillantini, M.G. et al. Alpha-synuclein in Lewy bodies. *Nature* **388**, 839-40 (1997).
185. Shibata, N. et al. Cu/Zn superoxide dismutase-like immunoreactivity in Lewy body-like inclusions of sporadic amyotrophic lateral sclerosis. *Neurosci Lett* **179**, 149-52 (1994).
186. Hardy, J.A. & Higgins, G.A. Alzheimer's disease: the amyloid cascade hypothesis. *Science* **256**, 184-5 (1992).
187. Hardy, J. & Allsop, D. Amyloid deposition as the central event in the aetiology of Alzheimer's disease. *Trends Pharmacol Sci* **12**, 383-8 (1991).
188. Glabe, C.G. Common mechanisms of amyloid oligomer pathogenesis in degenerative disease. *Neurobiol Aging* **27**, 570-5 (2006).
189. Davies, S.W. et al. Formation of neuronal intranuclear inclusions underlies the neurological dysfunction in mice transgenic for the HD mutation. *Cell* **90**, 537-48 (1997).
190. Perutz, M.F., Johnson, T., Suzuki, M. & Finch, J.T. Glutamine repeats as polar zippers: their possible role in inherited neurodegenerative diseases. *Proc Natl Acad Sci U S A* **91**, 5355-8 (1994).
191. Perutz, M.F. Glutamine repeats as polar zippers: their role in inherited neurodegenerative disease. *Mol Med* **1**, 718-21 (1995).
192. Perutz, M.F. Glutamine repeats and inherited neurodegenerative diseases: molecular aspects. *Curr Opin Struct Biol* **6**, 848-58 (1996).
193. Nagai, Y. et al. A toxic monomeric conformer of the polyglutamine protein. *Nat Struct Mol Biol* **14**, 332-40 (2007).
194. Bence, N.F., Sampat, R.M. & Kopito, R.R. Impairment of the ubiquitin-proteasome system by protein aggregation. *Science* **292**, 1552-5 (2001).
195. Arrasate, M., Mitra, S., Schweitzer, E.S., Segal, M.R. & Finkbeiner, S. Inclusion body formation reduces levels of mutant huntingtin and the risk of neuronal death. *Nature* **431**, 805-10 (2004).
196. Preisinger, E., Jordan, B.M., Kazantsev, A. & Housman, D. Evidence for a recruitment and sequestration mechanism in Huntington's disease. *Philos Trans R Soc Lond B Biol Sci* **354**, 1029-34 (1999).
197. Suhr, S.T. et al. Identities of sequestered proteins in aggregates from cells with induced polyglutamine expression. *J Cell Biol* **153**, 283-94 (2001).
198. Nagai, Y., Onodera, O., Chun, J., Strittmatter, W.J. & Burke, J.R. Expanded polyglutamine domain proteins bind neurofilament and alter the neurofilament network. *Exp Neurol* **155**, 195-203 (1999).

199. Matsumoto, G., Kim, S. & Morimoto, R.I. Huntingtin and mutant SOD1 form aggregate structures with distinct molecular properties in human cells. *J Biol Chem* **281**, 4477-85 (2006).
200. Huang, C.C. et al. Amyloid formation by mutant huntingtin: threshold, progressivity and recruitment of normal polyglutamine proteins. *Somat Cell Mol Genet* **24**, 217-33 (1998).
201. Schaffar, G. et al. Cellular toxicity of polyglutamine expansion proteins: mechanism of transcription factor deactivation. *Mol Cell* **15**, 95-105 (2004).
202. Nucifora, F.C., Jr. et al. Interference by huntingtin and atrophin-1 with cbp-mediated transcription leading to cellular toxicity. *Science* **291**, 2423-8 (2001).
203. Gunawardena, S. et al. Disruption of axonal transport by loss of huntingtin or expression of pathogenic polyQ proteins in *Drosophila*. *Neuron* **40**, 25-40 (2003).
204. Holmberg, C.I., Staniszewski, K.E., Mensah, K.N., Matouschek, A. & Morimoto, R.I. Inefficient degradation of truncated polyglutamine proteins by the proteasome. *EMBO J* **23**, 4307-18 (2004).
205. Scherzinger, E. et al. Huntingtin-encoded polyglutamine expansions form amyloid-like protein aggregates in vitro and in vivo. *Cell* **90**, 549-58 (1997).
206. Yang, W., Dunlap, J.R., Andrews, R.B. & Wetzel, R. Aggregated polyglutamine peptides delivered to nuclei are toxic to mammalian cells. *Hum Mol Genet* **11**, 2905-17 (2002).
207. Slow, E.J. et al. Absence of behavioral abnormalities and neurodegeneration in vivo despite widespread neuronal huntingtin inclusions. *Proc Natl Acad Sci U S A* **102**, 11402-7 (2005).
208. Unified Huntington's Disease Rating Scale: reliability and consistency. Huntington Study Group. *Mov Disord* **11**, 136-42 (1996).
209. Tetrabenazine as antichorea therapy in Huntington disease : a randomized controlled trial. *Neurology* **66**, 366-372 (2006).
210. de Yebenes, J.G. et al. Pridopidine for the treatment of motor function in patients with Huntington's disease (MermaiHD): a phase 3, randomised, double-blind, placebo-controlled trial. *Lancet Neurol* **10**, 1049-57 (2011).
211. A randomized, double-blind, placebo-controlled trial of pridopidine in Huntington's disease. *Mov Disord* **28**, 1407-15 (2013).
212. Bonelli, R.M., Mahnert, F.A. & Niederwieser, G. Olanzapine for Huntington's disease: an open label study. *Clin Neuropharmacol* **25**, 263-5 (2002).
213. Squitieri, F. et al. Short-term effects of olanzapine in Huntington disease. *Neuropsychiatry Neuropsychol Behav Neurol* **14**, 69-72 (2001).
214. Gimenez-Roldan, S. & Mateo, D. [Huntington disease: tetrabenazine compared to haloperidol in the reduction of involuntary movements]. *Neurologia* **4**, 282-7 (1989).
215. Holl, A.K., Wilkinson, L., Painold, A., Holl, E.M. & Bonelli, R.M. Combating depression in Huntington's disease: effective antidepressive treatment with venlafaxine XR. *Int Clin Psychopharmacol* **25**, 46-50 (2010).
216. Killoran, A. & Biglan, K.M. Therapeutics in Huntington's Disease. *Curr Treat Options Neurol* (2012).
217. de Tommaso, M., Specchio, N., Scirucchio, V., Difruscolo, O. & Specchio, L.M. Effects of rivastigmine on motor and cognitive impairment in Huntington's disease. *Mov Disord* **19**, 1516-8 (2004).
218. de Tommaso, M., Difruscolo, O., Scirucchio, V., Specchio, N. & Livrea, P. Two years' follow-up of rivastigmine treatment in Huntington disease. *Clin Neuropharmacol* **30**, 43-6 (2007).
219. Birks, J., Grimley Evans, J., Iakovidou, V. & Tsolaki, M. Rivastigmine for Alzheimer's disease. *Cochrane Database Syst Rev*, CD001191 (2000).
220. Emre, M. et al. Rivastigmine for dementia associated with Parkinson's disease. *N Engl J Med* **351**, 2509-18 (2004).

221. Brown, T.E. & Landgraf, J.M. Improvements in executive function correlate with enhanced performance and functioning and health-related quality of life: evidence from 2 large, double-blind, randomized, placebo-controlled trials in ADHD. *Postgrad Med* **122**, 42-51 (2010).
222. Paulsen, J.S. et al. Preparing for preventive clinical trials: the Predict-HD study. *Arch Neurol* **63**, 883-90 (2006).
223. Tabrizi, S.J. et al. Predictors of phenotypic progression and disease onset in premanifest and early-stage Huntington's disease in the TRACK-HD study: analysis of 36-month observational data. *Lancet Neurol* **12**, 637-49 (2013).
224. Pellegrini, J.W. & Lipton, S.A. Delayed administration of memantine prevents N-methyl-D-aspartate receptor-mediated neurotoxicity. *Ann Neurol* **33**, 403-7 (1993).
225. Kornhuber, J., Weller, M., Schoppmeyer, K. & Riederer, P. Amantadine and memantine are NMDA receptor antagonists with neuroprotective properties. *J Neural Transm Suppl* **43**, 91-104 (1994).
226. Matthews, R.T. et al. Neuroprotective effects of creatine and cyclocreatine in animal models of Huntington's disease. *J Neurosci* **18**, 156-63 (1998).
227. Tabrizi, S.J. et al. High-dose creatine therapy for Huntington disease: a 2-year clinical and MRS study. *Neurology* **64**, 1655-6 (2005).
228. Smith, K.M. et al. Dose ranging and efficacy study of high-dose coenzyme Q10 formulations in Huntington's disease mice. *Biochim Biophys Acta* **1762**, 616-26 (2006).
229. Menalled, L.B. et al. Comprehensive behavioral testing in the R6/2 mouse model of Huntington's disease shows no benefit from CoQ10 or minocycline. *PLoS One* **5**, e9793 (2010).
230. A randomized, placebo-controlled trial of coenzyme Q10 and remacemide in Huntington's disease. *Neurology* **57**, 397-404 (2001).
231. Hockly, E. et al. Suberoylanilide hydroxamic acid, a histone deacetylase inhibitor, ameliorates motor deficits in a mouse model of Huntington's disease. *Proc Natl Acad Sci U S A* **100**, 2041-6 (2003).
232. Napper, A.D. et al. Discovery of indoles as potent and selective inhibitors of the deacetylase SIRT1. *J Med Chem* **48**, 8045-54 (2005).
233. Ho, D.J., Calingasan, N.Y., Wille, E., Dumont, M. & Beal, M.F. Resveratrol protects against peripheral deficits in a mouse model of Huntington's disease. *Exp Neurol* **225**, 74-84 (2010).
234. Lagouge, M. et al. Resveratrol improves mitochondrial function and protects against metabolic disease by activating SIRT1 and PGC-1alpha. *Cell* **127**, 1109-22 (2006).
235. Chopra, V. et al. The sirtuin 2 inhibitor AK-7 is neuroprotective in Huntington's disease mouse models. *Cell Rep* **2**, 1492-7 (2012).
236. Chen, M. et al. Minocycline inhibits caspase-1 and caspase-3 expression and delays mortality in a transgenic mouse model of Huntington disease. *Nat Med* **6**, 797-801 (2000).
237. A futility study of minocycline in Huntington's disease. *Mov Disord* **25**, 2219-24 (2010).
238. Varma, H. et al. Selective inhibitors of death in mutant huntingtin cells. *Nat Chem Biol* **3**, 99-100 (2007).
239. Chu, W., Rothfuss, J., Chu, Y., Zhou, D. & Mach, R.H. Synthesis and in vitro evaluation of sulfonamide isatin Michael acceptors as small molecule inhibitors of caspase-6. *J Med Chem* **52**, 2188-91 (2009).
240. Heiser, V. et al. Identification of benzothiazoles as potential polyglutamine aggregation inhibitors of Huntington's disease by using an automated filter retardation assay. *Proc Natl Acad Sci U S A* **99 Suppl 4**, 16400-6 (2002).
241. Mary, V., Wahl, F. & Stutzmann, J.M. Effect of riluzole on quinolinate-induced neuronal damage in rats: comparison with blockers of glutamatergic neurotransmission. *Neurosci Lett* **201**, 92-6 (1995).

242. Schiefer, J. et al. Riluzole prolongs survival time and alters nuclear inclusion formation in a transgenic mouse model of Huntington's disease. *Mov Disord* **17**, 748-57 (2002).
243. Landwehrmeyer, G.B. et al. Riluzole in Huntington's disease: a 3-year, randomized controlled study. *Ann Neurol* **62**, 262-72 (2007).
244. Zhang, X. et al. A potent small molecule inhibits polyglutamine aggregation in Huntington's disease neurons and suppresses neurodegeneration in vivo. *Proc Natl Acad Sci U S A* **102**, 892-7 (2005).
245. Chopra, V. et al. A small-molecule therapeutic lead for Huntington's disease: preclinical pharmacology and efficacy of C2-8 in the R6/2 transgenic mouse. *Proc Natl Acad Sci U S A* **104**, 16685-9 (2007).
246. Poirier, M.A. et al. Huntingtin spheroids and protofibrils as precursors in polyglutamine fibrilization. *J Biol Chem* **277**, 41032-7 (2002).
247. Tanaka, M. et al. Trehalose alleviates polyglutamine-mediated pathology in a mouse model of Huntington disease. *Nat Med* **10**, 148-54 (2004).
248. Bodner, R.A., Housman, D.E. & Kazantsev, A.G. New directions for neurodegenerative disease therapy: using chemical compounds to boost the formation of mutant protein inclusions. *Cell Cycle* **5**, 1477-80 (2006).
249. Bodner, R.A. et al. Pharmacological promotion of inclusion formation: a therapeutic approach for Huntington's and Parkinson's diseases. *Proc Natl Acad Sci U S A* **103**, 4246-51 (2006).
250. Folk, J.E. & Finlayson, J.S. The epsilon-(gamma-glutamyl)lysine crosslink and the catalytic role of transglutaminases. *Adv Protein Chem* **31**, 1-133 (1977).
251. Fesus, L. & Piacentini, M. Transglutaminase 2: an enigmatic enzyme with diverse functions. *Trends Biochem Sci* **27**, 534-9 (2002).
252. Achyuthan, K.E. & Greenberg, C.S. Identification of a guanosine triphosphate-binding site on guinea pig liver transglutaminase. Role of GTP and calcium ions in modulating activity. *J Biol Chem* **262**, 1901-6 (1987).
253. Chen, J.S. & Mehta, K. Tissue transglutaminase: an enzyme with a split personality. *Int J Biochem Cell Biol* **31**, 817-36 (1999).
254. Pinkas, D.M., Strop, P., Brunger, A.T. & Khosla, C. Transglutaminase 2 undergoes a large conformational change upon activation. *PLoS Biol* **5**, e327 (2007).
255. Piacentini, M. & Colizzi, V. Tissue transglutaminase: apoptosis versus autoimmunity. *Immunol Today* **20**, 130-4 (1999).
256. Fesus, L. & Szondy, Z. Transglutaminase 2 in the balance of cell death and survival. *FEBS Lett* **579**, 3297-302 (2005).
257. Gundemir, S. & Johnson, G.V. Intracellular localization and conformational state of transglutaminase 2: implications for cell death. *PLoS One* **4**, e6123 (2009).
258. Gundemir, S., Colak, G., Feola, J., Blouin, R. & Johnson, G.V. Transglutaminase 2 facilitates or ameliorates HIF signaling and ischemic cell death depending on its conformation and localization. *Biochim Biophys Acta* **1833**, 1-10 (2013).
259. Jeitner, T.M., Muma, N.A., Battaile, K.P. & Cooper, A.J. Transglutaminase activation in neurodegenerative diseases. *Future Neurol* **4**, 449-467 (2009).
260. Muma, N.A. Transglutaminase is linked to neurodegenerative diseases. *J Neuropathol Exp Neurol* **66**, 258-63 (2007).
261. Roch, A.M., Noel, P., el Alaoui, S., Charlot, C. & Quash, G. Differential expression of isopeptide bonds N epsilon (gamma-glutamyl) lysine in benign and malignant human breast lesions: an immunohistochemical study. *Int J Cancer* **48**, 215-20 (1991).
262. Bowness, J.M., Venditti, M., Tarr, A.H. & Taylor, J.R. Increase in epsilon(gamma-glutamyl)lysine crosslinks in atherosclerotic aortas. *Atherosclerosis* **111**, 247-53 (1994).

263. Lorand, L., Hsu, L.K., Siefring, G.E., Jr. & Rafferty, N.S. Lens transglutaminase and cataract formation. *Proc Natl Acad Sci U S A* **78**, 1356-60 (1981).
264. Dieterich, W. et al. Identification of tissue transglutaminase as the autoantigen of celiac disease. *Nat Med* **3**, 797-801 (1997).
265. Marsh, M.N. Transglutaminase, gluten and celiac disease: food for thought. Transglutaminase is identified as the autoantigen of celiac disease. *Nat Med* **3**, 725-6 (1997).
266. Andringa, G. et al. Tissue transglutaminase catalyzes the formation of alpha-synuclein crosslinks in Parkinson's disease. *FASEB J* **18**, 932-4 (2004).
267. Junn, E., Ronchetti, R.D., Quezado, M.M., Kim, S.Y. & Mouradian, M.M. Tissue transglutaminase-induced aggregation of alpha-synuclein: Implications for Lewy body formation in Parkinson's disease and dementia with Lewy bodies. *Proc Natl Acad Sci U S A* **100**, 2047-52 (2003).
268. Kahlem, P., Green, H. & Djian, P. Transglutaminase action imitates Huntington's disease: selective polymerization of Huntingtin containing expanded polyglutamine. *Mol Cell* **1**, 595-601 (1998).
269. Zainelli, G.M., Ross, C.A., Troncoso, J.C. & Muma, N.A. Transglutaminase cross-links in intranuclear inclusions in Huntington disease. *J Neuropathol Exp Neurol* **62**, 14-24 (2003).
270. Karpuj, M.V., Becher, M.W. & Steinman, L. Evidence for a role for transglutaminase in Huntington's disease and the potential therapeutic implications. *Neurochem Int* **40**, 31-6 (2002).
271. Karpuj, M.V. et al. Transglutaminase aggregates huntingtin into nonamyloidogenic polymers, and its enzymatic activity increases in Huntington's disease brain nuclei. *Proc Natl Acad Sci U S A* **96**, 7388-93 (1999).
272. Chun, W., Lesort, M., Tucholski, J., Ross, C.A. & Johnson, G.V. Tissue transglutaminase does not contribute to the formation of mutant huntingtin aggregates. *J Cell Biol* **153**, 25-34 (2001).
273. Mastroberardino, P.G. et al. 'Tissue' transglutaminase ablation reduces neuronal death and prolongs survival in a mouse model of Huntington's disease. *Cell Death Differ* **9**, 873-80 (2002).
274. Lesort, M., Chun, W., Johnson, G.V. & Ferrante, R.J. Tissue transglutaminase is increased in Huntington's disease brain. *J Neurochem* **73**, 2018-27 (1999).
275. Jeitner, T.M. et al. N(epsilon)-(gamma-L-glutamyl)-L-lysine (GGEL) is increased in cerebrospinal fluid of patients with Huntington's disease. *J Neurochem* **79**, 1109-12 (2001).
276. Zhang, H. et al. Full length mutant huntingtin is required for altered Ca<sup>2+</sup> signaling and apoptosis of striatal neurons in the YAC mouse model of Huntington's disease. *Neurobiol Dis* **31**, 80-8 (2008).
277. Dedeoglu, A. et al. Therapeutic effects of cystamine in a murine model of Huntington's disease. *J Neurosci* **22**, 8942-50 (2002).
278. Karpuj, M.V. et al. Prolonged survival and decreased abnormal movements in transgenic model of Huntington disease, with administration of the transglutaminase inhibitor cystamine. *Nat Med* **8**, 143-9 (2002).
279. Van Raamsdonk, J.M. et al. Cystamine treatment is neuroprotective in the YAC128 mouse model of Huntington disease. *J Neurochem* **95**, 210-20 (2005).
280. Bailey, C.D. & Johnson, G.V. The protective effects of cystamine in the R6/2 Huntington's disease mouse involve mechanisms other than the inhibition of tissue transglutaminase. *Neurobiol Aging* **27**, 871-9 (2006).
281. Lesort, M., Lee, M., Tucholski, J. & Johnson, G.V. Cystamine inhibits caspase activity. Implications for the treatment of polyglutamine disorders. *J Biol Chem* **278**, 3825-30 (2003).
282. Fox, J.H. et al. Cystamine increases L-cysteine levels in Huntington's disease transgenic mouse brain and in a PC12 model of polyglutamine aggregation. *J Neurochem* **91**, 413-22 (2004).
283. Borrell-Pages, M. et al. Cystamine and cysteamine increase brain levels of BDNF in Huntington disease via HSP1b and transglutaminase. *J Clin Invest* **116**, 1410-24 (2006).

284. Prime, M.E. et al. Discovery and structure-activity relationship of potent and selective covalent inhibitors of transglutaminase 2 for Huntington's disease. *J Med Chem* **55**, 1021-46 (2012).
285. Pardin, C., Roy, I., Lubell, W.D. & Keillor, J.W. Reversible and competitive cinnamoyl triazole inhibitors of tissue transglutaminase. *Chem Biol Drug Des* **72**, 189-96 (2008).
286. Yamamoto, A., Lucas, J.J. & Hen, R. Reversal of neuropathology and motor dysfunction in a conditional model of Huntington's disease. *Cell* **101**, 57-66 (2000).
287. Carroll, J.B. et al. Potent and selective antisense oligonucleotides targeting single-nucleotide polymorphisms in the Huntington disease gene / allele-specific silencing of mutant huntingtin. *Mol Ther* **19**, 2178-85 (2011).
288. Pfister, E.L. et al. Five siRNAs targeting three SNPs may provide therapy for three-quarters of Huntington's disease patients. *Curr Biol* **19**, 774-8 (2009).
289. Dragatsis, I., Levine, M.S. & Zeitlin, S. Inactivation of Hdh in the brain and testis results in progressive neurodegeneration and sterility in mice. *Nat Genet* **26**, 300-6 (2000).
290. Kordasiewicz, H.B. et al. Sustained therapeutic reversal of Huntington's disease by transient repression of huntingtin synthesis. *Neuron* **74**, 1031-44 (2012).
291. McBride, J.L. et al. Preclinical safety of RNAi-mediated HTT suppression in the rhesus macaque as a potential therapy for Huntington's disease. *Mol Ther* **19**, 2152-62 (2011).
292. Grondin, R. et al. Six-month partial suppression of Huntingtin is well tolerated in the adult rhesus striatum. *Brain* **135**, 1197-209 (2012).
293. Boudreau, R.L. et al. Nonallele-specific silencing of mutant and wild-type huntingtin demonstrates therapeutic efficacy in Huntington's disease mice. *Mol Ther* **17**, 1053-63 (2009).
294. Drouet, V. et al. Sustained effects of nonallele-specific Huntingtin silencing. *Ann Neurol* **65**, 276-85 (2009).
295. Fire, A. et al. Potent and specific genetic interference by double-stranded RNA in *Caenorhabditis elegans*. *Nature* **391**, 806-11 (1998).
296. Harper, S.Q. et al. RNA interference improves motor and neuropathological abnormalities in a Huntington's disease mouse model. *Proc Natl Acad Sci U S A* **102**, 5820-5 (2005).
297. Boudreau, R.L., Martins, I. & Davidson, B.L. Artificial microRNAs as siRNA shuttles: improved safety as compared to shRNAs in vitro and in vivo. *Mol Ther* **17**, 169-75 (2009).
298. McBride, J.L. et al. Artificial miRNAs mitigate shRNA-mediated toxicity in the brain: implications for the therapeutic development of RNAi. *Proc Natl Acad Sci U S A* **105**, 5868-73 (2008).
299. Bennett, C.F. & Swayze, E.E. RNA targeting therapeutics: molecular mechanisms of antisense oligonucleotides as a therapeutic platform. *Annu Rev Pharmacol Toxicol* **50**, 259-93 (2010).
300. Gagnon, K.T. et al. Allele-selective inhibition of mutant huntingtin expression with antisense oligonucleotides targeting the expanded CAG repeat. *Biochemistry* **49**, 10166-78 (2010).
301. Miller, T.M. et al. An antisense oligonucleotide against SOD1 delivered intrathecally for patients with SOD1 familial amyotrophic lateral sclerosis: a phase 1, randomised, first-in-man study. *Lancet Neurol* **12**, 435-42 (2013).
302. Wolfgang, W.J. et al. Suppression of Huntington's disease pathology in *Drosophila* by human single-chain Fv antibodies. *Proc Natl Acad Sci U S A* **102**, 11563-8 (2005).
303. Snyder-Keller, A., McLearn, J.A., Hathorn, T. & Messer, A. Early or late-stage anti-N-terminal Huntingtin intrabody gene therapy reduces pathological features in B6.HDR6/1 mice. *J Neuropathol Exp Neurol* **69**, 1078-85 (2010).
304. Southwell, A.L. et al. Intrabodies binding the proline-rich domains of mutant huntingtin increase its turnover and reduce neurotoxicity. *J Neurosci* **28**, 9013-20 (2008).
305. Southwell, A.L., Ko, J. & Patterson, P.H. Intrabody gene therapy ameliorates motor, cognitive, and neuropathological symptoms in multiple mouse models of Huntington's disease. *J Neurosci* **29**, 13589-602 (2009).

306. Sonnino, S., Mauri, L., Chigorno, V. & Prinetti, A. Gangliosides as components of lipid membrane domains. *Glycobiology* **17**, 1R-13R (2007).
307. Maglione, V. et al. Impaired ganglioside metabolism in Huntington's disease and neuroprotective role of GM1. *J Neurosci* **30**, 4072-80 (2010).
308. Schneider, J.S. et al. A randomized, controlled, delayed start trial of GM1 ganglioside in treated Parkinson's disease patients. *J Neurol Sci* **324**, 140-8 (2013).
309. Jacobsen, J.C. et al. An ovine transgenic Huntington's disease model. *Hum Mol Genet* **19**, 1873-82 (2010).
310. Palfi, S. et al. Expression of mutated huntingtin fragment in the putamen is sufficient to produce abnormal movement in non-human primates. *Mol Ther* **15**, 1444-51 (2007).
311. Yang, S.H. et al. Towards a transgenic model of Huntington's disease in a non-human primate. *Nature* **453**, 921-4 (2008).
312. Chalfie, M., Tu, Y., Euskirchen, G., Ward, W.W. & Prasher, D.C. Green fluorescent protein as a marker for gene expression. *Science* **263**, 802-5 (1994).
313. Förster, T. Zwischenmolekulare Energiewanderung und Fluoreszenz. *Annalen der Physik* **437**, 55-75 (1948).
314. Kenworthy, A.K. Imaging protein-protein interactions using fluorescence resonance energy transfer microscopy. *Methods* **24**, 289-96 (2001).
315. Tsien, R.Y., Bacskai, B.J. & Adams, S.R. FRET for studying intracellular signalling. *Trends Cell Biol* **3**, 242-5 (1993).
316. Chen, Y., Mills, J.D. & Periasamy, A. Protein localization in living cells and tissues using FRET and FLIM. *Differentiation* **71**, 528-41 (2003).
317. Lleres, D., James, J., Swift, S., Norman, D.G. & Lamond, A.I. Quantitative analysis of chromatin compaction in living cells using FLIM-FRET. *J Cell Biol* **187**, 481-96 (2009).
318. Pollitt, S.K. et al. A rapid cellular FRET assay of polyglutamine aggregation identifies a novel inhibitor. *Neuron* **40**, 685-94 (2003).
319. Weiss, A. et al. Single-step detection of mutant huntingtin in animal and human tissues: a bioassay for Huntington's disease. *Anal Biochem* **395**, 8-15 (2009).
320. Schutzius, G. et al. A quantitative homogeneous assay for fragile X mental retardation 1 protein. *J Neurodev Disord* **5**, 8 (2013).
321. Bidinosti, M. et al. Novel one-step immunoassays to quantify alpha-synuclein: applications for biomarker development and high-throughput screening. *J Biol Chem* **287**, 33691-705 (2012).
322. Honarnejad, K. et al. FRET-Based Calcium Imaging: A Tool for High-Throughput/Content Phenotypic Drug Screening in Alzheimer Disease. *J Biomol Screen* **18**, 1309-20 (2013).
323. Karapetyan, Y.E. et al. Unique drug screening approach for prion diseases identifies tacrolimus and astemizole as antiprion agents. *Proc Natl Acad Sci U S A* **110**, 7044-9 (2013).
324. Griffin, M., Casadio, R. & Bergamini, C.M. Transglutaminases: nature's biological glues. *Biochem J* **368**, 377-96 (2002).
325. Nakaoka, H. et al. Gh: a GTP-binding protein with transglutaminase activity and receptor signaling function. *Science* **264**, 1593-6 (1994).
326. Begg, G.E. et al. Mutation of a critical arginine in the GTP-binding site of transglutaminase 2 disinhibits intracellular cross-linking activity. *J Biol Chem* **281**, 12603-9 (2006).
327. Van Der Meer, B.W., Coker, I., Chen, S.Y.S. Resonance Energy Transfer : Theory and Data. *VCH : New York* (1994).
328. Rizzo, M.A., Springer, G.H., Granada, B. & Piston, D.W. An improved cyan fluorescent protein variant useful for FRET. *Nat Biotechnol* **22**, 445-9 (2004).

329. Rizzo, M.A., Springer, G., Segawa, K., Zipfel, W.R. & Piston, D.W. Optimization of pairings and detection conditions for measurement of FRET between cyan and yellow fluorescent proteins. *Microsc Microanal* **12**, 238-54 (2006).
330. Wallrabe, H. & Periasamy, A. Imaging protein molecules using FRET and FLIM microscopy. *Curr Opin Biotechnol* **16**, 19-27 (2005).
331. Majoul, I., Straub, M., Duden, R., Hell, S.W. & Soling, H.D. Fluorescence resonance energy transfer analysis of protein-protein interactions in single living cells by multifocal multiphoton microscopy. *J Biotechnol* **82**, 267-77 (2002).
332. Alcor, D., Calleja, V. & Larijani, B. Revealing signaling in single cells by single- and two-photon fluorescence lifetime imaging microscopy. *Methods Mol Biol* **462**, 307-43 (2009).
333. Duncan, R.R., Bergmann, A., Cousin, M.A., Apps, D.K. & Shipston, M.J. Multi-dimensional time-correlated single photon counting (TCSPC) fluorescence lifetime imaging microscopy (FLIM) to detect FRET in cells. *J Microsc* **215**, 1-12 (2004).
334. Trettel, F. et al. Dominant phenotypes produced by the HD mutation in STHdh(Q111) striatal cells. *Hum Mol Genet* **9**, 2799-809 (2000).
335. DeLano, W.L. The PyMOL Molecular Graphics System. (DeLano Scientific, San Carlos, CA, USA, 2002).
336. Ruan, Q., Tucholski, J., Gundemir, S. & Johnson Voll, G.V. The Differential Effects of R580A Mutation on Transamidation and GTP Binding Activity of Rat and Human Type 2 Transglutaminase. *Int J Clin Exp Med* **1**, 248-59 (2008).
337. Murthy, S.N. et al. Conserved tryptophan in the core domain of transglutaminase is essential for catalytic activity. *Proc Natl Acad Sci U S A* **99**, 2738-42 (2002).
338. Sorger, P.K. Heat shock factor and the heat shock response. *Cell* **65**, 363-6 (1991).
339. Lunec, J. & Cresswell, S.R. Heat-induced thermotolerance expressed in the energy metabolism of mammalian cells. *Radiat Res* **93**, 588-97 (1983).
340. Wiemann, M., Busselberg, D., Schirmacher, K. & Bingmann, D. A calcium release activated calcium influx in primary cultures of rat osteoblast-like cells. *Calcif Tissue Int* **63**, 154-9 (1998).
341. Colak, G., Keillor, J.W. & Johnson, G.V. Cytosolic guanine nucleotide binding deficient form of transglutaminase 2 (R580a) potentiates cell death in oxygen glucose deprivation. *PLoS One* **6**, e16665 (2011).
342. Keillor, J.W., Chica, R.A., Chabot, N., Vinci, V., Pardin, C., Fortin, E., Gillet, S.M.F.G., Nakano, Y., Kaartinen, M.T., Pelletier, J.N., Lubell, W.D. The bioorganic chemistry of transglutaminase: From mechanism to inhibition and engineering. *Can J Chem* **86**, 271-276 (2008).
343. Kim, S.Y., Jeitner, T.M. & Steinert, P.M. Transglutaminases in disease. *Neurochem Int* **40**, 85-103 (2002).
344. Cooper, A.J., Jeitner, T.M. & Blass, J.P. The role of transglutaminases in neurodegenerative diseases: overview. *Neurochem Int* **40**, 1-5 (2002).
345. Jeitner, T.M., Pinto, J.T., Krasnikov, B.F., Horswill, M. & Cooper, A.J. Transglutaminases and neurodegeneration. *J Neurochem* **109 Suppl 1**, 160-6 (2009).
346. Menalled, L.B. & Chesselet, M.F. Mouse models of Huntington's disease. *Trends Pharmacol Sci* **23**, 32-9 (2002).
347. Suske, G. The Sp-family of transcription factors. *Gene* **238**, 291-300 (1999).
348. Johannessen, M., Delghandi, M.P. & Moens, U. What turns CREB on? *Cell Signal* **16**, 1211-27 (2004).
349. Chen, G. & Courey, A.J. Groucho/TLE family proteins and transcriptional repression. *Gene* **249**, 1-16 (2000).
350. Plomann, M. et al. PACSIN, a brain protein that is upregulated upon differentiation into neuronal cells. *Eur J Biochem* **256**, 201-11 (1998).

351. Schael, S. et al. Casein kinase 2 phosphorylation of protein kinase C and casein kinase 2 substrate in neurons (PACSIN) 1 protein regulates neuronal spine formation. *J Biol Chem* **288**, 9303-12 (2013).
352. Caron, N.S., Munsie, L.N., Keillor, J.W. & Truant, R. Using FLIM-FRET to measure conformational changes of transglutaminase type 2 in live cells. *PLoS One* **7**, e44159 (2012).
353. Evers, T.H., van Dongen, E.M., Faesen, A.C., Meijer, E.W. & Merckx, M. Quantitative understanding of the energy transfer between fluorescent proteins connected via flexible peptide linkers. *Biochemistry* **45**, 13183-92 (2006).
354. Berezin, M.Y. & Achilefu, S. Fluorescence lifetime measurements and biological imaging. *Chem Rev* **110**, 2641-84 (2010).
355. Trottier, Y. et al. Polyglutamine expansion as a pathological epitope in Huntington's disease and four dominant cerebellar ataxias. *Nature* **378**, 403-6 (1995).
356. Housman, D. Gain of glutamines, gain of function? *Nat Genet* **10**, 3-4 (1995).
357. Fuxreiter, M. & Tompa, P. Fuzzy complexes: a more stochastic view of protein function. *Adv Exp Med Biol* **725**, 1-14 (2012).
358. Khoshnan, A. & Patterson, P.H. The role of IkkappaB kinase complex in the neurobiology of Huntington's disease. *Neurobiol Dis* **43**, 305-11 (2011).
359. Lee, D.F. & Hung, M.C. Advances in targeting IKK and IKK-related kinases for cancer therapy. *Clin Cancer Res* **14**, 5656-62 (2008).
360. Quan, F., Janas, J. & Popovich, B.W. A novel CAG repeat configuration in the SCA1 gene: implications for the molecular diagnostics of spinocerebellar ataxia type 1. *Hum Mol Genet* **4**, 2411-3 (1995).
361. Sen, S., Dash, D., Pasha, S. & Brahmachari, S.K. Role of histidine interruption in mitigating the pathological effects of long polyglutamine stretches in SCA1: A molecular approach. *Protein Sci* **12**, 953-62 (2003).
362. Block-Galarza, J. et al. Fast transport and retrograde movement of huntingtin and HAP 1 in axons. *Neuroreport* **8**, 2247-51 (1997).
363. Sugars, K.L. & Rubinsztein, D.C. Transcriptional abnormalities in Huntington disease. *Trends Genet* **19**, 233-8 (2003).
364. DiProspero, N.A. et al. Early changes in Huntington's disease patient brains involve alterations in cytoskeletal and synaptic elements. *J Neurocytol* **33**, 517-33 (2004).
365. Hoffner, G., Island, M.L. & Djian, P. Purification of neuronal inclusions of patients with Huntington's disease reveals a broad range of N-terminal fragments of expanded huntingtin and insoluble polymers. *J Neurochem* **95**, 125-36 (2005).
366. Sathasivam, K. et al. Aberrant splicing of HTT generates the pathogenic exon 1 protein in Huntington disease. *Proc Natl Acad Sci U S A* **110**, 2366-70 (2013).
367. Ross, C.A. & Poirier, M.A. Protein aggregation and neurodegenerative disease. *Nat Med* **10 Suppl**, S10-7 (2004).
368. Caron, N.S., Desmond, C.R., Xia, J. & Truant, R. Polyglutamine domain flexibility mediates the proximity between flanking sequences in huntingtin. *Proc Natl Acad Sci U S A* **110**, 14610-5 (2013).
369. Gustafsson, M.G. Surpassing the lateral resolution limit by a factor of two using structured illumination microscopy. *J Microsc* **198**, 82-7 (2000).
370. Groenning, M. Binding mode of Thioflavin T and other molecular probes in the context of amyloid fibrils-current status. *J Chem Biol* **3**, 1-18 (2010).
371. Meyvis, T.K., De Smedt, S.C., Van Oostveldt, P. & Demeester, J. Fluorescence recovery after photobleaching: a versatile tool for mobility and interaction measurements in pharmaceutical research. *Pharm Res* **16**, 1153-62 (1999).

372. Howell, J.L. & Truant, R. Live-cell nucleocytoplasmic protein shuttle assay utilizing laser confocal microscopy and FRAP. *Biotechniques* **32**, 80-2, 84, 86-7 (2002).
373. Goedhart, J. et al. Structure-guided evolution of cyan fluorescent proteins towards a quantum yield of 93%. *Nat Commun* **3**, 751 (2012).
374. Waelter, S. et al. Accumulation of mutant huntingtin fragments in aggresome-like inclusion bodies as a result of insufficient protein degradation. *Mol Biol Cell* **12**, 1393-407 (2001).
375. Chai, Y., Shao, J., Miller, V.M., Williams, A. & Paulson, H.L. Live-cell imaging reveals divergent intracellular dynamics of polyglutamine disease proteins and supports a sequestration model of pathogenesis. *Proc Natl Acad Sci U S A* **99**, 9310-5 (2002).
376. Chung, M.Y. et al. Evidence for a mechanism predisposing to intergenerational CAG repeat instability in spinocerebellar ataxia type I. *Nat Genet* **5**, 254-8 (1993).
377. Zuhlke, C. et al. Spinocerebellar ataxia type 1 (SCA1): phenotype-genotype correlation studies in intermediate alleles. *Eur J Hum Genet* **10**, 204-9 (2002).
378. Calabresi, V., Guida, S., Servadio, A. & Jodice, C. Phenotypic effects of expanded ataxin-1 polyglutamines with interruptions in vitro. *Brain Res Bull* **56**, 337-42 (2001).
379. Moseley, M.L. et al. SCA8 CTG repeat: en masse contractions in sperm and intergenerational sequence changes may play a role in reduced penetrance. *Hum Mol Genet* **9**, 2125-30 (2000).